HIGH STRENGTH POLYISOBUTYLENE BASED STRUCTURES: SYNTHESIS, CHARACTERIZATON AND SUITABILITY FOR BIOMEDICAL APPLICATIONS

by
Nur Çiçek Kekeç Şenel
B.S., Chemistry, Middle East Technical University, 2013
M.S., Chemistry, Boğaziçi University, 2015

Submitted to the Institute for Graduate Studies
in Science and Engineering in partial fulfillment of
the requirements for the degree of
Doctor of Philosophy

Graduate Program in Chemistry
Boğaziçi University
2023

To Ünsal KEKEÇ and Rahmi GÜLTEKİN

ACKNOWLEDGEMENTS

First and foremost, I would like to express my sincere gratitude to my supervisor Prof. Nihan Nugay for her endless support and belief. I am grateful to her for generously sharing her experience, in-depth knowledge and awareness with me. I am also grateful to Prof. Turgut Nugay for sharing his support for all stage, constructive comments and knowledge throughout this project. I will always be in debt for not only their support but also being like a family.

I wish to extend my appreciation to Prof. Sinan Şen, Assist. Prof. Ayşe Ak and Assist. Prof. Fırat İlker for being my committee members and giving up from their time to evaluate my thesis. Also, I would like to thank Bilge Uluocak for NMR analysis and Burcu Selen Çağlayan for Raman and XPS analysis, and BAP for its support with project number 11121.

I also would like to thank my dearest friend Gizem Kırevliyası Pekküçük being like a long lost twin and by my side whenever I need her, and her husband Çağan Pekküçük for his support and friendship. Also, I would like to thank Zeynep Gültekin and Can Gültekin for not being like cousins but more like siblings and their profound love.

I owe my deepest gratitude to my family, especially my mother Funda Kekeç for her endless love and support throughout every stage of my life as both mother and father, my grandmother Sebahat Gültekin for not seeing me any different from her own children and love profoundly, my husband Cem Şenel for his endless love and support throughout this journey, I am sure he will stay with me for the rest of my life.

Finally, I would like to devote this thesis to my father Ünsal Kekeç and my grandfather Rahmi Gültekin even if they’re not here I will be forever grateful to them. Not only for this day but in every important stage of my life, they will always be nearby. They will remain the biggest heroes for me.

ABSTACT

HIGH STRENGTH POLYISOBUTYLENE BASED STRUCTURES: SYNTHESIS, CHARACTERIZATION AND SUITABILITY FOR BIOMEDICAL APPLICATIONS

In this study, there are two main focuses: (i) increasing the strength of polyisobutylene structures via interpenetrating network and polyurethane (PU) formation. Specifically, the latter strategy involves strengthening polyurethanes with the additional hydrogen-bonding sites in PIB soft domain and nanolayers, (ii) investigating the suitability of these high strength PUs for biomedical applications by comparing them with the commercial one.

In this context, PIB primary network was synthesized by using Thiol-ene (click) chemistry, in which HS-PIB-SH, prepared from HO-PIB-OH via esterification, reacted with a trifunctional allyl compound as a crosslinker. Sequential IPN method were preferred to be used for successful and controllable PIB/PS based IPN formation. The fundamental network characteristics, which are homogeneity of primary network, increased crosslink density and decreased mesh size, proved the successful IPN formation resulting in enhanced dimensional stability in solvents, tensile strength, thermal stability as well as creep resistance.

Newly synthesized high strength PIB-based PUs all showed that inert PIB barriers enhanced the protection of hydrolytically and oxidatively vulnerable carbamate bonds. Among them, sulfur addition aiming extra H-bonding sites in PIB soft phase of PUs was not very affective on static mechanical properties but improved thermal stability and surprisingly increased creep resistance of sulfur-containing PIB based PU (PIB_S-PU) via H-bonded S atoms (N-H…S) between hard and soft phases. Nanolayers addition to PIB_S-PU, on the other hand, enhanced elongation, tensile strength, creep resistance and hydrolytic-oxidative stability since as a co-chain extender/reinforcing filler, organically modified montmorillonite (OmMMT) covalently integrates hard PU segments, shields the vulnerable urethane linkages, and prevents the sulfur oxidation in soft segments.

Besides, suitability of these high strength PIB based PUs for biomedical applications were evaluated in terms of first preliminary surface properties including surface stiffness, charges, roughness, wettability, chemical functionalities, and dimensional stability in water medium. Then, calcification resistance, protein adsorption, cell attachment, cell viability and bacterial resistance of them were investigated. It has been found that these properties of high strength PUs were superior to clinically widely implanted PDMS-based polyurethane, Elast-Eon®, in the biomedical applications due to (i) increased hydrolytic and oxidative stability (ii) higher dimensional stability in PBS medium. In short, the commercial one was found to have lower *in vitro* biocompatibility as well as higher cytotoxicity than newly synthesized PIB based PUs.

ÖZET

YÜKSEK MUKAVEMETLİ POLİİZOBÜTİLEN BAZLI YAPILAR: SENTEZİ, KARAKTERİZASYONU VE BİYOMEDİKAL UYGULAMALARINA UYGUNLUĞU

Bu çalışmada 2 ana odak noktası bulunmaktadır: (i) iç içe geçen ağ ve poliüretan oluşumu yoluyla poliizobütilen yapılarının mukavemetinin arttırılması, özellikle, ikinci strateji kapsamında poliüretan yumuşak poliizobütilen fazının ek hidrojen bağı bölgeleri ve nano tabaka ilavesi ile güçlendirilmesi, (ii) bu yüksek mukavemetli poliüretan yapılarının biyomedikal uygulamalar için uygunluğunun ticari olan bir ürünle karşılaştırmalı olarak araştırılması.

Bu kapsamda, HO-PIB-OH’dan esterleşme yolu ile hazırlanan HS-PIB-SH’ın çapraz bağlayıcı olarak üç işlevli bir alil bileşiği ile reaksiyona girdiği Tiyol-en kimyası kullanılarak PIB birincil ağı oluşturulmuştur. Başarılı ve kontrol edilebilir poliizobütilen ve polistiren bazlı iç içe geçen ağ oluşumunda ardışık iç içe geçen ağ metodu tercih edilmiştir. Birincil ağ yapısının homojenliği, artan çapraz bağ yoğunluğu ve azalan ağ boyutu olan temel ağ özellikleri, çözücülerdeki gelişmiş boyutsal kararlılık, artan gerilme mukavemeti, termal kararlılık ve sürünme geri kazanımı ile sonuçlanan başarılı iç içe geçen ağ yapısı oluşumunu kanıtlamıştır.

Yeni sentezlenen yüksek mukavemetli poliizobütilen bazlı poliüretanların tümünde, inert PIB bariyerlerin hidrolitik ve oksidatif olarak savunmasız olan karbamat bağlarını koruduğu görülmüştür. Bunların yansıra, poliüretanların yumuşak PIB fazında ekstra hidrojen bağı bölgeleri oluşturmayı hedefleyen kükürt ilavesi, statik mekanik özellikler üzerinde çok etki olmasa da sert ve yumuşak fazlar arasındaki hidrojen bağlı kükürt atomları yoluyla kükürt içeren poliüretan (PIB_S-PU) yapısının termal kararlılığını ve şaşırtıcı bir şekilde sürünme direncini arttırmıştır. Öte yandan, PIB_S-PU yapısına eklenen nano tabakalar, eş-zincir genişletici/güçlendirici dolgu maddesi olan, organik olarak modifiye edilmiş montmorillonit (OmMMT), sert poliüretan segmentlerine kovalent olarak entegre ettiğinden, gelişmiş uzama, gerilme mukavemeti, sürünme direnci ve hidrolitik-oksidatif kararlılık hassas üretan bağlarını ve yumuşak fazda yer alan kükürt oksidasyonunu önlemiştir.

Ayrıca, bu yüksek mukavemetli poliizobütilen bazlı poliüretan yapılarının biyomedikal uygulamalar için uygunluğu, yüzey sertliği, yükleri, pürüzlülüğü, ıslanabilirliği, kimyasal işlevselliği ve su ortamındaki boyutsal kararlılığını içeren öncül yüzey özelliklerine göre değerlendirilmiştir. Ardından, kalsifikasyon direnci, protein adsorpsiyonu, hücre tutunması, hücre canlılığı ve bakteri direnci incelenmiştir. Yüksek mukavemetli PU’ların bu özelliklerinin (i) artan hidrolitik ve oksidatif kararlılık (ii) PBS ortamında daha yüksek boyutsal kararlılık nedeniyle biyomedikal uygulamalarda klinik olarak geniş çapta implante edilen PDMS bazlı poliüretan Elast-Eon®’dan üstün olduğu sonucuna varılmıştır. Sonuç olarak, yaygın ve ticari olarak kullanılan bu poliüretanın, yeni sentezlenmiş poliizobütilen bazlı poliüretanlardan daha düşük in-vitro biyouyumluluğa ve daha yüksek sitotoksisiteye sahip olduğu saptanmıştır.

TABLE OF CONTENT

LIST OF FIGURES

LIST OF TABLES

LIST OF SYMBOLS

a	Radius
a.u.	Arbitrary unit
cm	Cantimeter
cps	Counts per second
C_n	Characteristic ratio of polymer
$C_{2,r}$	Mass concentration of polymer film in the experimental solution before crosslinking
d	Density
E	Young's Modulus
eV	Electronvolt
F	Force
g	Gram
G	Shear Modulus
h	Hour
Hz	Hertz
keV	Kiloelectronvolt
kHz	Kilohetrz
kPa	Kilopascal
L	Liter
l	Average bond length
l_p	Final length of sample
l_0	Initial length of sample
M	Molarite
mg	Miligram
MHz	Megahertz
min	Minute
ml	Milliliter
mM	Milimolar
mm	Milimeter
mmHg	Millimeter of Mercury

mmol	Milimol
MPa	Megapascal
mW	Miliwatt
$\bar{M}_c$	Average molecular weight between crosslinks
$\bar{M}_n$	Number Average Molecular Weight
M_r	Molecular weight of the repeating unit
M_w	Weight Average Molecular Weight
M_w/M_n	Polydispersity Index
m	Mass
m_d	Dry weight of network
m_{ex}	Dry weight of network after extraction
m_s	Equilibrium weight of swollen network
nm	Nanometer
n	Number of bonds in the crosslinked system
ppm	Parts per million
Q	Volume swelling ratio
q_{cyc}	Volume swelling ratio in cyclohexane
q_{THF}	Volume swelling ratio in THF
q_w	Equilibrium weight swelling ratio
R	Gas constant
rpm	Revolutions per minute
$([r_0^{-2})]^{1/2}$	End-to-end distance of polymer chain
s	Second
T	Temperature
T_g	Glass transition temperature
T_m	Melting temperature
T_α	α-relaxation temperature
v/v	Volume/volume
vol	Volume
V_1	Molar volume of solvent
$v_{2,r}$	Volume fraction of relaxed film
$v_{2,s}$	Volume fraction of swollen film

W	Watt
wt	Weight
wt/v	Weight/volume
w	Depth
α	Alpha
δ	Chemical shift
Δl	Length change
ε	Strain
ϴ	Theta
µL	Microliter
µm	Micrometer
v	Poisson’s ratio
ξ	Mesh size
ρ_c	Crosslink density
ρ_{cyc}	Density of cyclohexane
ρ_p	Density of crosslinked polymer
σ	Tensile stress
$\bar{v}$	Specific volume of polymer
χ	Polymer-solvent interaction parameter
%	Percent

LIST OF ACRONYMS/ABBREVIATIONS

BSA	Bovine serum albumin
C.Albicans	Candida albicans yeast
DMA	Dynamic mechanical analysis
DSC	Differential scanning calorimeter
E.Coli	Escherichia coli bacteria
ECM	Extracellular matrix
EDX	Energy-dispersive X-ray
ELAS	Elast-Eon®E2A
Fg	Fibrinogen
IB	Isobutylene
OmMMT	Negatively charged montmorillonite nanolayers carrying the quaternary amine, $(CH_3)_3N+ (CH_2)_3NH_2)$
PBS	Phosphate-buffered saline
PIB	Polyisobutylene
PIB/PS IPN	Polyisobutylene/polystyrene based interpenetrating network
PIB_O	HO-PIB-OH
PIB_O-PU	Polyisobutylene based polyurethanes with HO-PIB-OH soft segments
PIB-PUU	Polyisobutylene based poly(urethane-urea)
PIB_S	HO-S-PIB-S-OH
PIB_S-PU	Polyisobutylene based polyurethanes with O-S-PIB-S-O- soft segments
PIB_S-PU/NC	Sulfur-containing polyisobutylene based polyurethane nanocomposite
PIB-SXA	Polyisobutylene based primary network
PU	Polyurethane
S.Aureus	Staphylococcus aureus bacteria
SBF	Simulated body fluid
SDS	Sodium dodecyl sulfate
SEM	Secondary electron microscope

TGA	Thermogravimetric analysis
TPIBSH	Dithiol telechelic polyisobutylene
UV	Ultraviolet
XPS	X-ray photoelectron spectroscopy
XRD	X-ray diffraction

1. INTRODUCTION

1.1. Polyisobutylene

Polyisobutylene (PIB) is a widely used commercial polymer because of its many useful properties, including its high flexibility at ambient temperature, thermal stability, and gas impermeability. According to these remarkable properties, in 1949, the National Bureau of Standards, which is currently named as the National Institute of Standards and Technology, had designated polyisobutylene (PIB) as a standard polymer to define “usual polymeric properties”, recognizing its significance [1].

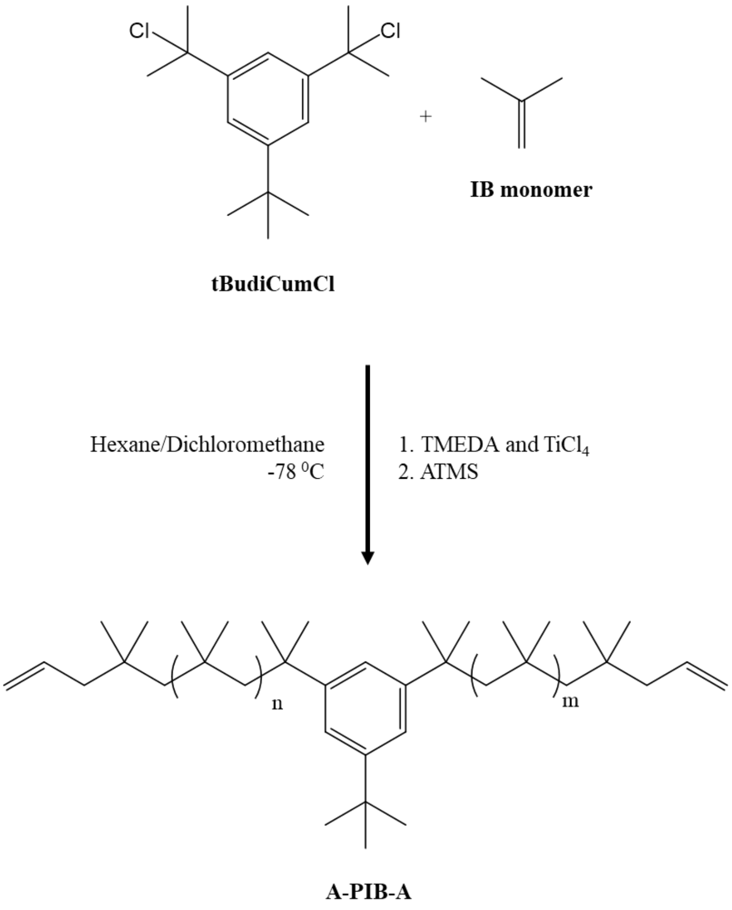

Figure 1.1: Cationic polymerization reaction of IB to form allyl telechelic PIB(A-PIB-A)

Cationic polymerization is a crucial method for generating polymers/copolymers with pre-determined monomer sequence and molecular weight. Isobutylene (IB), styrene, and their derivatives are the most important monomers polymerizing via a cationic polymerization mechanism and isobutylene is the most researched monomer because it polymerizes solely by a cationic mechanism (Figure 1.1), and its polymer (polyisobutylene – PIB-) is the only organic polymer, in comparison to many other ones, with such unique features such as good thermal and hydrolytic/oxidative stability, chemical resistivity and low permeability [2].

The accrued results of collaboration of 27 global research laboratories for a study of PIB sample, and the gathered results were used to determine what should be accepted as the standard viscoelastic properties of polymer samples. This collaborated study on PIB sample had a leading role for determining the general polymeric properties such as (i) the time-temperature superposition principle, generally used to specify the viscoelastic behavior of polymeric materials at long and short observation frequencies and/or times, and (ii) the influence of molecular weight on the viscosity of entangled polymers. Besides these important characteristics, polyisobutylene has some polymeric properties different from most of other polymer samples such as (i) a remarkably low permeability for small molecules penetration, (ii) low fragility (which is one of the weakest temperature-dependent viscosity and structural relaxation) and consequently, substantial inelastic scattering even much above the T_g (glass transition temperature) of polymeric material (iii) an obvious conformance to time-temperature super-positioning, which can be leaded by a quite low difference between the temperature-dependent pattern of chain and segmental relaxations, dissimilar to apparent breakdown of chains seen in some other polymer samples; for example, polypropylene and polystyrene (iv) more broadening in a mechanical segmental dispersion than the expected characteristic for a low fragility polymeric material (v) an exceptional spectrum of fast dynamics; which can be defined as having a “constant loss” pattern where the negligible changes in susceptibility with frequency. Therefore, these characteristics, which are differentiated from some common properties of other polymers, exemplify that polyisobutylene can be assumed as a unusual polymer [1].

The rapid changes in the rate of segmental relaxation in polymer structure (structural relaxation process) is mainly related with the glass transition in supercooled liquids [1]. Polyisobutylene rubbers can have a glass transition temperature as low as -76^{0}C. However, PIB materials have poor mechanical properties because of its low resistance to penetration and creeping; for example, they cannot be resisting to organic solvent penetration, such as benzene and toluene, and solvent containing materials such as oils and fats [3]. In order to improve the mechanical properties of polyisobutylene, and overcome other weaknesses of PIB material, like creeping and poor resistance to organic solvents without impairing their low permeability to gas, there are some reinforcing methods for PIB: (i) copolymer formation (ii) interpenetrating network formation (iii) polyurethane formation (iv) nanoparticle addition.

1.2. Reinforcing Methods for Polymers and Polyisobutylene (PIB)

1.2.1. Copolymer Formation

Polymers and their copolymers belong to the class of macromolecular compounds. Homopolymers show a uniform structure whereas copolymers have a heterogeneous composition. Understanding the composition (structure) and properties of copolymers requires the knowledge of their synthesis. At the synthesis stage of polymers, a wide variety of organic compounds might be categorized as monomers, and copolymerization refers to the chain polymerization process, where two or more of them are polymerized concurrently, and gives product named as a copolymer. Since different molecular chains can include different number of monomers, the term of copolymer refers to a combination of different-length macromolecules and has always been characterized by an average molecular weight (also distribution). Also, copolymers are classified according to their structures; (i) including single polymer chain are named as linear copolymers (such as block, alternating, block), (ii) containing polymeric side chains are known as branched copolymers (such as graft, star, brush) [4].

In addition to advances in synthetic polymer chemistry, thermoplastic elastomers (biphasic synthetic polymers), containing a continuous soft-rubbery matrix which is physically crosslinked glassy-plastic domains, one of the most widely utilized polymers in several applications; also block and graft copolymers are mainly preferred for these areas [5].

Block copolymers consist of two or more chemically different polymer chains which are linked by covalent bonds, and there are several potential molecular structures, i.e. -AB- diblock linear copolymer, -ABC- triblock linear copolymer, random and alternating block copolymer (see in Figure 1.2). However, one or maximum two covalent bonds may exist between two blocks. The characteristics of block copolymers significantly differ from those of random copolymers and blend of corresponding homopolymers. Because of their extraordinary microphase morphologies (and its separation also occur in the solid), block copolymers have attracted considerable study. Also, this morphology affects their properties and by adjusting the ratio of block lengths, type of comonomers and molecular weight distribution, it is possible to modify their architecture [4].

i) -AB- Diblock Linear Copolymer

ii) -ABC- Triblock Linear Copolymer

iii) Random Block Copolymer

iv) Alternating Block Copolymer

Figure 1.2: Various block copolymers with different structures: i) -AB- Diblock Linear Copolymer, ii) –ABC- Triblock Copolymer, iii) Random Block Copolymer, iv) Alternating Block Copolymer. Reprinted from [6].

Graft copolymers, an important type of commercial polymers, consist of a polymer backbone (base polymer in Figure 1.3) and polymer side chains (whose chemical composition are different from the backbone) linked to it. There are three different methods for preparing graft copolymers; (i) pre-synthesized polymer backbone and side chains are linked together using the in-chain-functionalities of base polymer and end-functionalities of side chains; it is called as a “grafting onto”, (ii) multifunctional base polymer acts as a macroinitiator and starts polymerization of side chain monomers grafted to the backbone; it is called as a “grafting from”, (iii) synthesis of polymer side with polymerizable end groups is followed by the polymerization of macromonomers to create the backbone; it is called as a “grafted through” [5].

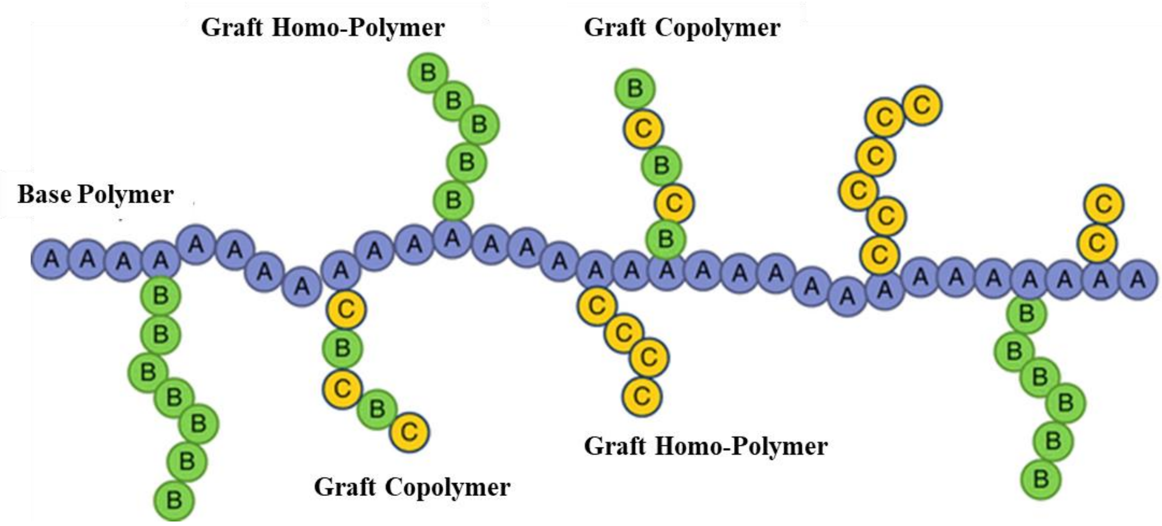

Figure 1.3: Idealized structure of graft copolymers. Reprinted from [7].

It is being investigated how to synthesize polyisobutylene combinations with polymers exhibiting strong mechanical properties to strengthen the mechanical properties of polyisobutylene. Blending and copolymer elaboration are two methods for creating long-lasting combinations of PIB and thermoplastic polymers.

As one of the few important literature examples, a variety of linear and three-arm star poly(styrene-b-isobutene-b-styrene) (PS–PIB–PS) block copolymers with different block compositions, which was synthesized by living carbocationic polymerization, was reported by Storey et al. [8]. Ionomer block copolymer has been generated from these block copolymers using PS block sulfonation. By introducing 5-20 mol% of sulfonate groups to the PS phases increases the tensile strength and modulus, and the resulting physical crosslinking can be stable at temperatures above the T_g of PS [8]. Later on, in 2006, Faust's research group prepared polyisobutylene-poly(alkyl methacrylate) block copolymers by using living cationic and anionic polymerization methods. By metalation of living PIB, they obtained stable macrocarbanion, which was used to initiate the anionic polymerization of tert-butyl methacrylate, and the final polyisobutylene-*b*-polymethacrylate block copolymers showed high blocking efficiency. Also, they stated that this triblock copolymer displayed zero-order drug release when loaded with PTx (paclitaxel drug) and coated on coronary stents in the contrast to SIBS/PTx systems, which is capable of delivering the drug straight to arterial walls. As a result, they reported that PMMA-*b*-PIB-*b*-PMMA/PTx system can be used as a drug delivery matrix for coronary stent coatings [9].

1.2.2. Interpenetrating Network (IPN) Formation

According to studies done to date, in order to generate a thermoplastic reinforced elastomeric material, combining different polymers inside an interpenetrating polymer network (IPN) structure, specified as a combination of two or more polymer network structures which are synthesized in juxtaposition, is an another and only alternative method [3]. In other words, IPN is an architecture including non-covalently attached but physically interlaced and inseparable multiple (two or more) networks [10]. Nevertheless, the interpenetrating polymer network (IPN) structure was discovered before phase morphology and separation concepts found today's meaning. Nowadays, it becomes clear that for most IPN systems, the interpenetration of polymer networks does not exist in a molecular scale, but they may be formed by finely separating phases into only ten nanometer scale in size. Numerous interpenetrating polymer network (IPN) systems, two or more polymers present in the architecture form continuous phases in a macroscopic level, display dual phase continuity.

Interpenetrating polymer network (IPN) architecture is most relevant with block copolymer structures in terms of many aspects. While the block length is determinative for the domains size in the block copolymer structure, the chain length between the crosslinks, defined as crosslinking level, has a primary role in determination of IPNs domain size. In detail, if the structure has short chain segments or blocks between crosslinks, they create small domains under many different conditions. Nevertheless, there are many significant differences between them; i.e., the short length of blocks plays an important role in increasing miscibility between polymer components; whereas, in the case of interpenetrating polymer networks, growing evidence indicates that increasing crosslink level reduces the miscibility of the system compared to the similar blend for system in which the linear component polymers are miscible [11].

There are many different methods to prepare interpenetrating polymer network (IPN) structures. More significant IPN structures can be defined as follow:

Sequential Interpenetrating Polymer Network (SeqIPN): One polymer network is prepared. Then, the monomer of second polymer is added into swollen first polymer network with initiator and crosslinker, and in-situ polymerization is completed. Therefore, the sequential interpenetrating polymer network (seqIPN) structures consist of two polymer network materials in which one of them is synthesized later than the other [11].

Simultaneous Interpenetrating Polymer Network (SimIPN): The monomers (or prepolymers) of both polymers are mixed into a same system with crosslinkers and initiators of them. Therefore, both polymerization reactions are carried through simultaneously however these reactions have not interfered each other [11].

Latex Interpenetrating Network: The latex interpenetrating polymer network, also named as an interpenetrating elastomer network, is prepared in a latex form including shell and core structures. After mixing two different latexes, this IPNs is obtained in a film form, crosslinking both polymer structures [11].

Gradient Interpenetrating Network: The interpenetrating network, in which the crosslink density or overall compositions of the polymers shows an alteration in different locations on a macroscopic level, named as a gradient IPN [11].

Thermoplastic Interpenetrating Network: They are hybrid structures between polymer blends and IPNs since they are obtained by physical crosslinking rather than chemical crosslinks. In detail, as in thermoplastic elastomer structures, thermoplastic IPNs are crosslinked at use temperature while flowing at elevated temperatures [11].

Semi-Interpenetrating Network: Semi IPNs mainly include two different polymer morphologies; that is, one or more polymers are branched or linear and one or more polymers are crosslinked in this structure [11].

When compared to conventional networks, **Thiol-ene networks** are superior because they can be formed rapidly and quantitatively under ambient atmospheric conditions, producing almost ideal, uniform polymer networks which are not afflicted with the heterogeneity typical of conventional radical-based photopolymerization processes [12].

Coatings, contact lenses, dental materials, and photolithographic procedures are just few of the many examples of where conventional (classic) radical-based photopolymerization involving methacrylates and acrylates; also, this polymerization allows for both temporal and spatial control via a chain-growth mechanism. In detail, biomaterials, nanotechnology, ultra-low stress networks, surface functionalization and selective functionalization of pre-prepared linear polymers are some of the fields that might benefit from the expanding of these technologies; however, oxygen inhibition, complex volume relaxation and stress development, complicated polymerization kinetics, the creation of extremely heterogeneous polymer/network systems are only a few of the critical issues that plague conventional (classic) photopolymerization reactions. On the other hand, photoinitiated Thiol-ene radical reactions are a potent approach for chemical synthesis and tunable materials production since they combine the advantageous of a light-mediated process with benefits of click reactions which can be initiated at particular times and locations. By combining chain-growth and step-growth mechanisms in a controllable manner, the Thiol-ene photopolymerization process is able to generate a homogenous polymer network architecture with much simplified polymerization kinetics, i.e., decreased stress and shrinkage, and oxygen inhibition, all of which address each of major drawbacks of classic photopolymerization reactions. Because of its unique advantageous, the thiol-ene photopolymerization process has recently been the comprehensive theoretical study and practical use in a variety of novel applications [12].

UV-initiated full seqIPN formation (by TEC and FRP) and semiIPN formation with linear polymer chains are shown in Figure 1.4. (In all cases, the components of the secondary network are diffused into the primary network.) [10].

In contrast to typical polymer blends, forced miscibility results from the entangled two crosslinked polymers, and the final materials shows impressive dimensional stability. Associations between polymers often results in higher resistance to degradation, improved mechanical properties, and a potentially synergetic combination of their component features. Although there are a variety of synthetic techniques for preparing IPNs, the in-situ method has been shown to be the most practical in the literature. Since the starting reaction medium contains all of the reactants, network formation might occur either simultaneously or more or less sequentially, based on the experimental conditions [10].

In literature, there are a few examples about PIB based interpenetrating networks. Vancaeyzeele et al. simultaneously combined a PIB network with a polystyrene (PS) one into an IPN architecture to enhance the mechanical properties of PIB mechanical properties. In their study, a PIB network was created by the alcohol addition between -OH end groups of HO-PIB-OH (a telechelic dihydroxypolyisobutylene) and pluri-isocyanate; and free-radical copolymerization was preferred to synthesis PS network from styrene monomer and divinylbenzene. The formation of IPN architecture occurred in situ process in which all components initially mixed and followed by the simultaneous network formation [3].

However, they reported that the highest interpenetration degree between PIB and PS phases was obtained by preparing PIB network first. As a result of this research, they reported that the inclusion of a PS network in IPN architectures significantly improved the mechanical properties of PIB, and the corresponding IPNs showed two mechanical relaxations that match to those PIB and PS enriched phases [3]. Also, a year later, the same research group worked on IPNs which was prepared by using simultaneous IPN strategy to combine poly(cyclohexyl methactylate) -PCHMA- and polyisobutylene -PIB- networks. Like in their previous study, they proved that the integration of PCHMA enhanced the mechanical properties of PIB networks in such IPN morphology [13].

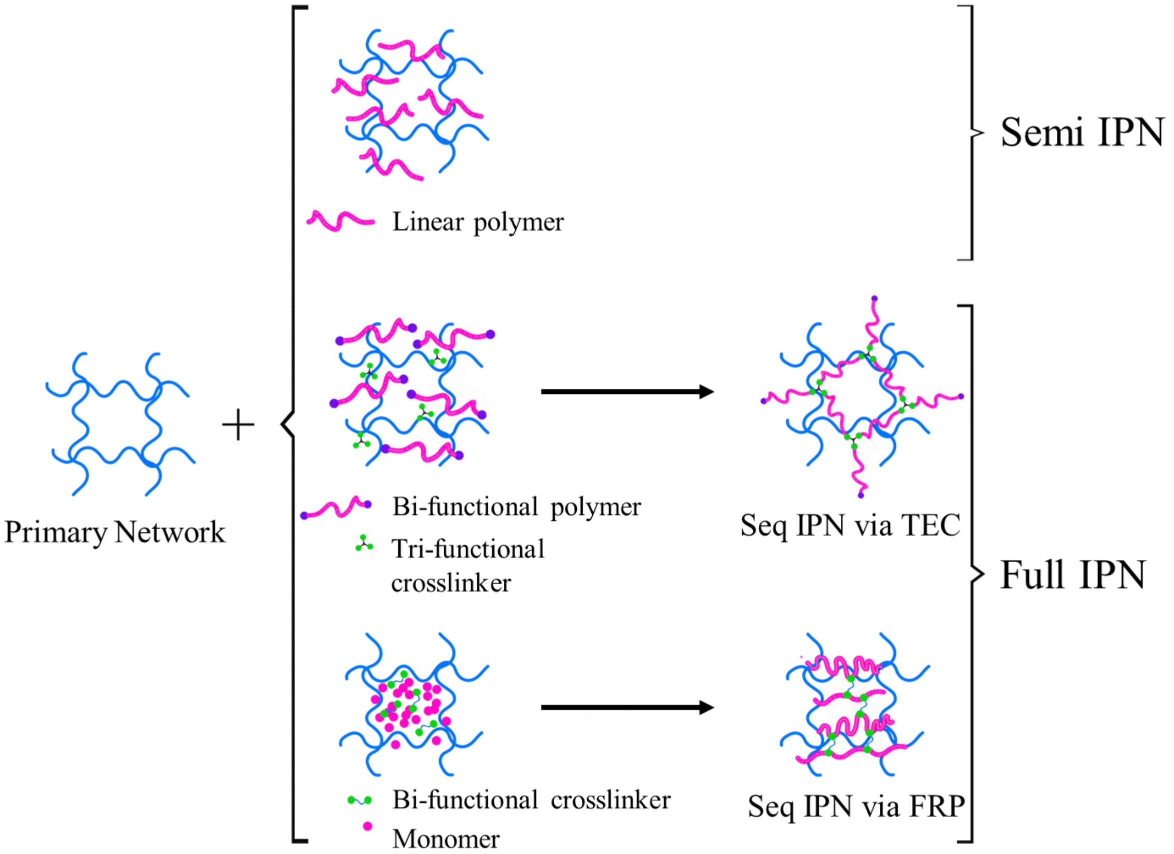

Figure 1.4: Full-IPN and Semi-IPN formation via sequential diffusion process [10].

In 2019, Kennedy’s and Nugay’s research groups published an article including the synthesis of PIB based primary networks from low molecular weight PIB chains via Thiol-ene (click) chemistry. In this study, to create PIB primary network HS-PIB-SH prepared via Dean-Stark apparatus and crosslinked with a trace amount triallyl compound (used as a crosslinker); and it was proven that Thiol-ene (click) chemistry yields new thiolated-PIB derivatives and this method is practical to obtain tight PIB primary networks from low molecular weight PIB precursors [14]. This successful strategy is the first important outcome this thesis study.

1.2.3. Polyurethane Formation

Polyurethane formation is one of the effective and intensively applied method in academia and industry. The term “polyurethane” refers to a diverse range of structures that may include urethane or carbamate groups; however, may consist of urea, carbamic acid ester groups. To make matters even confusing, these structures may also be copolymer of one another. As, in the most basic scenario, PUs are made up of two main structural components (or named as segments, phases); soft and hard segments, they are generally considered to be segmented polyurethanes. Typically, PUs are produced in two steps; (1) a macro diol (HO-macro-OH) is reacted with a stoichiometric excess of a small diisocyanate (OCN-R-NCO), which produces a prepolymer that is basically considered as a large diisocyanate, (2) a small diol (HO-small-OH), used as a chain extender, is added to the OCN-R-NHCO-O-macro-O-CONH-R-NCO, which is the product of (1), to create the final structure with the extended hard segment denoted by bold characters in Figure 1.5. [15].

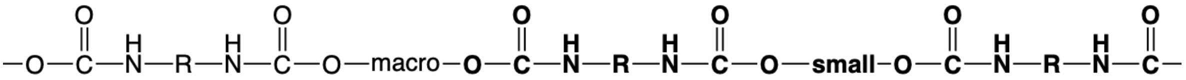

$$-O-\overset{\overset{O}{\|}}{C}-\overset{H}{N}-R-\overset{H}{N}-\overset{\overset{O}{\|}}{C}-O-\text{macro}-\mathbf{O}-\overset{\overset{\mathbf{O}}{\|}}{\mathbf{C}}-\overset{\mathbf{H}}{\mathbf{N}}-\mathbf{R}-\overset{\mathbf{H}}{\mathbf{N}}-\overset{\overset{\mathbf{O}}{\|}}{\mathbf{C}}-\mathbf{O}-\textbf{small}-\mathbf{O}-\overset{\overset{\mathbf{O}}{\|}}{\mathbf{C}}-\overset{\mathbf{H}}{\mathbf{N}}-\mathbf{R}-\overset{\mathbf{H}}{\mathbf{N}}-\overset{\overset{\mathbf{O}}{\|}}{\mathbf{C}}-$$

Figure 1.5: Structure of polyurethanes [15].

Chemical-physical-biological-processing characters of PUs are determined by the following main parameters (i) the nature (aromatic, aliphatic etc) and stoichiometry of starting materials (ii) the length (also molecular weight) the soft and hard segments (iii) the type and extend of hydrogen bonds observed between soft-hard segments and within the hard segments (iv) the phase separation degree between soft-hard segments (v) the compatibility between different segments (vi) thermal history of materials made of PUs. Further, the cooperation and interaction of each of them determines the final properties [15].

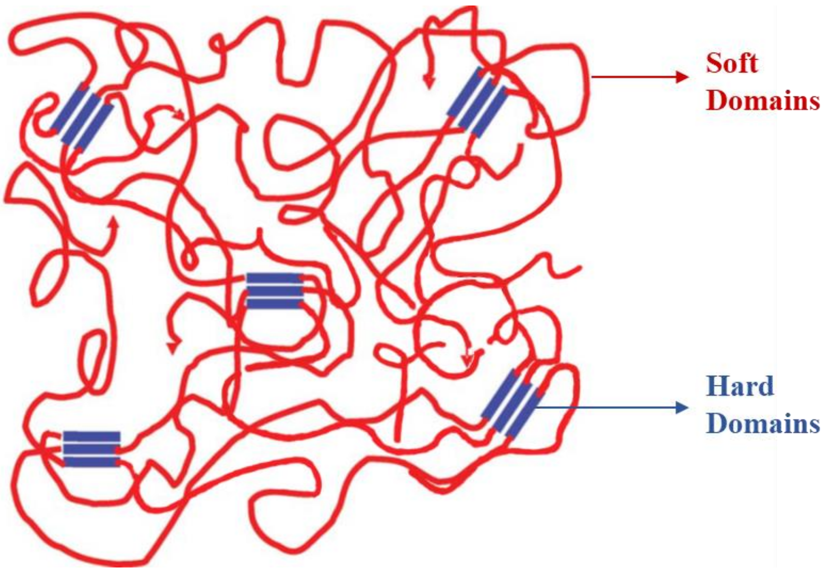

Figure 1.6: Idealized structure of polyurethane which has two-phase morphology.

The two-phase morphology of polyurethane thermoplastic elastomers is characterized by discrete domains of the hard segments which are scattered within the matrix of soft segments. (Figure 1.6)

Despite their superior mechanical and processing properties, conventional and commercially available PUs with soft segments made of polycarbonate, polyether, polydimethylsiloxane or a combination of them are vulnerable to oxidative, hydrolytic and biologic attacks and degrade rapidly when exposed to such chemical for extended periods of time [16].

The synthesis of HO-PIB-OH marked the beginning of extensive study on polyisobutylene based PUs. Incorporating HO-PIB-OH as the soft segment in place of conventionally used polyether and polyester soft phases would provide PUs that are biologically, hydrotically and oxidatively stable, according to the hypothesis that drove HO-PIB-OH research. Kang's et al. reported that the PIB soft segments, which is key component of butyl rubber and one of the best-known barrier rubbers, would make a significant difference in the barrier properties against moisture, hot air and gases. It was also deemed to be interesting to investigate how increasing the phase difference between the nonpolar PIB and polar urethane affected the final properties of polyurethanes [15].

In 1980, the first PIB based PUs were produced by combining well-defined HO-PIB-OH with common and traditional components (which are diisocyanates and chain extenders) utilized in polyurethane synthesis. As predicted, the characterized PIB based PUs exhibited improved hydrolytic, oxidative, thermal and barrier characteristics compared to conventional PUs while displaying moderate to poor mechanical properties. Even though the original researchers – one of whom is Joseph P. Keneddy, attempted to determine the cause(s) of the poor mechanical properties, they did not take into account the negative impacts induced by the absence of H-bonds and the significant phase separation between hard and soft domains [15].

After a few years, Ver Strate and colleagues attempted to create PUs from HO-PIB-OH derived by ozonolysis of butyl rubber (which is a copolymer of IB and only few amounts of isoprene); nonetheless, the mechanical properties of this product were likewise unsatisfactory. It was accurately identified that the presence of both primary and tertiary -OHs inside their diol parts ($HO-CH_2-PIB-CH_2-C(CH_3)_2-OH$) is one of the potential issues [15].

The finding of living IB polymerization marked the beginning of the second stage in this adventure. It is the first time that it has been possible to create well-defined PIBs with almost any molecular weight and narrow molecular weight distribution. Also, the most crucial point of this feature, linear -or three arm- telechelic polymer chains, containing $-NH_2$ and -OH termini, has been prepared [15].

At the beginning of 2000s, Yılgör's research group proposed that it is possible to create gradient interfaces between polar urea and nonpolar polyisobutylene phases by adding a compatibilizing agent such as PTMO - which is abbreviated as poly(tetramethylene oxide – in the appropriate proportions. Also, this can enhance the stress transfer from the soft PIB to reinforcing hard phases. The closeness of solubility parameter for PIB and PTMO suggested that HO-PTMO-OH might be used as a compatibilizing agent between both phases. A few years later, Yılgör's and Kennedy's research group worked together to demonstrate the beneficial effect of HO-PTMO-OH on the mechanical characteristics of polyisobutylene based PUs. They improved that the elongation and tensile strength of PUs were dramatically improved by the addition of 20% PTMO in soft segments. Compared to conventional PUs, these hybrid PIB/PTMO based PUs are softer and have better elastomeric properties [15, 17].

In 2008, Kennedy’s and Yılgör’s groups initiated the systematic research with the polyisobutylene based polyureas produced with H_2N-PIB-NH_2 chains for a soft domain. It was discovered that PIB based PUs have better mechanical properties when the hard domains consist of aliphatic diisocyanates, such as HMDI - aliphatic hexamethylene diisocyanate, with a longer chain extender, such as BDO - 1,4 Butanediol, than the conventional PTMO based PUs, which are the strongest polyurethanes when the hard domain includes an aromatic diisocyanate, such as MDI - diphenylmethanediisocyanate, with short chain extender (such as HDA - hexanediamine and HDO - hexanediol). The differences are largely due to the fact that the former combination (with a longer chain extender) creates more diffused and so less pronounced interphases between the hard phases and soft PIB phases. Predictably, as the percentage of hard domains in a material increases, its tensile strength increases but its elongation decreases. It’s interesting to note that the correlation is linear for both polyureas and may be extended to the origin. The proportionality of this result shows that the hard domains are uniformly distributed throughout the soft PIB phase that only the hard segments, not the soft segments, are responsible for tensile strength. Therefore, this mechanical behavior is not significantly influenced by the type and nature of chain extender [15].

Kennedy’s research group proved that 60-70% soft PIB phases yields almost full protection against hydrolytic and oxidative degradation of PUs, nonetheless, the mechanical strength is lower than anticipated for this category of materials. Then, same groups achieved that using hydrogen bond acceptor chain extenders – which is abbreviated as HACE – a novel idea in the synthesis of polyurethanes. (Figure 1.7) It was hypothesized that the unsatisfactory mechanical properties of 60-70% PIB based polyurethanes were the result of significant phase separation between polar urethane and nonpolar PIB phases which might be remedied by combining conventional chain extenders (CEs) with HACEs. HACEs served to lengthen hard segments, increase the amount of hydrogen bondings inside the hard phases and make the hard segments more flexible. They predicted that aliphatic saturated low molecular weight (between 150 and 650 g/mol) chain extenders with several hydrogen bonding, such as -N-, -O- and -OCOO-, accepting sites may accomplish these objectives. It was believed that low molecular weight was needed for molecular mobility under applied stress – for toughening and reinforcement. They experimentally proved that the optimal amount of HACEs for improving the mechanical strength of 70% PIB based PUs is between 5 and 7% [15, 18].

In the same time period, Kennedy's and Nugay's research groups reported an effective method for sulfur containing and -OH terminated PIB chains. Under moderate photochemical conditions, they reacted allyl terminated polyisobutylene (CH_2=CH-CH_2-PIB-CH_2-CH=CH_2) with cheap HO-CH_2CH_2-SH to synthesize HO-CH_2CH_2-S-PIB-S-CH_2CH_2-OH through Thiol-ene (click) chemistry and then to use this PIB-diol for the preparation of new PUs., which is another important outcome of this thesis study [16].

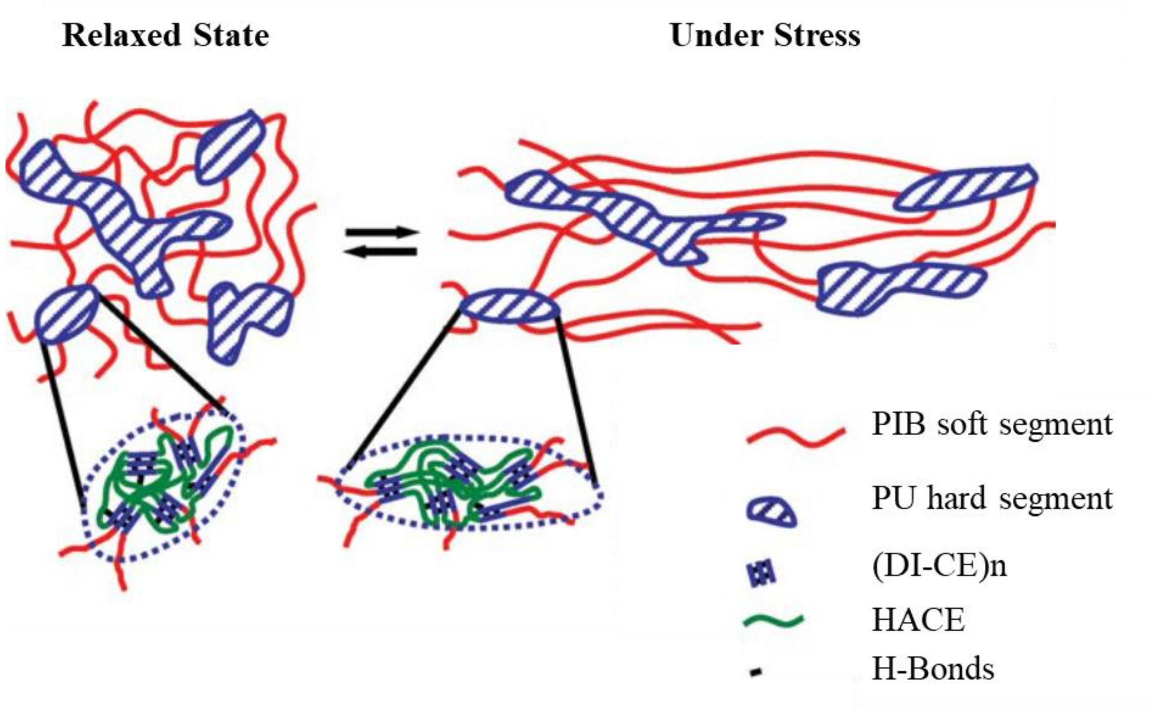

Figure 1.7: Idealized micromorphology of PIB-based HACE-reinforced PUs in the relaxed state and under stress. Reprinted from [15].

1.2.4. Nanocomposite Formation

In order to create new materials, nanotechnology is used as a useful tool in many scientific disciplines. On the other side, modifying materials at the nanoscale offers the chance to develop and produce new materials with improved properties and unheard-of performance. In composite systems, there are typically three basic matrix types; polymer, metal, and ceramic with different additives in different forms (i.e., fibers, fillers, particles); and nanocomposites are characterized by at least one nanoscale component. Nanofillers are used as reinforcing filler component in polymeric nanocomposites (which is abbreviated as PNCs) in different structures depending on the nanoscale dispersion (Figure 1.8) and are characterized according to their physical structure, chemical content/origin and particle morphologies. Also, these particles are represented by their morphologies and nano-dimension as one-dimensional linear particle (like carbon nanotubes), two-dimensional layered particle (like montmorillonite -MMT-) and three-dimensional powder particles (like silver nanoparticle) [19].

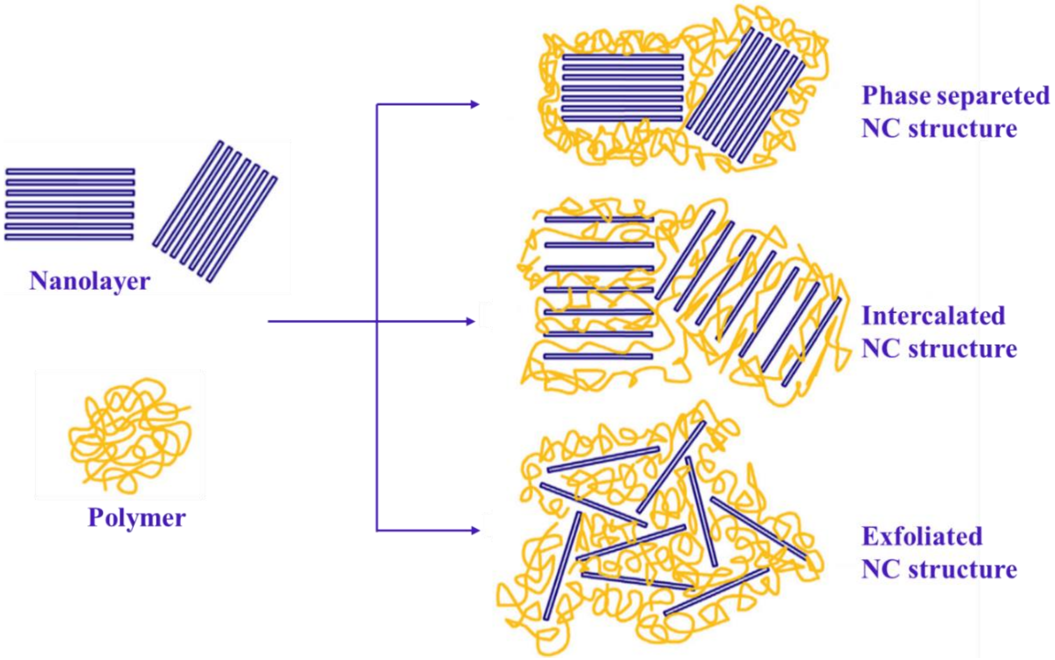

Figure 1.8: Possible types of polymer/nanolayer nanocomposite structures. Reprinted from [20].

In the end of 1985, Toyota Central Research Laboratory presented the “nanocomposite term for the first time, when they were successfully using nanocomposites made from clay-based montmorillonite (MMT) Nylon to make an automobile belt cover. After that, the area of polymer nanocomposites has been the subject of substantial research studies across the world. This is due to the fact that even at very low loadings, nanofillers may significantly improve the characteristics of polymer matrix through reinforcement because of high surface area [20].

Polyisobutylene rubbers can be strengthened by the addition of nanolayer. In 2016, Nugay et al. reported and discussed in detail that a trace amount (0.5 wt %) addition of organically modified montmorillonite (OmMMT) nanolayers to PUs, made with polyisobutylene diol soft segment and conventional hard segments of butane diol and diisocyanate, significantly improves the mechanical properties of materials. Layers of OmMMT act as a co-chain extender/reinforcing agents since the negatively charged MMT layers are electrostatically linked to the positively charged quaternary amine group, which defoliates it, and also the free -NH_2 groups of the OmMMT can react with isocyanates [21].

As stated above, PIB based polyurethanes were certainly exceptional; but their mechanical properties were moderate to poor because of the absence of H-bondings between the soft PIB and hard urethane segments and significant in incompatibility between them. Despite the fact that a considerable amount of work has been done to advance the development of PIB-based PUs, the mechanical strength and thermal stability of them, particularly the nanofilled PIB-based PU composite structures, should be further mentioned. Carbon nanotubes (which is abbreviated CNTs) are well-known to be appropriate reinforcing agents for high-performing polymeric composites due to their exceptional structural, chemical, mechanical stability and thermal characteristics. Li et al. reported that the thermal characteristics of multi-walled carbon nanotubes (MWCNTs)/PIB based PU nanocomposites were significantly improved at relatively low MWCNTs concentrations, also the tensile data of their study indicated that strong H-bondings allowed the external tensile loads to be transferred to MWCNTs over the PU-MWCNTs interfaces. It should be underlined that this H-bonding strategy has the potential to have wide-reaching benefits for the development of various PIB-based PU nanocomposites with enhanced performances [22].

The hydrolytically and oxidatively resistant new PIB-based PU (which were characterized in this study) were prepared by the use of $HO-CH_2CH_2-S-PIB-S-CH_2CH_2-OH$ soft segments, conventional hard segments (including urethane repeating units) of BDO and MDI, and OmMMT nanolayer. It is proposed that OmMMT nanolayers, when added in trace amounts, form covalent bonds with polyurethane chains and further enhanced the properties of final material by acting as reinforcing filler and co-chain extender. This is the additional important outcome of this thesis study [16, 21].

1.3. Polymers in Biomedical Applications

Over the decades, biomedical research has moved in a new path in which polymeric biomaterials have taken a place, and due to their biocompatibility and nontoxicity, polymeric materials are the subject of significant amount of research and developments in health care areas. Biomaterial development began with ceramics and metals and has progressed to the present day with the period of smart biocompatible natural and synthetic polymeric materials [23].

Any type of material intended for use of in biomedical applications must adhere to certain standards, and biocompatibility is the most important criterion among these others. The “biocompatibility” term refers to a substance that is physiologically/biologically acceptable and may be used to interact with human body to treat, asses, modify, or replace any organ or tissue without causing damage the body. Also, in the international dictionary of medicine and biology, it is described as the ability of prosthesis implanted in the body to remain in congruence with tissues without generating adverse modifications. Based on International Organization for Standardization (globally abbreviated as ISO) and Food and Drug Administration (globally abbreviated as FDA) regulations, any material intended for use in the pharmaceutical and/or medical fields must pass various in-vivo and in-vitro analyses, including hemocompatibility, cytotoxicity, genotoxicity, immunogenicity, mutagenicity etc. [23].

Due to their biocompatibility and different advantages, ceramic, metals, composites, and polymeric materials are called biomaterials, and owing to their wide-reaching benefits, biocompatible polymers have been widely studied in the medical area. By varying the monomer content during copolymerization or homopolymerization, the required chemical and physical characteristics of biocompatible polymers may be constructed with relative ease [23].

Materials that are biocompatible should not cause immunological responses and/or generate by products that are difficult to discard or may be metabolized by the body. Surface features such as surface energy, roughness, electrostatic effects, wettability, chemical functionalities, and protein adsorption of polymeric biomaterials will determine how cells respond to them since cells are extremely sensitive to their biologic environment. Despite their degradability and compatibility, certain synthetic polymeric materials lack these surface characteristics, so some surface modifications are required to make them compatible with biological systems for many biomedical applications. In Figure 1.9. some important biomedical application areas are shown [23].

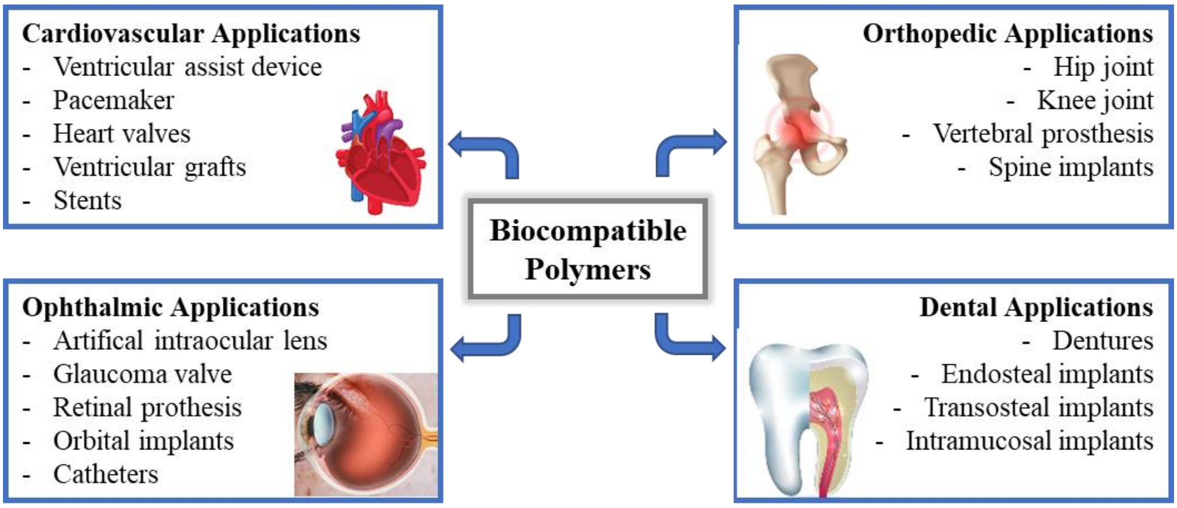

Figure 1.9: Examples of biomedical application areas where polymeric materials can be used. Reprinted from [23].

The chemical composition of polymeric materials governs important features such as degradability, crystallinity, solubility, hydrolytic and enzymatic stability. Such polymers as polyesters, polyurethanes, polycarbonates etc. are susceptible to hydrolytic breakdown. Widely utilized for cardio-vascular applications include synthetic polymers such as modified polyurethanes, polyvinylalcohol (PVA) and polytetrafluoroethylene (PTFE). To prevent immunological reactions, polymeric substrates are frequently coated with proteins like albumin.

PTFEs are frequently utilized in the production of heart valve rings, vascular grafts and sutures for mitral valve treatment. In addition, PUs are used in heart valve applications because of their promising properties such as hemocompatibility, flexibility, low thrombogenicity and biphasic nature. Also, polycarbonate urethane, one type of modified polyurethanes, has enhanced strength and oxidation resistivity as well as a low degradation degree, and polydimethylsiloxane-based PUs has also been applied to heart valves in order to increase hydrophobicity and calcification resistance [23].

1.3.1. Fundamentals In-vitro Biocompatibility Studies

1.3.1.1. Calcification

A series of segmented block copolymers known as polyurethanes (PUs) comprises alternating polyethers or polycarbonates, often referred to as the soft segments, and ureas or urethanes, frequently known as the hard segments. The chemical composition and molar ratio of its hard and soft segments can be easily modified for adapting to various conditions, and this alteration generates a broad range of physical properties for polyurethanes. These composite materials, having an elastomeric character, is attractively used for cardiovascular implantations, such as heart valves and artificial heart devices [24].

The longevity of mechanical heart valves and the biocompatibility of bioprosthetic heart valves may theoretically be combined in the polyurethane heart valves; however, ectopic calcification, defined as an improper biomineralization happening in soft tissues, of the polyurethane artificial heart valve surfaces significantly reduces the functionality of them in both in vivo and in vitro studies. Unfortunately, many examples in literatures have been hypothesized that calcification mechanism on polyurethane blood-contacting medical implants has a complex pathway and not been understood completely. Imachi et al. reported that surface deposition of thrombi and the cellular derbis has been proposed as the cause of the calcification on polymeric artificial heart valves [24, 25]. In addition, about the calcium deposition on artificial heart receiving a repeated stretching force Imachi et al. hypothesized that repeating stretching forces on implanted valves results the extension of polymer membrane; unfortunately, it causes some slackening between the polymer molecules and creating gaps in microscale. Due to blood-contacting, these microgaps are occupied with phospholipids and blood-proteins and then these structures attract positively charged calcium ion (Ca^{+2}) followed by negatively charged phosphate ion (PO_4^{-2}); and so calcium phosphate complexes (CaP) forms and localizes on the flexed region, tearing and cracking of the polyurethane heart valves [25].

Due to calcium deposition on implants impairing the functionality of artificial heart-valves (Figure 1.10), developments in PU artificial valve studies mainly have concentrated on alternative valve designing.

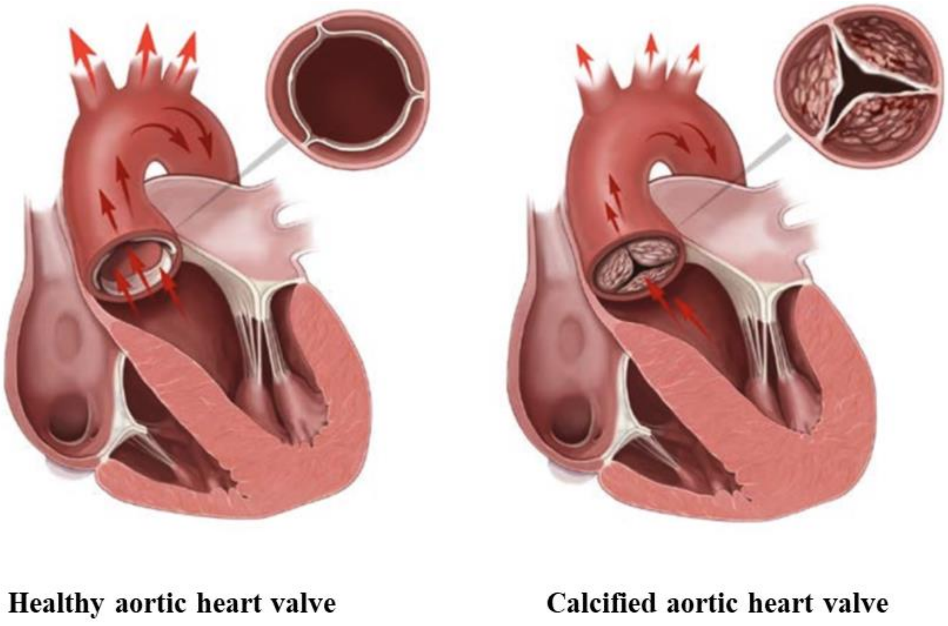

Figure 1.10: Schematic view of healthy and calcified aortic heart valve. Reprinted from [26].

Although these methods have not been successful probably because of the complex mechanism involving heart valve calcification in biological systems, altering the composite PUs to prevent polyurethane heart valve calcification has been the subject of few studies, i.e. blocking the reactive sites in PU structures. Also, Imachi et al. had focused on thickening of heart valve membrane and covering a membrane surface with an ion such as gold or carbon; and these strategies may postpone the creep fatigue and so it can hinder the occupation of phospholipids and blood proteins into microgaps on polyurethane membrane [25].

1.3.1.2. Protein Adsorption

Proteins, the most abundant and adaptable macromolecules in living systems, have a critical role in nearly all biological processes. With its wide variety of ligands, such as drugs, surfactants, fatty acids and different metal ions, proteins act as multifaceted macromolecules. Also, proteins readily demonstrate that they are interfacially active molecules by spontaneously accumulating at surfaces/interfaces. Some proteins have a tendency to adsorb substrates because of the nature of side chains that are found on their surfaces [27].

Proteins are amphoteric polyelectrolytes due to different characteristics of their amino acids. While some nonpolar amino acids are often preferred to be buried inside the protein structure, some polar and charged amino acids are generally located on the exterior of protein. Due to the long-ranged and strong electrostatic attraction between a charged adsorbent and oppositely charged side chains founded on amino acids, a substantial free energy change will occur, in favor of adsorption process. The stability of protein structure is related with different interaction concepts and their combinations, such as (i) hydrogen-bondings along polypeptide chains and between adjacent side chains, (ii) hydrophobic interaction between hydrophobic side chains, (iii) Van der Waals interactions and (iv) the Coulomb interactions between charged residual. In order to compete the same interactions and minimize the total free energy of a system, an adsorbent surface may cause protein denaturation by unfolding the protein structure during the adsorption process. Protein secondary structural components (α helix and β sheet) and super-secondary structures, or motifs, combine to generate a compact globular protein. If proteins are composed of multiple (more than one) domains, one domain may dominate the interfacial adsorption characteristic of whole multidomain-macromolecule structure [28].

Rather than surface properties, polymeric biomaterials utilized in medical devices are selected primarily on the basis of their bulk mechanical properties; however, the protein resistance of polymeric materials is generally related with hydrophilicity of their surface. For example, most hemodialysis catheters are made from polyurethanes and silicones since they provide an ideal and required balance of strength and flexibility; however, these and other widely used polymeric materials are unfortunately extremely vulnerable to nonspecific protein adsorption.

Surfaces that do not adsorb proteins surfaces that we refer to as “nonadsorbing” or “inert” for brevity - are part of the much broader field of biocompatible materials. Not protein adsorbing surfaces, shortly named as “inert” and “nonadsorbing” surfaces, belong to the considerably larger subject of biocompatible materials; commonly such as biosensors, prostheses, contact lens materials, artificial heart valves, implant materials, cosmetics, materials in food industry [71] and also newly drug delivery system, tissue engineering, patterned cell culture and analytical system materials. For the resistive character of these inert biomaterial surfaces, Ostuni et al. reported four molecular level characteristics for surfaces: (1) hydrophilic character (2) hydrogen bond acceptor content (3) a neutral electrical charge in total (4) not containing hydrogen bond donors [29]. Nevertheless, not all surfaces are not resistive for protein adsorption. For example, ionic surfactants, having a charged head group that attracts an oppositely charged amino acid residue of protein and alkyl chain that attracts non-polar parts on the surfaces as well as within this protein, are known to have a great affinity for associating with proteins in aqueous solutions [27].

During the implantation of blood-contacting medical devices, adsorption of plasma proteins promotes the thrombosis cascade and bacterial infection, eventually resulting im diminished in safety and efficacy of these devices. Likewise, protein adsorption causes biofouling and reduces the durability and sensitivity of implanted devices. [30] Despite the extensive literature on protein resistant devices and methods, thrombosis (thrombogenicity) and so inflammatory response are still serious issues for biomedical devices. Thrombosis, known as a coagulation cascade, actually is a healthy response of damaged tissues but a major cause of failure in synthetic biomaterials (i.e., polymeric vascular grafts). In detail, it follows a complex biological pathway in which firstly plasma protein adsorption occurs onto the implantation or foreign surfaces, then the adsorbed protein initiates platelet adhesion and consequently thrombus formation is observed. Therefore, as the initial stage in thrombus formation, protein adsorption has been an important area of research to better understand why and how it happens, and subsequently, how to design thromboresistant surfaces (Figure 1.11) [31].

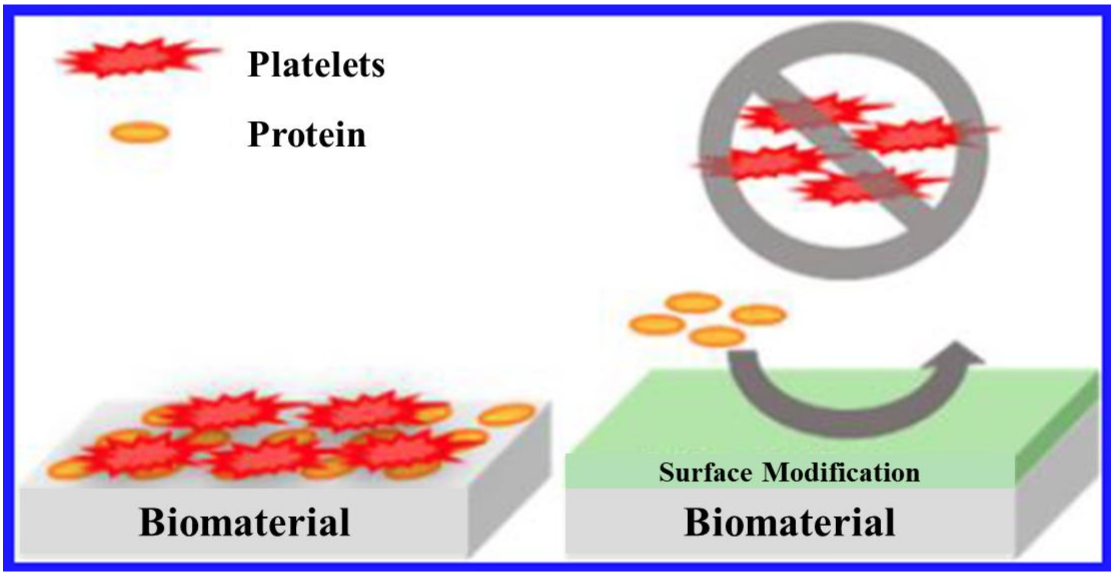

Figure 1.11: Schematic view of protein resistant polymeric biometarials with surface modification. Reprinted from [30].

1.3.1.3. Cell Attachments and Viability

Cell adhesion to surfaces is a key regulatory factor in a wide variety of biological mechanisms, including but not limited to activation, proliferation, migration, differentiation and or even simple survival. By modulating the degree of attachment to nearby tissues and inflammatory responses, these adhesive interactions between biomaterials and cells might determine the ultimate applicability of implanted medical devices/prostheses. Although it is now well accepted that specialized interactions between cell surface receptors and their ligands regulate the biological adhesion and responses, the impact of non-specific forces must also be taken in consideration. Currently, alteration in cell adhesion have been observed in a variety of disorders, including cancer, arthritis, atherosclerosis and osteoporosis. For example, cell adhesiveness is often decreased in human malignancies, allowing cancer cells to migrate, and losing their historical structure, which is the morphological characteristic of malignant tumor cells [32].

A series of physicochemical reactions take place between the material and cells interface when cells attach to the material surface. Protein adsorption to the surface of biomaterial occurs immediately after implantation into a living organism; this mediates the cell attachment and signals to the cell via cell adhesion receptors. Cell adhesion on the surfaces and releasing the active compounds can mediate the deposition of the ECM, cell proliferation and differentiation [32].

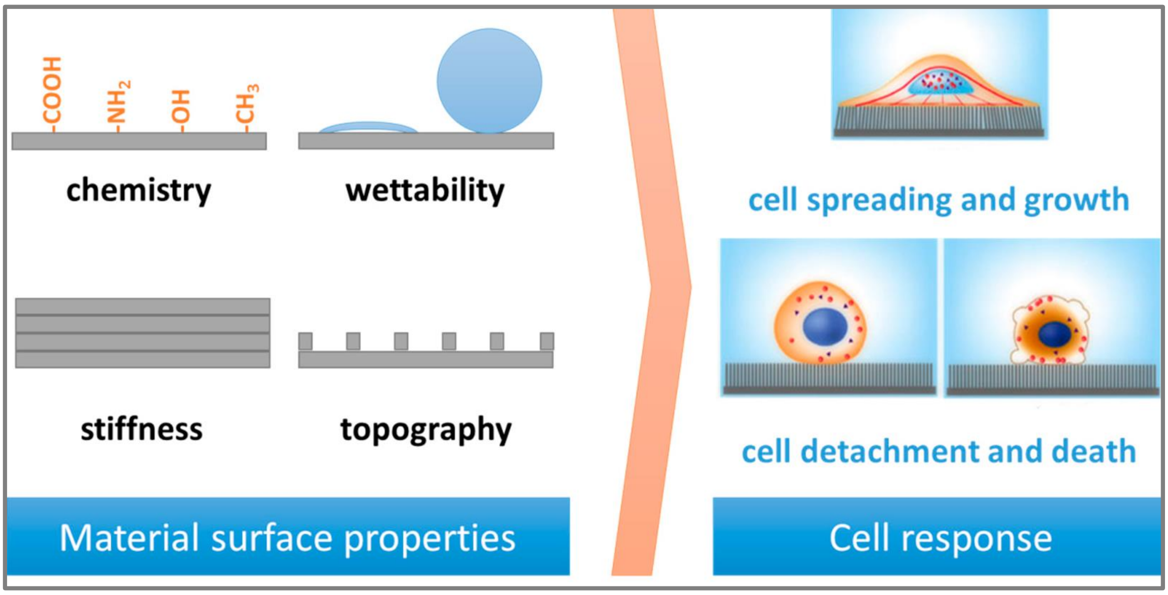

Figure 1.12: Schematic representation of the main surface properties and their direct effect on cell behavior. Reprinted from [32].

The development of various artificial biomaterials, applications and devices has taken into consideration the interfacial interactions between surfaces and cells/tissues, which show an strong correlation with many critical phenomena in living systems. The fabrication of implants and scaffolds for regenerative medicine and tissue engineering requires biomimetic materials that promote a favorable response from cells/tissues. However, bioinert polymers are necessary for most biomedical devices because of their interaction with blood and/or tissues, which can induce thrombosis and immunological responses if they are not inhibited. To be considered biocompatible, a material should be able to provide the necessary conditions and appropriate support for cellular activity including stimulation of molecular and mechanical mechanisms that would improve tissue regeneration, without inducing any adverse responses in the ultimate host, either locally or systemically. Therefore, the in-vitro biocompatibility of a biomaterial is primarily governed by its surface properties, including surface roughness, stiffness, surface charge, chemical functionalities, wettability, as well as cell interaction with the degradation products of scaffold [32]. The main and important surface properties that may affect cell behavior in terms of adhesion, proliferation, metabolism, morphology among others is summarized in Figure 1.12.

The adhesion and growth of cells on substrate can be regulated by surfaces with specific properties. A variety of methods have been preferred to physically modify the surface morphology, energy, and roughness, as well as introduce chemical groups that address the hydrophilicity or hydrophobicity behavior of surfaces [32].

1.3.1.4. Bacterial Resistance

Each year, 5% of hospitalized patients in the United States are affected by healthcare associated infections, which cost the healthcare system up to $4.5 billion yearly and result in almost 100.000 infection related deaths. Most of these infections are linked to the use of implantable medical devices, including medical heart valves, intravascular catheters, orthopedic implants, and urinary catheters. Polyurethanes are the most often utilized materials to produce vascular catheters due to their extensive range of mechanical properties, fatigue resistance and reasonably good hemocompatibility. They are also frequently used to manufacture various medical devices such as artificial organs, wound dressings, and drug-delivery devices. However, compared to other-to-other polymers, polyurethanes tend to perform only relatively well in bacterial adhesion investigations, making them more vulnerable to bacterial colonization and increasing the risk of infection [33].

The most active research is being done on antibacterial polyurethanes (also named as antibiotic polyurethanes) to improve their resistance to infection. In addition to preventing damage from microorganism induced erosion, antibacterial polyurethanes may prevent the growth and spread of pathogenic-bacteria in polyurethane materials; so it can be reduced diseases and these research into antibacterial polyurethanes has great importance. Research shows that the primary reason for material infection is the adhesion and growth of bacteria on the substrate surfaces, which results in the formation of a bacterial biofilm comprised of an ECM. Examples in literature shows that antibacterial polyurethanes can prevent the growth of bacterial biofilms by inclusion of disinfecting groups/elements such as quaternary ammonium salt, sulfur and silver. [34] Furthermore, it is possible to chemically modify the physicochemical properties of polymer surfaces to control the bacterial adhesion. In order to enhance the physicochemical properties and biocompatibility, many biomaterials incorporate additives, including organic polymers and stabilizers; however, microorganisms may metabolize these additives and use them to support biofilm formation, the content and features of the polymer surface greatly affect bacterial adhesion and growth [35].

Although PUs are comprehensively preferred for foams, coatings, fibers, elastomer and adhesives, and widely used in various biomedical applications (blood and tissue contacting devices); especially cardiologicals including heart valves, vascular protheses, cardiac assist devices, blood filters, catheters and artificial heart chambers due to their excellent mechanical and physical properties, stability in long-term implantation, physiologic acceptableness and comparatively high tolerable characteristic for blood-contacting [36]. Some commercial and medical grade PU examples are all listed in Table 1.1.

On the other hand, Kayırhan et al. worked on the polyurethane membranes prepared from diisocyanate and poly(propylene ethylene glycol), and focused on the increasing their surface hydrophilicity and enhancing hemocompatibility by oxygen and argon treatment. They reported that the applied surface treatment decreased the contact angle of surfaces and prevented the polyurethane membranes from oxidation and fibrinogen adsorption, which is well-known that fibrinogen adsorption contributes to surface induced thrombosis. As they stated, for further biomedical applications, the hemocompatibility of PUs should be enhanced to extent their implant periods and stability in human body [36].

Table 1.1: Some commercially available and medical grade PUs on the global market [37].

Trade name	Type	Manufacturers
Texin®	Polyether (Natural clear)	Bayer MaterialScience
Desmopan® DP 2590A	Polyester (Natural clear)	Bayer MaterialScience
Desmopan® DP 9370A	Polyether (Natural clear)	Bayer MaterialScience
Texin® 4210	TPU/PC blend (Opaque white)	Bayer MaterialScience
Tecofl ex®	Polyether	Lubrizol
Carbothane®	Polycarbonate	Lubrizol
Pellethane ®	Polyether	Lubrizol
Elastollan ® SP 806	Polyether	BASF
ChronoFlex ®	Polycarbonate	AdvanSource Biomaterials
Elast-Eon ®	Polydimethylsiloxane	AorTech

In the early 90s, Dr. Leonard Pinchuk discovered that conventional polyether-urethanes implantable biomaterials, such as those used in pacemaker lead insulators and the artificial vascular grafts being created by his team at Corvita Corporation, and it led the development of a new biomaterial. SIBS, poly(styrene-b-isobutylene-b-styrene), is the well-known drug eluting coating, which was developed by Boston Scientific Co. in coronary stents. Also, it has been implanted in over 6 million cardiac patients across the world, thanks to the living polymerization technique for PIB. As reported in the literature, PIB is an excellent biomaterial, whose blood and tissue compatibility are superior to those of silicone rubbers, and probably the greatest synthetic biomaterial currently known, but with superior mechanical properties. This discovery was the most significant result of SIBS development [15]. More in detail, SIBS was initially implemented in the medical field for the TAXUS® stent made by Boston Scientific Co. TAXUS®, which is a small balloon-expandable metallic stent with a permanent SIBS coating that gradually deliver paclitaxel medication into the coronary artery wall to ward against restenosis, is the biggest product launch in the history of medical devices. Also, studies on TAXUS® showed negligible biodegradation and limited tissue response, according to the data obtained, and this product gave them enough success and profit for establishment of InnFocus in 2004. InnFocus focused also to create SIBS-based solutions for usage in the ophthalmologic applications, and the first product developed was a glaucoma shunt [38]; meanwhile, they are currently studying on this area with thermally crosslinkable PIB to solve the intraocular lense problems [39].

According to the recently published study by the Nugay’s and Keneddy’s research groups, the key parameters for a calcification resistant and bioinert PIB based PUs, which were prepared for the first time in the literature and under optimized synthesis conditions, (i) using a precise stoichiometry of the PU formation process, in particular the utilization of highly purified MDI (ii) the solid content in the synthesis medium was raised until the point at which the increased viscosity rendered stirring impossible. With their results, they proved that this PIB based PU is a potential for a fully synthetic bioprosthetic heart valve because the preliminary investigations demonstrate that this material has an outstanding fatigue life [40].

Therefore, the overarching two main objectives of this thesis are (i) to design novel and original methods to increase the strength of polyisobutylene structures by interpenetrating network (IPN) and polyurethane (PU) formation, particularly for the latter one, via addition of extra hydrogen-bonding sites in PIB soft phase (with sulfur addition in chain) and organophilic nanolayers, which can be integrated with PU hard phase, and (ii) to conduct an in-vitro biocompatibility assay for these high strength PUs.

Since quite preliminary studies showed that PIB based PUs have also very impressive fatigue life, with the promising thesis results on suitability for biomedical applications it is believed that it is a very strong candidate for a fully synthetic bioprosthetic heart valve from now on.

2. EXPERIMENTAL

2.1. Materials

2.1.1. Polyisobutylene (PIB) Based Primary Network

The following chemicals were used for synthesis SH functionalized PIB chains. Toluene, p-toluene sulfonic acid (pTSA) and dried methanol (MeOH) were from Merck., and mercaptopropionic acid (MPA), anhydrous calcium chloride ($CaCl_2$) were from Sigma Aldrich. Hydroxyl telechelic polyisobutylene, HO-PIB-OH (M_n = 3000 g/mol), which is used for SH functionalized PIB chains, was prepared by collaborative laboratory members and the preparation and characterization of HO-PIB-OH have been described [16].

The following chemicals were used for preparation of PIB based primary network (PIB-SXA). Tetrahydrofuran (THF) was from Merck.; and 1,3,5-triallyl-1,3,5-triazine-2,4,6 (1H,3H,5H)-triazine (TATA) and 2,2-dimethoxy-1,2-diphenylethan-1-one (IRGACURE 651) were from Sigma Aldrich. Thiol telechelic polyisobutylene (HS-PIB-SH) of M_n = 3000 g/mol was the product of synthesis part of SH functionalization PIB chains.

2.1.2 Polyisobutylene (PIB) and Polystyrene (PS) Interpenetrating Networks

Styrene (C_8H_8), 2,2-dimethoxy-1,2-diphenylethan-1-one (IRGACURE 651) and divinylbenzene ($C_6H_4(CH=CH_2)_2$) were from Sigma Aldrich. Tetrahydrofuran (THF) was from Merck.

2.1.3 PIB Based PUs

The preparation of PIB based polyurethane structures were completed by our collaborative laboratory members in Akron University. The following materials were from Sigma-Aldrich. Methylene chloride (CH_2Cl_2) was distilled over CaH_2 under a N_2 atmosphere. Tetrahydrofuran (THF) was distilled from sodium benzophenone and after distillation, THF was stored over 3 Å molecular sieves (20 vol %) for at least 24 h before its usage. 4,4'- Methylenebis (phenyl isocyanate) (MDI) was distilled under reduced pressure and after distilllation, MDI was stored at -10^{0}C under a N_2 atmosphere. Dibutyltin dilaurate (DBTDL), tetramethylethylenediamine (TMEDA), titanium (IV) chloride ($TiCl_4$), and allyltrimethylsilane (ATMS), 2,2-dimethoxy-2-phenylacetophenone (DMPA), potassium permanganate ($KMnO_4$), glacial acetic acid (CH_3COOH), chloroform ($CHCl_3$), 2-mercaptoethanol ($HSCH_2CH_2OH$), and cobalt (II) chloride hexahydrate ($CoCl_2.6H_2O$ in reagent grade) were used as received without purification. 1,4-Butanediol (BDO) was dried under reduced pressure environment for at least 2 hours before its usage. PBS solution at pH 7.4 was prepared by dissolving the received phosphate-buffered saline powder in MilliQ water [16].

The following materials were from Fisher Scientific. Aqueous nitric acid solution (70 wt % HNO_3) was directly used for preparation of 50 wt % HNO_3 solution by diluting it with MilliQ water. Hydrogen peroxide (H_2O_2) was used as received and n-hexane were distilled over CaH_2 under a N_2 atmosphere like in methylene chloride distillation [16].

Elast-Eon® E2A (6 wt % BDO, 12 wt % PHMO, 33 wt % MDI, 49 wt % PDMS) pellets were from AorTech. ELAS pellets were solvent cast from tetrahydrafuran (THF), dried in air environment for 24 h, dried at 60^{0}C at least 24 h, and then annealed under vacuum (1 mmHg) at 100^{0}C for 16 hours, respectively. Optically transparent and slightly yellow ELAS films were obtained. Isobutylene (IB) monomer was from ExxonMobil Chemical Company and used for synthesis of HO-PIB-OH chains [16].

The synthesis procedure of 5-tertbutyl-1,3-bis(1-chloro-1-methylethyl) benzene (tBuDiCumCl) was described and it had been recrystallized from hexane under a nitrogen atmosphere before its usage [16].

The structure and preparation of OmMMT (negatively charged montmorillonite nanolayers carrying the quaternary amine, $(CH_3)_3N^+ (CH_2)_3NH_2$) were presented and discussed in our team members previous articles [21].

2.1.4 Calcification Analyses of PIB based PUs

Sodium chloride (NaCl), potassium chloride (KCl), magnesium chloride (anhydrous) ($MgCl_2$) and sodium sulfate (Na_2SO_4) were purchased from Sigma Aldrich. Sodium bicarbonate ($NaHCO_3$), di-potassium hydrogen phosphate trihydrate ($K_2HPO_4.3H_2O$), hydrochloric acid (HCl), Tris-hydroxymethyl aminomethane ($(HOCH_2)_3CNH_2$) were purchased from Merck and calcium chloride was purchased from J.T. Baker. The pH of SBF was adjusted to 7.4 with 1 M HCl solution and the SBF was filter sterilized with Stericup 0.22- µm filter purchased from Merck Millipore [41].

2.1.5 Protein Adsorption Analyses of PIB based PUs

Fibrinogen (F4129) was from Sigma Aldrich. BSA standard (Bradford Assay Kit) was from GeneMark (Lot # N00114). Sodium dodecyl sulfate, $C_{12}H_{25}NaO_4S$, (Lot # 154052) was from Fischer Scientific, and directly used for 5% w/v SDS solution with distilled water. Bradford Reagent (A 6931,0500) was from Applichem. Biosera Dulbeco’s Phosphate Buffer was used for PBS solution. Ethanol was from Merck Millipore.

2.1.6 Cell Attachment and Proliferation Analyses of PIB based PUs

Mouse connective tissue L929 cells was from ATCC. Dulbecco’s Modified Eagle’s Medium (DMEM), Foetal bovine serum (FBS), 1% penicilin/streptomycin, Tyripsin-EDTA solution (T3924) were from Sigma Aldrich.

The following materials were used for fixing the attached cells on polymer film surfaces. Glutaraldehyde solution was from Sigma Aldrich and ethanol was from Merck Millipore. Biosera Dulbeco’s Phosphate Buffer was used for PBS solution.

2.1.7 Bacterial Resistance Analyses PIB based PUs

3 different pathogenic organisms, Escherichia Coli bacteria, which is from ATCC and coded as *E.Coli* ATCC 25922, Staphylococcus Aureus bacteria, which is from ATCC and coded as *S.Aureus* ATCC 29215 and Candida Albicans yeast (*C.Albicans*), which is

kindly supplied by Acıbadem University, were used for qualitative antibacterial activity testing.

2.2. Instruments and Techniques

^{1}H Nuclear Magnetic Resonance (^{1}H-NMR) spectroscopy was generated by a Varian Gemini 400 MHz spectrometer with deuterated chloroform ($\delta CDCl_3$= 7.26 ppm) for investigating the polymeric structures of HO-PIB-OH and HS-PIB-SH samples at room temperature. In addition, other ^{1}H-NMR spectra related with preparation of PIB based PU samples were carried out by a Varian MERCURY 300 or Varian NMRS 500 spectrometers at 300 or 500 MHz, respectively using $CDCl_3$ and THF-d_8 at 30^0C. NMR analysis of PIB based PU samples were completed by our collaborative laboratory members.

For all dried polymer samples, Fourier Transform Infrared (FTIR) measurements were conducted with a Nicolet 380 FTIR spectrophotometer which is equipped with a Smart Diamond ATR head having 2cm^{-1} resolution between 400 and 4000 cm^{-1} range. Additional IR analysis of PIB based PU sample during their preparation stage were carried by on a Shimadzu FTIR 8300 spectrophotometer equipped with an ATR head using solution cast films and completed by our collaborative laboratory members.

SEM images, the thickness of HAP deposit on the surface of PIB based PU samples, PIB film and ELAS, the pattern of attached cells on the surface of PIB based PU samples, PIB film and ELAS, and the cross-sectional surface of fractured PIB-SXA and PIB/PS IPN membranes were analyzed by sputter coated polymer films with a thin layer of platinum and studied by field emission SEM (FEI-Philips XL30 ESEM-FEG). Surface composition of PIB-SXA was investigated by SEM analysis with Energy Dispersive X-Ray Spectroscopy (EDX) and elemental mapping for sulfur, oxygen, and carbon atoms on PIB-SXA surface. Surface morphology changes due to calcification analyses of PIB based PU samples, PIB film and ELAS were observed by field emission scanning electron microscopy [ESEM], Zeiss Ultra Plus, Bruker, MA as a before and after incubation comparison. Surface deposits (Ca, P etc.) after calcification studies were detected by energy- dispersive X- ray spectroscopy (EDX) (Bruker X flash 5010, 123 eV) connected to a field ESEM (Zeiss Ultra Plus; Bruker, MA). To support the biomedical analyses results, PBS deposition on ELAS and PIB_O-PU were compared by sputter coated polymer films with a thin layer of platinum and studied by field emission SEM (FEI-Philips XL30 ESEM-FEG). All samples before and after incubation were quick washed with 5 mL distilled water and dried at 37^0C for 24 hours for both instrumental analyses.

Raman Spectra of PIB-SXA were recorded by a Renishaw inVia Raman microscope with the following operation parameters; 785 nm 300 mW GaAs diode as the excitation source with ~2 mW laser intensity and 5 s acquisition time; total of 5 accumulations per spectrum. Before all measurements, Raman spectrum was calibrated by a silicon wafer peak at 520 cm^{-1}.

Thermogravimetric analysis of PIB-SXA and PIB/PS IPN samples were carried out using TA Instruments (TGA-Q500 instrument) under a continuous nitrogen flow with 10^0C/min heating rate from 30^0C to 600^0C to analyze of thermal stability of ~4 mg polymer samples. In addition, thermal properties of ~8 mg PIB based PU samples were analyzed by same TGA instrument with 10^0C/min heating rate from 20^0C to 600^0C.

UV initiated reactions of both primary network and interpenetrating network were carried out using a UV chamber which is equipped with an air circulation system and 365 nm UV lamps. UV initiated polymerization reactions were occurred in the Teflon mold which was exposed 6.5 mW cm^{-2} UV light at room temperature.

Number average molecular weights (M_n) and polydispersities of HO-PIB-OH and HS-PIB-SH (after SH modification for PIB-SXA and PIB/PS IPN parts) polymer chains were detected by Size Exclusion Chromatography (SEC) equipped by a Waters Isocratic HPLC Pump with Waters 2414 Refractive Index Detector and Four Waters Styragel colums (HR 3, HR 4, HR 4E and HR 5E) at 30^0C. The instrument was calibrated with polystyrene standards in the 400-180.000 range. Gel permeation chromatography (GPC) elugrams were recorded with a flow rate 0.35 mL THF, used as a mobile phase, per minute and samples were injected by a 100 μL Hamilton syringe. GPC data of HO-PIB-OH and HS-PIB-SH chains were analyzed using Gaussian deconvolution of the peaks by OriginLabs OriginPro

Software. GPC traces of PIB based PUs and ELAS were determined using a Viscotek GPCmax instrument and THF at a flow rate of 1.0 mL/min at 35^0C by our collaborative laboratory members.

Differential Scanning Calorimetry were performed with a DSC Q2000, TA Instrument working under a stabile nitrogen flow. For PIB-SXA and PIB/PS IPN, approximately 5.5 mg film sample were placed between aluminum pans, sealed by a quick press equipment, and heated with a 10^0C/min rate from -90^0C to 350^0C. For PIB based PU structures; ~8 mg of each sample was prepared with a same method and then heated with a 10^0C/min heating rate in the -90^0C to 250^0C range.

Permanent deformation of PIB-SXA and PIB/PS IPN samples was determined by using a Q800, TA Instruments – Universal Tensile Testing in the creep mode by applying constant stresses of 0.05 MPa at 24^0C for 15 min and followed by load removal (recovery) for 25 min at the same temperature. For time-dependent mechanical properties of PIB based PU samples, creep recovery and creep experiments were completed under 1 MPa constant stress and permanent deformation experiments of PIB based PU samples were performed under 1 MPa constant stress for 15 min, followed by load removal for 25 min at 25^0C by an isothermal creep test. Dynamic mechanical properties of PIB-SXA and PIB/PS IPN were determined by using a Universal Tensile Testing (Q800, TA Instrument) with a film tension clamp in a strain mode with 30% min/rate to 300% final strain. For PIB based PU samples, the film tension mode of same instrument (Q800, TA Instrument) was applied at 1 Hz and with a 3^0C/min heating rate from -100^0C to 250^0C.

Homogeneity of PIB-SXA were determined by measuring atomic percentages of surface (sulfur) and after calcification study, surface characters of PIB film, ELAS, PIB based PU samples against deposits were examined by determining the atomic percentages of surface deposits (Ca, P etc.) with a Thermo-Specific K-Alpha model X-Ray Photoelectron Spectrometer (XPS) with 15 scans under 150 eV passing energy and 10 scans under 50 eV passing energy, respectively. All binding energies for XPS analysis were referenced to the C1s line and peak intensities were determined by calculating the integral of all peaks, after subtraction of the S-shaped Shirley type background and fitting the curve to a combination of Lorentzian (30%) and Gaussian (70%) lines.

Swelling capacity of vacuum-dried networks were used for calculating mesh size of prepared network structures. PIB-SXA and PIB/PS IPN samples (~4 mg) were separately immersed in both cyclohexane (≥99,9% purity) and distilled THF at room temperature and length changes in their dimensions are recorded at different time intervals until reaching an equilibrium point. Before measuring the length of samples with travelling microscope, excess cyclohexane on surface was removed by gentle blotting with Kim-Wipe (tissue paper). Dimensional stabilities in PBS medium of PIB based PU samples were determined by swelling ratio % values determined according to above mentioned length change results recorded by travelling microscope.

3D Topographical imaging (as a 3D height image) of PIB film, ELAS and PIB based PU samples for surface roughness comparison were carried by atomic force microscopy using a universal scanning probe microscope [USPM] (Ambios Technology, Santa Cruz, CA). After solvent casting, thin polymer films were directly scanned in tapping mode with the cantilever oscillating at its resonance frequency of 170 kHz.

Surface hydrophobicity characters of PIB based PU samples were analyzed by measuring contact angles of surface/distilled water/air with a KSR CAM 101 instrument at room temperature.

Microshore (ASTM D-2240) hardness of PIB based PU samples was carried out by using ~0.5 mm thick films with a Micro-O-Ring Hardness Tester. For each sample, average of three to five data were reported in the Shore A scale. In addition, Shore A hardness character of PIB-SXA and PIB/PU IPN structures were tested using ~0.7 mm thick films with same instrument.

X-Ray diffraction (XRD) traces of PIB based PU samples were generated by a Rigaku D/Max-2200 Ultimate diffractometer with CuKα radiation, operating at 40 kV and 40 mA. XRD data of each polymer samples were collected from 1^0 to 70^0 (2θ) with 2^0/min rate.

The UV absorbance values of PIB base PU samples and ELAS were measured at 590 nm by a ThermoFisher MULTISKAN GO microplate reader spectrometer for protein adsorption and cell viability tests.

ChemiDoc Instrument is used for imaging the bacterial diffusion zone on the PIB based PU samples. These images were supported by optic camera images.

2.3. Syntheses, Preparation and Experiments

2.3.1. Syntheses of Thio Telechelic Polyisobutylene based Polymers, Primary and Interpenetrating Networks and Their Related Experiments

2.3.1.1. Synthesis of Thio Telechelic Polyisobutylene (HS-PIB-SH)

HO-PIB-OH was thiol end-capped by acid catalyzed esterification with mercaptopropionic acid (MPA) using a Dean and Stark apparatus (Figure 2.1). A typical procedure was as follows: HO-PIB-OH (7.5 g, 2.4 mmol) and MPA (2.7 g, 23 mmol) were dissolved in 120 mL toluene, heated to 50^0C, and then pTSA (0.033 g, 0.17 mmol) catalyst was added, finally the solution was stirred under reflux (130^0C) overnight.

Subsequently, the HS-PIB-SH polymer was precipitated in 0.5 L methanol. The solvent was decanted and final polymer product dried in vacuum oven at 30^0C [14].

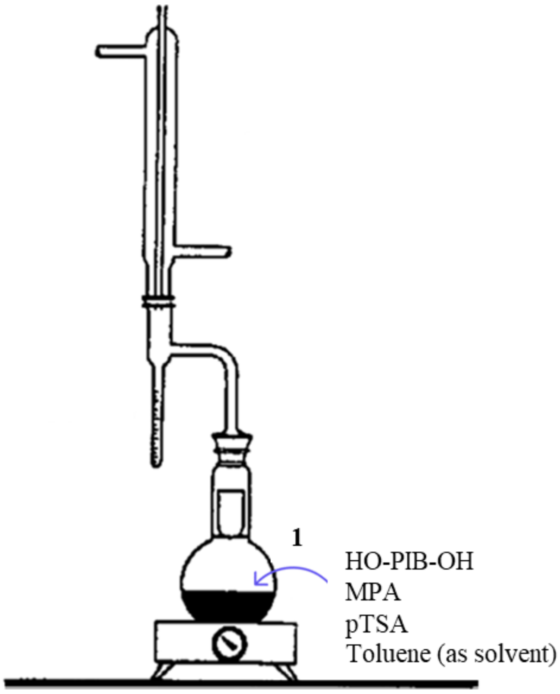

Figure 2.1: Esterification of HO-PIB-OH via Dean-Stark apparatus.

2.3.1.2. Synthesis of Thio Telechelic PIB based Primary Network (PIB-SXA) via Crosslinking

The PIB based primary network was prepared using an equimolar ratio (1:1) of HS-PIB-SH and TATA (as a crosslinker). A 10 ml vial was charged with HS-PIB-SH (0.583 g, 91.6 wt%) and TATA (0.039 g, 7.56 wt%) was added. DMPA (0.04 g, 0.76 wt%) was used as a photoinitiator and dissolved in 1 mL THF under a vigorous mixing. The homogeneous solution was poured in a Teflon mold and irradiated at 366 nm UV light with 4.67 mW/cm^2 intensity for an hour. The PIB-SXA network film was dried overnight in vacuum oven at 30^{0}C followed by post-curing for 30 minutes. The 0.2 mm thick films obtained were optically clear and had almost smooth surface [14].

2.3.1.3. Preparation of PIB-SXA and PS Interpenetrating Network (PIB-SXA/PS IPN)

The dried PIB-SXA network were used as a primary template for the preparation of sequential IPN structures. Pre-weighed PIB-SXA primary network was immersed in THF solution containing styrene monomer, crosslinker divinylbenzene, and photoinitiator

(IRGACURE 651). The molar ratio of styrene to divinylbenzene was set to 10:1 with 3 wt % initiator. The solution was poured on the PIB-SXA network film placed into a Teflon mold and this system was irradiated with 366 nm UV light (4.67 mW/cm^2 intensity) during overnight. After airdry, formed PIB/PS IPN structure was dried overnight in vacuum at 40^{0}C oven.

2.3.1.4. Swelling Studies of PIB-SXA and PS Interpenetrating Network (PIB-SXA/PS IPN)

All samples were dried in vacuum oven to remove the solvent used for curing. Two pieces of network films, which have different length but same thickness, were cut from vacuum-dried samples. For both primary and interpenetrating networks, one of them was used in swelling test with THF (which was as a solvent for synthesis part) and the other one was swollen in cyclohexane, which is a good solvent for PIB, at room temperature. For these two systems, a travelling microscope was used to determine the length change of samples for 4 days.

2.3.2. Synthesis of PIB based PUs

2.3.2.1. Synthesis of Allyl Telechelic PIB (A-PIB-A)

The preparation and characterization of allyl telechelic PIB (A-PIB-A), used for synthesis of HO-S-PIB-S-OH, have been completed by our collaborative group members [16].

2.3.2.2. Synthesis of HO-S-PIB-S-OH (PIB$_S$)

A well dried 50-mL round bottom flask containing DMPA (102 mg, 0.398 mmol), chloroform (18.8 mL) and A-PIB-A (10.955 g, 3.534 mmol) was stirred in the dark environment until the all A-PIB-A polymer dissolved. After the system was cooled by a water-ice bath, mercaptoethanol (0.75 mL, 11 mmol) was injected to the flask. The mixture was continued to stir a few additional minutes and irradiated with a medium pressure Hg lamp (Fusion UV, F300S) for 15 minutes, then the irradiated solvent was removed under reduced pressure The crude product was dissolved in hexane and well precipitated into methanol, respectively. The precipitated product was dissolved in hexane again, washed with water thrice and with brine twice, and finally dried over $MgSO_4$, filtered, dried. A colorless viscous liquid (10.6 g, 92.7%) product was obtained. HO-S-PIB-S-OH was synthesized by our collaborative laboratory members in USA [16].

2.3.2.3. Synthesis of PIB based PUs with O-S-PIB-S-O soft segment (PIB_S-PU)

The synthesis of 72.5PIB_S-PU was conducted in two sequent steps: (i) Freshly distilled MDI (1.9139 g, 7.648 mmol) dissolved in THF (4 mL) under a N_2 blanket was added to a well dried 50mL round bottom flask, and HO-S-PIB-S-OH (6.005 g, 1.888 mmol) was dissolved in THF (14 mL) was injected to the system in the flask. The solution was stirred and heated to 65^0C. Dibutyltin dilaurate, DBTDL (4.8 mg, 0.0076 mmol–0.48 mL of 10 mg/mL THF solution), was added as a catalyst and this “prepolymer” solution was stirred at 65^0C for 1 h. (ii) A deoxygenated solution of 1,4-Butanediol, BDO (0.4809 g, 5.3362 mmol) in THF (4mL) was prepared in a separate vial and injected in the stirred prepolymer solution. This system was stirred for another 3 h at 65^0C and poured in a 14x14 cm glass mold. The final product was air dried approximately 16 h and then dried in vacuum oven for 24 h at 60^0C. A colorless rubbery film was obtained, and ~250–350 μm thick film was optically clear. Synthesis of 72.5PIB_S-PU was completed by our collaborative laboratory members [16].

2.3.2.4. Synthesis of PIB based PU with HO-PIB-OH soft segment (PIB_O-PU)

The mechanism of the inifer polymerization of isobutylene, which yields di-tert-chloride telechelic polyisobutylene, tCl-PIB-Clt, were followed by a series of quantitative functionalization (dehydrochlorination, hydroboration, and oxidation) leading to HO-PIB-OH. Synthesis of 72.5 PIB_O-PU was completed by our collaborative laboratory members [16].

2.3.2.5. Preparation of Sulfur-containing PIB based PU nanocomposite (PIB_S-PU/NC)

For the synthesis of PIB_S-PU/Nanocomposite, a representative procedure was applied in three steps as follows: (i) A well dried 100 mL septum-sealed round bottom flask was equipped with a small Teflon coated stir bar; and freshly distilled 4,4’methylenebis (phenyl isocyanate) and MDI (2.0440 g, 8.168 mmol) dissolved in THF (4 mL) were added to the flask under a blanket of N_2. Then, HO-PIB-OH (6.0046 g, 1.888 mmol) in THF (12 mL) was injected to the system. The solution was stirred and heated to 65^0C. Dibutyltin dilaurate, DBTDL (5.2 mg, 0.0082 mmol 0.52 mL of 10 mg/mL THF solution), was added as a catalyst and this ‘prepolymer’ solution was stirred for 1h. (ii) Then, the chain extender 1,4-butanediol, BDO (0.4438 g, 4.925 mmol) dissolved in THF (4 mL) was prepared in a separate deoxygenated vial and injected to the “pre-polymer” solution. (iii) The mixture was stirred for additional 30 min at 65^0C and dispersed form of OmMMT (0.0406 g) in THF (8 mL), prepared in a separate deoxygenated vial, was injected. This system was stirred for additional 3 h at 65^0C and poured in a 14x14 cm glass mold. The final product was air dried ~16 h and then vacuum dried for 24 h at 60^0C oven. A colorless rubbery film was obtained, and it was optically clear. Synthesis of PIB_S-PU/Nanocomposite was completed by our collaborative laboratory members [21].

2.3.3. Preparation and Experiments for Calcification Analyses of PIB based PUs

2.3.3.1. Preparation of Simulated Body Fluid (SBF)

A cellular simulated body fluid (SBF), whose ion concentration equals to human blood plasma, was used for the calcification studies of ELAS and PIB based PU samples. 1000 mL of SBS was prepared in ion-exchanged and distilled water with nominal ion concentrations of 142 mM Na^+, 5 mM K^+, 1.5 mM Mg^{2+}, 2.5 Ca^{2+}, 147.8 Cl^-, 4.2 HCO_3^-, 1 mM HPO_4^2, 0.5 mM SO_4^{2-}. pH was adjusted to 7.4 with 1 M HCl. Then, solution was filter sterilized with Stericup 0. 22 µm filter (Merck Millipore). SBF was stored at 4^0C and was warmed to 37^0C before use [41].

2.3.3.2. Mineralization

Some studies in literature was followed by using a batch incubator at 37^0C for mineralization analyses. Each sample (0.5 × 1.0 × ~0.01 cm) was duplicated and incubated in 3 mL pre-warmed (37^0C) SBF solution, agitated for 28 days at 50 rpm. SBF solution of each sample was renewed with fresh ones once every 2 days and this process was repeated for 28 days [41].

2.3.4. Preparation and Experiments for Protein Adsorption, Cell Attachment and Proliferation, Bacterial Resistance Analyses of PIB based PUs

2.3.4.1. Protein Adsorption Studies

2.3.4.1.1. Standard Preparation for Standard Curve

1 mL BSA (Bradford Assay Kit) standard (2 mg/mL) was solved in 1 mL PBS at pH 7.4 and this 2 mL solution was used as a stock solution for following standards. By diluting the stock solution with distilled water in a different ratio, 7 standard solutions were prepared in different concentrations: 2 mg/mL, 1.5 mg/mL, 1 mg/mL, 0.5 mg/mL, 0.25 mg/mL, 0.125 mg/mL and 0.0625 mg/mL. For Bradford assay, prepared 3 sets of 200 µL for each standard solution and blank (distilled water was used as a blank solution in this experiment) in a 96-well plate, and 5 µL of blank and each standard solution were added to the wells containing Bradford reagent. The plate was shaken for 3 minutes and placed in UV cabin for measuring the absorbance values under 595 nm. (All steps were proceeded in dark room). For evaluating the standard curve equation, average of 3 sets was used for each concentration. By using UV Spectroscopy, the absorbance values of 7 BSA standards in different concentrations were obtained. Table 2.1 and Figure 2.2 summarize these results.

Table 2.1: UV absorbance results of BSA standards in different concentrations

BSA Conc. (mg/mL)	**2**	**1.5**	**1**	**0.5**	**0.25**	**0.125**	**0.0625**
UV Absorbance Values	0.829	0.68	0.609	0.481	0.397	0.356	0.355
	0.834	0.657	0.479	0.472	0.396	0.359	0.328
	0.81	0.685	0.578	0.482	0.392	0.345	0.327
AVERAGE	**0.824**	**0.674**	**0.555**	**0.478**	**0.395**	**0.353**	**0.337**

For obtaining this standard curve, the UV average absorbance values of each concentration were used. Since R^2 value of graph is higher than 0.95 the curve equation can be used for following Fg adsorption experiments.

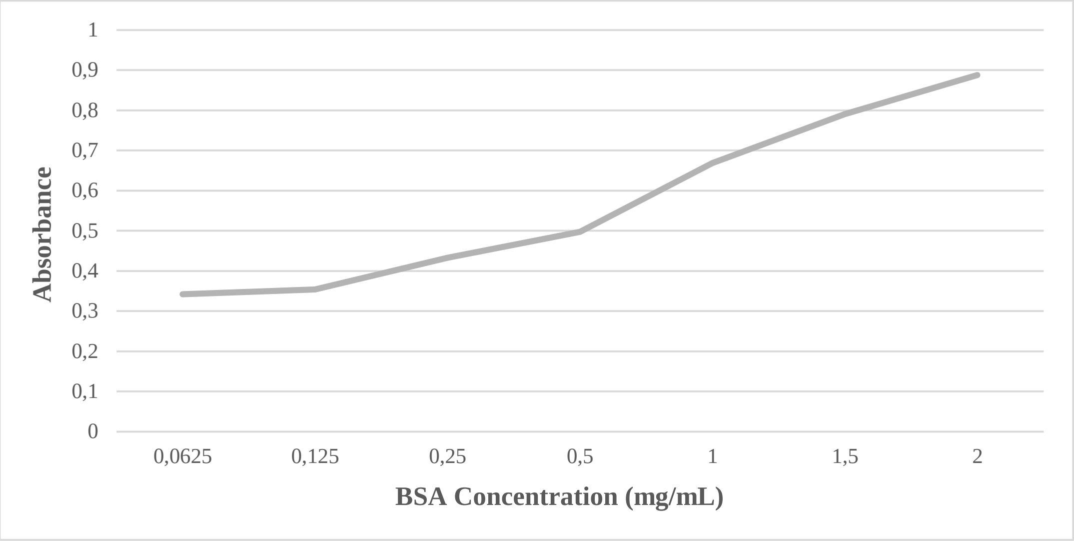

Figure 2.2: Standard curve of BSA standards in different concentrations

2.3.4.1.2. Fibrinogen (Fg) Preparation

Fg, stored at -20^{0}C, was removed from a refrigerator and 0.012 g Fg was slowly solved in 12 mL PBS (at pH 7.4). Obtained 1 mg/mL Fg solution was vortexed and then it was kept at 37^{0}C water bath for 1 hour to obtain clear and transparent solution. The homogeneous and clear solution was removed from water bath and filtered with 0.22 μm filter. (This Fg solution was prepared freshly before each experiment).

2.3.4.1.3. Fibrinogen (Fg) Adsorption Procedure

Before starting the Fg adsorption procedure, ELAS and PIB based PU film surfaces should be cleaned so all films were put under the 240 nm UV light during half an hour and then kept in ethanol solution overnight. All films were washed with 3 mL PBS for removing ethanol and cleaning. Cleaned films were placed in 24-well plate and 1 mg/mL fresh Fg solution were added to each well. The plate was kept 37^{0}C CO_2 incubator for 4 hours.

2.3.4.1.4. Eluting of Fibrinogen (Fg) with SDS

Incubated films were removed from Fg solution and washed with 500 μL PBS (at pH 7.4) twice in a 24-well plate. PBS was removed from well without disturbing film surface with attached proteins and film surfaces were covered with 300 μL SDS (5% w/v) solution to elute attached proteins. Films placed in SDS solution were shaken for 5 minutes, then they were removed from SDS solution and put in PBS at pH 7.4 for cleaning.

2.3.4.1.5. Bradford Assay

The SDS solutions containing eluted proteins of each film were used for Bradford Assay so the protein amount in SDS solution can be calculated directly and the results are equal to adsorbed proteins on film surfaces [29].

For each SDS solution so each sample, minimum 3 sets should be prepared in 96-well plates. Like in a standard curve determination part, 200 μL Bradford reagent were put in each well of 96-well plate. 5 μL SDS solution of films were added to each well and the 96-well plate was shaken for 3 minutes. Then, the plate was placed in UV cabin and the absorbance values were measured under 595 nm. (All steps were proceeded in dark room).

2.3.4.2. Cell Attachment and Proliferation Studies

2.3.4.2.1. Cell Attachment and Proliferation Protocols

Mouse connective tissue L929 cells, obtained from ATCC, were maintained in DMEM supplemented with 10% Foetal bovine serum (Sigma Aldrich) and 1% penicillin/Streptomycin (Sigma Aldrich) in CO_2 incubator at 37^0C [42] When cultures in 75 cm^2 flask reached confluence, they were trypsinized with 0.25 % (w/v) Trypsin-EDTA solution. $2x10^4$ cells were counted and plated on PIB based Polyurethane films in 48-well plate. They were allowed to attach on films for 24 h at CO_2 incubator.

For cell viability analysis, more than 4 sets (0.5x0.5cm in dimension) were prepared for each sample and $2.3x10^4$ cells were seeded on each sample. After 24 h, cell viability of films was evaluated by MTT assay. After 3 hours from the end of incubation, formed formazan products were dissolved with DMSO. The absorbance was measured at 570 nm in a microplate reader spectrometer.

2.3.4.2.2. Fixation of Attached Cells on Polymer Surface

Films held in cell medium were transferred from 48-well plate to 24-well plate and all films were washed with 500 μL PBS twice. After removing PBS, 300 μL 2.5% glutaraldehyde solution; rapidly denaturing protein and exploited by using it as a disinfectant, was added in each film wells and films were kept in 2.5% glutaraldehyde solution for 30 minutes. Then, glutaraldehyde was removed, and films were washed with 500 μL PBS twice. At the same time,

30%, 50%, 75%, 90% (v/v) and pure ethanol solutions were prepared, and films were put in 30%, 50%, 75%, 90% and pure ethanol solutions for 15 minutes, respectively. After 75 minutes, all films were transferred to clean 48-well plates and attached cells on films were directly analyzed with SEM.

2.3.4.3. Bacterial Resistance Analysis of New PIB based PUs

3 different pathogenic organisms, Escherichia Coli (*E.Coli* ATCC 25922) bacteria, Staphylococcus Aureus (*S.Aureus* ATCC 29215) bacteria and Candida Albicans (*C.Albicans*) yeast, were used for qualitative antibacterial activity testing known as Kirby-Bauer test. First, bacterial suspensions from 3 different organisms were prepared and incubated in a liquid culture medium with the film samples (in 0.5x0.5 cm dimensions). Then, the culture dishes put into a constant temperature incubator at 37^0C. After 18 h, the films were removed, and bacterial diffusion zone were analyzed. The optical images before and after film removals were taken via ChemiDoc instrument and optic camera [43].

2.3.4.4. Dimensional Stability of New PIB based PUs in PBS

To support all bio-related tests, length-change based swelling patterns, which were measured with Travelling Microscope, of dried PIB based PU and ELAS films were used for calculating swelling ratio ($\Delta l/l_0$) of samples. All films (~0.5-0.65 mm initial length) were immersed in PBS solution, which was used for cell attachment and cell viability analysis, at room temperature and length changes in their dimensions are recorded at regular time intervals until reaching an equilibrium swelling (more than 24 h). Before measuring the length changes of samples, excess PBS on surface was removed by gentle blotting with Kim-Wipe.

In addition to length change measurement, surface change and PBS crystals deposition on film surfaces were examined with SEM imaging. After 24 h PBS incubation at room temperature, samples were washed with distilled water and then, they were left for air-dry for 24 h. To remove residual water, samples were put to 25^0C vacuum oven for additional one day. The surfaces of PIB_O-PU and ELAS samples were checked with SEM to compare the changes on the sample surfaces before and after PBS exposition.

3. RESULT AND DISCUSSION

3.1. PIB based Interpenetrating Networks

Interpenetrating polymer networks (IPN) are a system composed of numerous physically intertwined, non-separable networks with no covalent bonds between them. IPN methodology is a technique for enhancing the mechanical characteristics of polymers and polymeric systems [10]. In order to improve the mechanical properties of PIB, and overcome other PIB weaknesses, like creeping and poor resistance to organic solvents without impairing their low permeability to gas, interpenetrating network formation method were used in this study.

3.1.1. Structural Property of PIB Based Primary Network (PIB-SXA)

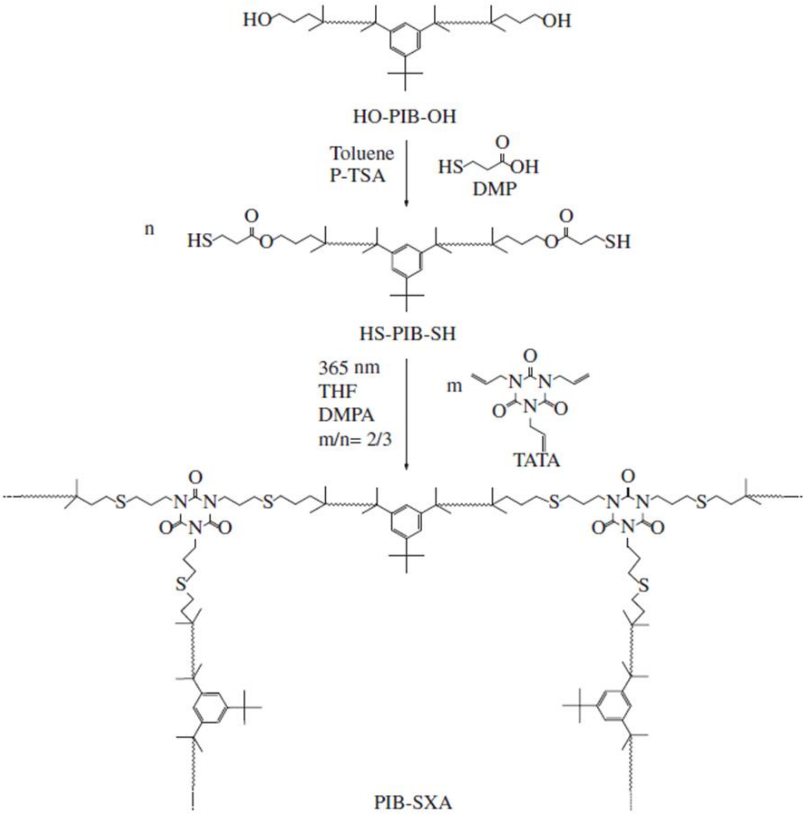

Figure 3.1: The synthesis and a structural element of HS-PIB-SH and PIB-SXA. Reprinted from [14].

Figure 3.1 outlines the synthesis strategy of thiol functional PIB and structural element of a PIB network obtained from dithiol telechelic PIB and multifunctional allyl based crosslinker. It is worth to say here that it was the first synthesis of telechelic HS-PIB-SH from telechelic HO-PIB-OH in the literature [14].

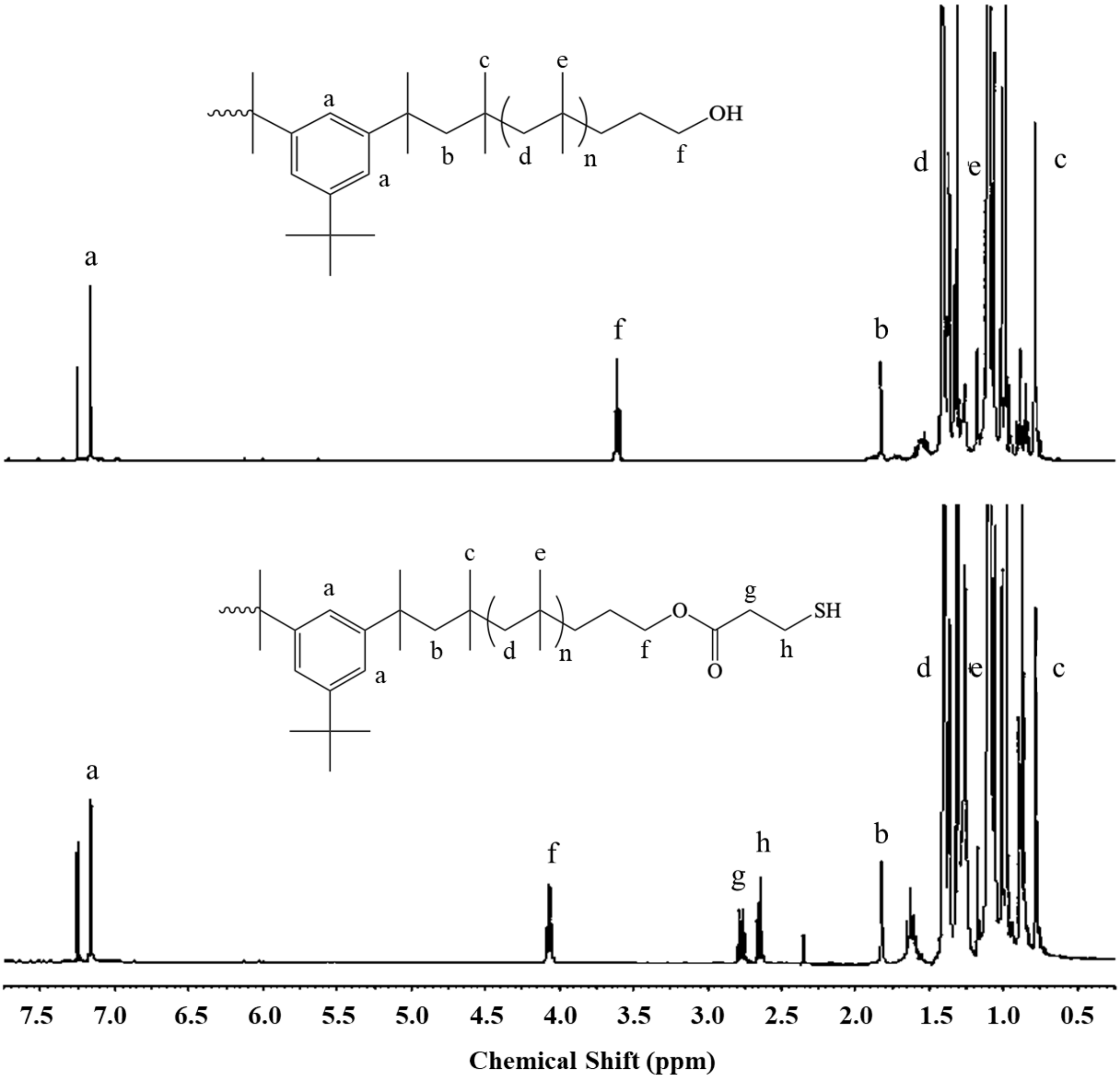

Figure 3.2: ^{1}H NMR Spectra of (a) hydroxyl telechelic PIB (HO-PIB-OH) (b) thiol functional PIB (HS-PIB-SH). Reprinted from [14].

After esterification reaction was completed, ^{1}H NMR results of initial and final samples were compared to prove the functionality success. The NMR spectrum of HO-PIB-

OH contains a resonance peak around 3.6 ppm due to the -C$\underline{H}_2$OH proton of the starting material (Figure 3.2(a)). However, there is not any resonance peak at same area of NMR spectrum for HS-PIB-SH (Figure 3.2(b)). Instead of that, around 4.2 ppm, an ester peak is observed, and the comparison of these peaks shows that 100% functionalization achieved [14].

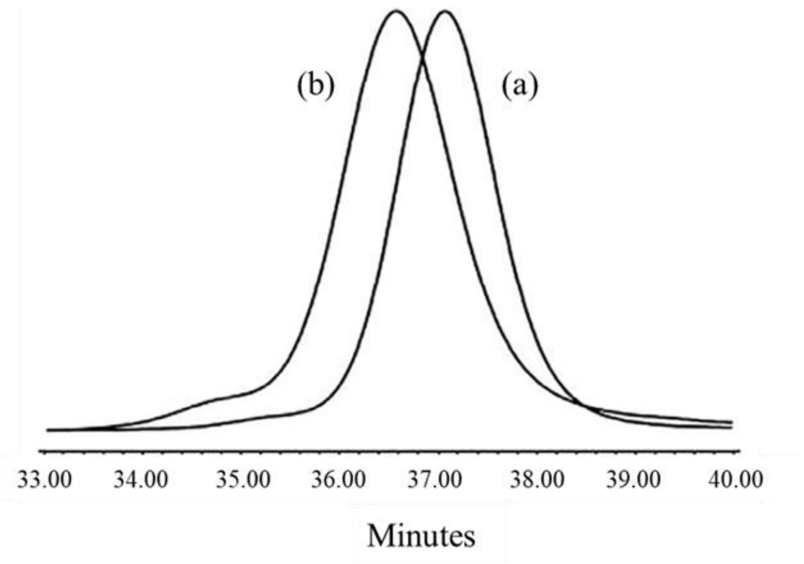

Figure 3.3: GPC traces of (a) hydroxyl telechelic PIB (HO-PIB-OH) (b) thiol functional PIB (HS-PIB-SH). Reprinted from [14].

In addition, average molecular weight, and M_w/M_n values of starting material (HO-PIB-OH) and the product of esterification reaction (HS-PIB-SH) were determined and their GPC traces (Figure 3.3) were compared. Slight change in M_n ($M_{n\ \text{HO-PIB-OH}}$ = 3180 g/mol and $M_{n\ \text{HS-PIB-SH}}$ = 3750 g/mol) and M_w/M_n values (from 1.06 to 1.10, respectively) confirms the nondestructive modification. According to these results, it can be safely concluded that thiol modification did not disrupt the molecular structure. [14]

FT-Raman analysis further confirmed the network structure and the success of functional group conversion, displaying the characteristic peak of C-H stretching in 680-760 cm^{-1} region, and the absence of characteristic peak from S-S stretching between 430-550 cm^{-1} is the evidence of that there was not any unwanted disulfide formation during network preparation step (Figure 3.4) [44].

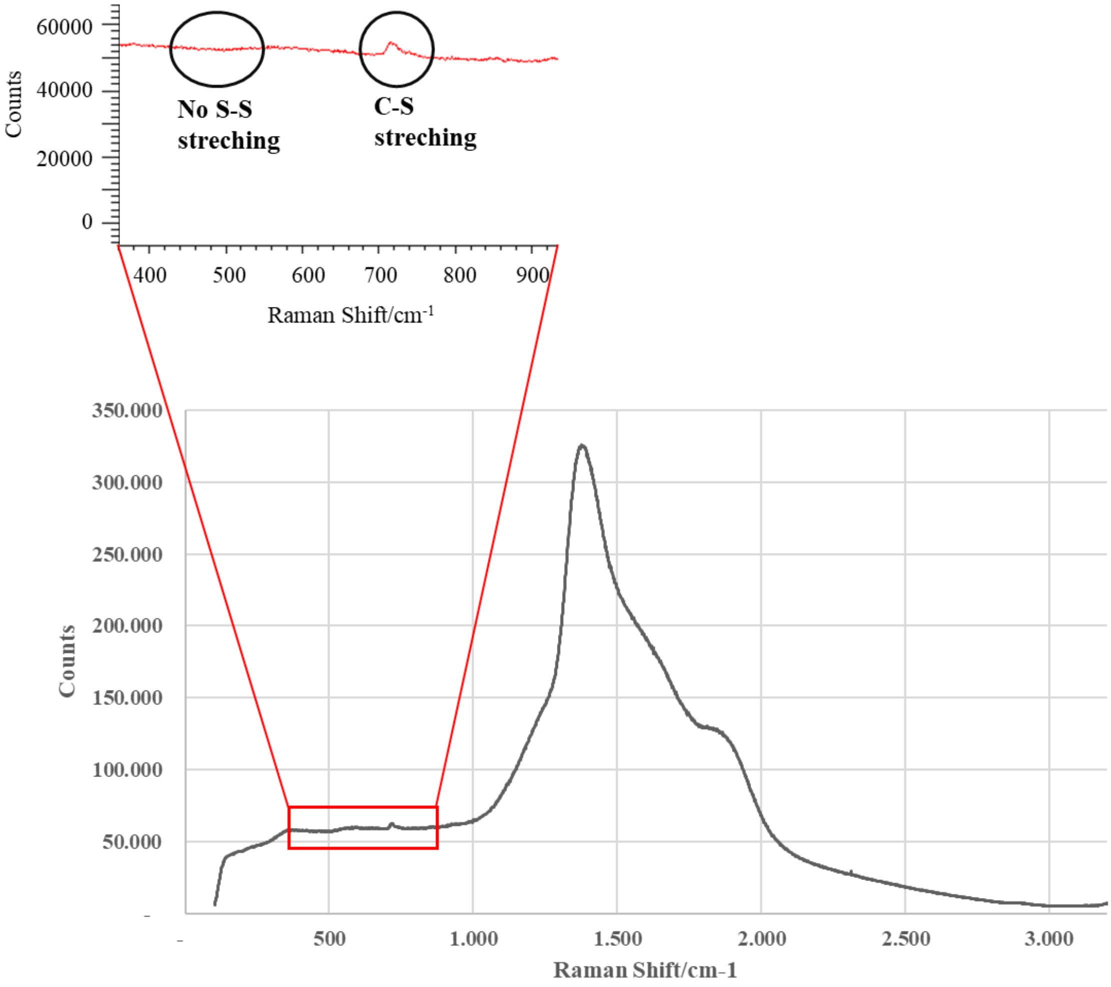

Figure 3.4: FT-Raman spectra of primary network (PIB-SXA).

3.1.2. Structural Property of PIB-SXA and PS Interpenetrating Network (PIB-SXA/PS IPN)

Figure 3.5 outlines the strategy for the preparation of PIB-SXA/PS IPN from PIB based primary network and styrene monomer via sequential interpenetrating network preparation method. It is worth to say here that although there are some examples about PIB and PS based IPNs [3], it was the first preparation of polyisobutylene and polystyrene based interpenetrating via sequential method.

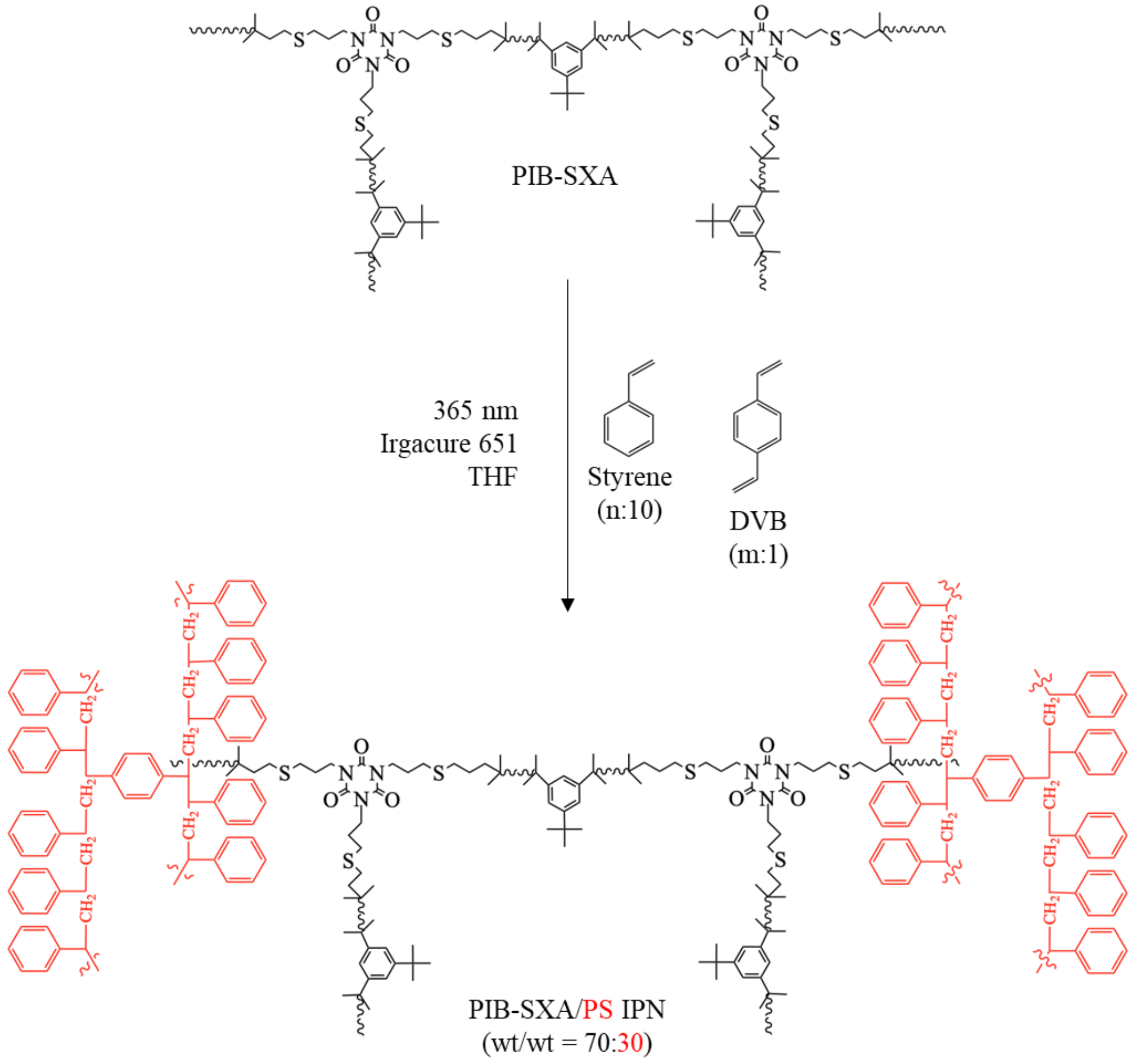

Figure 3.5: The synthesis and a structural element of PIB-SXA/PS IPN prepared from PIB based primary network (PIB-SXA) and styrene monomer via sequential technique.

Analysis of the extracted compound (~9%) by ^{1}H-NMR (Figure 3.6) shows that the prepared PIB-SXA/PS interpenetrating network contains trace amount of low molecular weight polystyrene and polyisobutylene without any unreacted styrene.

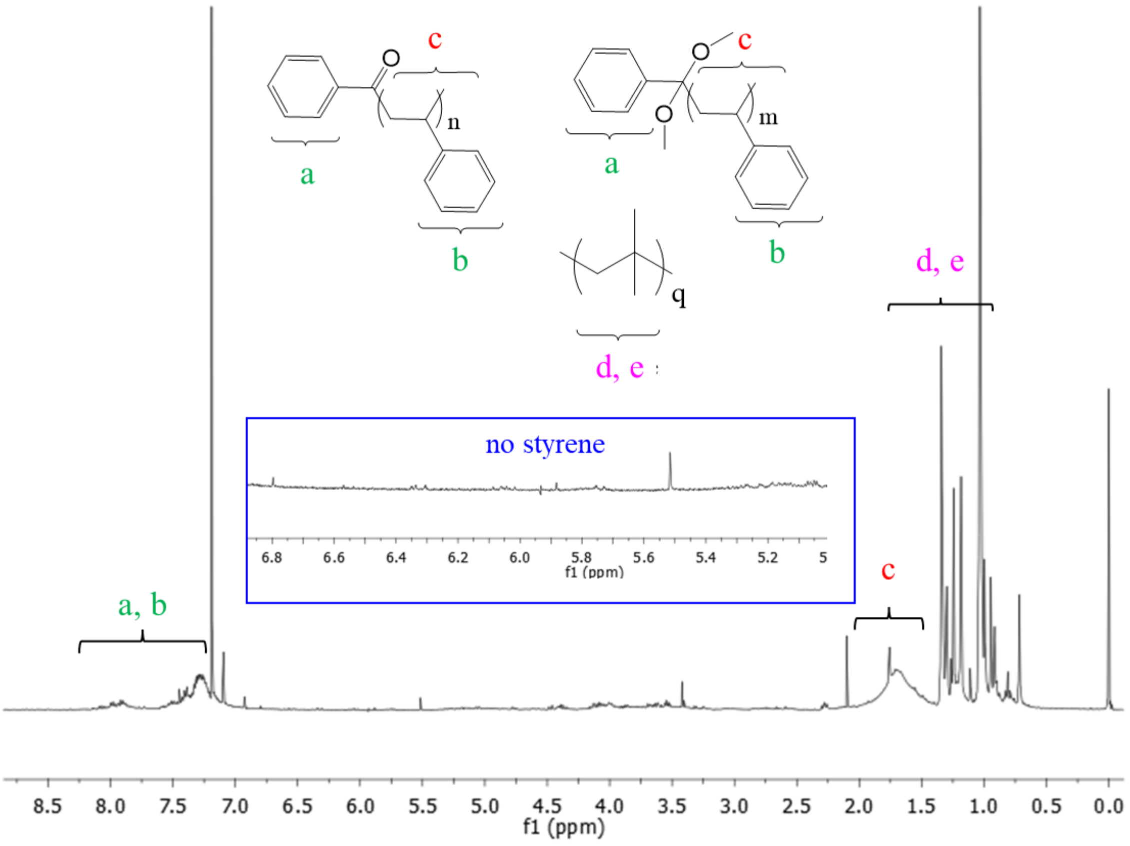

Figure 3.6: ^{1}H NMR spectra of a compound obtained after extraction of PIB-SXA/PS IPN with acetone

The chemical structure of synthesized PIB-SXA/PS IPN was also analyzed using FTIR spectroscopy. Due to sequential IPN synthesis, the comparison of PIB-SXA and PIB-SXA/PS IPN FTIR spectra can be easily applied.

The stacked FTIR spectra of PIB-SXA primary network and PIB-SXA/PS IPN is shown in Figure 3.7. The peak at 1596 cm^{-1} corresponds C-C in plane stretching of polystyrene ring showed peaks and other aromatic ring vibrations [45, 46] are detected at 1540 cm^{-1}. The weak band around 1038 cm^{-1} proves the presence of the aromatic ring of polystyrene. Dave et al. reported that this weak band is observed in 1018-1023 cm^{-1} range [47]; however, a reduced mobility (due to crosslinking) of the aromatic parts as the polymer is formed can cause a slight shift of this aromatic ring peak towards higher wavenumbers [48]. In addition, Vinodh et al. reported that increased crosslink density in structure also causes a decrease in the intensity of these PS bands [45].

As shown in ^{1}H-NMR spectrum, the prepared PIB-SXA/PS IPN sample contains a trace amount of styrene monomers, trace amount uncrosslinked PS and PIB chains, and presence of them is also detected with FTIR spectroscopy.

Brijmohan et al. reported that the peak around 697 cm^{-1} is the out of plane bending vibration of the styrene ring, 834 cm^{-1} is due to C-H out-of-plane vibration for para position and 756 cm^{-1}, one of the characteristic peaks for PS, is the out-of-plane bending vibration of C-H groups in the monosubstituted benzene ring in PS structure. These vibrations of styrene rings for PIB-SXA/PS IPN shifted higher wavenumbers and observed in 699, 873 and 764 cm^{-1} due to a lower mobility of the aromatic rings in network structure as explained above [48, 49].

As expected, the signal at 1683 cm^{-1}, which corresponds to C=C (double bond) stretching vibration of styrene vinyl group, disappeared after a successful polymerization of PS during IPN formation. [48]. However, the trace amount of not polymerized styrene monomer in PIB-SXA/PS IPN creates a peak at 1686 cm^{-1}. Tsyupura et al. reported that the presence of the absorbance peak at 1700 cm^{-1}, in a computer-simulated IR spectra, is the proof of a rigid and highly crosslinked model network, which does not contain C=O groups in structure [50].

As seen in FTIR spectra of PIB-SXA/PS IPN (Figure 3.7), there is a small peak around 1730 cm^{-1}. Shifting of this peak towards higher wavelength may be due to the difference between practical and computational methods, and different crosslink densities [50].

Finally, the broad peak around 3291 cm^{-1} is due to stretching vibrations of moisture which is also proved with thermogravimetric analysis [45] (see in Figure 3.15).

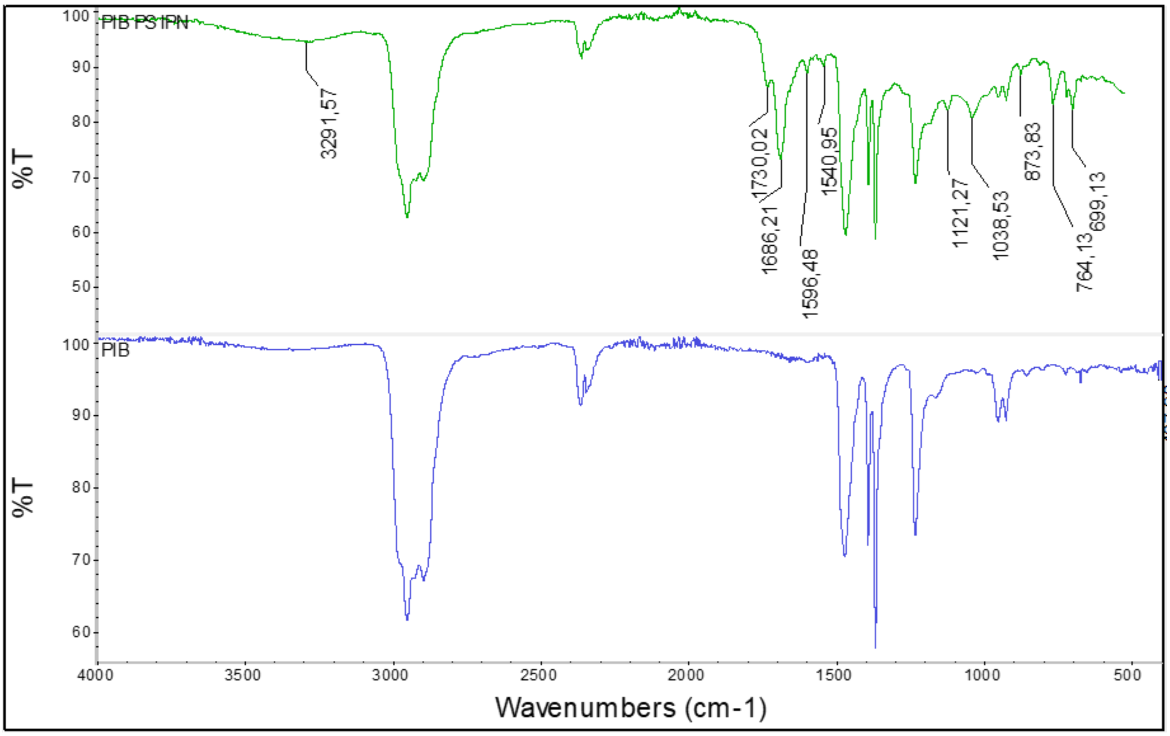

Figure 3.7**:** FTIR spectra of PIB-SXA/PS IPN (*green and upper one*) and PIB-SXA primary network (*blue and lower one*).

Both above mentioned molecular characterizations confirmed the successful synthesis of IPN structures.

3.1.3. Optical Property of PIB-SXA and PIB-SXA/PS IPN

The refractive indices of PIB and PS are 1.50 and 1.57 at 25^0C, respectively [14]. Because of their differences, an opacity of material is evidence of a phase separation between to networks in IPN. Therefore, the transparency of material verifies the quality of interpenetration degree of two phases. Vancaeyzeele's et al. reported that when PS network forms before the PIB part, the final IPN material becomes opaque (close to white), and this is indicative of a large phase separation between PIB and PS. Thus, the crosslinking of PIB network following PS formation cannot be adequate since final IPN structure mostly includes extended linear PIB chains, and although a sequential IPN synthesis method was applied, a macroscopic level phase separation occurs in final structure [3].

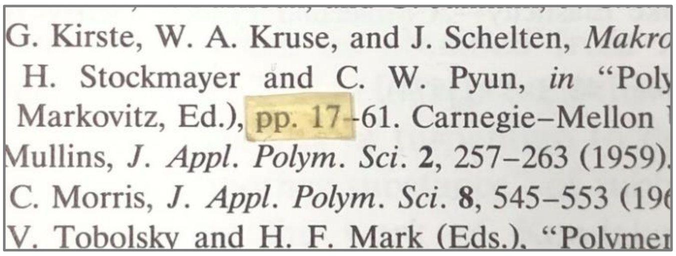

G. Kirste, W. A. Kruse, and J. Schelten, *Makr*
H. Stockmayer and C. W. Pyun, *in* "Pol
Markovitz, Ed.), pp. 17–61. Carnegie–Mellon
Mullins, *J. Appl. Polym. Sci.* **2**, 257–263 (1959).
C. Morris, *J. Appl. Polym. Sci.* **8**, 545–553 (19
V. Tobolsky and H. F. Mark (Eds.), "Polyme

Figure 3.8: Optic camera image of PIB-SXA/PS IPN

PIB-SXA/PS IPN, synthesized by sequential IPN method and PIB-SXA network was formed before the PS one, is very transparent (see in Figure 3.8). As reported by Vancaeyzeele's et al. the degree of interpenetration between networks is strongly correlated with the transparency of material and the domain size of polymers: a smaller polymer domain size and higher interpenetration degree of them creates a more transparent material. Therefore, the sequential IPN synthesis, in which the PIB network is formed before the PS part, results in improved interpenetration between both network phases [3].

Each individual network should be protected from chemical and/or physical threats thanks to interpenetrating network architecture. The PIB-SXA primary network and the PIB-SXA/PS IPNs are exposed to UV/VIS to show the correlation between crosslink density and UV absorbance capability. %Transmittance capacity of both PIB-SXA primary network and PIB-SXA/PS interpenetrating network were recorded between 190-750 nm and %Transmittance value at 350 nm of both samples were detected [3].

As seen in Figure 3.9, PIB-SXA/PS IPN is much more sensitive to UV irradiation than PIB-SXA primary network [3]. While %Transmittance of PIB-SXA primary network is equal to 99.85% at 350 nm, this value decreases to 91.05% for PIB-SXA/PS interpenetrating network. In addition, aromatic compounds in the PS part of IPN are well known to lead to yellowish material following UV irradiation.; however, the PS phase inside the IPN structure is protected from UV irradiation to a certain extent [3].

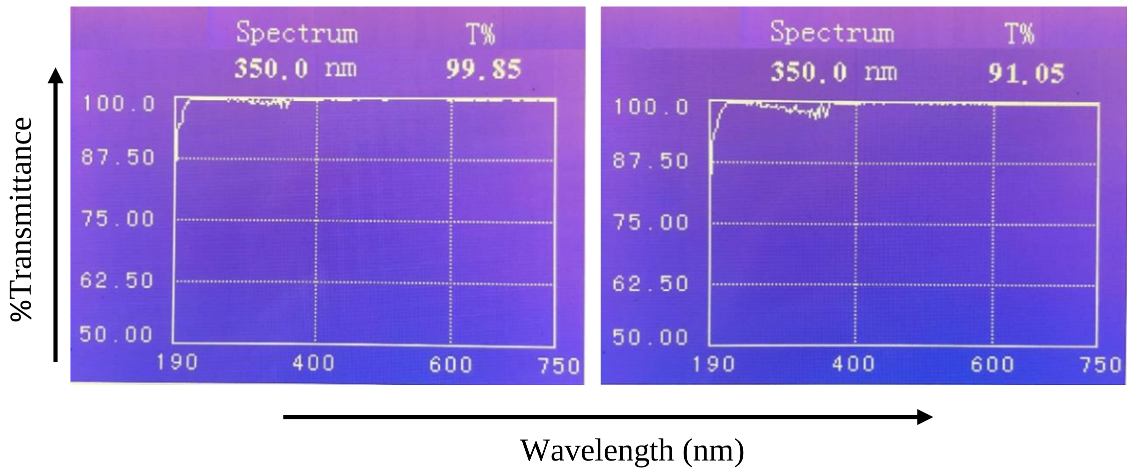

a) PIB-SXA

b) PIB-SXA/PS IPN

Figure 3.9: UV/VIS spectrum (at 350 nm) of (a) PIB-SXA primary network and (b) PIB-SXA/PS interpenetrating network.

The UV absorbance is directly proportional to PS contributed crosslink density of material. As shown in Table 3.2, the crosslink density of PIB-SXA/PS interpenetrating network (~0.0022 mol/L) is higher than PIB-SXA (~0.001 mol/L). As a result, PIB-SXA/PS interpenetrating network has higher absorbance thus lower %Transmittance [3, 51].

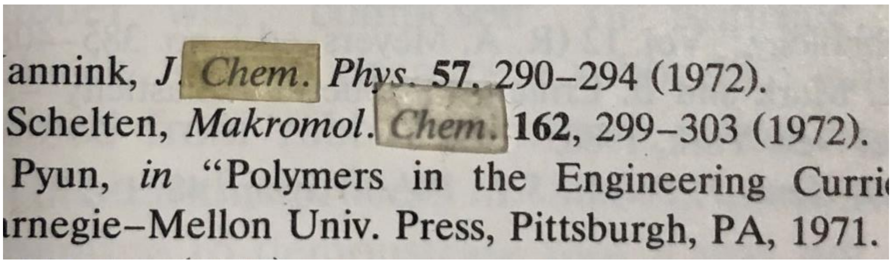

annink, *J. Chem. Phys.* **57**, 290–294 (1972).
Schelten, *Makromol. Chem.* **162**, 299–303 (1972).
Pyun, *in* "Polymers in the Engineering Curri
ırnegie–Mellon Univ. Press, Pittsburgh, PA, 1971.

Figure 3.10: Image of optical clarity of PIB-SXA Primary Network (*lower sample*) and PIB-SXA/PS Interpenetrating Network (*upper sample*)

In addition, sequential interpenetrating network formation with polystyrene did not affect VIS range transparency, thus PIB-SXA/PS IPN did not show any absorbance in visible range (380-740 nm) by exhibiting almost similar optical clarity with primary network as seen in Figure 3.8 and 3.10 [3].

3.1.4. Thermal Properties of PIB-SXA and PIB-SXA/PS IPN

It is commonly known that PIB rubbers have unique physical and mechanical properties which include resistivity for air and moisture permeability, high elasticity, and flexibility at extremely low temperatures; also, the glass transition temperature (T_g) of PIB can be as low as -76^{0}C [3]. After network formation, due to crosslinked structure, the glass transition temperature of PIB-SXA shifted to higher temperature and reached -57^{0}C [3, 52] (see in Figure 3.11).

Despite of their different single PIB network and IPN synthesis methods, Vancaeyzeele's et al. reported that the primary PIB network displays an α-relaxation with a peak centered at 30^{0}C, which corresponds to T_α of PIB, and a low temperature shoulder at -50^{0}C, also observed in other PIB based materials. [3]. Different synthesis and network preparation methods create difference in the crosslinking density and so in thermal glass transition temperature. With IPN formation, the glass transition temperature of PIB phase shifted to -54.13^{0}C (Figure 3.11). Since the thermal stability of polymers is enhanced by crosslinking, this 3^{0}C shifting (from -57^{0}C to 54.13^{0}C) is an expected result [52].

PIB-SXA/PS IPN synthesis is sequential, and the formation of polystyrene (PS) network occurred in the presence of PIB network. The network interpenetration degree significantly depends on the properties of particular polymer pair, and sometimes simultaneous IPN formation method and sometimes sequential formation, i.e., one after the other network, gives the best result [3].

The initial distribution of styrene in the PIB primary network directly affects the interpenetration degree and morphology of final structure. DSC measurements have carried out for also determining the glass transition temperature of PS phase. There are some examples in literature where no exploitable transition has been detected. In PIB-SXA/PS IPN structure, two minor heat flow changes have been determined. In many literature studies, T_g at 100^{0}C is often given for polystyrene [53]. Due to the network formation, higher thermal relaxation temperatures with crosslinking can be detected by the shift of T_g value of homopolymers to higher degree [11, 52]. Therefore, 4.96^{0}C increasing in T_g value belonging to PS part is an expected result. Also, in PS phase shows a second exothermic heat flow change at 164.21^{0}C because of multiple relaxation for PS phase depending on different crosslinking density. There is an example, in the literature, reported that PS single network shows α-relaxation at 132^{0}C [3]. 30^{0}C shifting to higher temperature for PIB-SXA/PS IPN is evidence for availability of higher crosslinking in PS phase of IPN than in primary PS network.

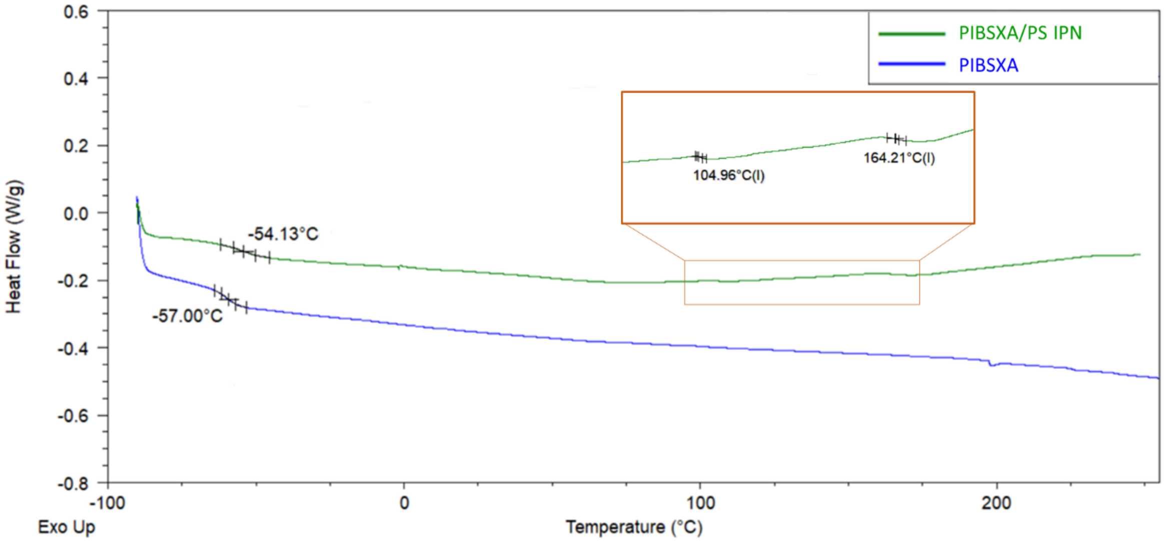

Figure 3.11: DSC curve of (a) PIB-SXA primary network (*lower and blue one*)
(b) PIB-SXA/PS IPN (*upper and green one*)

Thermal stability of polymeric materials has been determined using thermogravimetric analysis which has shown to be one of the most successful method for thermal studies. By blending with other polymers, it is possible to significantly alter the thermal stability of individual polymers. Regardless of the composition, the thermal characteristics of IPN systems are better than their corresponding homopolymers, and it is mainly based on the networking of primary phases. For example, Mathew et al. reported that poly(ether urethane)/poly(ethyl methacrylate) IPNs showed improved thermal properties due to the higher crosslink density in the networks [52].

In literature, 360-380^{0}C has regularly been shown as an onset of the degradation temperature of PIB [54]. The DTGA curve shows that PIB network is stable up 350^{0}C and after that degradation occurs rapidly. The degradation starts at about 360^{0}C and at 450^{0}C almost 98% degradation is complete. The onset the degradation temperature of PIB-SXA is higher than PIB homopolymer structure most probably due to the intensive crosslinking [11, 52].

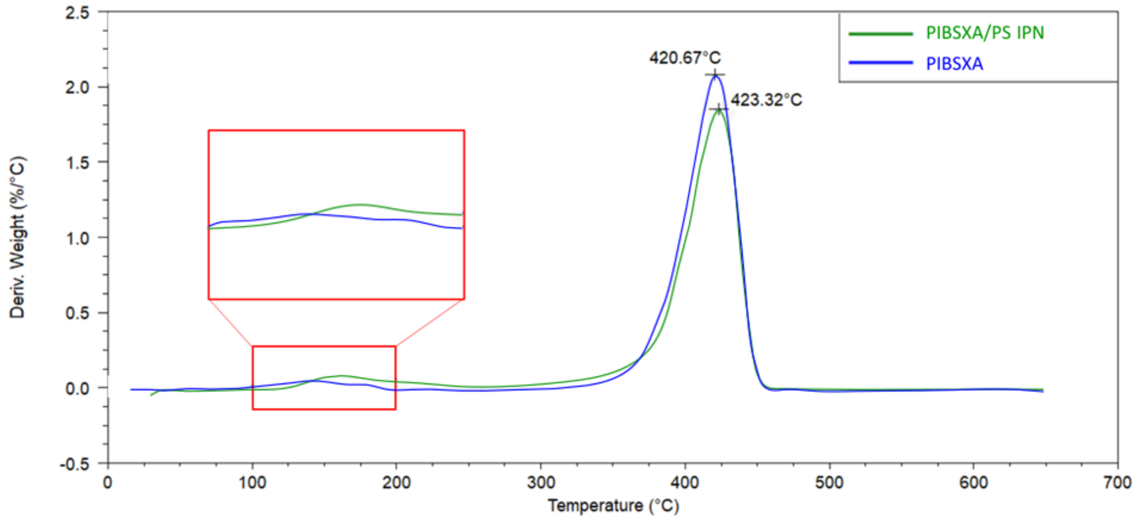

Figure 3.12: DTGA thermograms of (a) PIB-SXA primary network (*blue*) (b) PIB-SXA/PS IPN (*green*)

The molecular weight of PS decreases between 200^0C and 300^0C without the release of volatile compounds, also below 300^0C, random scission of PS chains takes place as follows [52, 55].

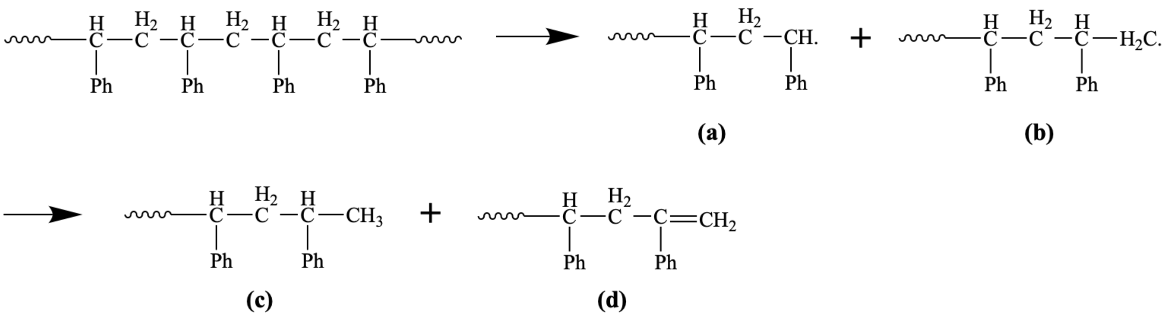

According to published studies, no volatile compounds are generated, and (a) and (b) give disproportionation reaction to produce (c) and (d) that are stable below 300^0C. However, above 300^0C, PS degrades and produces a mixture of styrene, toluene, methyl styrene, etc. [56]. In addition, Mathew et al. reported that polystyrene degrades in a single step and this degradation reaction starts at approximately 276^{0}C. Also, 96% PS degradation is almost completed ~385^{0}C with the major thermal degradation peak in the DTGA occurring at 360^{0}C. Because of close degradation temperature range of PIB and PS, the major peak of PS cannot be observed. However, the DTGA thermogram of PIB-SXA/PS IPN has a shoulder at 385-397^{0}C range which accepted as a thermal degradation of PS part in network system (Figure 3.12).

As a result, since IPNs have higher thermal stability than their pure polymer components due to increased crosslink density and higher entanglement density, the degradation temperatures of polymers in IPNs shifts to a higher temperature. Thus, the temperature shifting in PIB-SXA/PS IPN thermogram (according to thermogram of PIB-SXA and theoretical results about PS) is expected [52].

The TGA curve of PIB-SXA/PS IPN shows almost 10% degradation between 120^{0}C – 200^{0}C (insert of Figure 3.12). Kaya et al. reported that the presence of water has been indicated by the weight losses in TGA and DTGA ranging from 3 and 25% corresponding to the loss of crystallization water (between 50^{0}C and 150^{0}C) and coordination water (between 150^{0}C and 200^{0}C) in the sample at the beginning [57]. The presence of trace amount of water, most probably coming from insufficient drying during the whole process, in initial PIB-SXA/PS IPN was also shown in FTIR spectra (see in Figure 3.7).

3.1.5. Morphological and Mechanical Properties of PIB-SXA and PIB-SXA/PS IPN

SEM images comparison of PIB-SXA films, for both their air and Teflon surfaces, is the evidence of that there is homogeneous distribution of carbon, oxygen and sulfur elements in the network structure (Figure 3.13), on both side and there were not any UV light penetration problems during primary network preparation.

a) Air surface of PIB-SXA

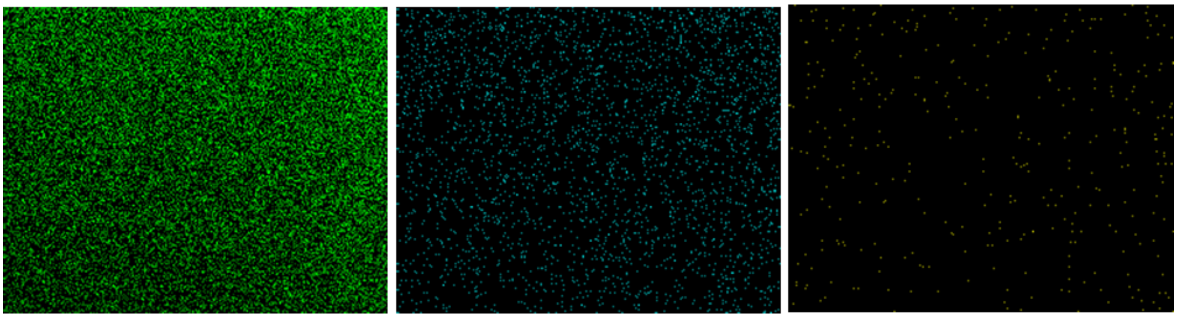

b) Teflon surface of PIB-SXA

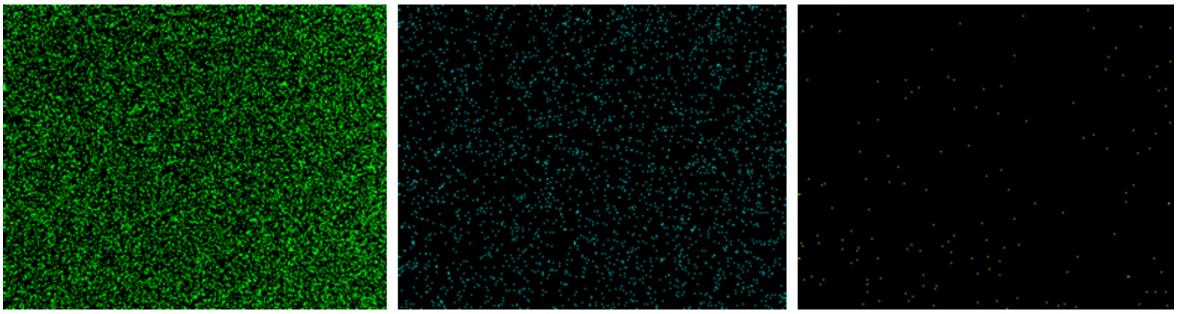

Figure 3.13: SEM images of PIB-SXA with carbon, oxygen and sulfur mapping, respectively (a: air surface and b: teflon surface.)

It is predicted that homogeneous network structures can be obtained by the help of Thiol-ene (click) chemistry. When compared to traditional photoinitiated systems, the overall easiness, mechanism, and durability of Thiol-ene photopolymerization reaction are superior. Since it forms homogeneous are predictable polymer network via a chain-growth and step-growth polymerization mechanisms, with greatly simplified polymerization kinetics, lack of sensitivity to oxygen inhibition, lowered stress and shrinkage. Therefore, Thiol-ene networks have significant advantages over traditional networks, including the fact that they can be formed rapidly and in large quantities under ambient atmospheric conditions, producing nearly ideal and uniform polymer networks free from the heterogeneity that often characterizes radical photopolymerization reactions. With these analyses, the homogeneity of Thiol-ene photopolymerization can be proved by the homogeneous distribution of carbon, oxygen, and sulfur elements in the primary network structure [12].

Dynamic mechanical properties of network films were determined by using a dynamic mechanical analyzer. The Young's modulus (*E*) was determined from the initial slope of graph which is equal to the ratio of tensile stress (σ) and strain (ε) [36],

$$E = \frac{\sigma}{\varepsilon}. \tag{3.1}$$

The strain value of initial (elastic) region can be predicted by using the following formula [36]:

$$\varepsilon = \frac{\Delta l}{l_0}, \tag{3.2}$$

where l_0 is the initial length of polymer film and Δl is the deformation. According to these data, the Young's Modulus (*E*) of PIB-SXA primary network film was calculated as 290 kPa (see in Figure 3.14).

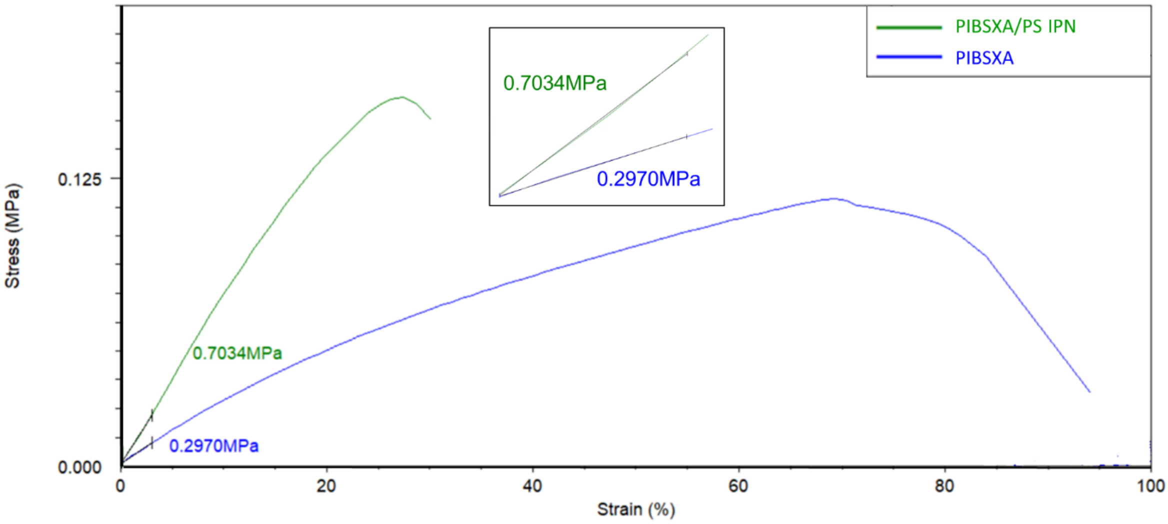

Figure 3.14: Stress-strain curve of PIB-SXA primary network (*blue*) and PIB-SXA/PS interpenetrating network (*green*).

Phase separation, which happens as a result of decrease in miscibility when monomers polymerize, is observed in multicomponent systems (especially in interpenetrating network systems). However, crosslinking, which results a decrease in phase separation and particularly in domain size, frequently leads to formation of 10-100 nm phase domains. In addition to domain size, shape of domain, the degree of continuity and interfacial bonding effect the phases and these characteristics create the morphological details, which have a strong impact on the physical and mechanical behavior of material [58].

As reported in literature [11, 58], interpenetrating network systems, which are made of two or more crosslinked polymers permanently entangled and bound together, have been defined as a relatively new type of polymer alloys. The IPN formation has the ability to reduce the degree of phase separation in final material when the reacting components are thoroughly mixed and polymer chains of different networks permanently interlocked together. Therefore, the physical and especially mechanical characteristics of polymers can be greatly enhanced by the IPN structure formation, and the improved interfacial bonding and increased crosslink density, occurring when two polymer networks interpenetrate one another, are related with this synergetic impact [59]. As a result, the limited phase separation due to increased crosslinking of polymer network cause an enhanced tensile modulus and tensile strength in IPNs structures.

The Young’s modulus (*E*) values were calculated from the initial slope of the Stress-Strain curves of PIB-SXA network and PIB-SXA/PS IPN. As seen in Figure 3.14, while the Young’s modulus of PIB-SXA is about 0.297 MPa, after interpenetration with PS, the *E* value increases more than two times, to 0.7034 MPa.

Vancaeyzeele’s et al. synthesized PIB single network with urethane-based crosslink which is a different method from Thiol-ene chemistry and so the Young’s modulus was reported as 0.2 MPa [3]. PIB-SXA network, on the other hand, shows higher indeed rigidity due to its effective crosslinking via special synthesis technique named as Thiol-ene chemistry [12]. In addition, same research group synthesized (70/30) PIB/PS IPN (wt%/wt%) via sequential method having approximately 2 MPa Young’s modulus. Although PIB-SXA/PS IPN and this network have same composition ratio, the difference in activation method for the crosslinking reactions (thermal vs UV) may result in lower rigidity (initial modulus) due to the less effective polymerization of styrene [3].

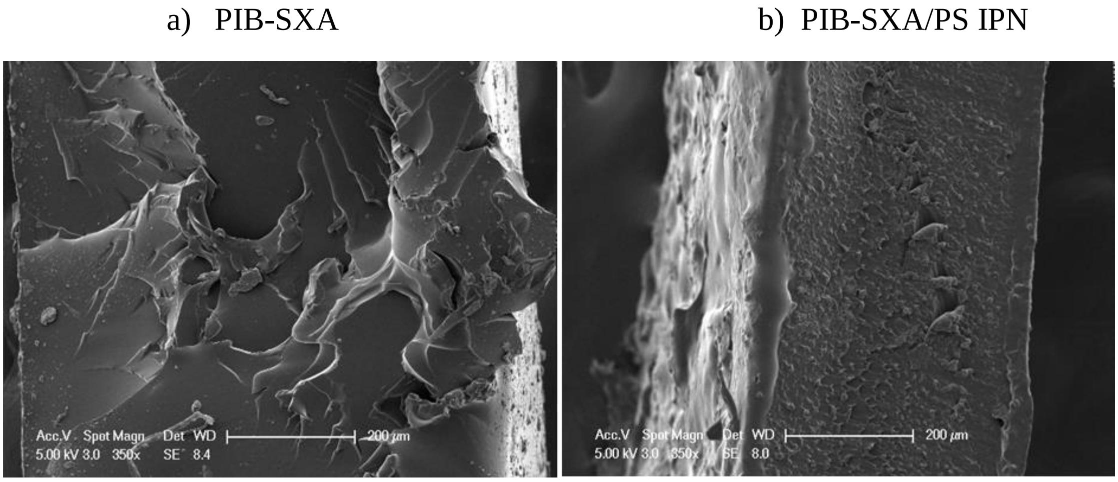

a) PIB-SXA

b) PIB-SXA/PS IPN

Figure 3.15: SEM images of (a) PIB-SXA and (b) PIB-SXA/PS IPN fracture surface after tensile testing.

Due to higher crosslink density and more interfacial bonding, elongation at break rapidly decreases to 65.16% for PIB-SXA/PS IPN structure. In detail, with same experimental conditions, while PIB-SXA network can reach 94.18% elongation to break, PIB-SXA/PS IPN only reaches 30.02%. Elongation at break of IPN structures has a tendency that is opposite of their tensile strengths, as is common in many other polymeric materials. Therefore, low modulus materials show a more ductile profile whereas high modulus polymers exhibit a brittle fracture [59]. Observations of cross-sectional surface of fractured PIB-SXA and PIB-PSXA/PS IPN membranes made with the aid of SEM are illustrated in Figure 3.18. While PIB-SXA (Figure 3.15a) exhibits a ductile like fracture surface, PIB-SXA/PS IPN shows a homogeneous and brittle fracture surface conforming high modulus value given in Figure 3.14, and not any pullout of domains can be observed (Figure 3.15b) [59].

A polymer deforms in response to an applied stress during mechanical test because the polymer chains gradually slide past one another. Creep is the term used to describe the gradual deformation (progressive deformation) of a material under constant stre~~ss~~ and isothermal circumstances. Also, it is generally understood that the change in conformations and reorganizations of the molecules (especially chains) in a polymeric material causes creep. Therefore, large-scale rearrangements of the atoms can also be observed if the polymeric material has enough molecular mobility as a result of increase in applied stress and temperature. On the other side, creep-recovery occurs after creep when the applied stress is taken off and the polymer chains in material return to their initial conformations and arrangements. Until today, the majority of creep and creep-recovery experiments have been conducted on reinforced plastics, adhesives and especially on thermoplastics in order to assess the durability of polymeric materials which are subjected to constant and continual stresses at different conditions over extended periods of time [60].

Deformation and permanent deformation of networks (both PIB-SXA and PIB-SXA/PS IPN) was determined by using a dynamic mechanical analyzer with creep mode under constant stresses of 0.05 MPa at 24^0C for 15 min, and creep recovery followed by removing applied stress for 25 min.

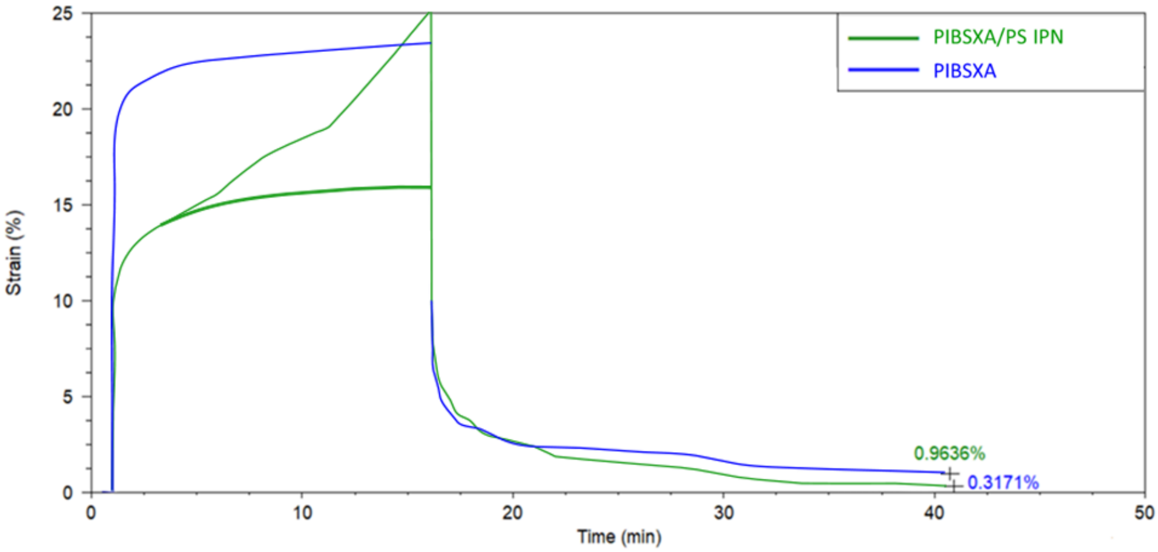

Figure 3.16: Creep behavior of PIB-SXA (*blue)* and PIB-SXA/PS IPN (*experimental result in green line, assumed data in green thick line*)

As seen in Figure 3.16, the permanent deformation of polymer PIB-SXA and PIB-SXA/PS IPN were approximately equal to 0.96 % and 0.32%, respectively, which indicates high network quality for both particularly for the latter. However, there are two unexpected rising points in strain% of PIB-SXA/PS interpenetrating network although stress value, equal to the experimental parameter of PIB-SXA primary network, is suitable for this material. Therefore, it is assumed that these sharp increase in strain% of IPN due to the tearing of the film during the experiment. After PIB-SXA/PS interpenetrating network sample reached ~15% strain at, the tearing of film from its defect points could start so strain% started to gradually increase until 12th minute. At this stage, the defect point could be completely torn thus a sharp increase in strain% could be observed after 12th minute to due to decreased cross-sectional area. If strain% of IPN was equal to 15%, which was just recorded before tearing begins; the strain% difference between PIB-SXA primary network and PIB-SXA/PS interpenetrating network would be consistent with their crosslink nature of them. In literature, there are many examples about crosslink density and dynamic creep behavior of polymer materials. Pavka et al. proved that the $\overline{M}_c$ for the arborescent thermoplastic elastomers (TPEs) and polymeric networks was found to rise with the increasing dynamic creep, stored energy, and loss energy. Therefore, more slack was simply provided in these materials via greater $\overline{M}_c$ values. More strain could be applied as $\overline{M}_c$ values rise before running into a resistance to deformation, which would appear as physical crosslinking, chemical crosslinking and entanglement at the junction of the rubbery and glassy phases. Thus, more dynamic creep was possible due to increased slack in the polymeric network structure. As a result, increasing crosslink density and decreasing $\overline{M}_c$ provide higher strain% value but lower permanent deformation behavior [61].

As a result, although PIB-SXA/PS interpenetrating network sample tore during creep testing and completed experiment with lower cross-sectional area, highly crosslinked PIB-SXA/PS interpenetrating network has ~15% stain with 0.32% permanent deformation, while PIB-SXA has ~23% strain with 0.96% permanent deformation. It is assumed by this study that if PIB-SXA/PS interpenetrating network sample did not tear during creep testing, its permanent deformation value could be lower than 0.32%; however, despite of this situation, creep recovery performance of PIB-SXA/PS interpenetrating network is higher than PIB-SXA [60, 62].

The origin of hardness measurements is based on the testing of metal samples, and they can be easily and rapidly performed for testing of solid samples. Also, these types of tests are useful for specification and quality control reasons. In literature, there are many examples related with hardness measurements of composite filling materials, and these tests are classified and defined by the dimensions and shape of indenter, and the applied force. In detail, when a force is applied to a solid material, such as composites, metals, glassy polymers and calcified tissues, a permanent indentation is created, and the hardness value generally equals to the load per unit surface area of indentation [63].

Additionally, some hardness tests, such as Shore hardness, can be performed elastomeric materials. Like in other hardness measurements, Shore hardness testing can be used for quick and simple quality control procedures. However, in contrast to the tests mentioned above, the characteristics of what being quantified are entirely different. When it comes to elastomeric materials, the indentation is mostly elastic in nature which means it may be recovered.

Therefore, depending on the type of test, the indenter shape changes and for Shore hardness measurements, the appropriate equation is [63]:

$$F = \frac{2aEw}{1-v_2}, \tag{3.3}$$

where F = force, E = Young's Modulus, a = the radius of the indenter, w = the depth of indentation, and v = Poisson's ratio.

Because of elastomeric materials are reasonably incompressible [63], v is taken as 0.5 and Eq. (3.4) becomes:

$$F = \frac{8}{3aEw}. \tag{3.4}$$

As can be seen from the equations above, there is a direct relation between Young's modulus (E) and the degree of indentation (w) against a constant force (F). Therefore, there should be a direct relationship between Young's modulus (E) and Shore hardness as well as Shear (rigidity) modulus (G), as for elastomers at minor strains "E=3G".

Shore A hardness testing was carried out using Micro-O-Ring Hardness Tester. The minimum dwell time of 1 s was used to minimize creep effects and test carried out approximately 22^{0}C. Both PIB-SXA and PIB-SXA/PS IPN have close thickness value, which are equal to ~0.7 mm, and a minimum five readings was used to calculate the mean value of Shore A hardness for each sample. According to these experimental conditions, while average Shore A hardness value of PIB-SXA is equal to 81.7 and PIB-SXA/PS IPN approximately exhibits 88.2. This result is quite reasonable since the modulus and hardness are directly proportional to each other and both increase with the increased crosslink density.

3.1.6. Network Properties of PIB-SXA and PIB-SXA/PS IPN

3.1.6.1. Gel Fraction of PIB-SXA

The leaching test was used to determine the gel fraction of prepared primary networks film by identifying unreacted starting materials. The gel fraction of films was calculated by following formula based on leaching percentage:

$$Gel\ Fraction = \frac{m\prime}{m}\ x\ 100\ \%\ , \tag{3.5}$$

where *m* is the mass of dry network film after curing and *m'* is the mass of dry network film after leaching test [44].

According to above formula, the gel fraction of primary network was calculated as 90%. It is the evidence of that the yield of network formation reaction was very high.

3.1.6.2. Density Determination of PIB-SXA

Pycnometer was used to determine the density of PIB-SXA network by following formula:

$$Density\ (polymer) = \frac{w_p + d_w}{w_2 + w_p - w_3}\ , \tag{3.6}$$

where d_w is the density of water, w_p is the weight of polymer network, w_2 is the weight of empty pycnometer and water, w_3 is the weight of empty pycnometer, water and polymer. According to that, the density of polymer network was calculated as 0.9096 g/cm^3.

3.1.6.3. Swelling Properties of PIB-SXA and PIB-SXA/PS IPN

In network systems, crosslink density is an important knowledge since it effects the mechanical properties of them and how they behave in practical applications. The crosslinked structure of polymers was characterized by the calculation of $\overline{M}_c$ and mesh size, which decreases with the increasing crosslinking density. Since swelling data of the polymers are used in the calculation of $\overline{M}_c$, the $\overline{M}_c$ values should reflect the same trends as those for swelling. It is also known that interpenetration of one polymer network with another increases the effective crosslinking density, resulting in a lower $\overline{M}_c$ for IPN structure [44].

All samples were dried in vacuum oven to remove the solvent used in curing. Two pieces of network films, which have different length but same thickness, were cut from vacuum-dried samples. For both primary and interpenetrating networks, one of them was used in swelling test with THF (which was as a solvent for synthesis part) and the other one was swollen in cyclohexane, which is a good solvent for PIB, at room temperature. For these two systems, a travelling microscope was used to determine the exact length change of samples for 4 days. The volume swelling ratio [44] of network films was calculated by:

$$Q = \frac{v_{2,r}}{v_{2,s}}, \tag{3.7}$$

where $v_{2,r}$ is the volume fraction of polymer of relaxed film in THF and $v_{2,s}$ is the volume fraction of polymer of swollen film in cyclohexane. Equilibrium polymer volume fraction variables were calculated by following formulas [14]:

$$v_{2,s} = \left[1 + \frac{(q_{cyc}-1)\rho_p}{\rho_{cyc}}\right]^{-1}, \tag{3.8}$$

$$v_{2,r} = \left[1 + \frac{(q_{THF}-1)\rho_p}{\rho_{THF}}\right]^{-1}, \tag{3.9}$$

where q_{cyc} is the volume swelling ratio of network films after equilibrium swelling in cyclohexane, q_{THF} is the volume swelling ratio of network films after equilibrium swelling in THF. ρ_p is the density of polymer film (0.9096 g/cm^3) which was calculated at 3.1.6.2.,

ρ_{cyc} is the density of cyclohexane (0.7781 g/cm^3) and ρ_{THF} is the density of THF (0.8892 g/cm^3).

According to Flory’s original equilibrium swelling theory, an initially non-solvated and crosslinked network sample swells by absorbing solvent until the rise in elastic energy of the polymer chains constituting the network balances the loss in free energy caused by mixing of polymer chains with solvent molecules [64]. For both PIB-SXA and PIB-SXA/IPN, the average molecular weight between crosslinks ($\bar{M}_c$) was calculated using the method defined by Peppas and Merrill, 1977 to characterize swollen networks [14, 64, 65]:

$$\frac{1}{\bar{M}_{c,s}} = \frac{2}{\bar{M}_n} - \frac{(\frac{\bar{v}}{V_1})\ x\left[\ln(1-v_{2,s})+v_{2,s}+\chi\,(v_{2,s})^2\right]}{\left[(v_{2,s})^{1/3}-\frac{1}{2}v_{2,s}\right]}\ , \tag{3.10}$$

where “s” indicates swelling based calculations.

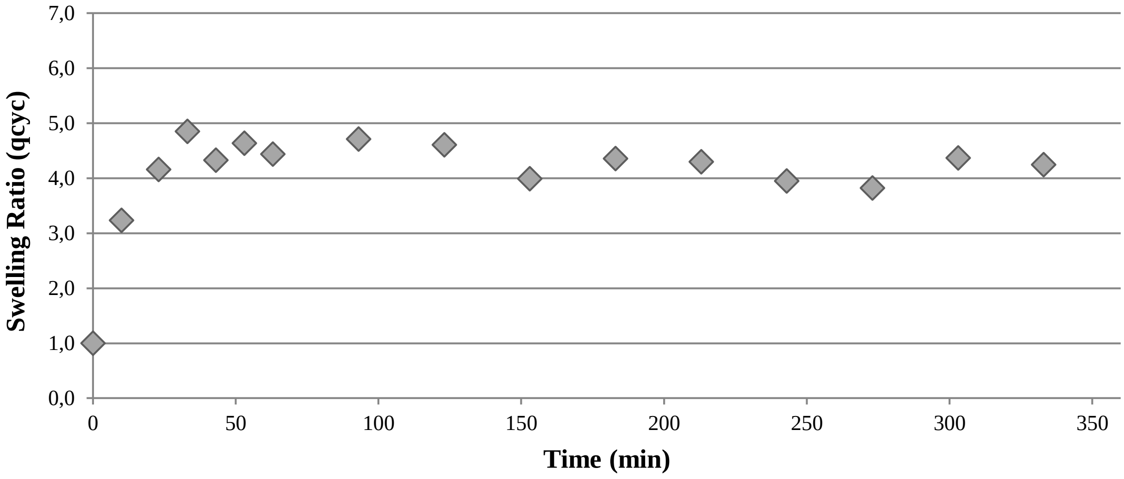

Figure 3.17: Swelling trend of PIB-SXA primary network in cyclohexane medium at room temperature (*used data for $\bar{M}_c$ calculation).

For the characterization of PIB-SXA primary network, $\bar{M}_{c,s}$ is the number average molecular weight between crosslinking points, $\bar{M}_n$ is the number average molecular weight of the uncrosslinked HS-PIB-SH polymer chains (2018 g/mol), χ is the polymer-solvent interaction parameter (0.403 for cyclohexane - PIB systems) [14], $\bar{v}$ is the specific volume of polymer (1.10 cm^3/g for PIB) [14], V_1 is the molar volume of solvent (108.1 mL/mol for cyclohexane), and $v_{2,r}$ and $v_{2,s}$ are the volume fractions of polymer in the relaxed gel and swollen gel, respectively [14]. (Figure 3.17)

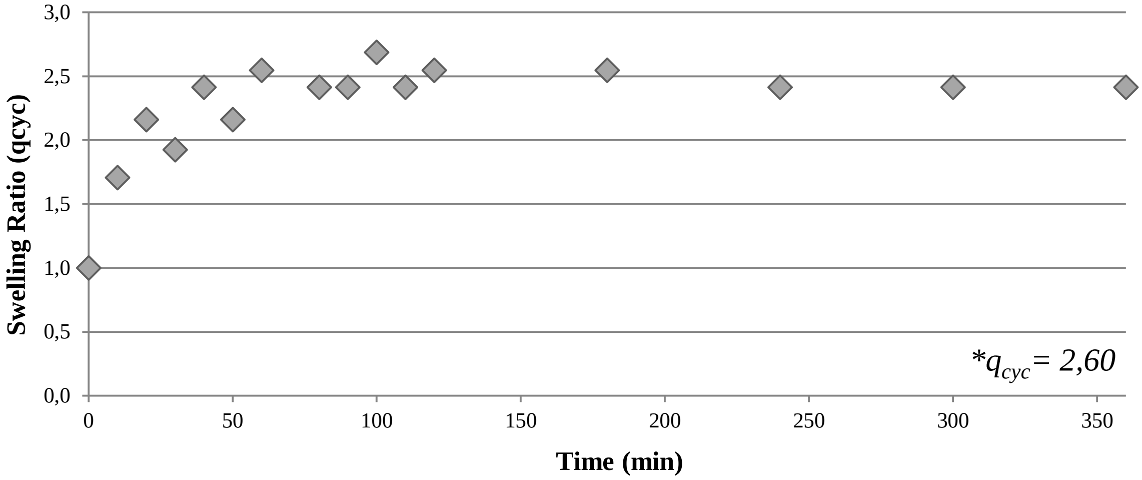

Figure 3.18: Swelling trend of PIB-SXA/PS IPN in cyclohexane medium at room temperature. (*used data for $\overline{M}_c$ calculation)

For the characterization of PIB-SXA/PS interpenetrating network, $\overline{M}_{c,s}$ is the number average molecular weight between crosslinking points, $\overline{M}_n$ is the number average molecular weight before crosslinking (which is the average value: 1061.075 g/mol), $\bar{v}$ is the specific volume of the polymers (which is the average value: 1.0275 cm^3/g), V_1 is the molar volume of solvent (for cyclohexane: 108.76 mL/mol and for THF: 79.76 cm^3/mol), and χ is the Flory–Huggins interaction parameter of polymer-solvent (which is the average value: 0.4515), $v_{2,r}$ and $v_{2,s}$ are the volume fractions of polymer in the relaxed gel and swollen gel, respectively (Figure 3.18).

For both network systems, the shear modulus (G) was calculated from the Young's modulus (E) value by following formula [44]:

$$G = \frac{E}{2(1+v)}\,, \tag{3.11}$$

where v is a Poisson's ratio and assumed to be 0.5 for this experiment [44]. The average molecular weight between crosslinks $\bar{M}_{c,T}$ [64] was calculated from tensile testing by using the following equation where "*T*" indicates tensile stiffness-based calculations:

$$\frac{1}{\bar{M}_{c,T}} = \frac{G\ x\ Q^{1/3}}{R\ x\ T\ x\ C_{2,r}} + \frac{2}{\bar{M}_n}, \tag{3.12}$$

where $C_{2,r}$ is the mass concentration of polymer film in the experimental solution before crosslinking step (0.335 g/mL in THF for PIB-SXA and 0,306 g/mL in THF for PIB-SXA/PS IPN), T is the temperature at which tensile testing were applied (298 K) using TA instrument in a strain mode and R is the gas constant (8.31 kPa L/mol K).

The crosslink density of polymer networks (ρ_c) was predicted by following equation [14, 44, 64]:

$$\rho_c = \frac{1}{v\ x\ \bar{M}_n}, \tag{3.13}$$

The mesh size of polymer networks [14, 44] was determined as described by Lee et al. [65]. The average end-to-end distance of the polymer chain in the unperturbed (solvent-free) state was determined by the following equation:

$$([r_0^{-2})]^{1/2} = l\ x\ C_n^{1/2}\ x\ n^{1/2}, \tag{3.14}$$

where $([r_0^{-2})]^{1/2}$ is the end-to-end distance of polymer chain in the unperturbed state, l is the average bond length (0.154 nm for both PIB-SXA and PIB-SXA/PS IPN) [14], C_n is the characteristic ratio of polymer (6.73 for PIB-SXA [14] and 8.765 for PIB-SXA/PS IPN) and n is the number of bonds in the crosslinked network system which was calculated as:

$$n = 3\ \frac{\bar{M}_c}{M_r}, \tag{3.15}$$

where M_r is the molecular weight of repeating unit of network system (56.11 g/mol for PIB-SXA and 80.13 g/mol for PIB-SXA/PS IPN).

According to these terms, mesh size of polymer networks can be determined by following formula [14, 44]:

$$\xi = \left(v_{2,s}\right)^{-\frac{1}{3}}([r_0^{-2})]^{\frac{1}{2}} . \tag{3.16}$$

Table 3.1. summarizes mesh size, crosslink density and $\bar{M}_c$ of polymer networks depending on swelling properties and tensile stiffness.

Table 3.1: Average molecular weight between crosslinks ($\bar{M}_c$), crosslink density (ρ_c), and mesh size (ξ) of network obtained from swelling studies and tensile testing of PIB-SXA primary and PIB-SXA/PS interpenetrating networks

PIB-SXA	**SWELLING DATA**	**TENSILE DATA**
$\bar{M}_c$ (g/mol)	906.7	900.2
ρ_c (mol/L)	0.001	0.001
ξ (nm)	4.94	4.93
PIB-SXA/PS IPN	**SWELLING DATA**	**TENSILE DATA**
$\bar{M}_c$ (g/mol)	441.5	456.2
ρ_c (mol/L)	0,0022	0,0021
ξ (nm)	3,3	3,4

Although different formulation steps were followed for $\bar{M}_{c,T}$ and $\bar{M}_{c,s}$ calculations as explained above, the results are very close to each other. It has also found that the $\bar{M}_c$ determined by elastic modulus differed little from the $\bar{M}_c$ derived only from swelling because chains defects in network structure had a lesser impact on swelling than on tensile behavior [44, 64]. The comparable results of swelling and tensile testing indicate successful crosslinking in the PIB-SXA primary network and PIB-SXA/PS interpenetrating network. Also, according to the comparative data of PIB-SXA and PIB-SXA/PS IPN, the decrease in $\bar{M}_c$ and mesh size (ξ), and increase in crosslink density (ρ_c) are proof of successful interpenetration of one polymer network (PIB-SXA) with another (PS).

3.2. New PIB based Polyurethanes

Polyurethane thermoplastic elastomers have a two-phase morphology in which the hard segments create distinct hard domains distributed in a soft segment matrix. Conventional and commercially available polyurethanes, including polycarbonate, polyether or polydimethylsiloxane soft segments or a combination of them, exhibit excellent mechanical, but are susceptible to hydrolytic–oxidative biological attacks and degrade rapidly after prolonged exposure to such chemicals [16].

More than two decades ago, PIB soft segment-based PUs were developed. It was hypothesized that (i) the incompatibility between the hard (polar urethane) and soft (nonpolar PIB) segments would result in outstanding phase separation between both phases, and (2) due to saturated PIB segments, the hydrolytic and oxidative stability of PIB based PUs would be exceptional. Also, to provide hydrolytic, oxidative, and chemical stability, PIB is utilized in a wide variety of products such as wire insulators, automotive inner tubes and many more. However, due to the absence of H-bondings between both polar hard and nonpolar soft segments, and excessive incompatibility between both phases, the mechanical properties of these early PIB based PUs were moderate to low despite of their outstanding hydrolytic and oxidative stability [18].

In this topic, the effect of sulfur-containing new polyisobutylene diol ($HO-CH_2CH_2-S-PIB-S-CH_2CH_2-OH$) usage and addition of organically modified montmorillonite (OmMMT) nanolayers on the mechanical properties of PIB based PUs were evaluated.

3.2.1. Sulfur-Containing PIB based PUs

Sulfur-containing PIB based polyurethane was prepared using a new polyisobutylene diol $HO-CH_2CH_2-S-PIB-S-CH_2CH_2-OH$ soft segment and conventional hard segments of BDO and MDI, and a new polyurethane containing 72.5% soft segment (PIB) and 27.5% hard segment was obtained (Figure 3.19). In this study, the sulfur effect on morphology, tensile strength, elongation, hydrolytic stability, creep resistance and thermal properties are evaluated and compared to similar polyurethane (PIB_O-PU) synthesized with HO-PIB-OH.

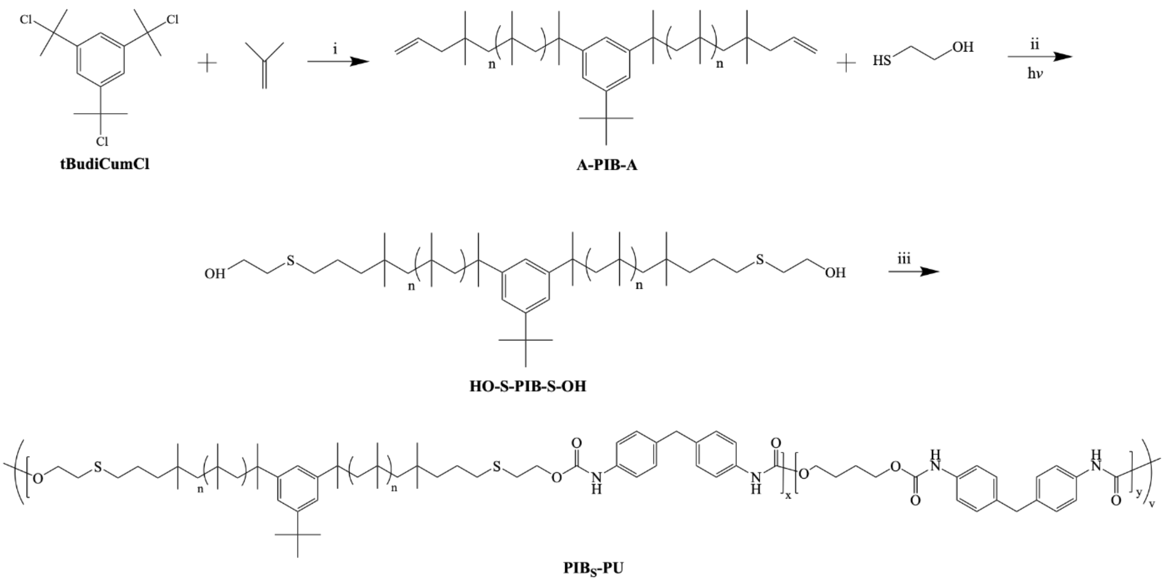

Figure 3.19: Reaction mechanism of PIB$_S$-PU synthesis (i=$TiCl_4$, TMEDA, ATMS, hexane, CH_2Cl_2; ii=DMPA, $CHCl_3$; iii=MDI, BDO, DBTDL, THF). Reprinted from [16].

3.2.1.1. Molecular Characterization

The a,ω-primary hydroxyl telechelic PIB (HO-S-PIB-S-OH) was synthesized quantitatively using photochemical Thiol-ene click reaction involving HS-CH_2CH_2-SH and A-PIB-A, followed by water washing. The ^{1}H NMR spectrum of HO-S-PIB-S-OH was shown in Figure 3.20. The methylene and methyl protons of PIB responsible for resonances between 0 and 2.0 ppm. The -S-CH_2-CH_2-O*H* proton occurs as a triplet at 2.22 ppm. The triplets at 2.57 and 2.82 ppm are caused by methylene protons close to sulfur atom whereas the doublet of triplets at 3.80 ppm is related to the methylene protons close to the -OH group (Figure 3.20) [16].

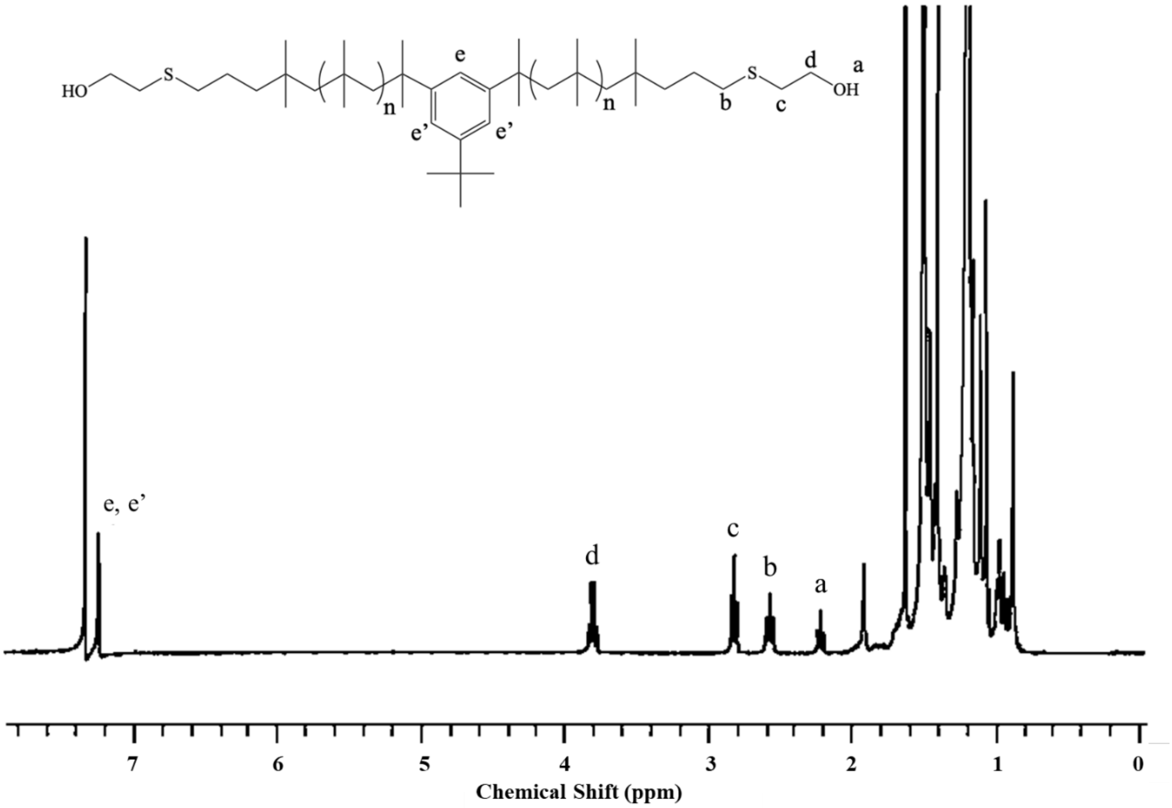

Figure 3.20: ^{1}H NMR spectrum of HO-S-PIB-S-OH (in $CDCl_3$) together with assignments. Reprinted from [16].

Figure 3.21 summarizes the ^{13}C NMR spectrum of A-PIB-A (i) and HO-S-PIB-S-OH (ii) and shows (1) the lack of $–CH_2–\underline{C}H=\underline{C}H_2$ carbons (116.95, 136.33 ppm) as well as an upfield shift of $-\underline{C}H_2–CH=CH_2$ carbon (from 50.53 to 45.08 ppm), (2) the presence of $–\underline{C}H_2-OH$ at 60.41 ppm, (c) the presence of $-\underline{C}H_2-S-\underline{C}H_2-CH_2-OH$ carbons at 32.86 and 35.28 ppm, and (d) the existence of $-CH_2-\underline{C}H_2-CH_2-S-CH_2-CH_2-OH$ carbon (one of the former allylic carbons) at 24.99 ppm [16].

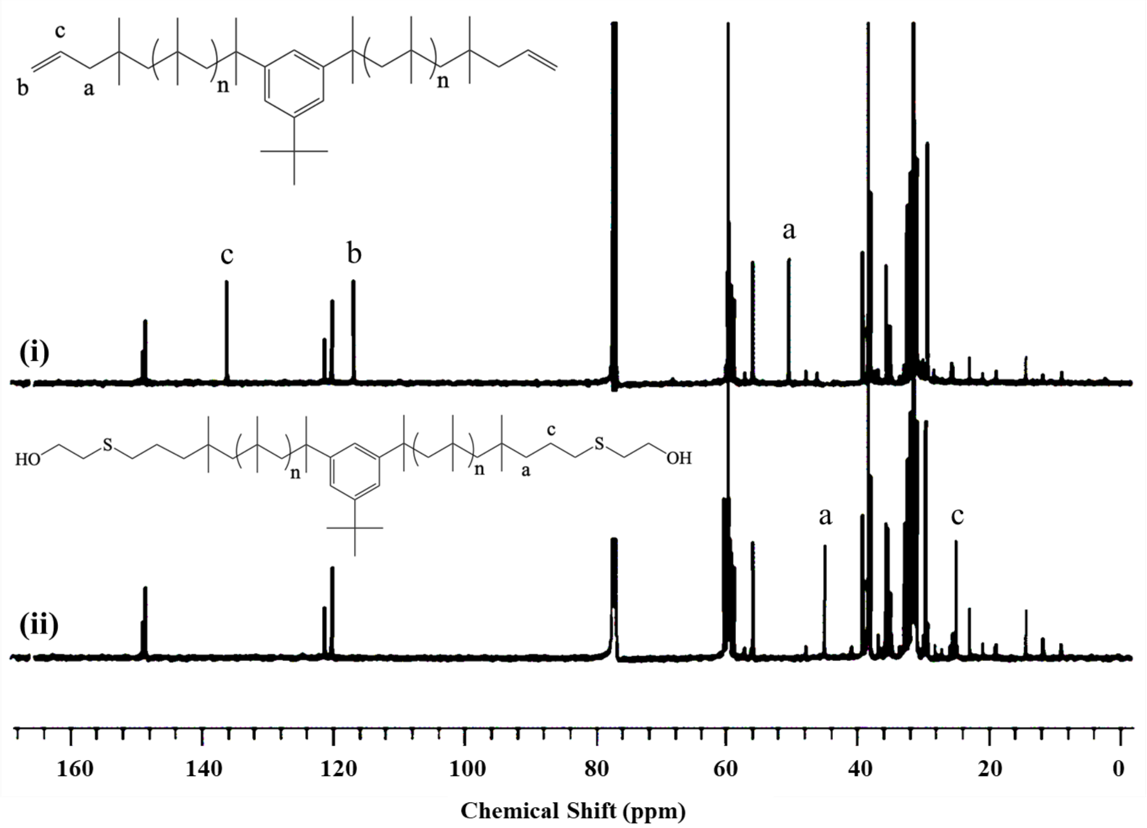

Figure 3.21: ^{13}C NMR spectrum of (i) A-PIB-A and (ii) HO-S-PIB-S-OH (in $CDCl_3$). Reprinted from [16].

Consequently, the successful preparation of HO-S-PIB-S-OH was proven by ^{1}H NMR, which also revealed the quantitative functionalization, and ^{13}C NMR spectra. The GPC trace of HO-S-PIB-S-OH exhibits the characteristics of a material with a well-defined low polydispersity (PDI = 1.02) (shown in Figure 3.22). Polymerization is indicated by the shift of the narrow peak.

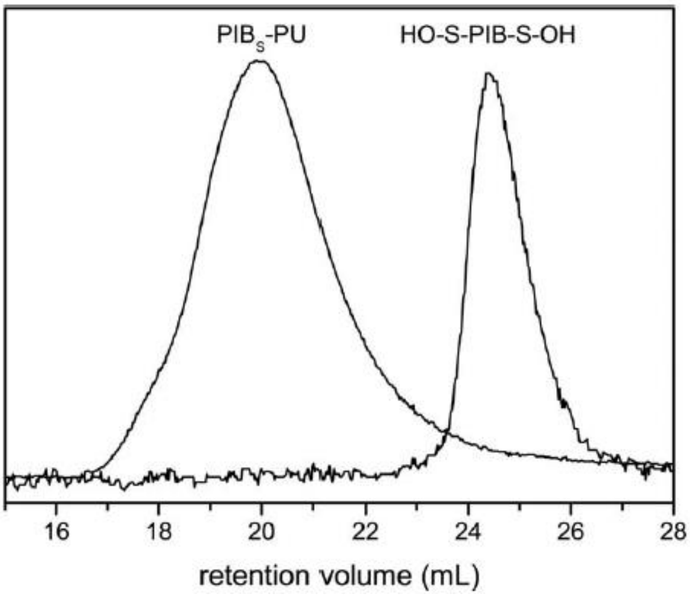

Figure 3.22: GPC traces of HO-S-PIB-S-OH and PIB$_S$-PU. Reprinted from [16].

(M_w ~ 3300 g/mol) associated with HO-S-PIB-S-OH to lower retention volumes (M_w ~ 160,000 g/mol). After polymerization, there is almost no unreacted HO-S-PIB-S-OH left (as shown by the absence of a hump at 25 mL in the PIB$_S$-PU trace). The PIB$_S$-PU trace exhibits only slight shoulder at ~18 mL which is most likely caused by allophanates [16].

^{1}H NMR of PIB$_S$-PU is shown at Figure 3.23 with assignments. The multiplets at 8.54 and 8.62 ppm are because of urethane linkages. The identifying signals of the hard and soft segments (of this PIB based polyurethane structure) are easily discernible. The triplets at 2.54, 2.74, and 4.20 ppm, respectively, represent the -C$\underline{H}_2$-S-CH$_2$-CH$_2$-O-, the -CH$_2$-S-C$\underline{H}_2$-CH-O-, and -CH$_2$-S-CH$_2$-C$\underline{H}_2$-O- protons. The singlet at 3.82 ppm is due to the methylene protons between the aromatic ring of MDI and the multiplet at 4.13 ppm indicates the methylene protons close to oxygen of BDO. Also, the resonances that occurs between 7.03 and 7.36 ppm point to the aromatic protons of MDI as well as the residue of the initiator that was used for the preparation of PIB$_S$-PU [16].

Polyurethane thermoplastic elastomers have a two-phase morphology in which the hard segments form separate domains being spread out within a matrix of soft segments, and the molar ratio of each hard and soft segments is determined by relative signal intensities in Figure 3.23. Based on ^{1}H NMR spectroscopy, the computed experimental molar ratio of

1/4.16/2.74 for PIB/MDI/BDO is extremely close to the theoretical molar ratio of 1/4.05/2.82. In addition, the various aliphatic protons of PIB and BDO contribute to resonances between 0-2 ppm. The signal at 7.64 ppm is attributable to the urea protons (NH) generated in the presence of moisture during PIB$_S$-PU synthesis. The extremely small resonance at 10.78 ppm presumably results from allophanate N-H protons and the NH allophanate content in the structure, computed by ^{1}H NMR spectroscopy, is around 2% of total NH protons, within the experimental error [16].

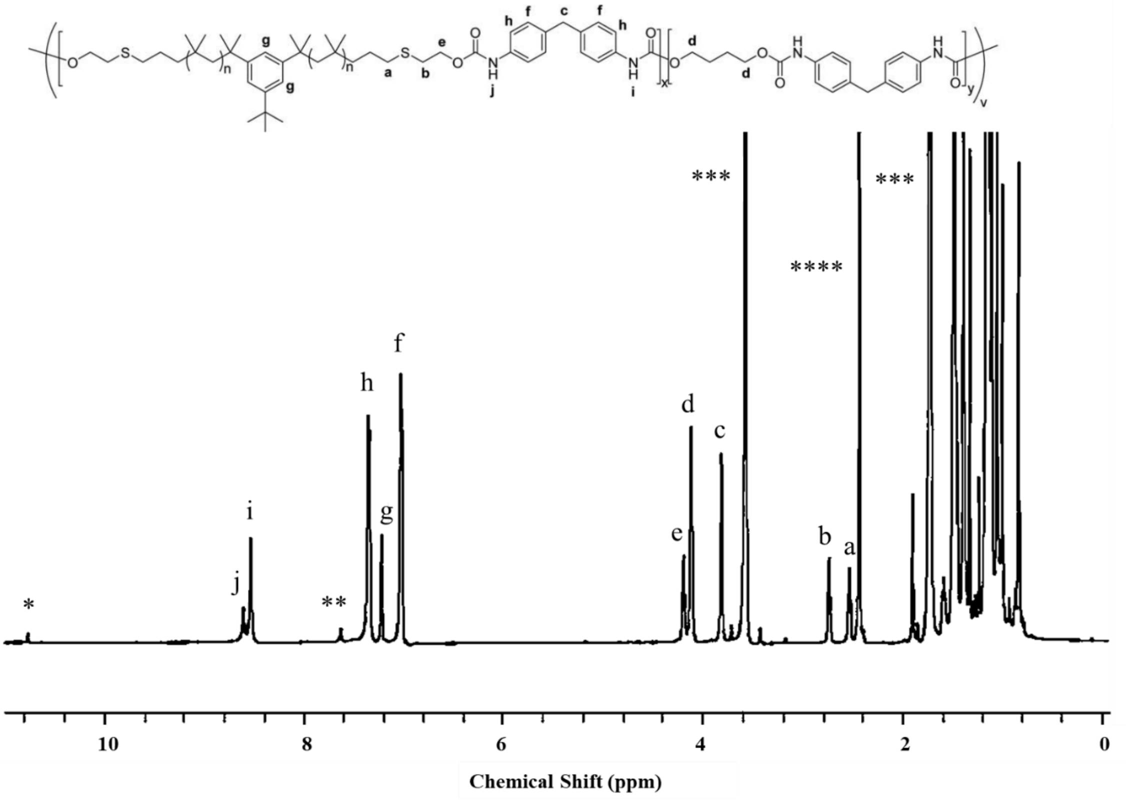

Figure 3.23: ^{1}H NMR spectrum of PIB$_S$-PU (prepared with 72.5 wt % HO-S-PIB-S-OH, 21.7 wt % MDI and 5.8 wt % BDO) in THF-d8. (*NH of allophanate; **NH of urea; ***residual solvent; ****water.). Reprinted from [16].

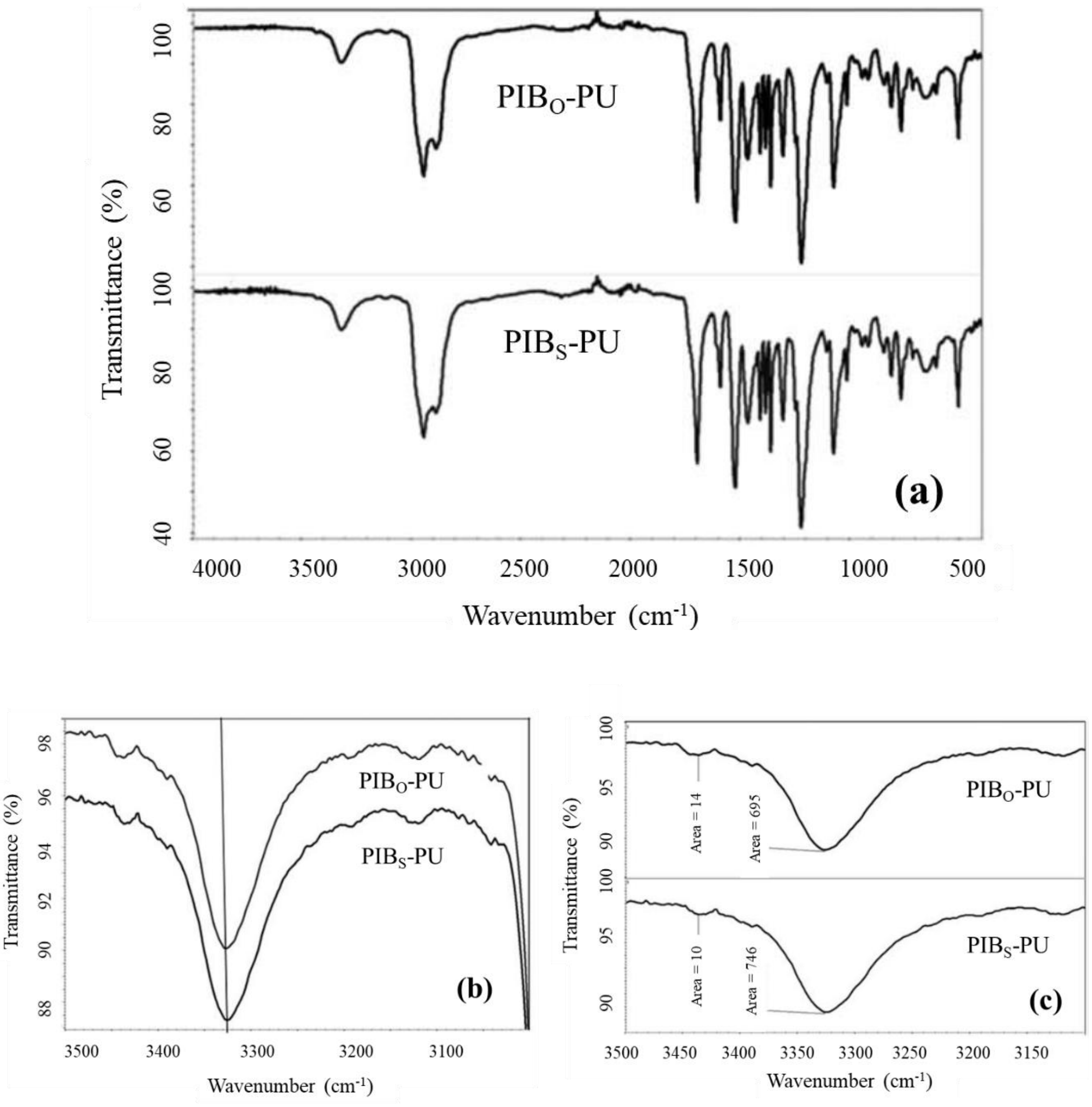

Figure 3.24: (a) FTIR spectra of PIB$_O$-PU and PIB$_S$-PU; (b) and (c) expanded 3100–3500 cm^{-1} range. Reprinted from [16].

FTIR spectroscopy is a potent method for understanding the microstructure of polyurethane in general and hydrogen bonding in particular. Figure 3.24 summarizes FTIR spectra of PIB$_O$-PU and PIB$_S$-PU in the 500-4000 cm^{-1} and their comparison. The absence of absorption peak at 2225 cm^{-1} signifies the lack of NCO and means the complete conversion to polyurethane. The adsorption at 1699 cm^{-1} is the characteristic peak of N-H….O=C bonds in PUs, which is another proof of PU formation [16, 66].

Figure 3.24 (b and c) also highlights peak positions and peak areas of NH stretching in the 3200–3500 cm^{-1} range. Specifically, stretching of H-bonded N (i.e., N-H…O=C and N-H…O) and free NH are attributed the adsorptions at 3327 and 3446 cm^{-1}, respectively. The red shift of the N-H stretching from 3327 cm^{-1} (for PIB$_\mathrm{O}$-PU) to 3322 cm^{-1} (for PIB$_\mathrm{S}$-PU) presumably represents an increase in H-bonding which is due to N-H…S in PIB$_\mathrm{S}$-PU. Coleman et al. reported similar findings regarding hydrogen bonding in polyurethanes at various temperatures. Consequently, FTIR spectra of them indicates that PIB$_\mathrm{S}$-PU has a slightly higher H-bond energy compared to PIB$_\mathrm{O}$-PU. This statement is consistent with other findings that, the H acceptor ability of -S- is greater than that of -O- or O=C in methionine containing peptides [16, 66].

Observed variations in peak areas support our conclusion that N-H…S bonding occurs in PIB$_\mathrm{S}$-PU. The peak area related with N-H…C=O stretching at ~3327 cm^{-1} is considerably larger in PIB$_\mathrm{S}$-PU than in PIB$_\mathrm{O}$-PU, which implies (i) conversion of the free NH to N-H…S, N-H…O=C, or N-H…O, and (ii) an increase in the adsorption coefficient with increasing in H-bond strength, although that for free NH (at ~3446 cm$^{-1)}$ is less. (Figure 3.24c). Earlier researchers have examined the H-bonding capacity of sulfides thoroughly and concluded that -S- can be as good as or better than -O- as an H-bond acceptor [16].

3.2.1.2. Mechanical Properties

Figure 3.25. depicts the stress–strain traces of PIB$_\mathrm{O}$-PU, PIB$_\mathrm{S}$-PU and ELAS and Table 3.2 provides a summary of ultimate strengths and elongations. Since its hard segments content (39%) [31] is much greater than that of PIB-based PUs (26.5%), ELAS (which includes 61% soft segment [31] displays the highest stress and toughness. PIB$_\mathrm{S}$-PU and PIB$_\mathrm{O}$-PU have comparable elastic moduli, but PIB$_\mathrm{S}$-PU is less tough in the plastic region and hence has a lower ultimate strength. Despite stronger and more H-bonds in PIB$_\mathrm{S}$-PU, it is surprisingly weaker (exhibits lower stress) than PIB$_\mathrm{O}$-PU. This is likely owing to differing

microstructures, i.e., the big S atoms in PIB$_S$-PU reduce the self-organization of hard segments [16].

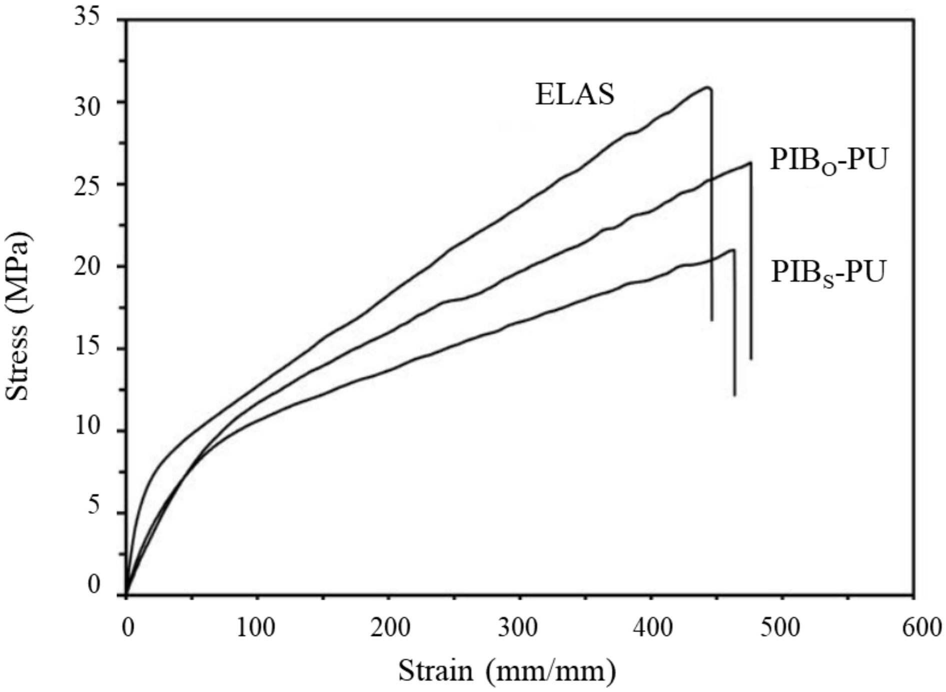

Figure 3.25: Stress–strain traces of PIB$_O$-PU, PIB$_S$-PU, and ELAS.
Reprinted from [16].

Figure 3.26 depicts storage moduli and tan delta of PIB$_S$-PU and PIB$_O$-PU as a function of temperature. Relaxation temperatures are quite comparable except PIB$_S$-PUs exhibits less damping mostly due to H-bonded S restricting molecular motions and hence raising the storage modulus. The length of the rubbery plateaus, that is, the temperature range over which the storage modulus varies little due to entanglement coupling, and the plateau moduli are, however, significantly different. The rubbery plateau of PIB$_S$-PU is significantly longer than that of PIB$_O$-PU. This data shows that H…S is responsible for chain entanglements and diffuse interphases between the hard and soft segments [16].

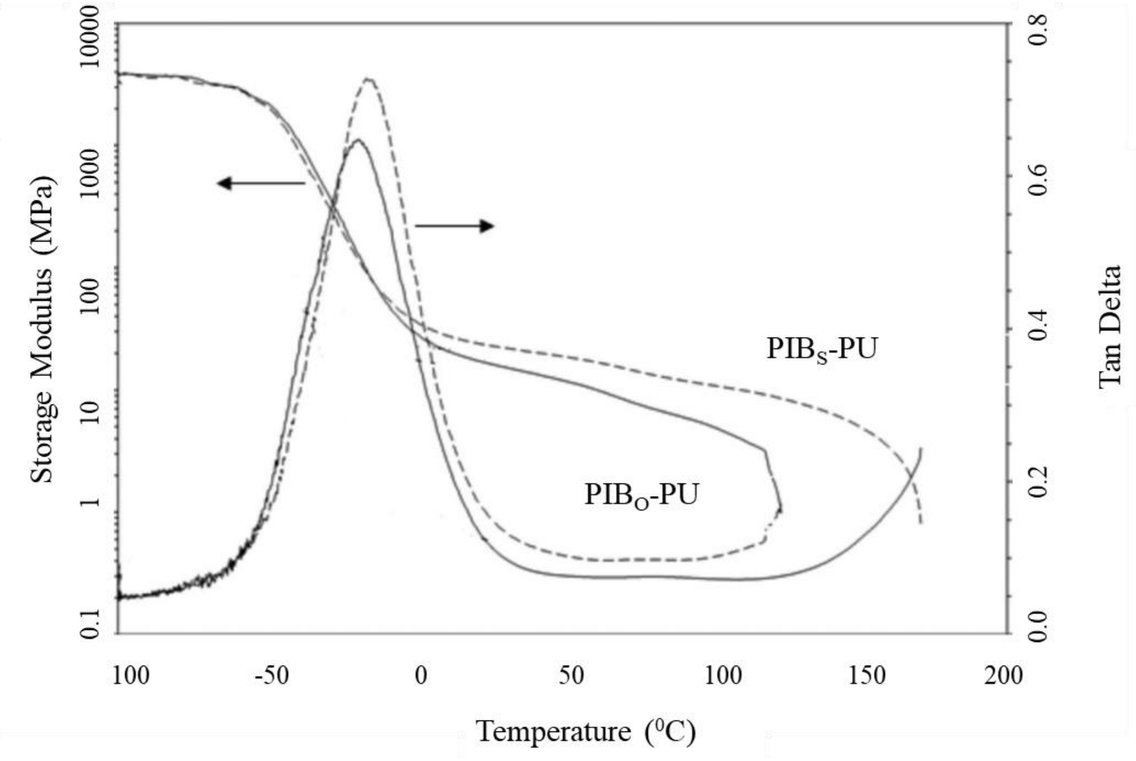

Figure 3.26: DMA thermograms of PIB$_O$-PU (----) and PIB$_S$-PU (- - -).
Reprinted from [16].

Figure 3.26 depicts the time dependence of creep compliance for PIB$_O$-PU and PIB$_S$-PU. Creep, which is the time dependent deformation under load, of PIB$_S$-PU was ~36% lower than that of PIB$_O$-PU, indicating that considerable chain entanglements and diffuse interphases between hard and soft segments generated by H…S bonds in addition to H…O bonds. This is further supported by the prolonged rubbery plateau.

Strain recovery following the removal of results in permanent deformation. Figure 3.28 displays extremely similar strain recoveries for PIB$_O$-PU and PIB$_S$-PU, indicating, very similar, small permanent sets for these PIB-based polyurethanes; precisely, 93.4% and 91.5% strain recoveries correspond to ~0.69% permanent deformation for both PUs.

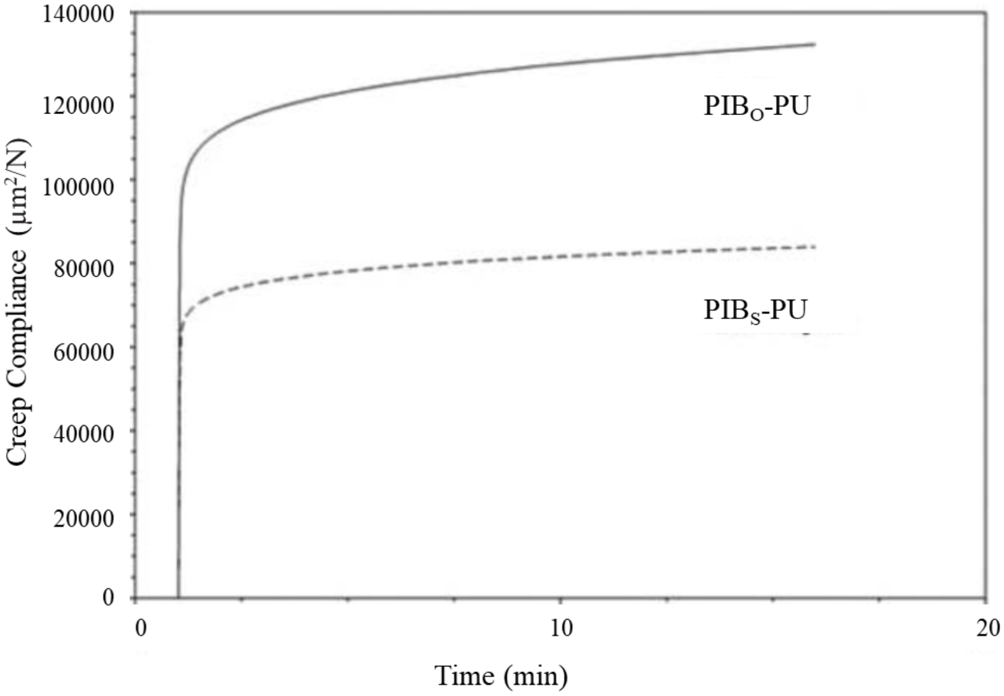

Figure 3.27: Tensile creep compliance versus time of PIB$_O$-PU (––––) and PIB$_S$-PU (- - -). Reprinted from [16].

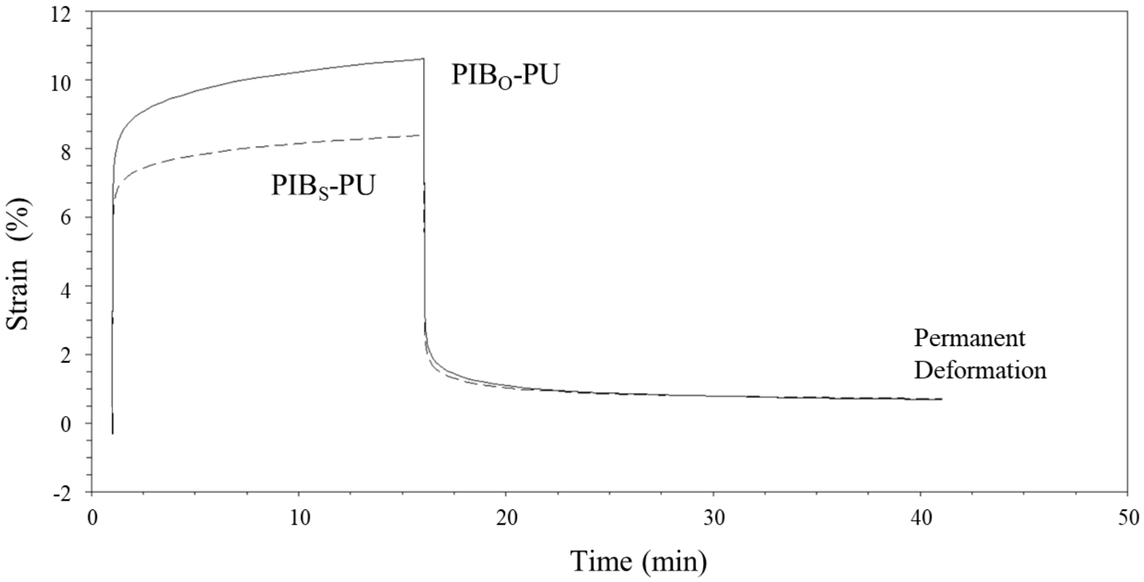

Figure 3.28: Strain (%) versus time of PIB$_O$-PU (––––) and PIB$_S$-PU (- - -).

3.2.1.3. Morphological Properties

The nanometer scale elemental analysis of $\mathrm{PIB_S}$-PU provided by EDX coupled with SEM, and S-mapping was used to better examine the distribution of S atoms on the sample surfaces (Figure 3.29). Consequently, the elemental composition (especially C, O and S) and dispersion of S atoms on film surfaces clearly reveal uniform distribution [16].

XRD traces of $\mathrm{PIB_O}$-PU and $\mathrm{PIB_S}$-PU are shown in Figure 3.30. Both materials contain PIB, BDO and MDI, which are extremely comparable ingredients, therefore it is not unexpected that XRD analyses of them provide similar outcomes. However, there are slight differences between XRD patterns of them to focus on as they result in substantial differences in static and dynamic mechanical properties; (i) due to lateral self-organization of hard domains, $\mathrm{PIB_S}$-PU displays a broder peak at ~14^{o}, (ii) the shoulder at ~20^{o} is mostly attributable to lateral distances between molten aliphatic chains, and (iii) due to second-order distances, $\mathrm{PIB_S}$-PU displays a broder low-intensity signal in the region of 30-50^{o} [16].

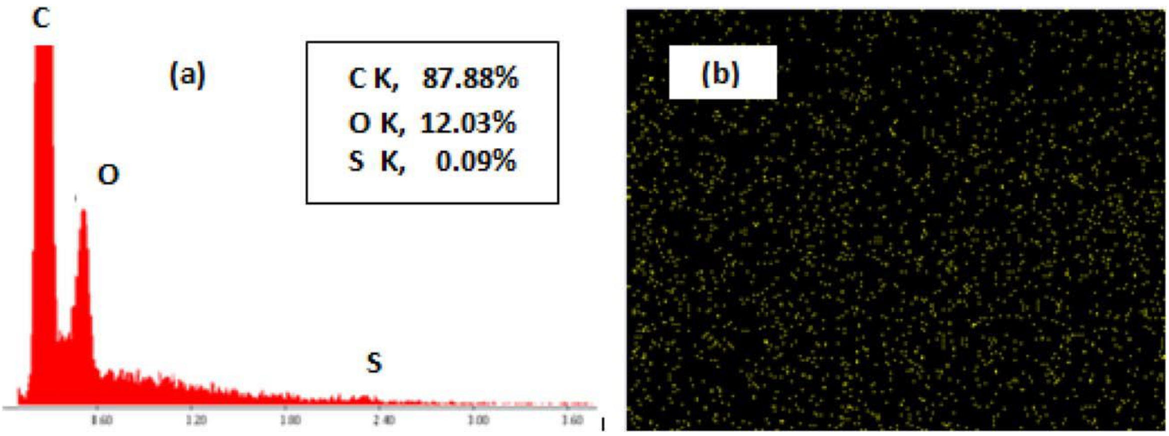

Figure 3.29: SEM–EDX spectra of (a) $\mathrm{PIB_S}$-PU, and (b) dispersion of surface S atoms on the film surface. Reprinted from [16].

In detail, the low self-organization of hard and soft segments was indicated with the slight broadening of the peak at ~14^{o} and weaker second-order signals in the 30-50^{o} range. Due to the atomic size difference between S and C, the correlation lengths are larger in $\mathrm{PIB_S}$-PU than in $\mathrm{PIB_O}$-PU, so the molecular segregation is more obvious [16].

Despite of the less intense and broader XRD peaks of PIB_S-PU, which are indicative of random low periodicity crystals, PIB_O-PU has a narrower XRD peak which implies larger crystallites. The larger H-bonded S atoms, as also shown by DSC thermograms, disturb chain alignment and crystallinity, and lower hard domain size and periodicity diminish the mechanical strength, whereas H. . .S bonds limits extensibility (see also Figure 3.31) [16].

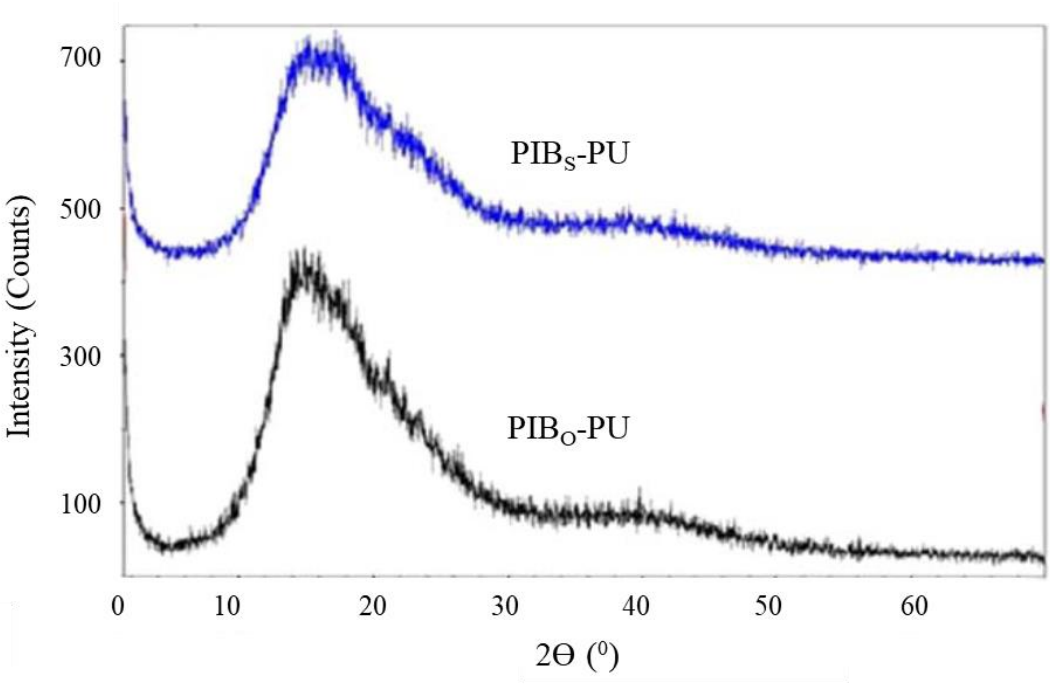

Figure 3.30: XRD traces of PIB_O-PU and PIB_S-PU. Reprinted from [16].

3.2.1.4. Thermal Properties

Figure 3.31 and 3.32 summarize thermal properties PIB_O-PU and PIB_S-PU, and their comparison. The soft phase (PIB) transition is drops by ~5^0C in the presence of S atoms, and a variety of intermediate hard phases, most likely random small crystals with low periodicity, are supported by the less defined broad transitions between -30^0C and 150^0C, which are supported by XRD and higher degradation temperature in TGA [16].

Crystalline melting points, like glass transitions, provide information on crystallinity and crystal sizes. As shown by XRD, the slightly lower heat of fusion of PIB_S-PU may be attributed to less crystalline hard domains and lower periodicity, and the broad T_m peak with shoulder is another result of random low periodicity crystals. The shift of PIB_S-PU's T_m to higher temperature (from 185.43^{0}C to 193.33^{0}C in Figure 3.31) may be caused by (i) melting of thicker small crystals at higher temperatures, (ii) restriction of chain motions because of H…S bonding, (iii) or both (i) and (ii) [16].

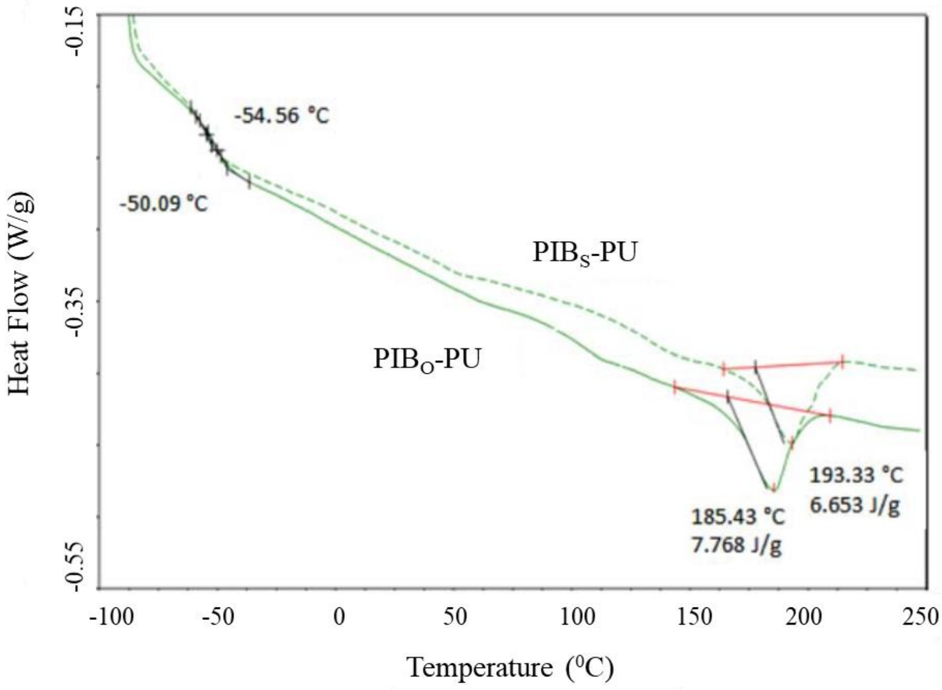

Figure 3.31: DSC thermograms of PIB$_O$-PU (----) and PIB$_S$-PU (- - -). Reprinted from [16].

Decomposition temperatures of PIB$_O$-PU and PIB$_S$-PU are shown in Figure 3.32. For PIB$_O$-PU, the peaks at 321^{0}C and 418^{0}C correspond to the degradation of the hard polyurethane phase and the soft PIB phase, respectively. The shift of hard phase degradation to higher temperatures (from 321^{0}C to 336^{0}C) in the presence of sulfur atoms, most likely result H. . .S bonding and polar interactions, and it appears that sulfur in PIB$_S$-PU causes a ~15^{0}C increase in the hard phase heat stability. On the contrary, when compared to C-C bonds, S-C bonds have lower bond dissociation energies, hence soft phase degradation occurs at lower temperatures (~406^{0}C) [16].

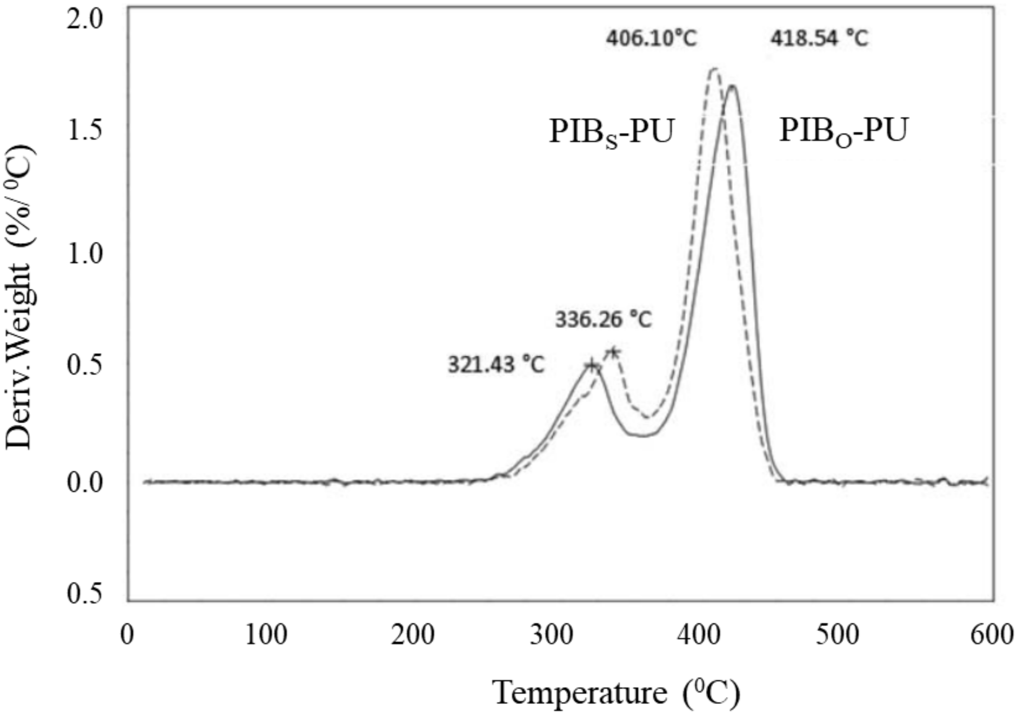

Figure 3.32: DTGA thermograms of PIB_O-PU (––––) and PIB_S-PU (- - -). Reprinted from [16].

3.2.1.5. Hydrolytic and Oxidative Stability

It is reported that PIB_S-PU has superior stress retention whereas PIB_O-PU has better strain retention, and it has stated that the reason of these results may be the oxidation of sulfur in PIB_S-PU to sulfoxides (~84%) and sulfones (~16%) detected after immersion in PBS.

Therefore, small amount of residual O_2 in PBS medium can oxidize polyurethane parts and the resulting sulfoxide and/or sulfones can stiffen the polymer.

Nitric acid exposure was shown to be less damaging to PIB_S-PU than ELAS since PIB_S-PU showed >60% strain retention and >80% stress retention whereas only 52% strain and 50% stress retentions were observed for ELAS. In addition, both PIB_S-PU and PIB_O-PU have similar stress retention %, but PIB_O-PU surprisingly has better strain retention, which is consistent with the lack of sulfur oxidation that would stiffen PIB_S-PU.

In sum, it is proved that PIB_S-PU and PIB_O-PU are both more resistant to hydrolysis and oxidation than ELAS [16].

3.2.2. Sulfur - Containing PIB based PU Nanocomposites

$HO\text{-}CH_2CH_2\text{-}S\text{-}PIB\text{-}S\text{-}CH_2CH_2\text{-}OH$ soft segment (as in PIB_S-PU), conventional hard segments of BDO and MDI, and organically modified montmorillonite (OmMMT) nanolayers were utilized to synthesize S-containing PIB based polyurethane nanocomposite (PIB_S-PU/NC). It contains 72.5% PIB and 0.5% OmMMT, and the organophilic nanolayer effect on morphology, tensile strength, elongation, hydrolytic stability, creep resistance and thermal properties are analyzed in this study [21].

Schematic view of PIB_S-PU/NC is demonstrated in Figure 3.33 by labeling various H-bonds in this nanocomposite structure. Negatively charged defoliated OmMMT nanolayers with multiple -OH groups and the modifier $N^+(CH_3)_3CH_2\,CH_2\,CH_2\text{-}NH_2$ (which is electrostatically bound to OmMMT) on their surfaces are represented by the horizontal white ovals. The formulas in gray squares indicate the polyurethane/urea hard segments, whereas S-containing PIB soft segments are shown by red wavy lines (~ ~ ~). Also, the sketch of PIB_S-PU/NC highlights urea groups, which may be formed if the terminal $-NH_2$ groups of the modifier reacted with isocyanate, the potential H-bonds between three main components: hard segments, soft segments and OmMMT.

In sum, under this heading, co-extender/reinforcing filler mission of OmMMT was evaluated in line with these properties [21].

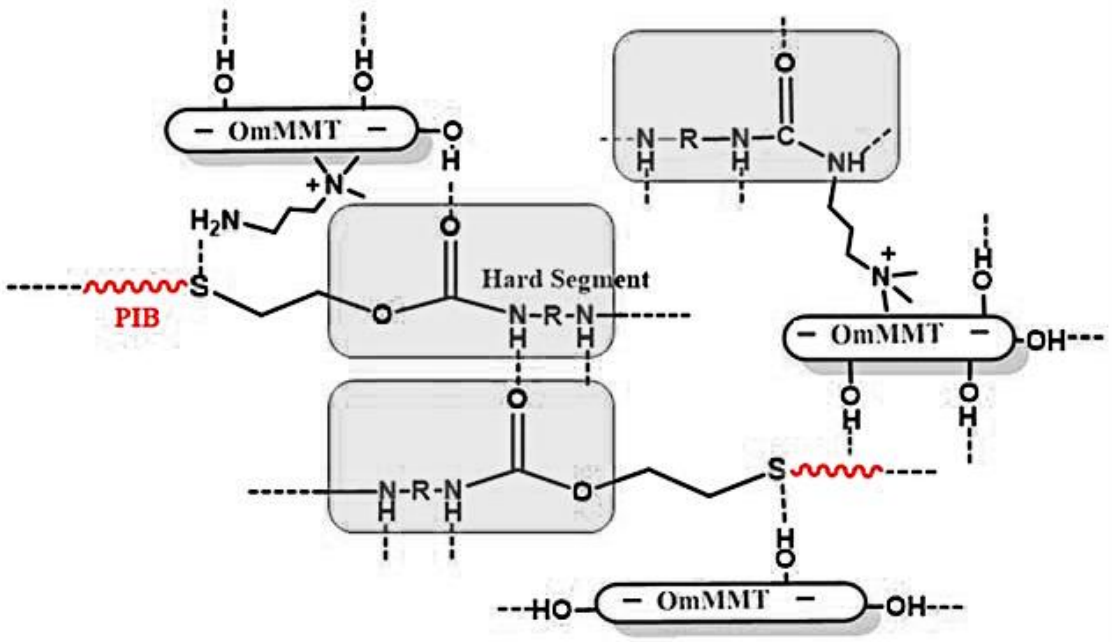

Figure 3.33: Idealized microarchitecture of PIB$_S$-PU/NC highlighting various H bonds between constituents. Reprinted from [21].

3.2.2.1. Molecular Characterization

C=O stretching regions in PIB$_S$-PU and PIB$_S$-PU/NC are shown in Figure 3.34. Due to overlapping of two bands at ~1730 cm^{-1} and ~1701 cm^{-1}, which correspond to the free and H-bonded C=O absorptions, respectively, the broad C=O adsorption is observed. It is common to see the splitting of the C=O stretching into two components, however, due to the presence of the aromatic rings in the chain, both the free and H bonded C=O stretching occurs at lower wavenumbers than those stated in the literature [21].

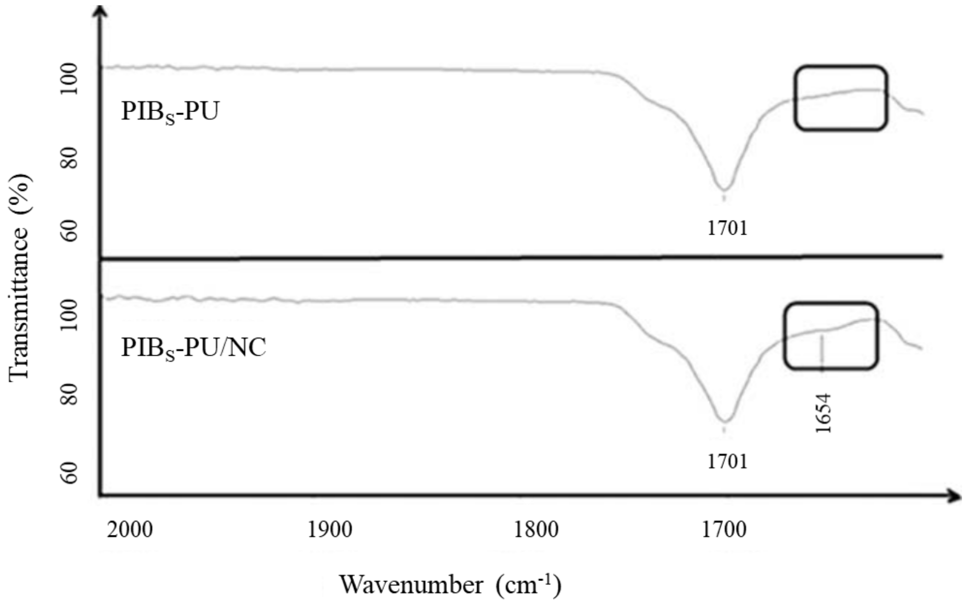

Figure 3.34: FTIR spectra in the C=O stretching region of PIB_S-PU and PIB_S-PU/NC. Reprinted from [21].

Because of the formation of urea linkages by the reaction between the amine of the modifier on OmMMT and isocyanate, 0.5% OmMMT addition results in a considerable adsorption at 1654 cm^{-1}. Also, Nugay et al. reported that the carbonyl of urea in polyurethane-urea model compounds shifted from 1639 cm^{-1} to 1647 cm^{-1} as a result of improved H-bonding [21]. However, the broadening of this adsorption band implies disorder due to hydrogen bonding [67], and Woniak-Braszak et al. similarly ascribed the broadening of the C=O stretching band to disorder resulting from H-bonding [21, 68].

N-H wag is responsible for the broad absorption at 670 cm^{-1} in the FTIR spectrum of PIB_S-PU/NC (see in Figure 3.35) since only primary and secondary amines create broad bands between 910 cm^{-1} and 665 cm^{-1}. Also, hydrogen bonds will be derived from the amine of the modifier attached to OmMMT [21].

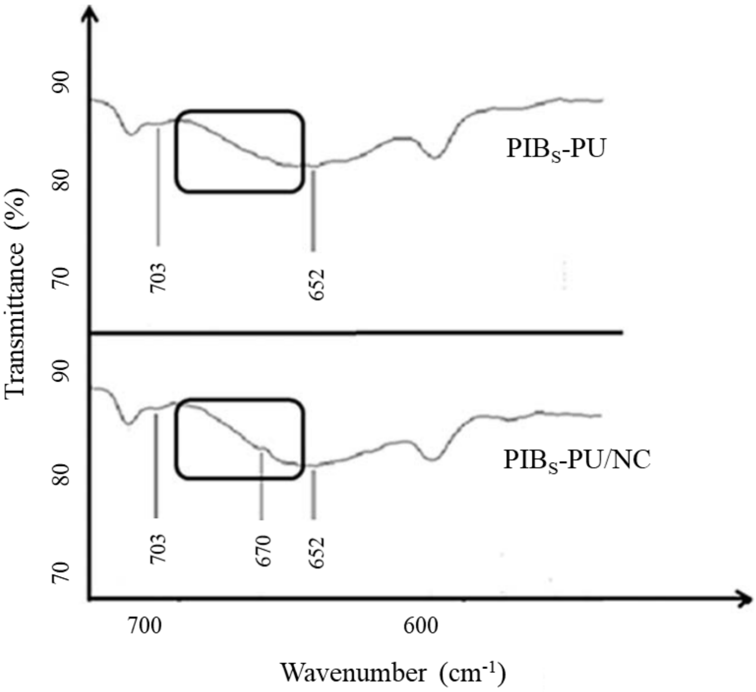

Figure 3.35: FTIR spectra in 750-550 cm^{-1} region of PIB$_S$-PU and PIB$_S$-PU/NC. Reprinted from [21].

Figure 3.36 demonstrates that the NH-associated absorption at 3325 cm^{-1} in PIB$_S$-PU broadens and shifts to 3322 cm^{-1} in PIB$_S$-PU/NC. In addition, two new absorptions at 3408 cm^{-1} and 3419 cm^{-1}, both of which are related with H-bonded Si-OHs, are also observed in PIB$_S$-PU/NC. Based on these results, it is likely that different H-bonds can be formed between surface/edge -OH and/or -NH$_2$ groups of OmMMT [21].

In conclusion, FTIR spectroscopy of PIB$_S$-PU/NC indicates the formation of different types of H-bonds between the surface -NH$_2$ and -OH groups of OmMMT and the S, N, and O atoms within the chain [21].

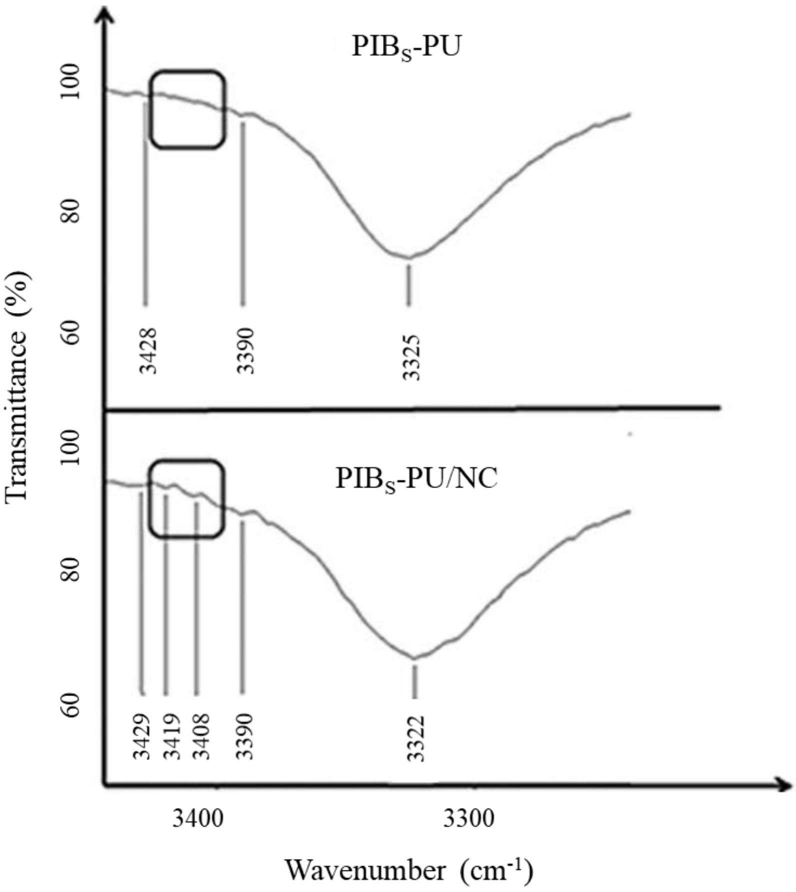

Figure 3.36: FTIR spectra in the NH stretching region of PIB$_S$-PU and PIB$_S$-PU/NC. Reprinted from [21].

3.2.2.2. Mechanical Properties

Traces of storage modulus and tan delta of PIB$_S$-PU and PIB$_S$-PU/NC as a function of temperature are depicted in Figure 3.37. Multiple H-bonds that constrain the molecular movements/motions, so increasing the modulus and shortening the rubbery plateau, are likely responsible for the higher relaxation temperature and decreased damping of PIBs-PU/NC. Also, creep experiments provide evidence of the shortened rubbery plateau (see in Figure 3.37) [21].

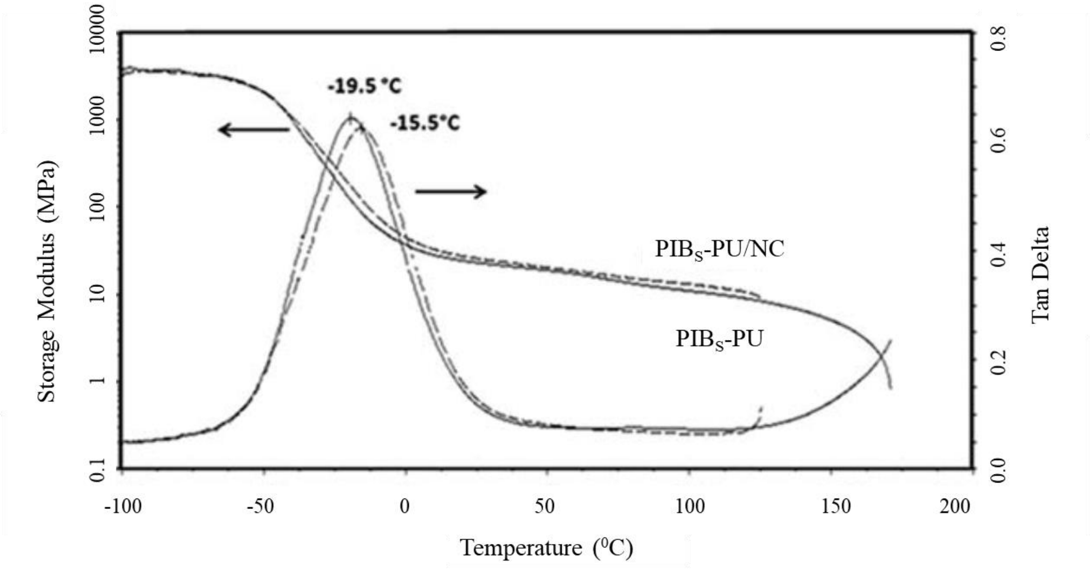

Figure 3.37: DMA traces of PIB$_S$-PU (----) and PIB$_S$-PU/NC (- - -). Reprinted from [21].

The results of creep and creep recovery experiments demonstrating time-dependent deformation in terms of percent strain are shown in Figure 3.38. Under constant stress, PIB$_S$-PU deforms somewhat more than PIB$_S$-PU/NC, which displays lower creep strain. These findings suggest that the nanocomposite (NC) is resistant to the uncoiling of chain entanglements and as a result, exhibits a decreased creep rate because of H-bondings [21].

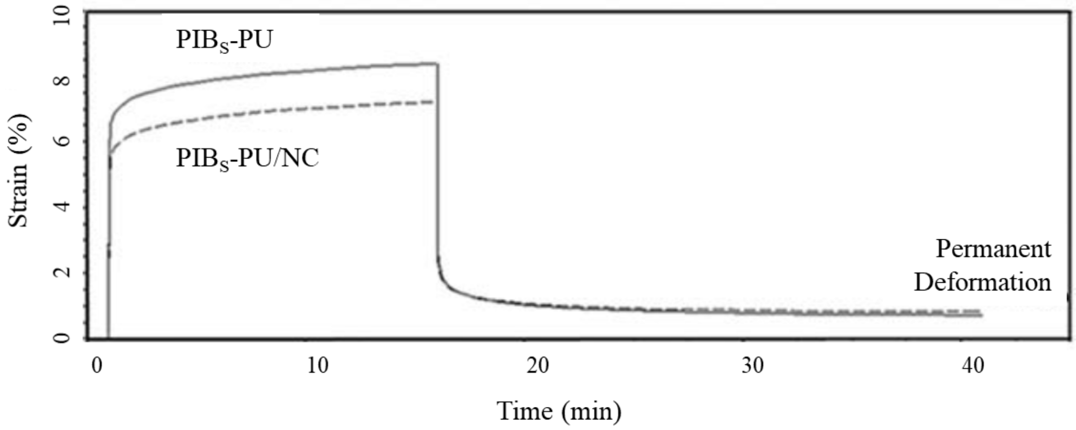

Figure 3.38: Strain (%) versus time of PIB$_S$-PU (----) and PIB$_S$-PU/NC (- - -) (1 MPa load for 15 min, at 25^{0}C). Reprinted from [21].

In addition, extremely low permanent deformation (~0.8%) is observed in either PIB$_S$-PU and PIB$_S$-PU/NC, indicating a very high degree of dimensional stability. It is clear that a trace amount (0.5%) of OmMMT addition in the presence of sulfur atoms decreases not only creep strain but also permanent deformation [21].

3.2.2.3. Morphological Properties

XRD traces of PIB$_S$-PU and PIB$_S$-PU/NC are shown in Figure 3.39 as well as the effect of OmMMT nanolayers on microstructure.

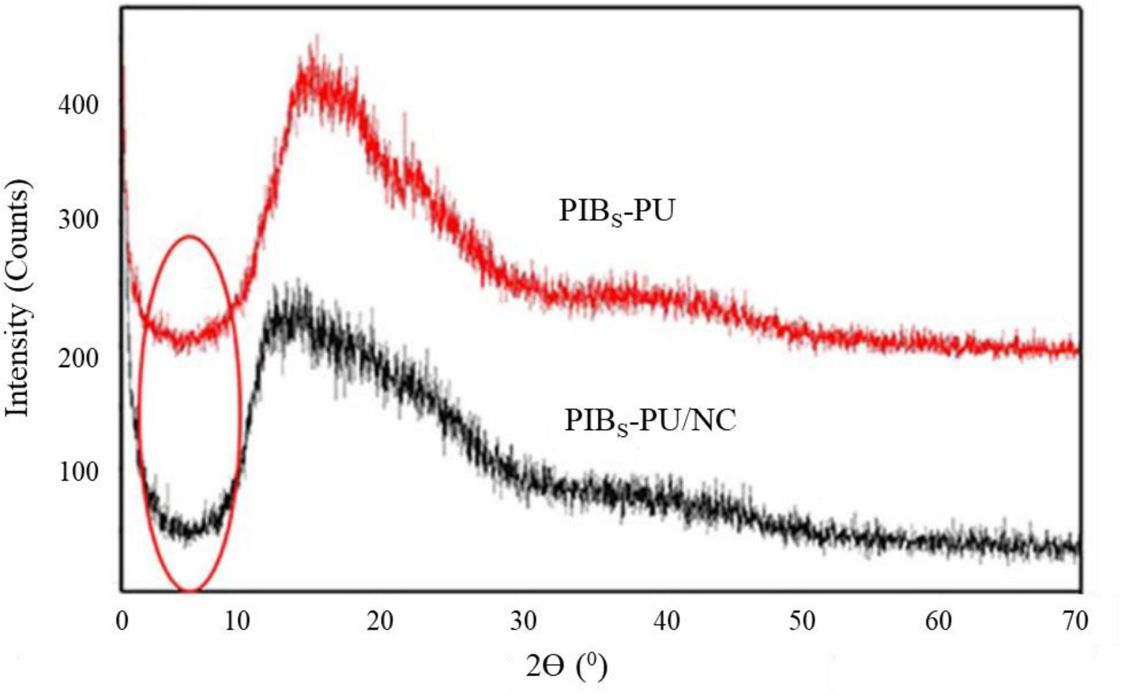

Figure 3.39: XRD traces of PIB$_S$-PU and PIB$_S$-PU/NC. Reprinted from [21].

The lack of the characteristic diffraction peak of OmMMT, which is at 7.04^0 (encircled in Figure 3.39), implies silica layers have been exfoliated inside the PU matrix. Clay may exfoliate due to the formation of H-bonds between surface/edge -OH groups of OmMMT and in-chain -NH- groups. In both PIB$_S$-PU and PIB$_S$-PU/NC, the broader peak at ~14^0 results from the lateral self-organization of hard segments. Also, the shoulder at ~20^0 is caused by lateral distance between aliphatic chains, and the broad low intensity signal in the 30^0–50^0 range to second order distances.

In addition, the peak-broadening at ~14^0 of PIB_S-PU/NC XRD trace, as well as the weaker second order signals, show that the self-organization of soft domains has diminished. Despite the fact that H-bonded sulfur atoms disrupt the chain alignment and crystallinity (which is also shown by DSC traces in Figure 3.40), enhanced hydrogen bonding between PU chains and OmMMT counteracts the impact of reduced hard-domain periodicity, and this results in increased tensile strength and decreased extensibility (see also in Table 3.2) [21].

3.2.2.4. Thermal Properties

Thermal transitions of PIB_S-PU and PIB_S-PU/NC are depicted in Figure 3.40. There are two well-defined high temperature endotherms between 170^0C and 220^0C in the DSC trace of PIB_S-PU/NC, and the soft phase T_g of the nanocomposite is somewhat lower than that of PIB_S-PU.

In addition, different types of H-bonds in the hard domain and generated between the -NH_2 and/or -OH groups of OmMMT and S and O atoms in the chain. XRD trace is another evidence about these H-bonds cause the formation of random and small low periodicity crystals. (see in Figure 3.40). The transition of soft segment in PIB_S-PU/NC rises somewhat as a result of the formation of hydrogen bonds between the -NH_2 groups of OmMMT and S and/or O atoms in the chain.

Significantly, the urea linkage between -NH_2 groups of OmMMT and S and/or O atoms in the chain likely contribute for the increased strength that is seen at a small crystalline melting endotherm in PIB_S-PU/NC at 220^0C [21].

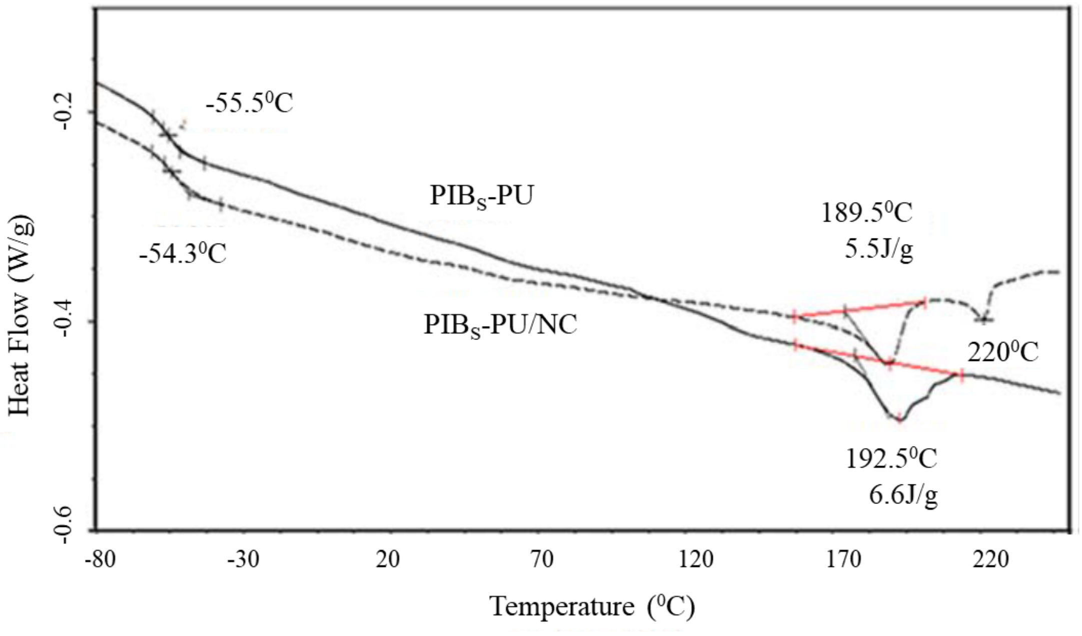

Figure 3.40: DSC thermograms of PIB_S-PU (––––) and PIB_S-PU/NC (- - -). Reprinted from [21].

3.2.2.5. Hydrolytic and Oxidative Stability

It was found that there are no discernible differences between PIB_S-PU and PIB_S-PU/NC in terms of their hydrolytic stability, as detected by PBS test, indicating that these samples showed negligible degradation. Also, with the compared strain retention data of PIB_S-PU and PIB_S-PU/NC, it was suggested that the oxidation of sulfur in the PIB chains is less likely in the presence of OmMMT (albeit in trace amount). Similar approaches for enhanced resistance to photo- and thermo-aging in the modified bitumen composites were reported by Nugay et al. who attributed this result to the reduced O_2 diffusion by MMT layers [21].

In sum, increased H-bonding between PU chains and OmMMT compensates for reduced hard domain periodicity, hence increasing tensile strength of PIB_S-PU/NC and decreasing its extensibility (i.e., elongation %) as summarized in Table 3.2. Enhanced H-bonding raises the relaxation temperature (-19.5^{0}C for PIB_S-PU and -15.5 for PIB_S-PU/NC) and modulus, also decreases damping. Apparently, adding a trace amount of OmMMT enhances the ultimate strength, creep, and permanent deformation of PIB_S-PU/NC [16, 21].

Table 3.2: (a) Tensile properties of PIB_O-PU, PIB_S-PU, PIB_S-PU/NC and ELAS before exposure, (b) Tensile strength and Elongation (%) of PIB_O-PU, PIB_S-PU, PIB_S-PU/NC and ELAS after exposure to HNO_3 for 4 h at room temperature, and after exposure to PBS at 55^0C.

	Before Exposure			
(a)	**Tensile Stress (MPa)**	**Elongation (%)**	**Young's Modulus**	**Hardness (Shore A)**
PIB_O-PU	26.1 ± 0.6	526 ± 20	16	81.8
PIB_S-PU	20.7 ± 0.5	447 ± 25	16	82.5
PIB_S-PU/NC	24.3 ± 0.7	351 ± 17	19	89.6
ELAS	30.6 ± 1.1	436 ± 20	38	91.5

	After Exposure to HNO_3 at 25^0C		**After Exposure to PBS at 55^0C**	
(b)	**Tensile Stress (MPa)**	**Elongation (%)**	**Tensile Stress (MPa)**	**Elongation (%)**
PIB_O-PU	21.3 ± 0.4	478 ± 21	23.5 ± 0.3	454 ± 14
PIB_S-PU	16.7	280	17.9 ± 0.5	193 ± 43
PIB_S-PU/NC	20.6 ± 0.6	314 ± 15	20.7 ± 0.5	324 ± 13
ELAS	15.2 ± 0.1	226 ± 7	21.1 ± 0.2	298 ± 3

Consequently, even a trace amount of OmMMT improves the hydrolytic and oxidative resistance of PIB_S-PU, most likely due to the organically modified montmorillonite nanolayers shielding the vulnerable urethane linkages and preventing the sulfur oxidation [21].

3.3. New PIB based PUs for Biomedical Designs

As a unique class of polymer, polyurethanes can have a wide variety of uses due to the ease with which their properties can be modified by changing the chemical composition of the material. Therefore, they are widely utilized as adhesives, foams, coatings, fibers and elastomers, and they also have several medical uses when they come into touch with blood or tissue, such as in catheters, heart valves, vascular prosthesis, cardiac assist devices, pacemaker lead insulation, blood filters, and artificial heart chambers. This class of polymers is used in these types of applications due to its outstanding mechanical and physical properties, stability during extended implant periods, reasonably good blood tolerance, and physiological acceptability. Nevertheless, if the PUs is to be utilized in more biomedical applications, their biocompatibility with blood should be enhanced [36].

To improve the hemocompatibility of PUs, PIB can be preferred as a soft segment of them. While PIB-containing materials are used in commercial applications such as adhesives, inner tubes and liners, condenser caps and pharmaceutical stoppers, there are few studies on biomedical applications of these materials due to their excellent tissue and blood compatibility [38, 43]. In this study, it is aimed to investigate in-vitro biocompatibility of newly synthesized PIB based PUs whose structure given in Figure 3.41.

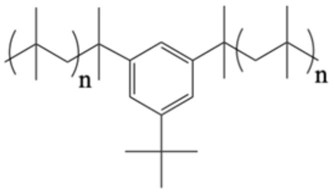

PIB

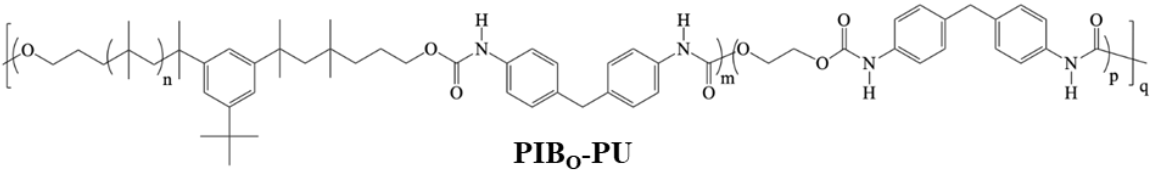

PIB$_O$-PU

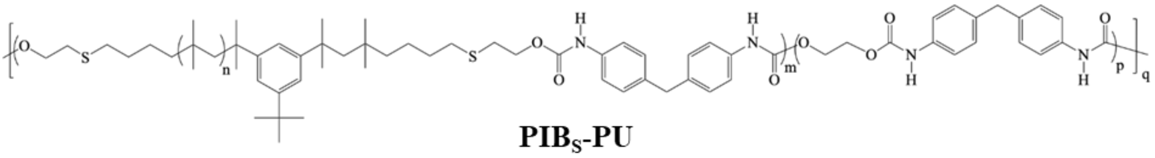

PIB$_S$-PU

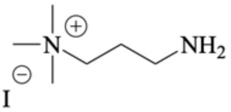

ATMPA$^+$ I$^-$ (Modifying agent for montmorillonite)

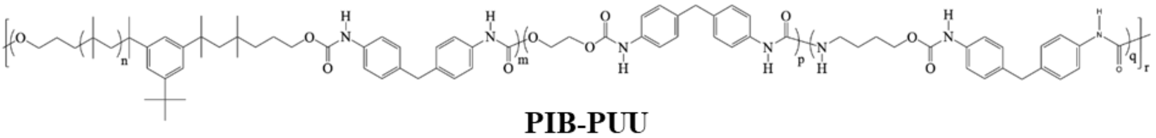

PIB-PUU

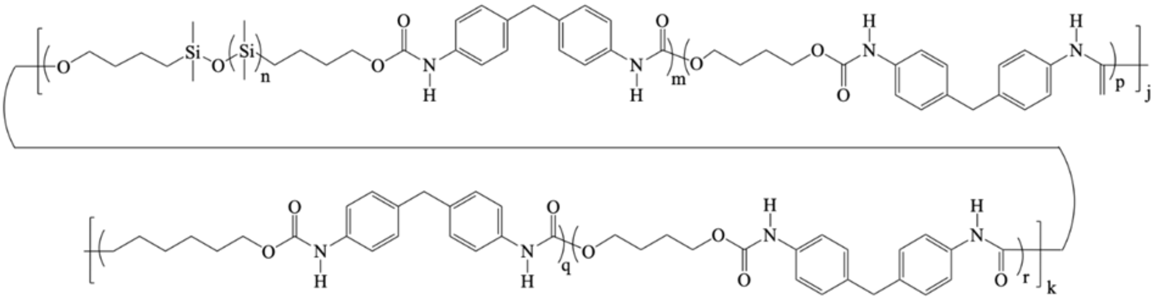

ELAS

Figure 3.41: Structural formula and abbreviations of polymers (PIB, PIB based PUs and ELAS) and the modifying agent of montmorillonite. Reprinted from [41].

3.3.1. Preliminary Surface Properties of PUs

Surface-biomaterial interactions are influenced by both proteins, the first step where the biomaterial begins to connect the sample surface, and surface properties. Besides material type and chemical structure (which are main chemical properties of polymer), surface energy, charges, contact angle, and morphology (which are main physical properties of polymers) should be considered as important parameters for biological properties and biocompatibility of surfaces [32]. To predict the calcification, protein adsorption, cell attachment and cell viability pattern of PIB based PU samples and ELAS, and compare their result, the preliminary surface properties of them and the importance of these properties should be evaluated.

The surface properties, such as stiffness, surface charge, chemical functionalities, roughness, and wettability are all the main parameters for determining in-vitro biocompatibility of biomaterials, and the results of in-vitro biocompatibility studies can be explained by more than one parameter [32]. Table 3.3 summarizes the main physical and surface properties, considered to affect in vitro biocompatibility, of PIB based PU and ELAS samples used in this study.

Table 3.3: The main physical and surface properties of the samples

Sample Code	**Contact Angle (^{0})**	**Surface Roughness (RMSD in nm)**	**Shore A Hardness**	**Equilibrium Swelling Ratio (%)**
PIB$_S$-PU/NC	71.47	121	89.6	2.7
PIB$_O$-PU	85.51	25	81.8	1.8
PIB-PUU	71.65	24	-	3.2
PIB$_S$-PU	73.1	39	85.2	3.4
ELAS	92.57	45	91.5	3.7

3.3.1.1. Surface Wettability

Surface properties in terms of surface wettability with respect to their hydrophobicity or hydrophilicity have an important role in influencing the biological response of a biomaterial. Since the displacement of water from the surface of a hydrophilic material constitutes a large energy barrier to adsorption by proteins, hydrophobicity of material surfaces enhances the protein adsorption and (in parallel) cell adhesion capacity [69].

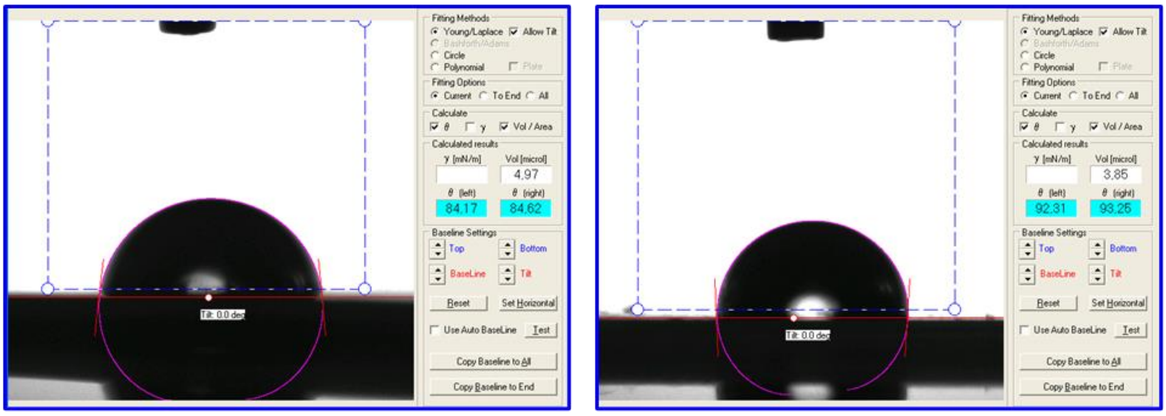

a) PIB$_O$-PU

Fitting Methods: ● Young/Laplace ☑ Allow Tilt ○ Circle ○ Polynomial
Fitting Options: ● Current ○ To End ○ All
Calculate: ☑ θ ☐ γ ☑ Vol / Area
Calculated results: γ [mN/m] Vol [microl] 4,97 θ (left) 84,17 θ (right) 84,62
☐ Use Auto BaseLine
Tilt: 0.0 deg

b) ELAS

Fitting Methods: ● Young/Laplace ☑ Allow Tilt ○ Circle ○ Polynomial
Fitting Options: ● Current ○ To End ○ All
Calculate: ☑ θ ☐ γ ☑ Vol / Area
Calculated results: γ [mN/m] Vol [microl] 3,85 θ (left) 92,31 θ (right) 93,25
☐ Use Auto BaseLine
Tilt: 0.0 deg

Figure 3.42: KSR CAM 101 image of (a) PIB$_O$-PU and (b) ELAS samples with distilled water

Average of minimum 10 measurements were reported in Table 3.3. According to these results and surface wettability characteristic of samples, ELAS should be expected to yield higher protein adsorption and cell adhesion results.

3.3.1.2. Surface Hardness

There is evidence that substrate rigidity affects the modulation of cell attachment, proliferation, and differentiation. The mechanism between ECM and seeded-cell, which has a strong correlation with a cell adhesion, mainly depends on softness and stiffness. Generally, it has been shown that stiffer substrates are less compatible with the adhesion and proliferation of cells, while cells responded stronger to stiffer substrate [32]. Moreover, a rigid behavior, preventing a strong attachment with the cell membrane, drastically lower the cell viability. As seen in Table 3.3, Shore A hardness (92.57) of ELAS is higher than all PIB based PU samples since its hard segment ratio (39%) [31] is greater than all PIB based PU samples (27.5%). As a result, ELAS should be expected to yield low cell attachment and adhesion results.

3.3.1.3. Surface Roughness

For cell adhesion and proliferation, the morphology of surface is a vital factor. Therefore, to obtain the desired interaction between biological agent and polymer surface, modification of surface attributes of the polymer substrates, such as roughness, morphology besides the physico-chemical composition, is required. It has been shown that cells orient and arrange themselves along surface-treatment-induced grooves. Increase of surface roughness on polymer, which leads to increase surface area, frequently enhanced the cell adhesion but it depends on the seeded cell type, polymer substrate and also roughness value [70].

Surface roughness strongly affects cellular morphology, phenotype expression and cell proliferation in vitro as well as in vivo. Topographical features of the material surfaces at nano or micro scale such as grooves, fibers, wells, ridges, pores, nodes, and steps have been evaluated as a function of the cellular response, which is the result of its interaction with different chemistry, geometries, and structures on the surfaces. The roughness of the sample surface can be evaluated in 3 different groups, exhibiting their own influences: nano-roughness (less than 100 nm), micro-roughness (100 nm – 100 µm), and macro-roughness (100 µm – 1 mm) [32].

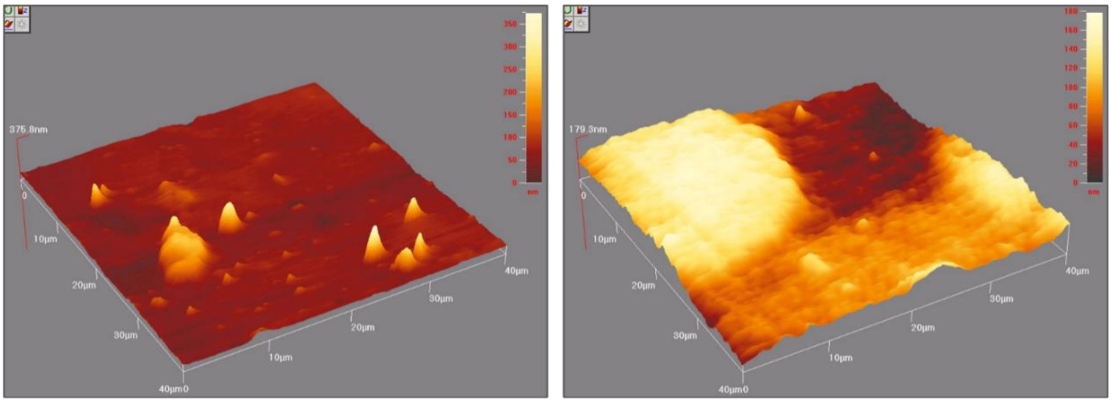
a) PIB$_O$-PU

b) ELAS

Figure 3.43: 3D AFM image of surfaces of (a) PIB$_O$-PU and (b) ELAS samples

Increasing in root mean square (rms) surface roughness for values higher than 4.0 nm inhibited cell stretching and so supported the presence of round-shaped cells. As a result, the lower surface roughness ratios promote and point out a better cell adhesion [32]. Therefore, due to difference between their surface roughness, it is expected that the protein adsorption and cell attachment capacity of ELAS (~45 nm roughness) and PIB_O-PU (~25 nm roughness) should be different in theory. However, an increase in surface roughness, as a consequence of the formation of valleys and peaks, [71] inhibit the cell stretching and so encourage the existence of round-shaped cells [32]. Moreover, Ovcharenko et al. mentioned that rough and porous surfaces are known to cause a more inflammatory response than smoother and structured surfaces [72].

As a result, surface roughness is a parameter that affects the results of in-vitro studies at many different points.

3.3.2. Hydrolytic Stability, and Dimensional Stability in PBS

Conventional polyurethanes that are commercially available and comprise polycarbonate, polyether or polydimethylsiloxane soft segments (or different combinations of them) are known to have outstanding mechanical and processing properties, However, they are naturally vulnerable to hydrolytic, oxidative, biological attack, and rapidly degrade upon long-term exposure to such chemical agents (i.e., PBS, nitric acid etc.). Hydrolytic stability is also important parameter for long-term biomedical applications due to water-based medium of human body [16] Therefore, PIB based PUs exhibit exceptional hydrolytic and oxidative resistance due to the protection of susceptible urethane linkages by chemically highly resistant PIB soft segments [16, 21].

The main disadvantage associated with the long-term application (i.e., artificial heart valve) is the polymeric structure biostability [73]. The greater swelling of the polymer, used in cardiac surgery, leads to cardiac tamponade, which is a serious medical condition, and results in compression on the heart and decrease in cardiac function. Therefore, minimal swelling support the maintenance of cardiac function after surgery [74]. Also, the reduced water permeability, demonstrated by contact angle attempts, which may be advantageous in heart valve applications, avoiding the regurgitation by passage of blood [73]. To evaluate the biostability of PIB based PUs and compare these samples with ELAS, the commercially available, swelling patterns of them in PBS medium, a salt-based water solution, was observed.

Length-change based swelling patterns of dried PIB based PU and ELAS samples were used for calculating swelling ratio (%). All films (~0.5 – 0.65 mm initial length) were immersed in PBS solution, which was used for cell attachment and cell viability tests, at room temperature and length change in their dimensions are recorded at regular time interval for 24h same as cell attachment and viability studies. According to their swelling data, their swelling ratio (%) values were calculated by following formula; where l_p is the length of the sample after PBS incubation at relevant time and l_0 is the length of the sample before incubation.

$$Swelling\ Ratio\ \% = \frac{l_p - l_o}{l_0}\ x\ 100, \tag{3.17}$$

where l_p is the length of the sample after PBS incubation at relavent time and l_0 is the length of the sample before incubation.

Swelling ratio (%) changes of all samples are shown in Figure 3.44 in two separate zones. Then, equilibrium swelling ratio values as a percentage were determined from swelling-deswelling averages. In detail, looking at 10th minute data, it can be easily understood that the fastest swelling was seen in ELAS and it was having a trouble to reach the swelling equilibrium in PBS. Therefore, it can be easily said that ELAS shows the most unstable swelling characteristic. In addition, the most stable and lowest swelling was seen at PIB_O-PU, which is fastest to reach an equilibrium. Moreover, the initial swelling ratio of PIB_S-PU is high, but it recovered quickly and at the end of 24 h, it reached an equilibrium. PIB based PU samples showed higher dimensional stability in PBS which mediates the bio-based studies.

After 24 h PBS incubation, samples were washed with distilled water and then the surfaces of PIB_O-PU and ELAS samples were checked with SEM to compare the changes on the sample surfaces before and after PBS exposition.

As seen in Table 3.3 and Figure 3.44, the highest PBS (so water) uptake observed at ELAS sample. Jeong et al. reported that the protein adsorption increased with increasing with water uptake capacity of the polymer films [75, 76]. As a result, ELAS should be expected to yield the highest protein adsorption result.

Since the proportion of water absorbed by polyurethane polymers achieves a constant value within 4 hours of immersion [77], 24 hours incubation in PBS was adequate to detect a main difference between PIB_O-PU and ELAS, which is PDMS based polyurethane. Also, a thorough examination of the content of PBS reveals that it is quite comparable to SBF (see in Table 3.4). Consequently, calcification results early, and this study are anticipated to have comparable outcomes.

Table 3.4: The ingredients comparison of PBS and SBF solutions [78].

PBS INGREDIENT	**SBF INGREDIENT**
INORGANIC SALTS	**INORGANIC SALTS**
Calcium Chloride	Calcium Chloride
Magnesium Chloride (hexahydrate)	Magnesium Chloride (hexahydrate)
Potassium Chloride	Potassium Chloride
Potassium Phosphate, Monobasic (Anhydr.)	Di-potassium Hydrogen Phosphate Trihydrate
Sodium Chloride	Sodium Chloride
Sodium Phosphate, Dibasic (Anhydr.)	Sodium Hydrogen Carbonate
	Sodium Sulfate
OTHER COMPONENTS	**OTHER COMPONENTS**
D-Glucose	Tris-hydroxymethyl Aminomethane
Sodium Pyruvate	1M (mol/l) Hydrochloric Acid
Phenol Red • Na	
Sodium Bicarbonate	

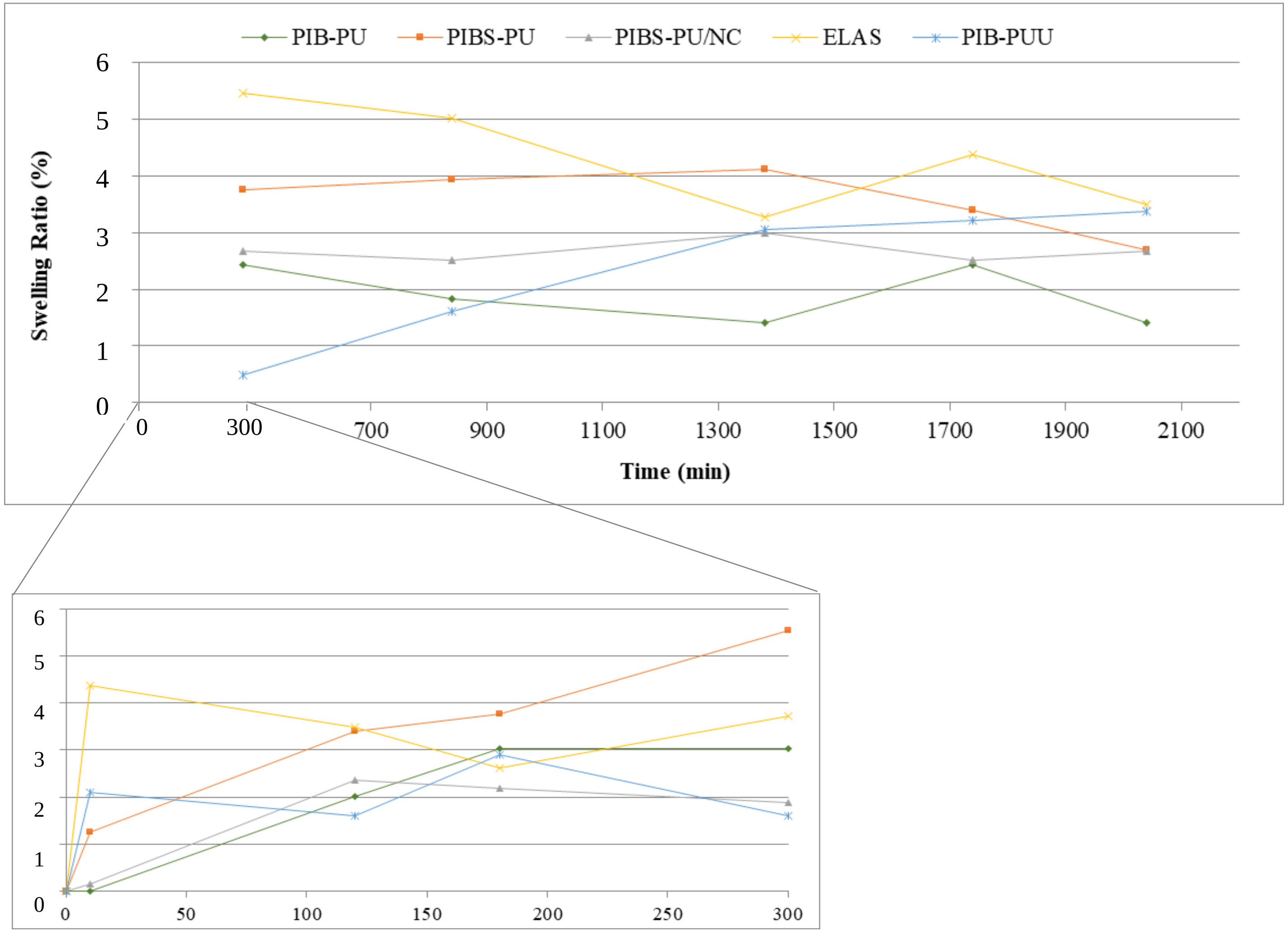

Figure 3.44: Length based swelling ratio change of PIB based PUs and ELAS samples versus time.

As seen in Figure 3.45; SEM images as well as EDX spectrum of PIB$_O$-PU indicated the complete absence of PBS crystals after 24 h incubation**.** PIB phase (soft phase) covered the surface of PIB$_O$-PU, which is containing 27.5 wt % PU as a hard phase, and it provides an outstanding hydrolytic stability to sample. In this way, the swelling of PIB$_O$-PU is negligible and lower than ELAS (see in Figure 3.46) so incubation of PIB$_O$-PU in aqueous PBS is not expected to affect the surface (or bulk) morphology of PIB$_O$-PU [41]. As a result, absence of deposition of PBS crystals on PIB$_O$-PU surface is a meaningful outcome.

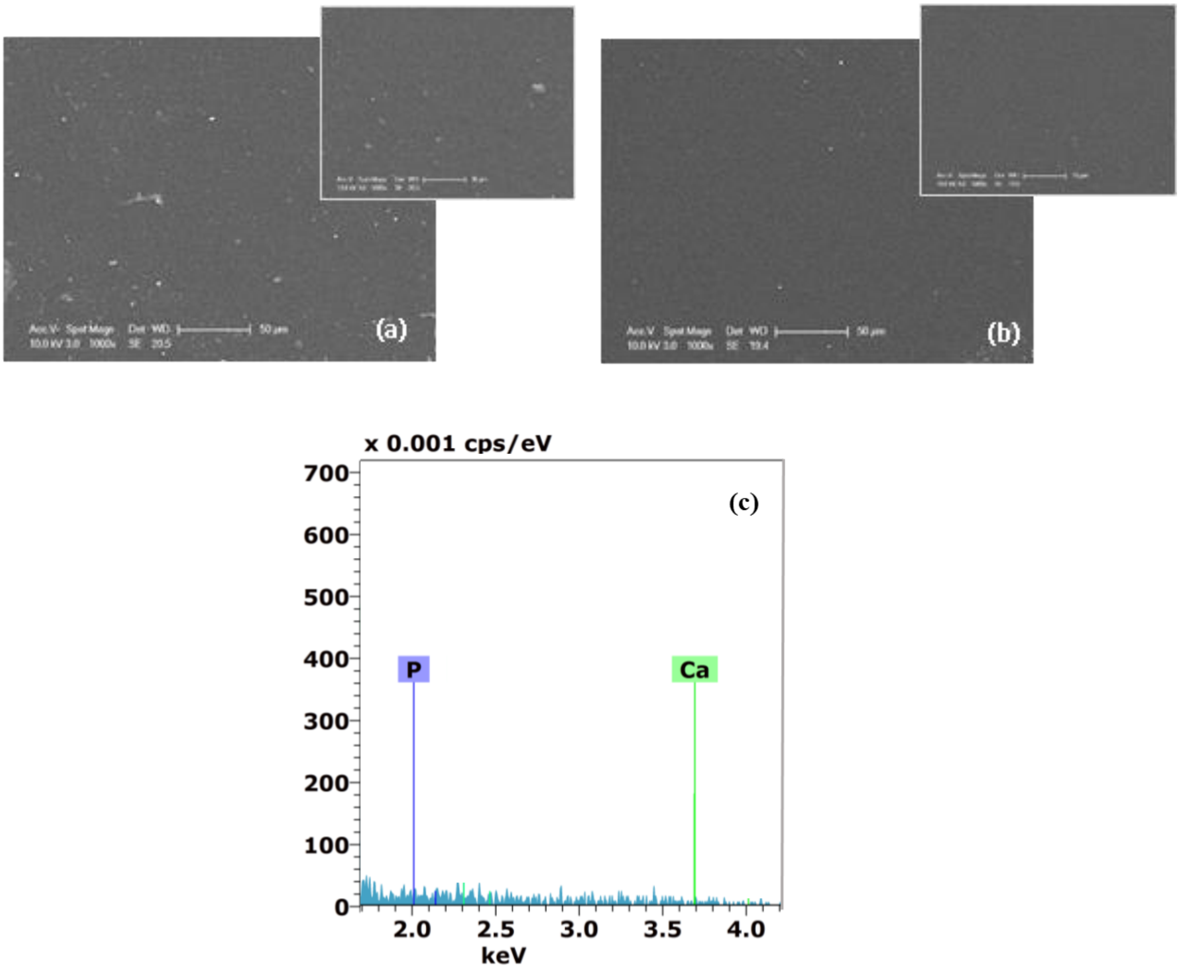

Figure 3.45: Scanning electron microscopy images of PIB$_O$-PU surfaces (a) before and (b) after 24h PBS incubation, (c) Energy-Dispersive X-Ray Spectroscopy (EDX) spectra after SBF incubation for calcification analysis [41].

Moreover, as seen in Figure 3.46, SEM images as well as EDX spectrum of ELAS indicated the deposition of PBS crystals on sample surface after 24h incubation.

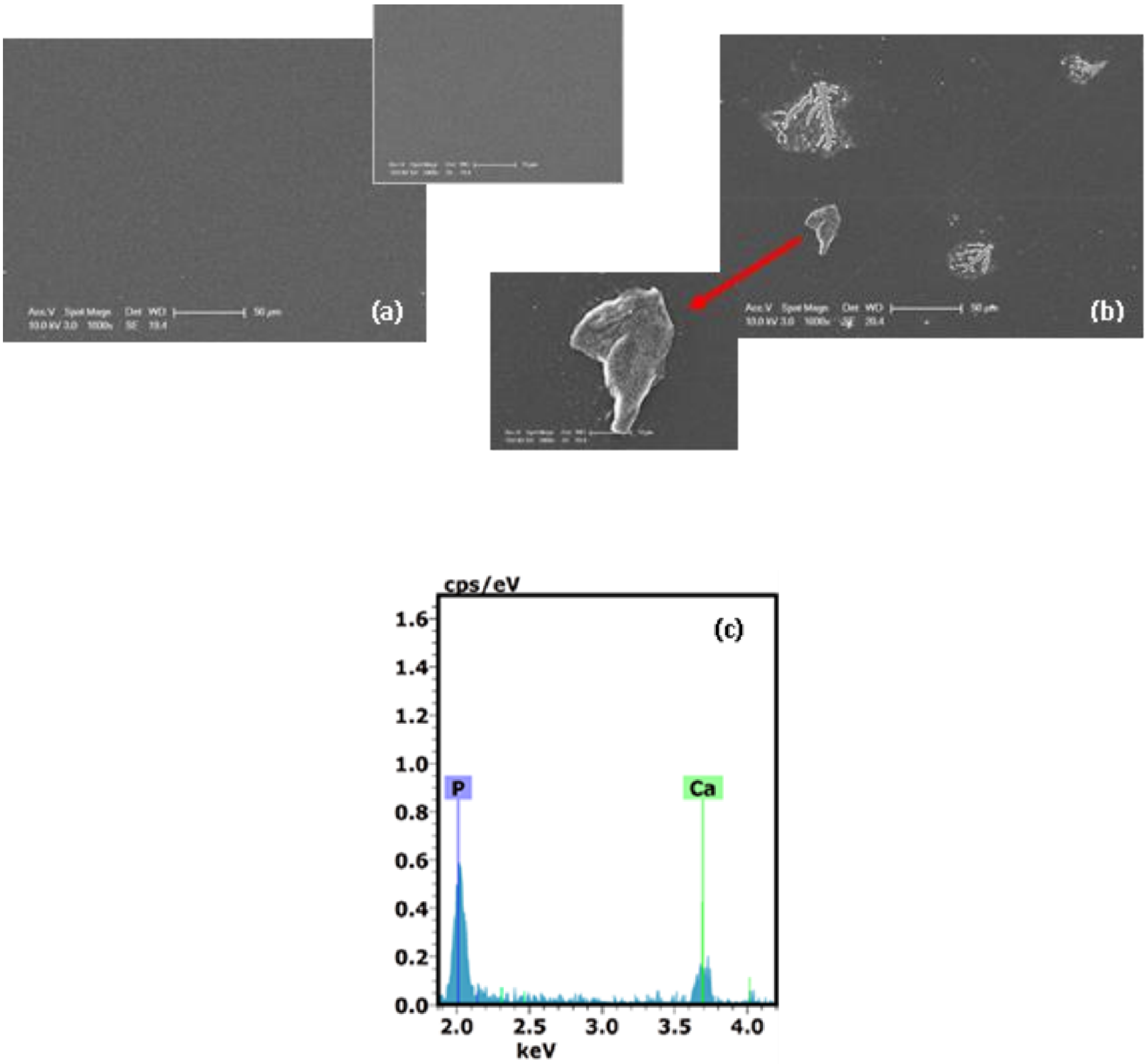

Figure 3.46: Scanning electron microscopy images of ELAS surfaces (a) before and (b) after 24h PBS incubation, (c) EDX spectra after SBF incubation for the calcification analysis [41].

In detail, ELAS is a polyurethane structure with dihydroxy-terminated polydimethylsiloxane (PDMS diol) soft segment, which is a challenging structure since it has an unusual viscoelastic behavior and degree of control over structure morphology because of its ultralow T_g and excessive nonpolar character [77]. It can be reported that the extensive PBS crystals on ELAS surface may be due to chelation of positive charged calcium ions at -O- sites placed in the PDMS soft segments [41].

Consequently, while PBS crystals were not observed on PIB_O-PU samples, due to the presence of PIB phase (soft phase), covering the surface of PIB_O-PU and proving an outstanding hydrolytic stability to sample, the -Si-O- sites of the PDMS segments in the ELAS structure are more susceptible to hydrolysis and it may cause the hydrolytic cleavage, adsorption, and deposition on sample surface [41].

The absence of barrier such as PIB, bio-application capability of ELAS is expected to lower than PIB based PUs in terms of many parameters.

3.3.3. Critical In-vitro Biocompatibility Evaluation of New PIB based PUs

3.3.3.1. Calcification

Mineral deposition, such as calcification, on implanted biomaterials restricts their clinical applicability and biocompatibility. Deposition of crystalline calcium phosphates like hydroxyapatite ($Ca_{10}(PO_4)_6(OH)_2$), HAP, on implanted polymeric materials is extremely undesirable since it reduces their function and long-term stability. Calcification of implanted synthetic heart valves, cardiac assist devices, etc. causes pathological stiffness and degeneration, although mineral deposition on bones and teeth is a natural and normal process. Therefore, the dysfunction caused by calcification must be reduced or avoided whenever possible [41].

Consequently, to evaluate the in-vitro biocompatibility, the calcification resistance of PIB based PUs was questioned in this study and the results were compared with ELAS, conventional non-PIB based PUs.

3.3.3.1.1. ELAS

The analytical results, obtained by SEM, EDX, AFM and XPS instruments, of ELAS sample, which is used as a control material, are summarized in Figure 3.47.

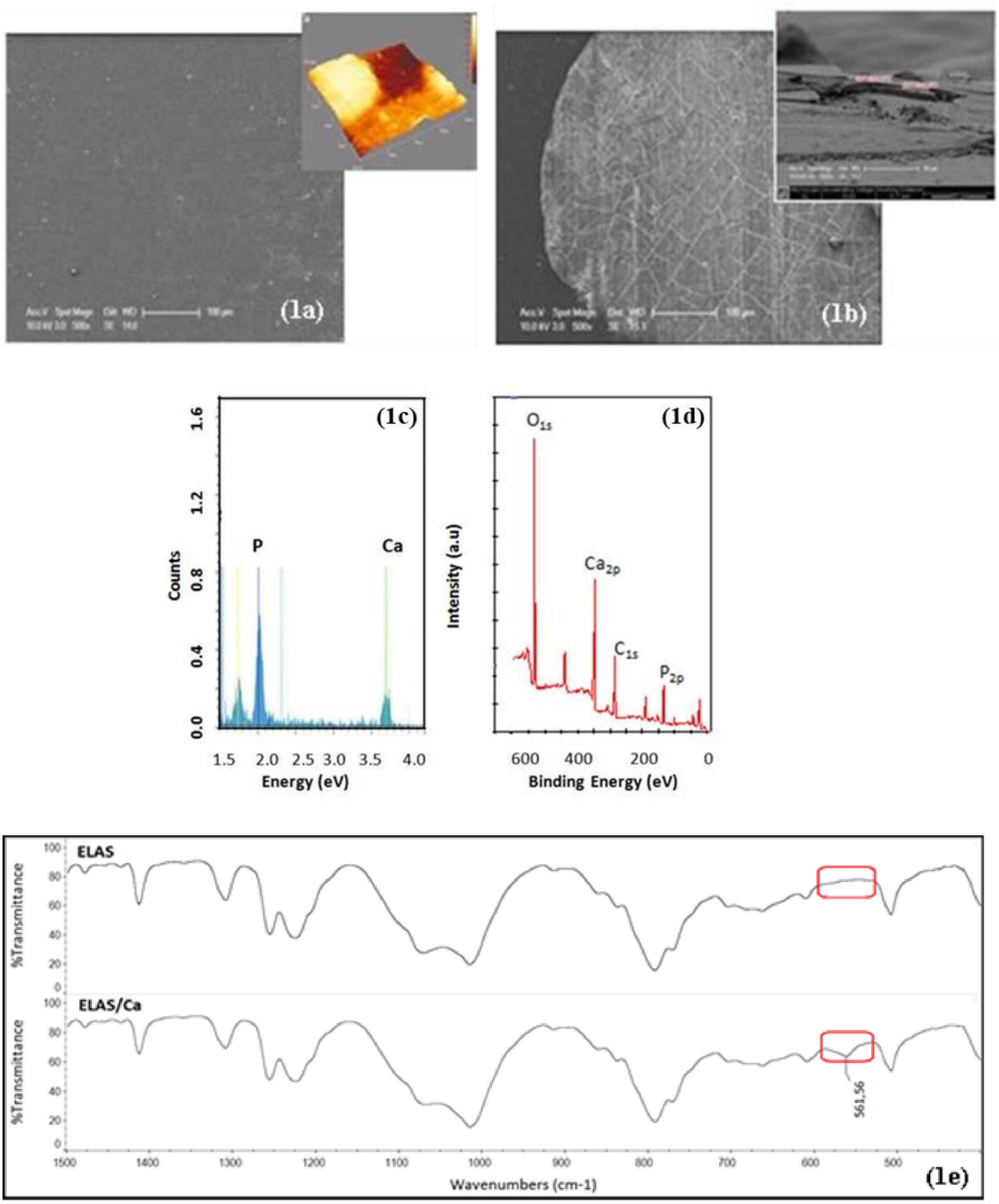

Figure 3.47: (1a) SEM images before SBF incubation for 28 days and the AFM image of ELAS surface is also inserted (1b,c,d) SEM image, EDX spectra and XPS spectra of ELAS after 28-day SBF incubation, respectively (1e) FTIR spectra before (ELAS coded) and after (ELAS/Ca coded) 28-day SBF incubation. Reprinted from [41].

The surface roughness value of ELAS sample, before SBF incubation, was determined as 41.99 nm (RMSD) via AFM spectroscopy (see in Figure 3.47.1a, inset) so it can be defined as a satin surface whose roughness is lower than 0.6 micron. [79] However, after 28-day SBF incubation, extensive calcification was observed on ELAS surface. As seen in Figure 3.47.1b, there was a ~5.75-micron-thich calcium phosphate (CaP) deposition on ELAS [41].

Ca and P deposition are supported by the FT-IR spectra of incubated ELAS (Figure 3.47.1e), which displays a strong characteristic 561 cm-1 band associated with the triply degenerate bending mode, ν4, of the O-P-O group of HAP [41].

EDX and XPS spectra after being incubated are shown in Figure 3.47.1d and 1e, respectively. Particularly, encrustation by calcium-deficient HAP is indicated by a ratio of calcium to phosphorus by XPS that is higher than unity (Ca/P 1.24, with Ca = 13.46% and P = 10.82%, respectively). Some Ca^{+2} may have been replaced by Mg^{+2} and/or Na^{+} during incubation (EDX reveals Na^{+} at ~1.0 keV, not indicated in the picture) [41].

Consequently, like the artificial heart valves made of silicon rubber, well known to calcify, ELAS surface is not calcification resistant as shown by FTIR, AFM, XPS, SEM and EDX analyses. Chelation of Ca^{+2} at —O— sites in soft segments of ELAS may lead to extensive calcification on surface [41].

3.3.3.1.2. PIB_O-PU

The analytical results, obtained by SEM, EDX, AFM and XPS instruments, of PIB_O-PU sample are summarized in Figure 3.48.

It was shown that the surface of PIB-PUs containing 72.5- wt% PIB was covered by PIB and it exhibited exceptional hydrolytic and oxidative resistance, as well as negligible water swelling due to inert segments (CH_2 and CH_3) at the surface inhibiting the diffusion [41]. Therefore, immersion PIB- PU in an aqueous SBF solution, conveniently used for calcification analyses, is not anticipated to undamaged the film structure, alter its surface or bulk morphology of sample [41].

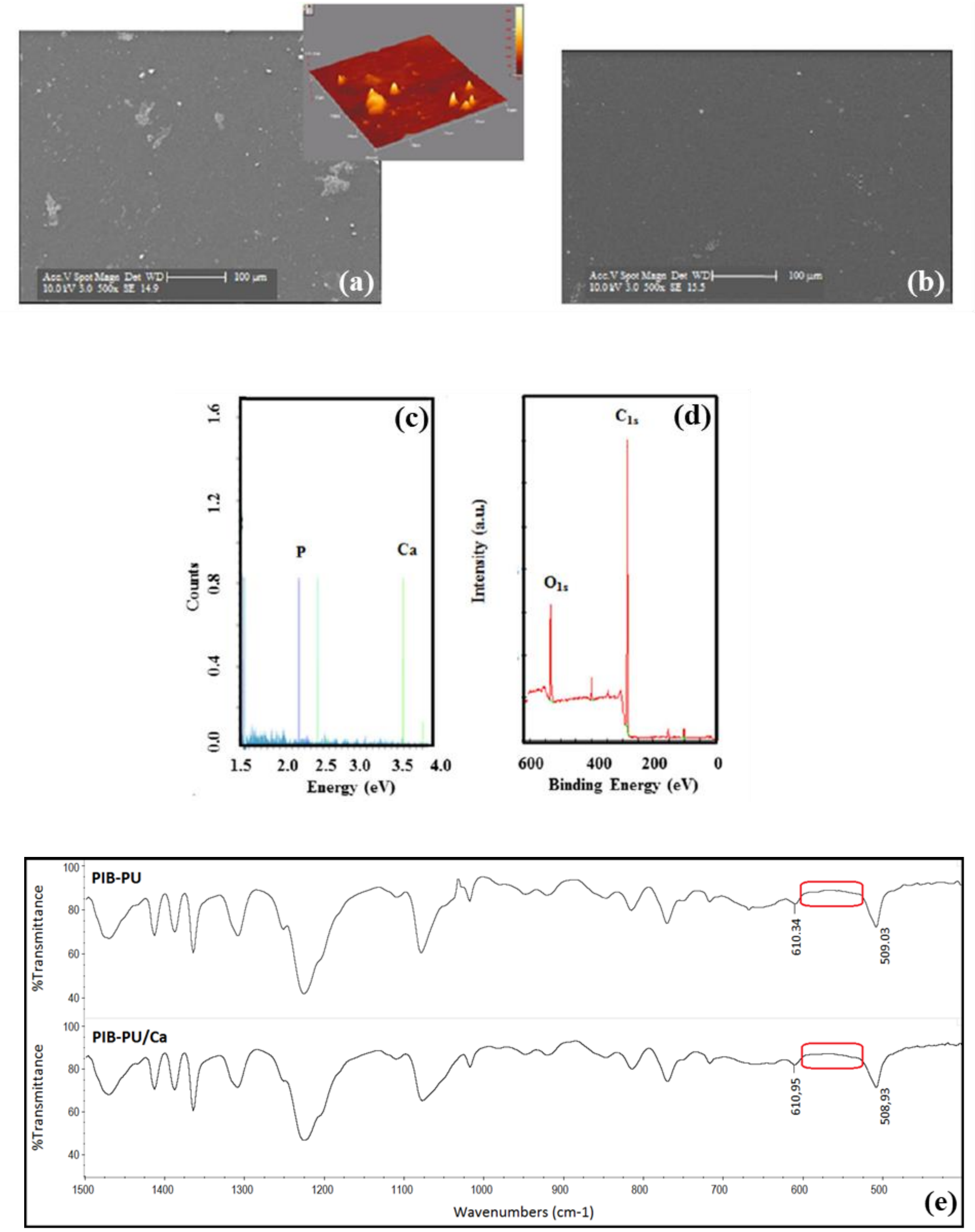

Figure 3.48: (a) SEM images before SBF incubation for 28 days and the AFM image of PIB_O-PU surface is also inserted in (a) SEM image, (b,c) EDX spectra and XPS spectra of PIB_O-PU after 28-day SBF incubation, respectively, (e) FTIR spectra before (PIB-PU coded) and after (PIB-PU/Ca coded) 28-day SBF incubation. Reprinted from [41].

The comparable quantitative results show that layers with hydrophobic groups correlates with the lack of mineralization so almost no calcification was observed for polymers lacking charged functional groups eg. PET and PTFE [80].

Figure 3.48.a,b depict SEM and AFM (inset) images of PIB- PU demonstrating the lack of calcification following 28-day incubation on a smooth satin surface with 24.88- nm roughness (rms value). This was also supported by EDX, XPS, and FT- IR spectra: the FTIR spectra lacked the characteristic band at 561 cm^{-1} associated with the triply degenerated bending mode, ν4, of O─P─O, and the other characteristic band at 1036 cm^{-1} assigned to the vibrations of phosphate group of hydroxyapatites [81, 82] does not observed in FTIR spectra after incubation as an absence of Ca and P deposition. EDX indicated an absence of Ca and P, also XPS showed a minor surface deposition of Ca and P (0.46% for both). These results suggest that PIB- PU with 72.5% PIB composition is resistant to calcification [41].

3.3.3.1.3. PIBS-PU

Kepa et al. have reported that increasing number of sulfonic groups in the polymer structure leads to the acceleration of mineral deposition such as calcium. In literature, early studies showed that the sulfonic groups in structure were more effective than carboxylate groups in polyamide copolymer at inducing mineralization which is related with the acid dissociation constants of these functional groups. Early studies on self-assembled monolayers showed that minimal mineral deposition is observed on the substrate surface with cationic and neutral groups and no mineralization is on the layer with hydrophobic groups while anionic groups at the surface have induced Ca and P mineralization in SBF [80]. Because mineral nucleation is related with the electrostatic interaction between Ca^{+2} ions and substrate surface. Tanahashi et al. have also reported that the highest mineralization capacity belonged to phosphate group and mineralization tendency of carboxylate groups followed the phosphate functionalized structure [80, 83]. The sulfate-based structure also showed significant Ca and P mineralization however the mineral nucleation capacity of sulfate group has not as yet directly compared to other functional groups [80].

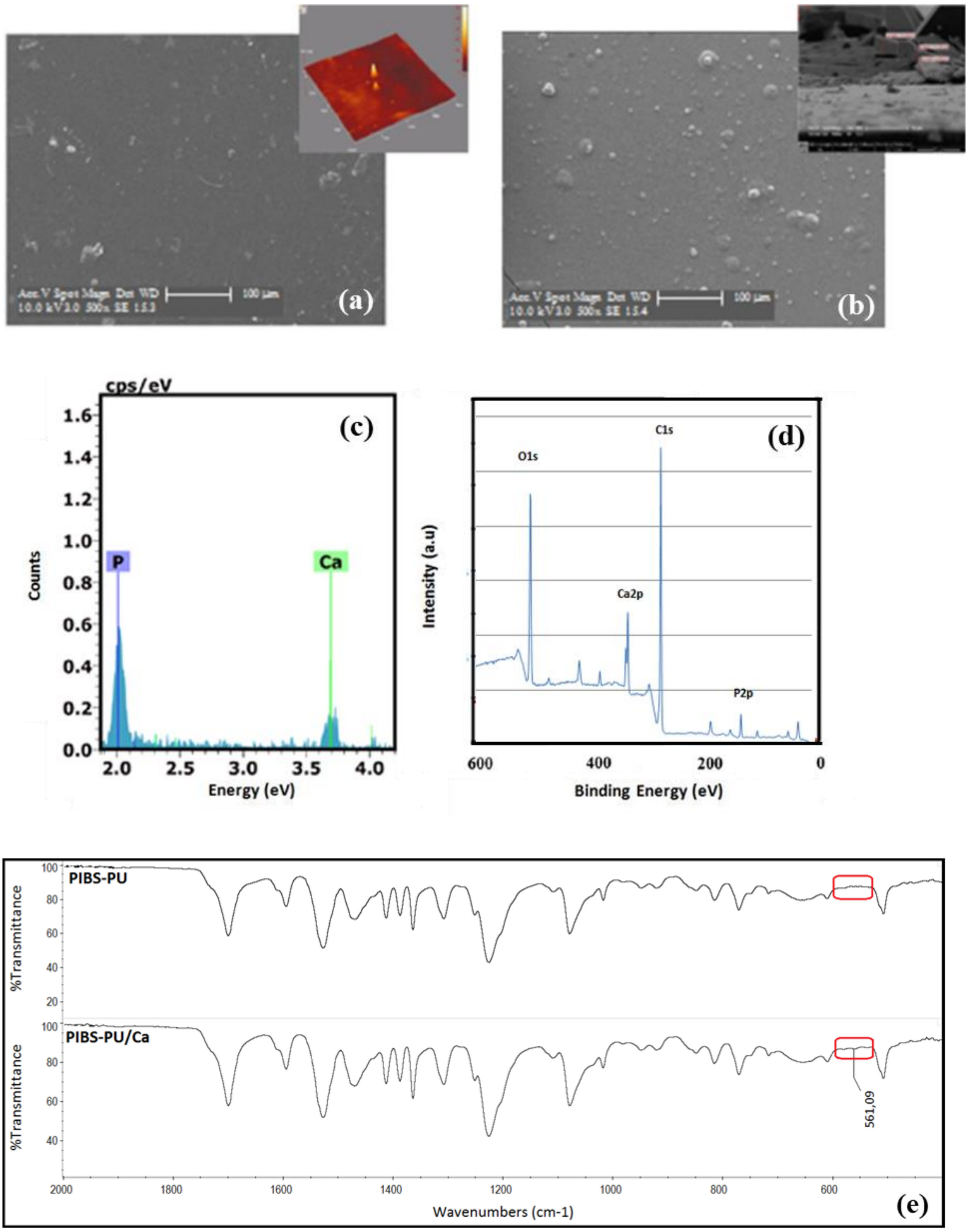

Figure 3.49: (a) SEM images before SBF incubation for 28 days and the AFM image of PIB_S-PU surface is also inserted in (a) SEM image, (b,c) EDX spectra and XPS spectra of PIB_S-PU after 28-day SBF incubation, respectively, (e) FTIR spectra before (PIB_S-PU coded) and after (PIB_S-PU/Ca coded) 28-day SBF incubation. Reprinted from [41].

The analytical results, obtained by SEM, EDX, AFM and XPS instruments, of PIB_S-PU sample are summarized in Figure 3.49.

Figure 3.49.a,b depict SEM and AFM (inset) images of PIB_S- PU demonstrating the modest encrustation with around 11.92- micron- thick mineralization over a wide and originally smooth (~39 nm roughness) surface area.

As suggested by XPS results, calcium deficient HAP is observed on PIB_S-PU film because Ca/P molar ratio (Ca = 5.28% and P = 4.22%) is about 1.25. The lower Ca/P molar ratios than 1.67 (Ca/P < 1.67) are generally observed after longer calcification times. Because the longer incubation in SBF results the substitution of some Ca^{2+} ions by Mg^{2+} and Na^{+} ions. In this study, Mg and Na appears at around 1.3 keV and 1.0 keV in EDS spectrum (not shown). Also, a characteristic FTIR band at 561 cm−1 associated with the O─P─O bond in HAP slightly appears after incubation as proof of calcification on PIB_S-PU surface [41].

Since sulfone groups were reported to promote mineralization, the calcification on PIB_S- PU surface might have been enhanced by sulfoxide (~84%) and/or sulfone (~16%) groups that originated from the oxidation of sulfur by minute amounts of O_2 dissolved in the SBF medium [16, 41].

3.3.3.1.4. PIB-PUU

Figure 3.50 summarizes surface analytical results of PIB-PUU (which was prepared by our collaborative laboratory members for a different project and was used for only comparison study in this part) before and after incubation in SBF solution.

Ca and P deposition is supported by the existence of a strong absorption at 561 cm^{-1} in the FTIR spectra of incubated PIB- PUU, indicating the presence of a triply degenerate bending mode, ν4, of O─P─O in HAP [41].

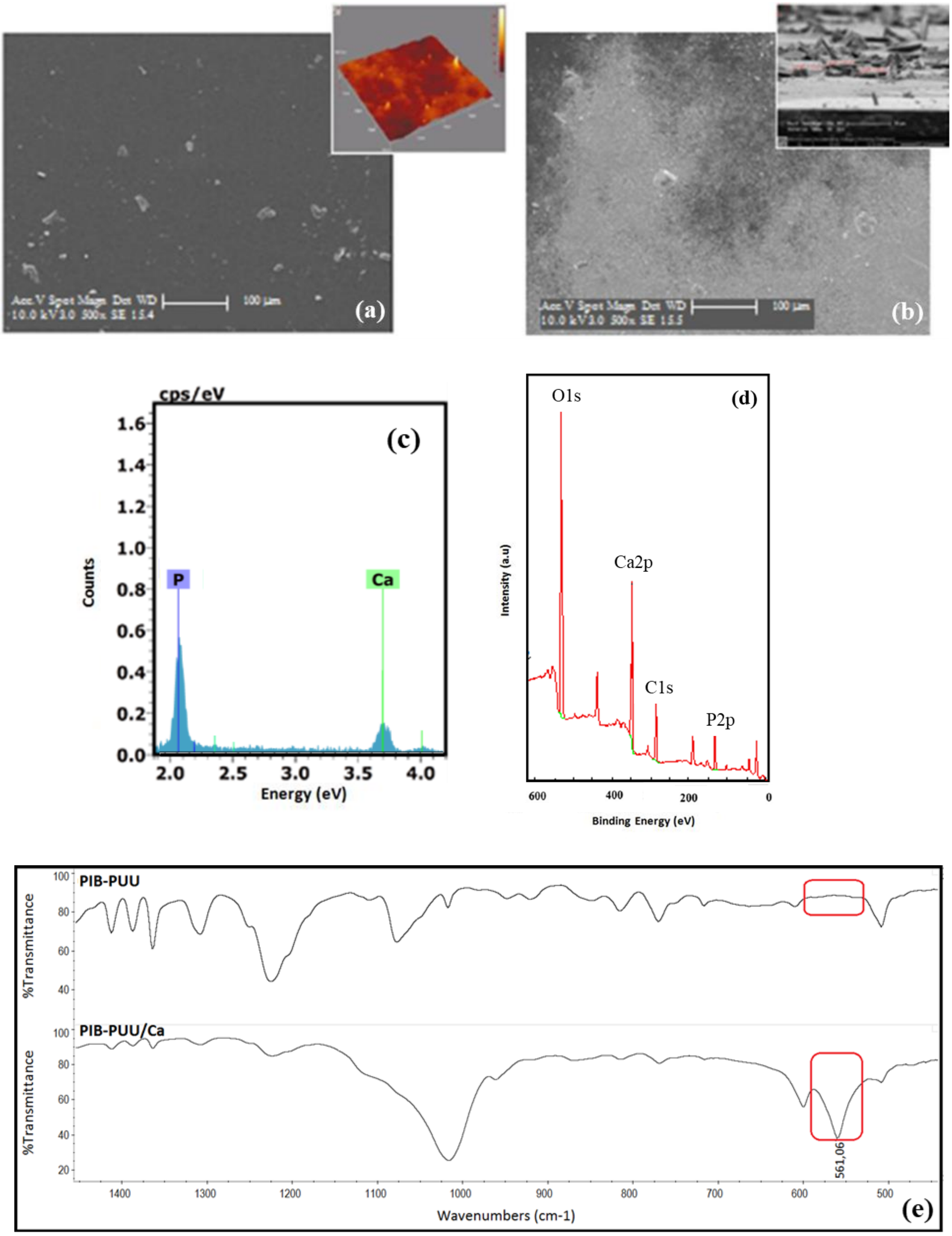

Figure 3.50: (a) SEM images before SBF incubation for 28 days and the AFM image of PIB-PUU surface is also inserted in (a) SEM image, (b,c) EDX spectra and XPS spectra of PIB-PUU after 28-day SBF incubation, respectively, (e) FTIR spectra before (PIB-PUU coded) and after (PIB-PUU/Ca coded) 28-day SBF incubation. Reprinted from [41].

As seen in Figure 3.50.a,b, SEM and AFM images further indicate calcification after SBF incubation and show a strong deposition (~2.50 micron- thick encrustation) on an originally satin surface (~3.94 nm roughness). Also, EDX spectrum (Figure 3.50.c.) showed that Ca/P molar ratio is approximately 1.23 (Ca = 15.93% and P = 12.88%) which means calcium- deficient HAP deposition like PIB$_S$-PU. Presence of Na and Mg in solution (EDX spectra of incubated PIB-PUU showed peaks at ~1.3 and ~1.0 keV, respectively), positively charged ions other than Ca^{+2} can contribute the formation of hydroxyapatite during the equilibration of calcification in SBF (and it creates calcium-deficient HAP deposition on sample surface. The fact that the amounts of Ca and P on PIB-PUU are greater than those on PIB$_S$-PU (Figure 3.49.c), most likely due to a greater abundance of urea groups on PIB-PUU than chelating S sites in PIB$_S$-PU. The higher deposition of Ca and P is related with the higher N content in structure and more phase-separated nature of PIB-PUU. It is known that due to the electronegative character, the nitrogen of urea linkages can create additional binding sites for Ca^{+2} ions and these interactions lead to higher Ca and P deposition [41]. Moreover, in the hard segment of structure (polyurethane-urea), controlled combination of linear and bifurcated hydrogen bond exists [67]. The intense hydrogen bond case results in the formation of compact and more phase-separated structure which makes it possible for Ca^{+2} chelation. Thus, positively charged calcium ions form a complex with electronegative nitrogen, act as a donor atom, of urea linkages of hard domains in the coordination sphere. During the long calcification process, firstly Ca^{+2} ions bind through the chelation, then they will attract PO_4^{-3} ions and propagate the Ca and P deposition [41]. Consequently, these results suggest that PIB- PUU surfaces are prone to calcification.

3.3.3.1.5. PIB$_S$-PU/NC

PIB$_S$-PU was prepared by the use of HO-S-PIB-S-OH plus the conventional diisocyante MDI and chain extender BDO. Although the presence of -S- in polyurethane structure results in the formation of additional hydrogen bonds improving the mechanical properties of material, sulfonic groups in the polymer structure cause an increased mineral deposition such as calcium [16].

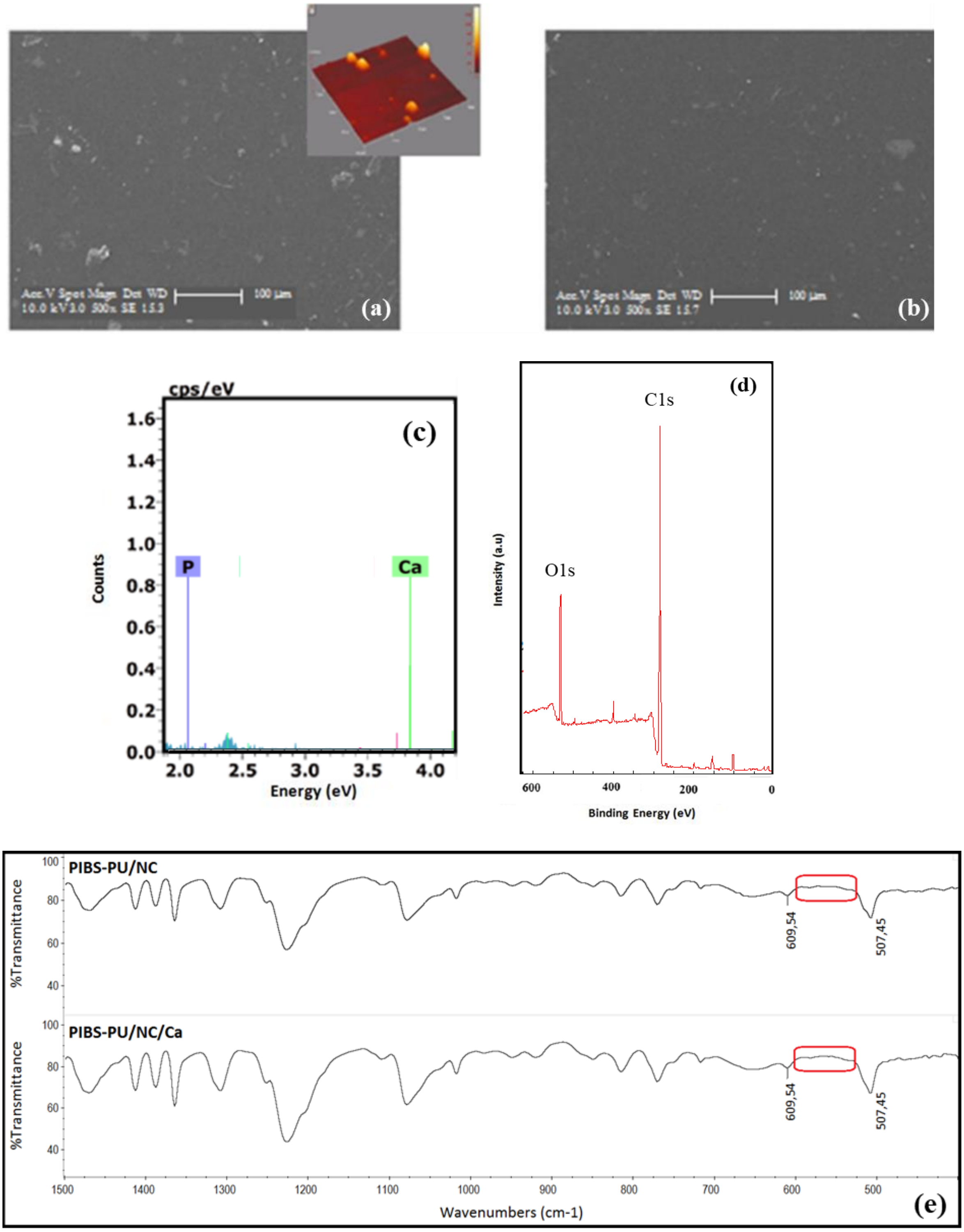

Figure 3.51: (a) SEM images before SBF incubation for 28 days and the AFM image of PIB$_S$-PU/NC surface is also inserted in (a) SEM image, (b,c) EDX spectra and XPS spectra of PIB$_S$-PU/NC after 28-day SBF incubation, respectively, (e) FTIR spectra before (PIB$_S$-PU/NC coded) and after (PIB$_S$-PU/NC/Ca coded) 28-day SBF incubation. Reprinted from [16].

Even though sulfur content promoted the mechanical strength of this material, it is diminished due to the substantial amounts of PIB in its soft phase. This deficiency may also remedied by strengthening the PIB_S-PU with trace amount (0.5%) of montmorillonite (MMT) modified with a quaternary ammonium salt, 3-amino-N,N,N-trimethylpropan-1-ammonium ($ATMPA^+I^-$) [41, 84].

As mentioned in 3.2.2.2., the mechanical strength of this nanocomposite was significantly better to those of unreinforced PIB_S-PU [21]. Also, the calcification pattern of both PIB_S-PU and PIB_S-PU/NC were examined. Figure 3.51 is a summary of the surface analytical data of PIB_S-PU/NC before and after 28-day incubation. The FT-IR spectra showed the lack of the characteristic band at 561 cm^{-1}, and SEM images (which showed free of calcification on surface) of sample were supported by EDX data which showed that the absence of Ca an P. Also, the negligible mineralization on PIB_S-PU/NC surface was substantiated by XPS results (which showed Ca = 0.65% and P = 0.397%) [41].

Although PIB_S-PU prone to calcification, the calcification resistance of PIB_S-PU/NC can be explained by that amine-modified MMT (reinforcing agent) was not found to promote mineral deposition since it is likely to be hidden inside the bulk. In the other hand, calcification would not occur if quaternary amine-modified MMT was present on the surface because it would repeal Ca^{+2} ions responsible for the process [41].

As a result, the addition of the MMT or quaternary ammonium salt to PIB_S-PU inhibits mineralization by decreasing Ca from 5.28% to 0.65% and P 4.22% from to 0.397%, however, some of sulfur atoms in soft phase may have oxidized to sulfoxide by a trace amount of water in SBF solution, resulting in the extremely modest levels of mineralization detected by XPS [41].

3.3.3.2. Protein and Cell Studies

3.3.3.2.1. Protein Adsorption on Polymer Surfaces

Quantitative analysis on protein adsorption was conducted by using UV spectrometer. For calculating the attached Fg amount to surface, the standard curve equation (see in Figure 2.2) and absorbance values were used. The 4 best experiment results were shown in Table 3.5. For comparing the protein adsorption capacity of samples, the average value of 4 experiment was used.

Table 3.5: UV absorbance results of solutions contained eluted Fg after adsorption on sample surfaces.

	UV Absorbance (Mean Values)				
Set #	**PIB$_O$-PU**	**PIB$_S$-PU**	**PIB$_S$-PU/NC**	**PIB-PUU**	**ELAS**
1	0,314	0,315	0,308	0,307	0,315
2	0,302	0,309	0,302	0,313	0,306
3	0,340	0,339	0,323	0,324	0,376
4	0,308	0,325	0,300	0,337	0,295
Average	**0,316**	**0,322**	**0,308**	**0,320**	**0,323**

After determining the best experiment sets, their average absorbance value was put instead of y at the standard curve equation ($y = 0.0981x + 0.1751$) and concentration of adsorbed protein on each surface was calculated. Before calculating the protein amount on surface from the standard curve equation, the absorbance values of PBS, which was used as a blank solution in each measurement, were considered. Table 3.6 summarizes the adsorbed protein amount on all films.

Table 3.6: Average adsorption values and Fg amounts on sample surfaces.

Samples	**UV Adsorption**	**Protein (µg/ml)**	**Protein (µg/cm^2)**
PIB$_S$-PU/NC	0,308	1,36	16,7
PIB$_O$-PU	0,316	1,43	17,6
PIB-PUU	0,32	1,48	18,2
PIB$_s$-PU	0,322	1,50	18,4
ELAS	0,323	1,51	18,6

Since the protein adsorption increases with increased water uptake capacity of the polymer films [77]. It is an expected result that the highest PBS (so water) uptake observed at ELAS sample (Figure 3.44), which caused the greatest Fg adsorption capacity than other PIB based PU films (see in Figure 3.52).

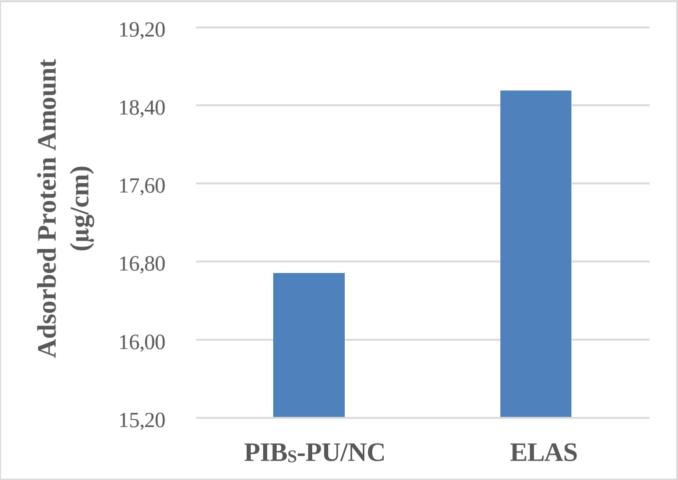

Figure 3.52: Protein (Fg) adsorption comparison of least and most active samples, PIB$_S$-PU/NC and ELAS, respectively.

In literature, many different methods were used to examine protein adsorption on polymeric material surfaces such as quartz crystal microbalance with dissipation monitoring (QCM-D) [31] and Bradford assay [85]. In this Bradford study, 1 mg/mL protein solution was used and according to its results, for ELAS showed the highest protein adsorption on its surface (18,6 µg/cm^2) mainly due to its hydrophobicity as explained above. Balaji et al. proved that polyether-based PU structure adsorbed app. 30 µg Fg per cm^2 by applying Bradford assay [85] and it is higher than all PIB based PU samples and also ELAS because of the lower stability of ester linkage. In addition, Cozzens et al. studied on the concentration based competitive protein adsorption on polyisobutylene-based thermoplastic polyurethanes and proved that increased concentration of protein solution increases the adsorbed amount by changing Fg solution concentration from 50 µg/mL to 100 µg/mL. This double increase also increased the amount of absorbed protein on Elast-Eon® 2A, having a same content with ELAS coded sample in this study, by 1.4 times [31]. Considering these studies, it can be said that results of this study are consistent with the examples in literature.

3.3.3.2.2. Cell Attachment and Cell Viability on Polymer Surfaces

Mouse connective tissue L929 cells, obtained from ATCC, were used for both studies. In the cell attachment test, cells were allowed to attach on films for 24 h at CO_2 incubator and after fixation of cells, the qualitative analysis of attached cells on different sample surfaces was obtained by SEM images.

For cell viability, the cytotoxic effects of each polymer should be examined. In literature, there are many studies about cell viability of polymers and in these studies, cell viability on polymers were checked in different times such as 3 h, 9 h, 24 h, 48 h. To predict the toxic effect on in vivo systems, while an early cytotoxic response can be taken within 3 hours after starting the cell interactions, cytotoxicity after 24 hours is essential when taking into consideration the 24-hour blood circulation and clearance time. Therefore, 24 h data of MTT assay was used to evaluate the cell viability on polymer surfaces [75, 86]. For comparing the quantitative cell viability capacity of polymer samples, MTT assay was performed, and the cell viability order of samples was predicted from the average optical density values of them at 570 nm (by using the coloring properties of MTT chemical reagent with living cells) [75, 86, 87]. Based on the results of this study, the cell viability order of samples is determined according to the Relative Growth Rate (RGR) was calculated as following: RGR: 100% x ODsample/ODcontrol. (Polystyrene based tissue cell plates (TCPs) was used as a control group). He et al. used the MTT assay to determine the potential toxicities of PTFE and PU based vascular grafts which follows the cell survival in a biomaterial-conditioned medium. Additionally, the cytotoxicity was determined using average optical densities at 570 nm measuring growth and was categorized into a range of RGR of 100%, which corresponds to grade 0 – 5 (where grade 5 means the zero growth) [86]. The RGR of L929 cells was above 100% (according to TCP control group) in ELAS and PIB based PU experiments (see in Figure 3.53).

However, the results of this experiment were not considered sufficient to make a quantitative comparison with the literature data because the quantitative results in literature were obtained with minimum 3 independent experiments with five-eight replicates and within different end points (such as 24 h, 48 h, 72 h etc.) [86]. However, due to the quantity of used samples, cell viability study with only 1 MTT assay (at 24 h) with 4 replicates per sample was used to predict the cytotoxicity ordering of samples (see in Table 3.7).

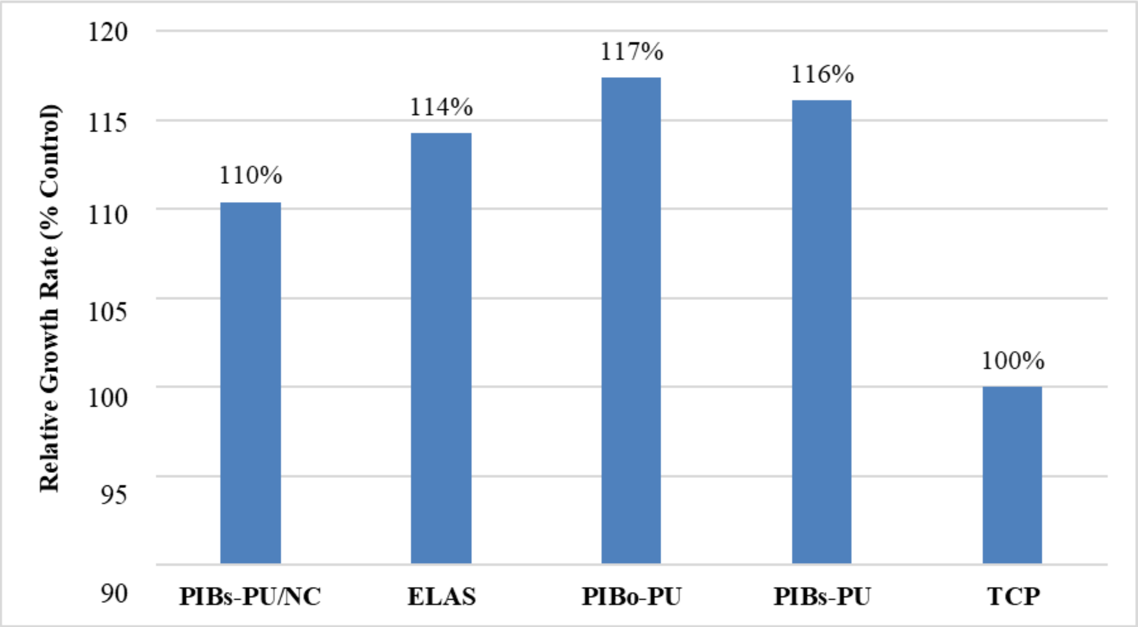

Figure 3.53: Relative growth rate (% control) of mouse fibroblast L-929 cells by absorbance measurement at OD_{570nm} by the MTT assay and using TCP surface as a control.

The cytotoxicity criteria are shown in Table 3.7. RGR values of grade 3–5 is regarded as cytotoxic whereas grade 0–1 is considered non-cytotoxic [86]. As seen in Figure 3.53, the RGR of mouse fibroblasts (L929) was above 100 % in ELAS and all PIB based PU samples' experiment group and so their cytotoxicity level reached at grade 0.

Table 3.7: Cytotoxicity criteria based on relative growth rate (% control) values [86].

Relative growth rate (%)	≥100	75-99	50-74	25-49	1-24	0
Cytotoxicity Grade	0	1	2	3	4	5

According to these data, as expected, TCP has the lowest cell viability result at 24h and because of its polystyrene nature. For this study, polystyrene based tissue culture plates were used. Polystyrene surfaces are mainly composed of hydrophobic natured phenyl groups, which are harmful to cell anchorage since they are not naturally found in the body [88]. Therefore, since polystyrene surface has extremely low surface energy, it is cell repellent due to the little adsorption of proteins on the cell membrane [89]. In addition, polystyrene was reported to be calcifying [41]. As a result, the cytotoxicity grades of PIB based PU samples and ELAS are lower than TCP used as a control.

According to protein adsorption, cell attachment and cell viability studies, the connection between these results are tried to designate. In detail, Table 3.8 summarizes the adsorbed protein (Fg) amount and the qualitative order of cell attachment on each film surface, and the quantitative order of cell viability capability of samples.

Table 3.8: The adsorbed Fg amount and the qualitative order of cell attachment on each film surface, and the quantitative order of cell viability capability of samples.

Samples	**Adsorbed Fg Amount on Surface (µg/cm^2)**	**Protein Adsorption Order *(Quantitative**)***	**Cell Attachment Order *(Qualitative*)***	**Cell Viability Order *(Quantitative**)***
PIB$_S$-PU/NC	16.7	1	1	4
PIB$_O$-PU	17.6	2	2	1
PIB-PUU	18.2	3	3	-
PIB$_S$-PU	18.4	4	4	2
ELAS	18.5	5	5	3

**Qualitative results rely on the first-hand observation (1: the lowest, 5: the highest)*
***Quantitative results depend on numerical data (1: the lowest, 5: the highest)*

The sample based detailed explanation of these analyses below.

3.3.3.2.3. ELAS

As seen in Table 3.8, the highest Fg adsorption was on ELAS film surface mainly due to the highest contact angle related hydrophobicity of the surface since when adsorbing to more hydrophobic surfaces, proteins preferentially lose their α-helix secondary structures and adopt an unfolded β-sheet conformation [69].

As explained in Section 3.3.1.1, surface wettability of biomaterials in relation to its hydrophobicity or hydrophilicity has a significant impact on its biological response, and surface hydrophobicity improves protein adsorption and (concurrently) cell adhesion capacity of biomaterials [69, 90]. Therefore, like in Fg adsorption results, ELAS has a great tendency for cell attachment and the qualitative observation of attached cell on its surfaces, shown in Figure 3.54 with SEM images, supports this approach.

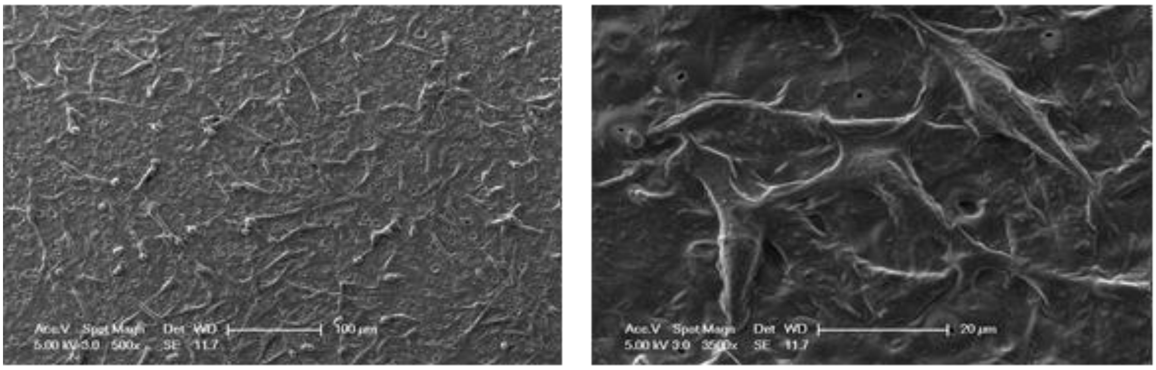

Figure 3.54: Scanning electron microscopy images of L929 cells attached on the material surface of ELAS (The “flattened” appearance of adherent cells is shown in 3500x SEM image).

In addition, since the surface roughness levels above 4.0 nm impeded cell stretching and promoted the occurrence of round-shaped cells, lower surface roughness ratios encourage and indicate a better fibroblast cell adhesion [32]. Therefore, the cell attachment capability of ELAS surface is greater than that of PIB_O-PU surface (Table 3.8).

Protein adsorption and cell adhesion capacity of ELAS surface are in a same pattern because the cell adhesion has been based upon the physical, chemical, and mechanical properties of material. In general, an adsorption of proteins onto a polymer surface, which is defined as a “hard attachment”, is accepted as the first step of the cell attachment mechanism onto polymer surfaces and it is followed by a more dynamic “softer” layer with the interactions between these proteins and related cells [91]. Therefore, the cell attachment mainly depends on the protein adsorption onto a polymer.

Consequently, these results can be explained by more than one preliminary surface properties discussed in 3.3.1. According to surface roughness, the protein adsorption capacity and cell attachment difference between ELAS (RMS = ~ 45 nm roughness) and PIB_O-PU (RMS = ~25 nm roughness) (Table 3.3) is theoretically acceptable. However, ELAS showed a lower cell viability so higher cytotoxicity in the MTT assay. An increase in surface roughness, as a consequence of the formation of valleys and peaks, [71] inhibit the cell stretching and so encourage the existence of round-shaped cells [32] and more inflammation is triggered by rough and porous surfaces than by smooth and structured ones. [72]. As a result, due to its surface roughness, lower spreading of cells was observed on ELAS surface and the viability of cell on ELAS surface has a low ratio. Furthermore, a stiff behavior of sample surface that prevents a firm connection with the cell membrane greatly reduces the cell viability [32] so Shore A hardness results, as well as surface roughness, consistently support the cell viability capability of samples. Also, compared to other PIB based PU samples in PBS medium, ELAS has also the highest swelling capacity (Figure 3.44 and Table 3.3). This result is closely related its lowest hydrolytic stability mentioned above. This low stability of ELAS can be also verified with the vucol riched surface appearance in SEM images given in Figure 3.54 after PBS mediated cell attachment studies.

Finally, chemical composition on sample surface has a significant impact on biocompatibility. ELAS is a commercially available PDMS-based polyurethane, and our samples were mainly prepared as PIB based PU. Although both structures include urethane linkage in their hard segments, the hydrolytic stability of PIB based PU samples is higher than ELAS since PIB soft segment, in PIB based PU structures, proportionally pretends as a barrier on the urethane linkage in the hard segment [16, 21]. Due to its lower stability, the urethane part of ELAS is more open to hydrolysis in PBS medium so during the 24-hour cell studies, amine and hydroxyl groups begin to form on the surface of ELAS. It is assumed that these formations cause to death of cells on ELAS surface because the role of amines and hydroxyl groups on toxicity was proven in literature [32]. Especially, Jeong et al. mentioned that the increased amount of hydroxyl group on sample surface, producing metabolites such as ellagic and gallic acids, have a toxic effect on the seeded-cells [75]. As a result, due to having the lowest hydrolytic stability compared to PIB based PU samples [16, 21], the lower cytotoxicity of ELAS is acceptable.

As a result, the bio-application capability of ELAS is lower than PIB-based PU samples in terms of many parameters.

3.3.3.2.4. PIB$_S$-PU

As seen in Table 3.8, PIB$_S$-PU shows high protein adsorption trend despite of its lower contact angle pattern. However, as explained in 3.3.1; protein adsorption can be affected by several surface parameters and sulfonation is one of them since it affects the surface properties. It is reported that the sulfonate group concentration on the polyurethane substrates directly affects Fg uptake and ex vivo platelet adhesion on polymer surfaces. Therefore, while Fg adsorption was reduced in the low-sulfonated materials, the concentration of Fg on the surfaces significantly increased in the higher-sulfonated materials. In addition, because of significantly greater adsorption levels and less displacement of initially deposited protein (Vroman effect), Fg adsorption behavior significantly differs from the conventional unsulfonated PU samples. In general, surfaces with increasing hydrophilicity tend to be more “dynamic” regarding protein adsorption. Also, Santerre et al. reported that plasma-surface interaction is significantly influenced by the presence of sulfonate groups because of the hydrophilicity which is a determinant parameter for protein adsorption [92]. Therefore, due to sulfur content of PIB$_S$-PU, which could have been enhanced by sulfoxide (~84%) and/or sulfone (~16%) groups that arose via oxidation of sulfur by minute quantities of O_2 dissolved in water-based solutions, the higher protein adsorption trend of PIB$_S$-PU is not surprising [16, 93].

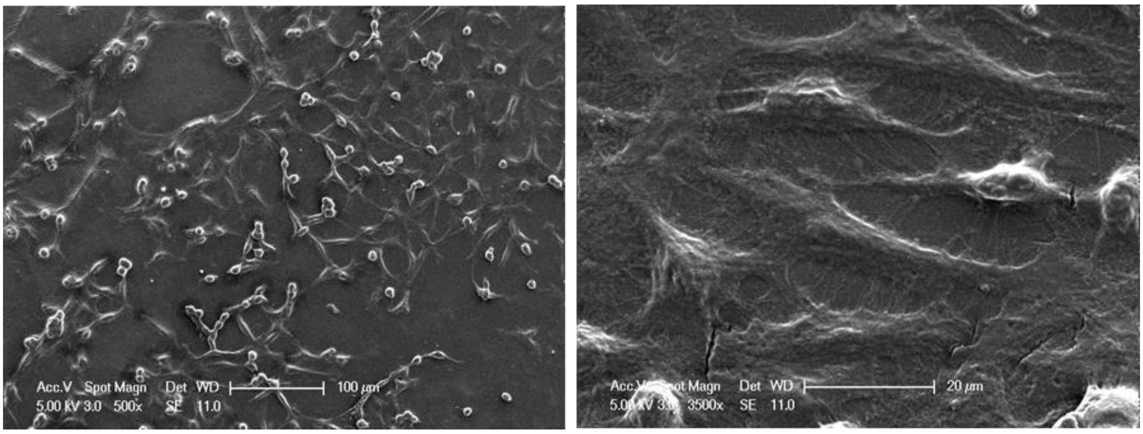

Figure 3.55: Scanning electron microscopy images of L929 cells attached on PIB$_S$-PU surfaces (The “flattened” appearance of adherent cells is shown in 3500x SEM image).

Proteins, such as from the serum, are adsorbed on the surface of non-biological substrate, which lack any ligand for particular cell surface receptor recognition and these adsorbed proteins allow cells to interact with the surface of these substrates. In literature studies, related with cell behavior on nonbiological samples, surfaces, whose chemical composition, and structure are defined, are used because these surface properties have an impact on cell spreading and adsorption via both conformations of adsorbed protein, needed for cell attachment, and receptors on cell surface. The rearrangements in protein structure may take place during the protein adsorption process on polymer substrates, and it is mainly influenced by the polymer type and the orientation of adsorbed protein. When adsorbing on a sample surface, the natural conformation of fibronectin molecule, having a high flexibility, may alter by unfolding into an expanded shape and the biological functions of protein are affected by this type of conformations. Kowalczynska et al. reported that cell adhesion is advanced by the conformation of adsorbed fibronectin molecule on sulfonated polymer substrates. Therefore, like in Fg adsorption study, despite of its hydrophilicity, a qualitative result for greater number of attached cells on PIB_S-PU surface is an expected result (Figure 3.55) [94].

In addition, cell viability on PIB_S-PU is higher than on ELAS but lower than on PIB_O-PU. The main reason of them is the sulfur content of PIBS-PU sample. As explained above, in water-based medium, such as PBS, sulfone and/or sulfoxide groups arises by oxidizing of sulfur with trace amounts of O_2 in PBS [16, 93]. Although the sulfonated structure enhances the protein adsorption and directly promote cell adhesion on surface, it reduced the viability of cells. In detail, Kowalczynska et al. stated that the cells spread relatively quickly on surface including sulfonic group and were significantly polarized within 2 h. The interaction between surfaces, having a high sulfonic group density, and highly polarized cells, creating a less ordered adhesive structure, is weak while the spread cells on surfaces, having a low sulfonic density, form a relatively strong interaction [94].

As a result, sulfonic groups on PIB_S-PU support protein and cell adhesion but the polarization of cells on surface cause the decrease in viability. Furthermore, the swelling ratio of PIB_S-PU is higher than PIB_O-PU due to its lower hydrolytic stability than PIB_O-PU [31]. Also, its water permeability is lower than ELAS and it is acceptable as explained above.

3.3.3.2.5. PIB$_S$-PU/NC

As seen in Table 3.8, the lowest protein adsorption was observed on PIB$_S$-PU/NC. Surface-protein interactions are influenced by both protein and surface properties. Besides material type and chemical structure, which are main chemical properties of polymer, surface energy, charges, contact angle, and morphology, which are main physical properties of polymers, should be considered as important parameters for biological properties and biocompatibility of surfaces. As previously mentioned, PIB$_S$-PU/NC structure contains 0.5% MMT whose structure is shown in Figure 3.33 and 3.41 and homogeneously separated quaternary amine structure's function and resist protein adsorption [95].

The important role in influencing the biological response of a biomaterial of hydrophilicity was explained in previous parts. In addition to that, the lower cell adhesion tendency of PIB$_S$-PU/NC is expected due to its lower contact angle value (~71.47^0) referring to higher hydrophilicity. Adding a trace amounts (0.5%) of montmorillonite (MMT) modified with a quaternary ammonium salt, 3-amino-N,N,N-trimethylpropan-1-ammonium (ATMPA$^+$I$^-$) mechanically reinforced the PIB based PU material and the roughness of polymer structure directly affected from this modification. [16, 30, 41] Therefore, highest roughness value of PIB$_S$-PU/NC (with 121 nm surface roughness) is not surprising result [32]. As explained in previous parts, higher roughness ratios indicated lower fibroblast cell adhesion on biomaterial surface (see in Figure 3.56).

Although the surface hardness values of PIB$_S$-PU (Shore A is 85) and PIB$_S$-PU/NC (Shore A is 90) are very close to each other (Table 3.3), cell adhesion tendency of PIB$_S$-PU is higher than PIB$_S$-PU/NC. Because the sulfur content also increases the cell interaction with surface while the increased roughness significantly affects the cell attachment process. Therefore, the limited amount of attached cell, shown in Figure 3.56, may be because of the oxidation of some of the sulfur atoms in PIB$_S$-PU/NC to sulfoxide by minute amounts of water in PBS [16, 77].

In addition, the positively charged groups coming with quaternary ammonium salt-based intercalant in PIB$_S$-PU/NC reduced the cell viability on surface like in protein adsorption mechanism. Jeong et al. proved that cationic structures more strongly interact (electrostatic interaction) with negatively charged lipid bilayers than anionic and neutral parts. However, like as polycations, positively charged quaternary amine groups act on the cells very quickly and induce the cell death within 9 h by disrupting the cell plasma membrane allowing the release of the intracellular material. In general, it can be said that the rate of cytotoxicity action significantly varied across the groups mostly and mostly depended on the charged of the substrate surfaces since the cell membrane is negatively charged [75].

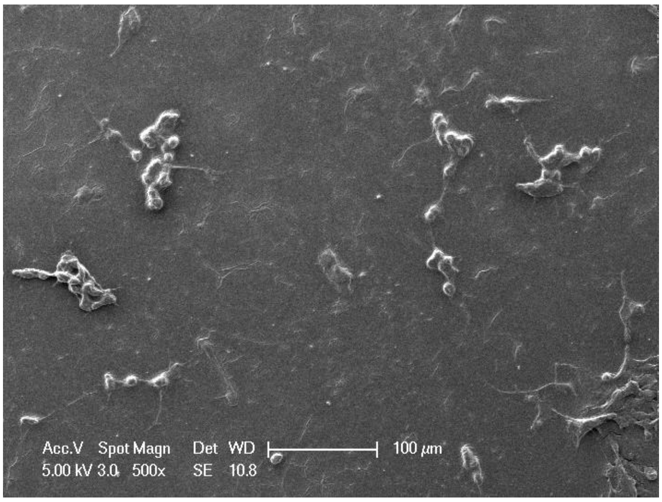

Figure 3.56: Scanning electron microscopy image of L929 cells attached on PIB$_S$-PU/NC surfaces.

As a result, both sulfonic and positively charged quaternary amine parts reduced the cell viability on surface for PIB$_S$-PU/NC. The cell viability order of PIB$_S$-PU/NC is lower than both PIB$_O$-PU and PIB$_S$-PU but higher than ELAS.

Furthermore, the hydrolytic stability, observed in PBS medium, of PIB$_S$-PU and PIB$_S$-PU/NC were not significantly different and trace amount OmMMT addition in the presence of sulfur atoms supports the dimensional stability [21]. As a result, the water permeability capacity of PIB$_S$-PU/NC is lower than PIB$_S$-PU and ELAS but higher than PIB$_O$-PU.

3.3.3.2.6. PIB-PUU

As seen in Table 3.8, PIB-PUU; which was synthesized with 92.2/7.8 mole % urethane/urea composition [67] adsorbs higher amount of Fg, which is approximately 18.2

$\mu g/cm^2$ than other PIB based PU samples. Protein–surface interactions are influenced by the protein's properties on one side and by the surface properties on the other side. Important parameters that have to be considered include surface energy, polarity, charge, and morphology [95]. Therefore, during biocompatibility studies, surface composition of polymers should be considered. As seen in introduction part, in addition to urethane linkage, PIB-PUU contains urea linkage so its nitrogen amount in structure is higher, which is indirectly relevance with contact angle and equilibrium swelling ratio. Yin et al. proved that nitrogen provides a high protein adsorption capability and long-lasting stability of action for substrate [96]. In addition, both oxygen and nitrogen rich surfaces seem to promote adsorption and in turn cell adhesion [97]. Therefore, due to nitrogen and oxygen content addition of urea linkage, PIB-PUU exhibits higher protein adsorption trend.

The creation of novel biomaterials, which will significantly enhance the biocompatibility, is mainly based on the functionalization of polymer surfaces. For surface modification, there are two main methods: (i) biological and (ii) physicochemical such as grafting polymerization, oxidation, acid treatment, photolithography, flame treatment and others. Typically, this kind of surface modification always results in a change in surface energy, which directly affects the interfacial interactions. However, Kostadinova et al. reported that certain polymer surfaces have comparable surface energy while have a different chemical structure and composition. It is clear that other factors than surface energy affect the bio-conductivity characteristic of polymeric materials. For example, chemical composition of polymeric material has an important effect on biocompatibility of them. Numerous chemical groups, such as amine, carbonyl, carboxyl and hydroxyl, have been identified as key players in adjusting the circumstances of attached and attachment of cells on the polymeric surfaces. As mentioned in literature, the presence of some specific chemical groups is correlated with the capacity and capability of macrophages, which are defined as special cells served in the initiation of immune systems by detecting and destructing of bacteria and other harmful organisms, to form massive and multinuclear cells on the surface of various polymeric surfaces. According to the chemical groups, $(CH_3)_2N$-> -OH> -CO-NH-> -SO_3H> -COOH> -COONa, the probability of macrophage fusion reduces. When CHO cells, a kind of mammalian cells, were incubated on a functionalized polymer surface, a comparable hierarchy was also seen in which cell adhesion and growth declined in the following order: -CH_2NH_2 > -CH_2OH> -$CONH_2$ > -COOH. As a summary, in literature, there are many examples about amine rich films/surfaces enhanced the conditions for the cell adhesion and since the presence of amine groups on the surface enhances the interaction of cells with polymeric surfaces [98].

Moreover, because of their low surface energy, or poor wettability, materials with noble bulk properties, such as stability, morphology, hardness, are frequently unable to be used in bio-applications. Thus, the surface modification of materials, such as polymers, is considered as an important application by material scientists and there are many examples and procedures have been used to raise the surface energy of materials by adding hydrophilic groups, such as hydroxyl, carboxyl, amine, to their surfaces. For example, since 1990s, it has been widely known that positively charged surfaces, including amine groups, increase the attachment of endothelial and fibroblast cells to those surfaces at neutral pH. Amine groups advance the adsorption/attachment of molecules that mediate the cell adhesion, such as fibrinogen and fibronectin, in a suitable conformation that is similar to the natural physiological structure of them. Also, Strbkov´a et al. reported that since amine groups of substrates are protonated in neutral pH aqueous medium, positive surface charge is increased and the positively charged amine included surfaces enhanced the attachment and growing of fibroblast cells [99]. As a result, increasing in an electrostatic interaction between the cells and amine groups on the material surface enhances the cell-surface interaction and so cell adhesion on surface [99, 100].

In addition, it has been shown in many studies that the surface charge density can affect the cell attachment and proliferation. Mammalian cells are well known to have a net negative charge according to electrophoretic measurements. As a result, electrostatic repulsion can be preferred to reduce the cell adhesion by using the interaction between negative charged surfaces and cells. Ferrari et al. reported that both negative and positive ions can be used to increase the cell differentiation and biocompatibility of the material surfaces. In their study, increased osteoblast and fibroblast cell adhesion and spreading were seen on the polymeric hydrogel surfaces which are modified with positive charges as opposed to neutral or negative charged surfaces. Also, changing cell behavior has been accomplished by adding chemical functionalities to material surfaces. In their study, the effect of different chargeable functional groups ($-CH_2NH_2$, $-CONH_2$, $-CH_2OH$, $-COOH$) on polyethylene surfaces have been evaluated and the best cell adhesion, spreading and growth rate were carried out on polar and positively charged surfaces, functionalized with amine groups, while more restricted spreading and growth was seen on the negatively charged surfaces, modified with carboxyl acid groups. [32, 99] In summary, despite of its hydrophilic surface nature (~72^0) (Table 3.6), increased amine content in PIB-PUU structure, cell adhesion on substrate surface is in higher amount (Figure 3.57).

In addition, the swelling ratio of PIB-PUU is lower than PIB_O-PU but very close to ELAS. As explained above, the water uptake capacity directly affects the protein adsorption pattern and the swelling ratio order of these 3 samples is same with their Fg adsorption patterns so the equilibrium swelling ratio difference between PIB-PUU and PIB-PU is meaningful [31, 75, 76].

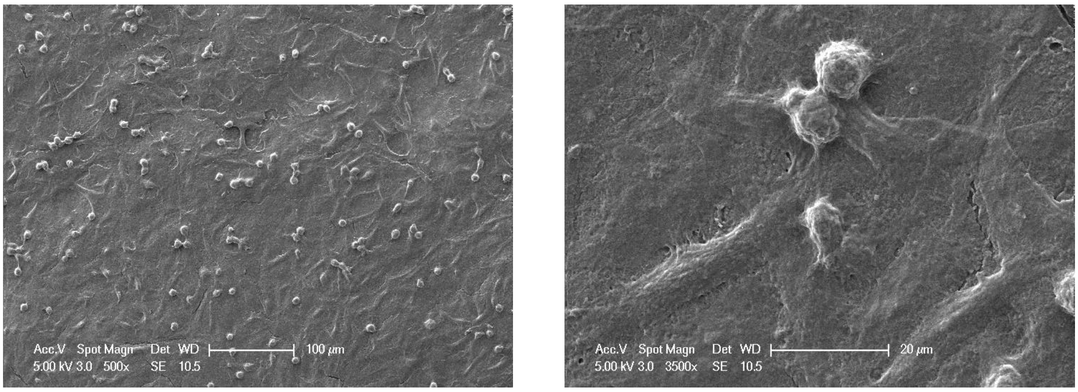

Figure 3.57: Scanning electron microscopy images of L929 cells attached on PIB-PUU surfaces. The “flattened” appearance of adherent cells is shown in 3500x SEM image).

3.3.3.3. Bacterial Resistance of PIB based PUs for Biomedical Applications

PIB-free polyurethane-based products can lead the bacteria growth, proliferation and reproduction under a certain humidity and temperature condition and if these types of products are preferred for human usage, such as packaging, food processing and healthcare, there is a possibility to damage a human health. However, with antibacterial modification, such as quaternary ammonium salt, silver, iodine, zinc oxide addition, in PU structures can decrease these bad effects [34, 43, 101]. Polyisobutylene content can be one of these modifications due to its unique characteristics which are inert and hydrophobic nature [16, 43].

Qualitative antibacterial activity tests were performed with three pathogenic organisms, Escherichia Coli (*E.Coli*) bacteria, Staphylococcus Aureus (*S.Aureus*) bacteria and Candida Albicans (*C.Albicans*) yeast. After removal of the films from the cultured medium bacterial diffusion zones were optically analyzed. No diffusion zone (bacteria-free zone) was observed under all film samples., which were evaluated against *E.Coli*, which is a facultative anaerobic bacterium, and *C.Albicans*, which is a facultative anaerobic fungal pathogen, (see in Figure 3.58).

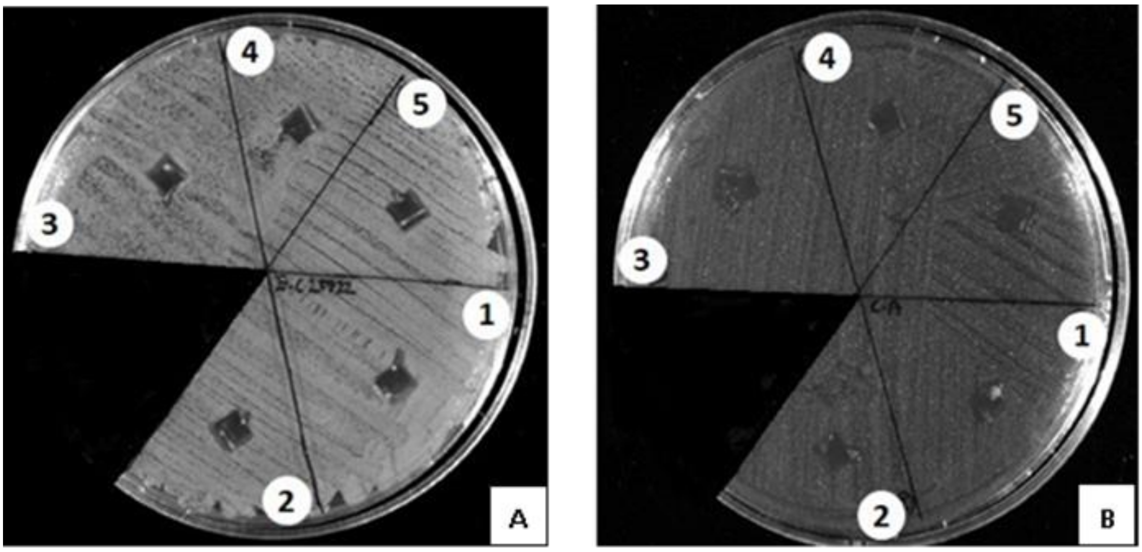

Figure 3.58: CemiDoc images of samples (1: PIB-PUU, 2: PIB$_{O}$-PU, 3: PIB$_{S}$-PU, 4: PIB$_{S}$-PU/NC, 5: ELAS) incubated in *E.Coli* (A) and *C.Albicans* (B) for 18 h (The images were taken after removal of films to evaluate the bacterial growth are under the specimens).

Therefore, according to microscopic and optic camera images, it can be said that samples have bacterial resistance against *E.Coli* and *C.Albicans* since visible bacterial adhesion in macro level cannot be observed.

Bacterial resistance results for PIB-based PU samples are not surprising because the samples contain 72.5% polyisobutylene as a soft phase. PIB phase leads a relatively low surface energy to them and so PIB parts can easily move to surface of sample and act as a partially inert barrier on urethane linkages in the hard phase [16, 43].

Since the main anaerobic character of *E.Coli* and *C.Albicans* organisms, despite of inert barrier property of PIB phase, the bacterial resistance of samples should be evaluated according to other parameters such as (i) physicochemical properties of polymer surfaces, (ii) additives, (iii) surface (iv) hydrophobicity and (v) roughness of polymer samples etc.

No diffusion zone on ELAS sample is not surprising because due to its lower hydrolytic stability and PIB barrier absence for oxygen passage, *E.Coli* and *C.Albicans* organisms may have been exposed to oxygen and this situation may have prevented their adhesion and growing on ELAS sample. In detail, although *C.Albicans* has frequently been called a facultative anaerobe and its aerobic growth has been thoroughly investigated, there are few studies and publications in the literature that describe anaerobic growth. Therefore, it is assumed *that C.Albicans* could not grow in an oxygen-rich environment due to its main anaerobic character [102]. In addition, the same approach can be used for *E.Coli* set of ELAS.

Despite of its facultative character, the enzyme composition of cells (more than 20% of genomes) should be extensively modified for adapting from anaerobic to aerobic metabolism so it is assumed that growth of *E.Coli* in an oxygen-rich environment should be not too easy [103]. As a result, no bacterial adhesion on ELAS in *E.Coli* and *C.Albicans* experiment is not surprising.

Due to anaerobic growth nature of *E.Coli* and *C.Albicans*, diffusion zone on the PIB based PU samples can be expected. However, the characteristic and composition of the polymer surface significantly influence the bacterial adhesion and growth. In literature, there are many studies about this topic. In detail, surface hydrophobicity and roughness play a significant role in the surface adhesion. Increased bacterial adhesion (i.e. *S.Aureus*) have been generally observed on hydrophobic or less hydrophilic surfaces since removing of water from between microorganisms and substrate surface is significantly easier for the hydrophobic surfaces. Moreover, bacterial adhesion is mainly related with the surface roughness of biomaterial since the bacterial adhesion and biofilm formation could be promoted by the irregularities, such as peaks and valleys, on the polymeric substrate surfaces. A greater surface area for bacterial colonization can be created by depressions and elevations on the biomaterial surface, and these surface features can also shield microorganisms from shear forces [35]. As seen in Table 3.3, surfaces of PIB-based PU samples have a hydrophilic character, and their surface roughness values are lower than ELAS (except for PIB$_S$-PU/NC). As a result, despite of the anaerobic growth character of *E.Coli* and *C.Albicans*, and inert barrier effect of PIB phases, qualitatively no diffusion zone is not surprising. In addition to these parameters, Ioannou et al. reported that the quaternary ammonium compounds (OACs) in the biomaterial substrate cause a damage in cell membrane and then cell leakage principally because of their extensive adsorption to the bacterial membrane [104]. Therefore, due to MMT content of PIB$_S$-PU/NC, bacterial adhesion was not observed despite of its high surface roughness.

On the other hand, while all PIB based PU samples showed a resistance against *S.Aureus*, bacterial growth are was observed under the ELAS sample within 18h leading decreasing bacteria free zone area (see in Figure 3.59).

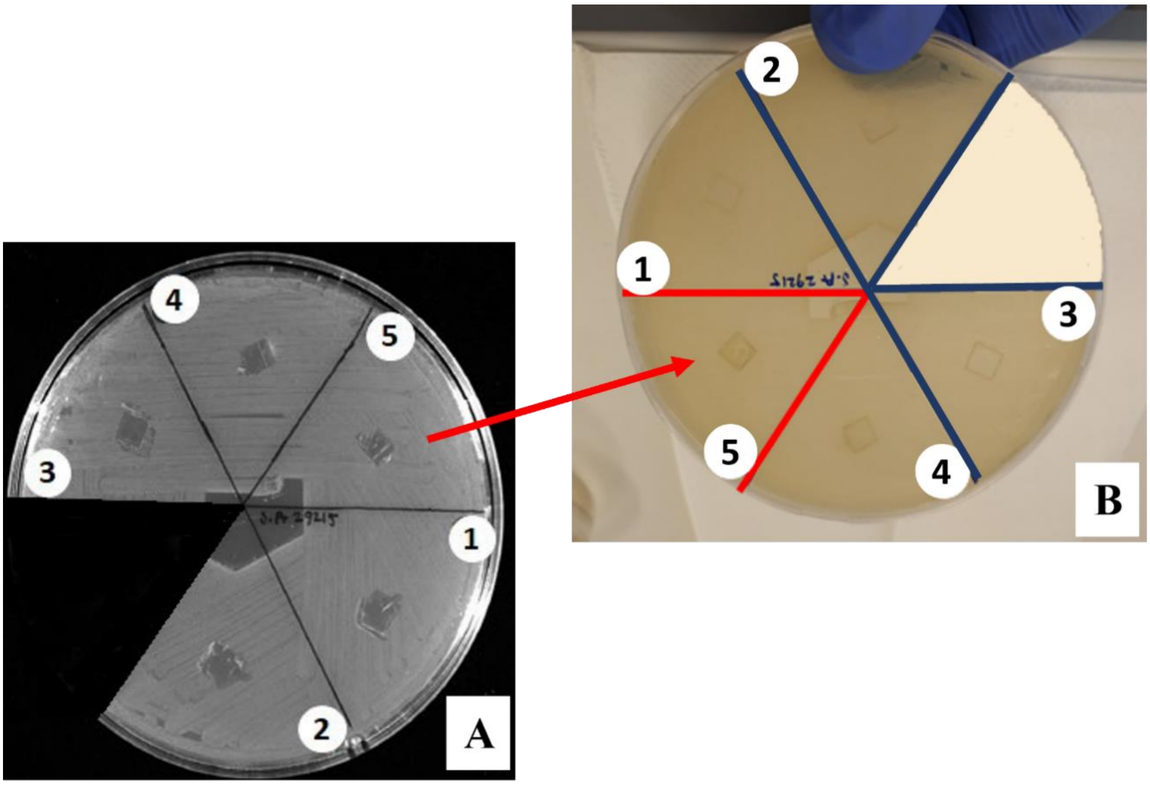

Figure 3.59: CemiDoc (A) and optic camera (B) outcomes of samples (1: PIB-PUU, 2: PIB$_O$-PU, 3: PIB$_S$-PU, 4: PIB$_S$-PU/NC, 5: ELAS) incubated in *S.Aureus* for 18 h. (CemiDoc and optic camera images were taken without film and with film, respectively.)

Masalha et al. reported that there are relatively few knowledges about the regulatory systems, operating in *S.Aureus* bacteria, in literature, but these details about transduction system is crucial to understanding how oxygen affects the expression of virulence genes, which are present and/or have an active role in a genome of microorganism and so are responsible for the pathogenic activity of an infective agent, in *S.Aureus* [105].

As reported in several in vitro studies, the generation of virulence factor can be impacted by a change in oxygen concentration of environment.

Additionally, these studies indicated that generating of toxic shock syndrome by *S.Aureus*, related with pathogenicity, significantly depends on the presence of oxygen ion. Therefore, due to the oxygen dependence of *S.Aureus*'s pathogenic effect, the sample most affected by *S.Aureus* was ELAS due to its lower hydrolytic stability and PIB barrier absence for oxygen passage [16, 21, 105]. Moreover, qualitatively no diffusion zone was observed in all of the PIB-based PU samples since PIB phases act as an inert barrier and can prevent the oxygen passage, which is needed for anerobic *S.Aureus* growth.

4. CONCLUSION

PIB based primary network structure (PIB-SXA) was synthesized by dithiol telechelic PIB and multifunctional allyl based crosslinker via Thiol-ene (click) chemistry for the first time in literature. The product was then characterized in terms of static and dynamic mechanical, thermal and morphological analyses by using NMR, Universal Tensile Testing, DSC, TGA, Raman Spectroscopy, FTIR Spectroscopy, XRD, SEM-EDX techniques. According to successful results of PIB based primary network structures (PIB-SXA), PIB and PS based interpenetrating network structure (IPN) was prepared via sequential IPN protocol. Fundamental network characterizations such as M_c, degree of crosslinking as well as mechanical characterizations such as elastic modulus and creep were all evaluated. IPN exhibited typical network characteristics like extensibility and solvent resistance. Higher mechanical and thermal strength than primary network, PIB-SXA, proved the successful PIB and PS based interpenetrating network formation.

In addition, polyisobutylene based polyurethane structures were first supported via addition of extra hydrogen bonding sites (sulfur) and nanoparticles (OmMMT). These newly synthesized PIB based PUs were then examined by the help of molecular characterizations techniques (NMR, GPC, FTIR spectroscopy), static and dynamic mechanical analyses (Universal Tensile Testing), hydrolytic and oxidative stabilities, thermal analyses (TGA and DSC) and morphological analyses (SEM-EDX and XRD). Results showed that not only mechanical and thermal strength increases with these additions also characteristic oxidative and hydrolytic stability of PIB based polyurethanes retained extensively.

Since polyurethane-based structures are being extensively used in cardiovascular applications, biomedical performance of newly synthesized PIB based PUs were examined in terms of calcification, protein adsorption and cell attachment-viability patterns. Since all these biostability performances mainly depend on the dimensional stability in PBS medium, first, swelling characteristics of all PU samples were evaluated. SEM images of PIB_O-PU indicated the complete absence of PBS crystals on the films after 24h incubation whereas ELAS surface was rich in PBS crystals. To support the calcification, protein and cell adhesion data, the cytotoxicity of PIB_O-PU, PIB_S-PU, PIB_S-PU/NC, PUU surfaces were analyzed via MTT study. Besides, Kirby-Bauer disc diffusion method was used to investigate the possible qualitative bacterial resistance to *E.Coli*, *S.Aureus* and *C.Albicans.*

The conclusive remarks on above mentioned *in vitro* biocompatibility results can be listed as follows;

i. PIB$_{O}$-PU showed the highest calcification resistance while ELAS had the highest deposition on surface. (PIB$_{O}$-PU > PIB$_{S}$-PU/NC > PIB$_{S}$-PU > PIB-PUU > ELAS)

ii. The highest and lowest protein adsorptions were observed on ELAS and PIBS-PU/NC surfaces, respectively. (ELAS > PIB$_{S}$-PU > PIB-PUU > PIB$_{O}$-PU > PIB$_{S}$-PU/NC)

iii. Like protein adsorption, the highest and lowest cell adhesion capacity belong to ELAS and PIBS-PU/NC surfaces, respectively. (ELAS > PIB$_{S}$-PU > PIB-PUU> PIB$_{O}$-PU > PIB$_{S}$-PU/NC)

iv. The highest and lowest cell viability were determined on PIB$_{O}$-PU and PIB$_{S}$-PU/NC surfaces, respectively. (PIB$_{S}$-PU/NC > ELAS > PIB$_{S}$-PU > PIB$_{O}$-PU)

v. All polyurethanes were resistive against *E.Coli* and *C.Albicans*; whereas ELAS exhibited low resistance against to *S.Auerus*.

vi. PIB$_{O}$-PU showed the most stable swelling characteristic in PBS; however, reaching to the swelling equilibrium in PBS for ELAS takes longer time. *(PIB$_{O}$-PU > PIB$_{S}$-PU/NC > PIB-PUU > PIB$_{S}$-PU > ELAS).*

It has been found that among all polyurethanes, ELAS exhibits the highest protein adsorption, cell attachment capacity, calcification and low cell viability as well as low bacterial resistance particularly against *S.Auerus*.

It can be safely concluded that newly synthesized PIB based PUs have higher *in vitro* biocompatibility and lower cytotoxicity than widely used ELAS. All these results make PIB based PUs quite promising for more widespread biomedical applications.

PUBLICATIONS as THESIS OUTCOMES:

1. **Kekec, N.C**., M.B. Akolpoğlu, U. Bozuyuk, S. Kizilel, N. Nugay, T. Nugay, and J.P. Kennedy, “Calcification resistance of polyisobutylene and polyisobutylene- based materials”, *Polymer Advanced Technologies*, Vol. 30, pp. 1836-1846, 2019

2. Kurnaz, E., E. Helvacioglu, **N.C. Kekec**, N. Nugay, T. Nugay and J.P. Kennedy, “High-molecular-weight polyisobutylenes (PIBs) and PIB networks from liquid PIBs by thiol-ene clicking”, *Journal of Polymer Science: Part A: Polymer Chemistry*, Vol.57, pp. 1197-1208, 2019.

3. Toth, K., **N.C. Kekec**, N. Nugay and J.P. Kennedy, “Polyisobutylene-Based Polyurethanes. VIII. Polyurethanes with -O-S-PIB-S-O- Soft Segments”, *Journal of Polymer Science, Part A: Polymer Chemistry*, Vol. 54, pp. 1119-1131, 2016.

4. Nugay, N., K. Toth, **N.C. Kekec**, T. Nugay and J.P. Kennedy, “Polyisobutylene-Based Polyurethanes X: PU Nanocomposites with S-Containing Soft Segments” *Journal of Polymer Science, Part A: Polymer Chemistry*, Vol. 54, pp. 2760-2765, 2016

REFERENCES

1. Kunal, K., M. Paluch, M. Ronald, J.E. Puskas, Y. Chen and A.P. Sokolov, "Polyisobutylene: A Most Unusual Polymer", *Journal of Polymer Science: Part B: Polymer Physics*, Vol. 46, pp. 1390–1399, 2008.

2. Kostjuk, S.V., H.Y. Yeong and B. Voit, "Cationic Polymerization of Isobutylene at Room Temperature", *Journal of Polymer Science: Part A: Polymer Chemistry*, Vol. 51, pp. 471–486, 2013.

3. Vancaeyzeele, C., O. Fichet, J. Laskar, S. Boileau and D. Teyssie, "Polyisobutene/ Polystyrene Interpenetrating Polymer Networks: Effects of Network Formation Order and Composition on the IPN Architecture", *Polymer*, Vol. 47, pp. 2046-2060, 2006.

4. Hagiopol, C., "Copolymers", *Reference Module in Material Science and Materials Engineering*, Elsevier, 2016.

5. Wang, W., W. Lu, N. Kang, J. Mays, and K. Kunlun Hong, "Thermoplastic Elastomers Based on Block, Graft, and Star Copolymers", in *Elastomers*, pp. 97-120, 2017.

6. Samaddar, P., A. Deep and K.H. Kim, "An Engineering Insight into Block Copolymer Self-assembly: Contemporary Application from Biomedical Research to Nanotechnology", *Chemical Engineering Journal*, Vol. 342, pp. 71-89, 2018.

7. Sherazi, T.A., "Graft Polymerization" in *Encyclopedia of Membranes*, pp. 886-887, 2016.

8. Storey, R.F., B.J. Chisholm and K.R. Choate, "Synthesis and Characterization of PS-PIB-PS Triblock Copolymers", *Journal of Macromolecular Science, Part A: Pure and Applied Chemistry*, Vol. 31:8, pp. 969-987, 1994.

9. Cho, J.C., G. Cheng, D. Feng and R. Faust, “Synthesis, Characterization, Properties, and Drug Release of Poly(alkyl methacrylate-b-isobutylene-b-alkyl methacrylate)”, *Biomacromolecules,* Vol. 7, pp. 2997-3007, 2006.

10. Yang, T., 2012, *Mechanical and Swelling Properties of Hydrogels,* Ph.D. Thesis, KTH Royal Institute of Technology.

11. Sperling, L.H., “Interpenetrating Polymer Networks: An Overview”, *Advance in Chemistry*, Vol. 239, pp. 3-38, 1994.

12. Hoyle, C.E. and C.N. Bowman, “Thiol-ene Click Chemistry”, *Angewandte Chemie International Edition,* Vol. 49, No. 9, pp. 1540-1573, 2010.

13. Vancaeyzeele, C., O. Fichet, B. Amana, S. Boileau and D. Teyssie, “Polyisobutene/ Polycyclohexyl Methacrylate Interpenetrating Polymer Networks”, *Polymer*, Vol. 47, pp. 6048- 6956, 2006.

14. Kurnaz, E., E. Helvacioglu, N.C. Kekec, N. Nugay, T. Nugay and J.P. Kennedy, “High-molecular-weight Polyisobutylenes (PIBs) and PIB Networks from Liquid PIBs by Thiol-ene Clicking”, *Journal of Polymer Science: Part A: Polymer Chemistry*, Vol. 57, pp. 1197-1208, 2019.

15. Kang, J., G. Erdodi, and J.P. Kennedy, “Polyisobutylene-Based Polyurethanes with Unprecedented Properties and How They Came About”, *Journal of Polymer Science, Part A: Polymer Chemistry.* Vol. 49, pp. 3891-3904, 2011.

16. Toth, K., N.C. Kekec, N. Nugay and J.P. Kennedy, “Polyisobutylene-Based Polyurethanes. VIII. Polyurethanes with -O-S-PIB-S-O- Soft Segments”, *Journal of Polymer Science, Part A: Polymer Chemistry*, Vol. 54, pp. 1119-1131, 2016.

17. Erdodi, G., J. Kang, J.P. Kennedy, E. Yilgor and I. Yilgor, “Polyisobutylene-based Polyurethanes. III. Polyurethanes Containing PIB/PTMO Soft Co-segments”, *Journal of Polymer Science, Part A: Polymer Chemistry*, Vol. 47, pp. 5278-5290, 2009.

18. Erdodi, G., J. Kang and J.P. Kennedy, “Polyisobutylene-based Polyurethanes. VI. Unprecedented Combination of Mechanical Properties and Oxidative/Hydrolytic Stability by H-bond Acceptor Chain Extenders”, *Journal of Polymer Science, Part A: Polymer Chemistry*, Vol. 48, pp. 2361-2371, 2010.

19. Zaferani, S.H., “Introduction of Polymer-based Nanocomposites”, *Polymer-based Nanocomposites for Energy and Environmental Applications*, pp. 1-25, 2018.

20. Valapa, R.V., S. Loganathan, G. Pugazhenthi, S. Thomas and T.O. Varghese, “Chapter 2 - An Overview of Polymer–Clay Nanocomposites”, *Clay-Polymer Nanocomposites*, pp. 29-81, 2017.

21. Nugay, N., K. Toth, N.C. Kekec, T. Nugay and J.P. Kennedy, “Polyisobutylene-Based Polyurethanes X: PU Nanocomposites with S-Containing Soft Segments” *Journal of Polymer Science, Part A: Polymer Chemistry*, Vol. 54, pp. 2760-2765, 2016.

22. Li, Y., K. Hu, H. Jiao, X. Liu, Q. Wang, G. Pan, X. Zhang and T. Wang, “*In Situ* Polymerization, Thermal, Damping, and Mechanical Properties of Multiwalled Carbon Nanotubes/Polyisobutylene-based Polyurethane Nanocomposites”, *Polymer Composites*, Vol. 36, pp. 198-203, 2015.

23. Sharma, S., T.T. Aiswarya, I. Mirza and S. Saha, “Biocompatible Polymers and Their Applications”, *Encyclopedia of Materials: Plastics and Polymers*, pp. 796-819, 2022.

24. Alferiev, I., S.J. Stachelek, Z. Lu, A.L. Fu, T.L. Sellaro, J.M. Connolly, R.W. Bianco, M.S. Sacks and R.J. Levy, “Prevention of Polyurethane Valve Cusp Calcification with Covalently Attached Bisphosphonate Diethylamino Moieties”, *Journal of Biomedical Materials Research: Part A*, Vol. 66A(2), pp. 385-395, 2003.

25. Imachi, K., Y. Abe, T. Chinzei, K. Mabuchi, K. Babal, H. Matsuura, A. Kouno, T. Ono, S. Mochizukil, Y.P. Son, K. Imanishi and I. Fujimasa, 1998, *Heart Replacement Artificial Heart 6*, Springer-Verlag, Tokyo.

26. Tallahassee Memorial Healthcare, 2021, https://www.tmh.org/, accessed on: January 19, 2023.

27. Xi, M. and B. Zhang, “Interaction of Plasma Proteins with Tri-quaternary Ammonium Salt Cationic Surfactant Studied by QCM-D”, *Chinese Journal of Chemistry*, Vol. 33, pp. 253-260, 2015.

28. Hlady, V., J. Buijs and H.P. Jennissen, “Methods for Studying Protein Adsorption”, *Methods Enzymol*, Vol. 309, pp. 402-429, 1999.

29. Ostuni, E., R.G. Chapman and R.E. Holmlin, S. Takayama and G.M. Whitesides, “A Survey of Structure-Property Relationships of Surfaces that Resist the Adsorption of Protein”, *Langmuir,* Vol. 17, pp. 5605-5620, 2001.

30. Ngo, B.K.D. and M.A. Grunlan, “Protein Resistant Polymeric Biomaterials”, *ACS Macro Letters*, Vol. 6, pp. 992-1000, 2017.

31. Cozzens, D., A. Luk, U. Ojha, M. Ruths and R. Faust, “Surface Characterization and Protein Interactions of Segmented Polyisobutylene-Based Thermoplastic Polyurethanes”, *Langmuir*, Vol. 27, pp. 14160-14168, 2011.

32. Ferrari, M., F. Cirisano and M.C. Morán, “Mammalian Cell Behavior on Hydrophobic Substrates: Influence of Surface Properties”, *Colloids Interfaces*, Vol. 3(2), pp. 48, 2019.

33. Xu, L.C. and C.A. Siedlecki, “Antibacterial Polyurethanes” In *Advances in Polyurethane Biomaterials,* pp. 247-284, 2016.

34. Wang, C.H., G.G. Hou, Z.Z. Du, W. Cong, J.F. Sun, Y. Xu and W.S. Liu, “Synthesis, Characterization and Antibacterial Properties of Polyurethane Material Functionalized with Quaternary Ammonium Salt”, *Polymer Journal*, Vol. 48, pp. 259-265, 2016.

35. Lima, J.C., N.J. Andrade, N.F.F. Soares, S.O. Ferreira, P.E. Fernandes, C.C.P. Carvalho, J.P. Lopes and J.F.L. Martins, “The Hydrophobicity and Roughness of a Nasoenteral

Tube Surface Influences the Adhesion of A Multi-Drug Resistant Strain of *Staphylococcus Aureus", Brazilian Journal of Microbiology*, Vol. 42, pp. 489-498, 2011.

36. Kayirhan, N., A. Denizli and N. Hasirci, "Adsorption of Blood Proteins on Glow-Discharge-modified Polyurethane Membranes", *Journal of Applied Polymer Science*, Vol. 81, pp. 1322-1332, 2001.

37. Wang, W., and C. Wang, "3-Polyurethane for Biomedical Applications: A Review of Recent Developments", *The Design and Manufacture of Medical Devices*, pp. 115-151, 2012.

38. Pinchuk, L., I. Riss, J.F. Batlle, Y.P. Kato, J.B. Martin, E. Arrieta, P. Palmberg, R.K. Parrish, B.A. Weber, Y. Kwon and J.M. Parel, "The Use of Poly(styrene-block-isobutylene-block-styrene) as a Microshunt to Treat Glaucoma", *Regenerative Biomaterials*, Vol. 3(2), pp. 137-142, 2016.

39. Pinchuk, L., "The Use of Polyisobutylene-based Polymers in Ophthalmology", *Bioactive Materials*, Vol. 10, pp. 185-194, 2022.

40. Deodhar, T., N. Nugay, T. Nugay, R. Patel, G. Moggridge and J.P. Kennedy, "Synthesis of High Molecular Weight and Strength Polyisobutylene-Based Polyurethane and Its Use for the Development of a Synthetic Heart Valve", *Macromolecular Rapid Communications*, Vol. 44(1), pp. 2200147, 2023.

41. Kekec, N.C., M.B. Akolpoğlu, U. Bozuyuk, S. Kizilel, N. Nugay, T. Nugay and J.P. Kennedy, "Calcification Resistance of Polyisobutylene and Polyisobutylene- based Materials", *Polymer Advanced Technologies*, Vol. 30, pp. 1836-1846, 2019.

42. Hacking, S.A., and A. Khademhosseini, "Chapter II.1.3 – Cells and Surfaces in vitro", *Biomaterials Science (Third Edition)*, pp. 408-427, 2013.

43. Barczikai, D., J. Domokos, D. Szabó, K. Molnar, D. Juriga, E. Krisch, K.S. Nagy, L. Kohidai, C.A. Helfer, A. Jedlovszky-Hajdu, J.E. Puskas, “Polyisobutylene—New Opportunities for Medical Applications”, *Molecules,* Vol. 26(17), pp. 5207, 2021.

44. Yang, T., H. Long, M. Malkoch, E. Kristofer Gamstedt, L. Berglund and A. Hult, “Characterization of Well-defined Poly(ethylene glycol) Hydrogels Prepared by Thiol-ene Chemistry”, *Journal of Polymer Science, Part A: Polymer Chemistry,* Vol. 49, pp. 4044-4054, 2011.

45. Vinodh, R., A. Abidov, M.M. Peng, C.M. Babu, M. Palanichamy, S.C. Cha and H.T. Jang, “A New Strategy to Synthesize Hypercross-linked Conjugated Polystyrene and Its Application Towards CO_2 sorption”, *Fibers and Polym*ers, Vol. 16, pp. 1458–1467, 2015.

46. Bhutto, A.A., D. Vesely and B.J. Gabrys, “Miscibility and Interactions in Polystyrene and Sodium Sulfonated Polystyrene with Poly(vinyl methyl ether) PVME Blends. Part II. FTIR”, *Polymer*, Vol. 44(21), pp. 6627-6631, 2003.

47. Dave, V.J. and H.S. Patel, “Synthesis and Characterization of Interpenetrating Polymer Networks from Transesterified Castor Oil Based Polyurethane and Polystyrene”, *Journal of Saudi Chemical Society*, Vol. 21(1), pp. 18-24, 2017.

48. Hermán, V., H. Takacs, F. Duclairoir, O. Renault, J.H. Tortai and B. Viala, “Core Double–shell Cobalt/Graphene/Polystyrene Magnetic Nanocomposites Synthesized by *In Situ* Sonochemical Polymerization”, *RSC Advances*, Vol. 5, pp. 51371-51381, 2015.

49. Brijmohan, S.B., S. Swier, R.A. Weiss and T.M. Shaw, “Synthesis and Characterization of Cross-linked Sulfonated Polystyrene Nanoparticles”, *Industrial and Engineering Chemistry Research*, Vol. 44(21), pp. 8039–8045, 2005.

50. Tsyurupa, M.P., Y.A. Borisov, Z.K. Blinnikova, N.P. Platonova, A.V. Ul’yanov, A.K. Buryak and V.A. Davankov, “On the Origin of Absorbance Band Around 1700 cm^{-1} in

FTIR Spectra of Hypercrosslinked Polystyrene", *Protection of Metals Physical Chemistry of Surfaces,* Vol. 50, pp. 59–63, 2014.

51. Kato, K., Y. Ikeda and K. Ito, "Direct Determination of Cross-Link Density and Its Correlation with the Elastic Modulus of a Gel with Slidable Cross-Links", *ACS Macro Letters*, Vol. 8(6), pp. 700-704, 2019.

52. Mathew, A.P., S. Packirisamy and S. Thomas, "Studies on the Thermal Stability of Natural Rubber/Polystyrene Interpenetrating Polymer Networks: Thermogravimetric Analysis", *Polymer Degradation and Stability*, Vol. 72, pp. 423–439, 2001.

53. Rieger, J., "The Glass Transition Temperature of Polystyrene", *Journal of Thermal Analysis*, Vol. 46, pp. 965-972, 1996.

54. Parada, C.M., 2018, "*A New Generation of Functional Polyisobutylenes for Advanced Applications*", The University of Southern Mississippi.

55. Faravelli, T., M. Pinciroli, F. Pisano, G. Bozzano, M. Dente and E. Ranzi, "Thermal Degradation of Polystyrene", *Journal of Analytical and Applied Pyrolysis*, Vol. 60, pp. 103-121, 2001.

56. Guyot, A., "Recent Developments in the Thermal Degradation of Polystyrene—A Review", *Polymer Degradation and Stability*, Vol. 15(3), pp. 219-235, 1986.

57. Kaya, İ., A. Bilici and M. Saçak, "Study on Synthesis, Characterization, Thermal Stability and Conductivity Properties of a New Conjugated Oligoazomethine and Some of its Metal Complexes", *Journal of Inorganic and Organometallic Polymers and Materials*, Vol . 443, 2009.

58. Trakulsujaritchok, T., "Interpenetrating Polymer Networks", *Burapha Science Journal*, Vol. 11(2), pp. 77-88, 2006.

59. Hsieh, T.T., K.H. Hsieh, G.P. Simon, C. Tiu and H.P. Hsu, “Effect of Crosslinking Density on the Physical Properties of Interpenetrating Polymer Networks of Polyurethane and 2-Hydroxyethyl Methacrylate-terminated Polyurethane”, *Journal of Polymer Research*, Vol. 5, No. 3, pp. 153-162, 1998.

60. Rao, K.V., G.S. Ananthapadmanabha and G.N. Dayananda, “Effect of Cross-linking Density on Creep and Recovery Behavior in Epoxy-Based Shape Memory Polymers (SMEPs) for Structural Applications”, *Journal of Materials Engineering and Performance*, Vol. 25, pp. 5314-5322, 2016.

61. Pavka, P.A., 2013, “*Effect of Network Structure on The Quasi-Static, Fatigue, Creep, Thermal and Fiber Properties of Polyisobutylene-Based Thermoplastic Elastomers*”, M.Sc. Thesis, The University of Akron.

62. Nicholson, L.M. and T.S. Gates, “The Influence of Cross-Link Density on the Creep Compliance of an Advanced Polyimide”, *Journal of Thermoplastic Composite Materials*, Vol. 14, pp. 477-488, 2001.

63. Meththananda, I.M., S. Parker, M.P. Patel and M. Braden, “The Relationship Between Shore Hardness of Elastomeric Dental Materials and Young’s Modulus”, *Dental Materials*, Vol. 25, pp. 956-959, 2009.

64. Peppas, N.A. and E.W. Merrill, “Crosslinked Poly(vinyl Alcohol) Hydrogels as Swollen Elastic Networks”, *Journal of Applied Polymer Science*, Vol. 21, pp. 1763-1770, 1977.

65. Lee, Y., D.N. Kim, D. Choi, W. Lee, J. Park and W.G. Koh, “Preparation of Interpenetrating Polymer Network Composed of Poly(ethylene glycol) and Poly(acrylamide) Hydrogels as a Support of Enzyme Immobilization”, *Polymers For Advanced Technologies*, Vol. 18, pp. 852-858, 2008.

66. Coleman, M.M, K.H. Lee, D.J. Skrovanek and P.C. Painter, “Hydrogen Bonding in Polymers. 4. Infrared Temperature Studies of a Simple Polyurethane”, *Macromolecules*, Vol. 19(8), pp. 2149-2157, 1986.

67. Toth, K., N. Nugay and J.P. Kennedy, "Polyisobutylene-Based Polyurethanes. IX. Synthesis, Characterization, and Properties of Polyisobutylene-Based Poly(urethane-ureas)", *Journal of Polymer Science Part A: Polymer Chemistry*, Vol. 54, pp. 2361–2369, 2016.

68. Woniak-Braszak, A., M. Baranowsky, K. Jurga, B. Brycki, E. Mikuli and K. Hoderna-Natkaniec, "Complementary Study of Molecular Dynamics and Domain Sizes in Heterogenous Nanocomposites PBT/DA-C_{60} and PBT/TCNEO-C_{60}", *Journal of Applied Physics*, Vol. 115(20), pp. 204914, 2014.

69. Kyriakides, T. R. "Molecular Events at Tissue–Biomaterial Interface", *Host Response to Biomaterials*, pp. 81–116, 2015.

70. Neděla, O., P. Slepička and V. Švorčík, "Surface Modification of Polymer Substrates for Biomedical Applications", *Materials*, Vol. 10(10), pp. 1115, 2017.

71. Tallawi, M., E. Rosellini, N. Barbani, M.G. Cascone, R. Rai, G. Saint-Pierre and A.R. Boccaccini, "Strategies for the Chemical and Biological Functionalization of Scaffolds for Cardiac Tissue Engineering: A Review", *Journal of Royal Society Interface*, Vol. 12, pp. 20150254, 2015.

72. Ovcharenko, E.A., A. Seifalian, M.A. Rezvova, K.Y. Klyshnikov, T.V. Glushkova, T.N. Akenteva, L.V. Antonova, E.A. Velikanova, V.S. Chernonosova, G.Y. Shevelev, D.K. Shishkova, E.O. Krivkina, Y.A. Kudryavceva, A.M. Kudryavceva and L.S. Barbarash, "A New Nanocomposite Copolymer Based on Functionalised Graphene Oxide for Development of Heart Valves", *Scientific Reports*, Vol. 10, pp. 5271, 2020.

73. Dean, IV. H., 2012, "*Development of Biopoly Materials for use in Prosthetic Heart Valve Replacements*", M.Sc. Thesis, Colorado State University.

74. Fujita, M., G.M. Policastro, A. Burdick, H.T. Lam, J.L. Ungerleider, R.L. Braden, D. Huang, K.G. Osborn, J.H. Omens, M.M. Madani and K.L. Christman, "Preventing Post-

surgical Cardiac Adhesions with a Catechol-functionalized Oxime Hydrogel”, *Nature Communications*, Vol. 12, pp. 3764, 2021.

75. Jeong, H., J. Hwang, H. Lee, P.T. Hammond, J. Choi and J. Hong, “ In Vitro Blood Cell Viability Profiling of Polymers Used in Molecular Assembly”, *Nature*, Vol. 7, pp. 9481, 2017.

76. Akkas, T., C. Citak, A. Sirkecioglu and F.S. Güner, “Which is More Effective for Protein Adsorption: Surface Roughness, Surface Wettability or Swelling? Case Study of Polyurethane Films Prepared from Castor Oil and Poly(ethylene glycol)”, *Polymer International*, Vol. 62, pp. 1202-1209, 2012.

77. Chaffin, K.A., A.J. Buckalew, J.L. Schley, X. Chen, M. Jolly, J.A. Alkatout, J.P. Miller, D.F. Untereker, M.A. Hillmyer and F.S. Bates, “Influence of Water on the Structure and Properties of PDMS Containing Multiblock Polyurethanes”, *Macromolecules*, Vol. 45, pp. 9110-9120, 2012.

78. Kokubo, T. and H. Takadama, “How Useful is SBF in Predicting In Vivo Bone Bioactivity?”, *Biomaterials*, Vol. 27, pp. 2907-2915, 2006.

79. Miller, J.D., S. Veeramasuneni, J. Drelich, M.R. Yalamanchili and G. Yamauchi, “Effect of Roughness as Determined by Atomic Force Microscopy on the Wetting Properties of PTFE Thin Films”, *Polymer Engineering and Science*, Vol. 36(14), pp. 1849- 1855, 1996.

80. Kepa, K., L. Coleman and L. Grøndahl, “In Vitro Mineralization of Functional Polymers”, *Biosurface and Biotribology,* Vol. 1, pp. 214-227, 2015.

81. Ducheyne, P., S. Radin and L. King, “The Effect of Calcium Phosphate Ceramic Composition and Structure on In Vitro Behavior. I. Dissolution.” *Journal of Biomedical Materials Research*, Vol. 27(1), pp. 25-34, 1993.

82. Filgueiras, M.R., G.L. Torre and L.L. Hench, “Solution Effects on the Surface Reactions

of a Bioactive Glass”, *Journal of Biomedical Materials Research*, Vol. 27, pp. 445-453, 1993.

83. Tanahashi, M. and T. Matsuda, “Surface Functional Group Dependence on Apatite Formation on Self-assembled Monolayers in a Simulated Body Fluid”, *Journal of Biomedical Materials Research*, Vol. 34(3), pp. 305-315, 1998.

84. Nugay, N., T. Nugay and J.P. Kennedy, “Minute Amounts of Organically Modified Montmorillonite Improve the Properties of Polyisobutylene-based Polyurethanes”, *Journal of Polymer Science, Part A: Polymer Chemistry*, Vol. 51, pp. 4076-4087, 2013.

85. Balaji, A., S.K. Jaganathan, A.F. Ismail and R. Rajasekar, “Fabrication and Hemocompatibility Assessment of Novel Polyurethane-based Bio-nanofibrous Dressing Loaded with Honey and *Carica Papaya* Extract for the Management of Burn Injuries”, *International Journal of Nanomedicine.* Vol. 11, pp. 4339-4355, 2011.

86. He, W., Z. Hu, A. Xu, R. Liu, H. Yin, J. Wang and S. Wang, “The Preparation and Performance of a New Polyurethane Vascular Prothesis”, *Cell Biochemistry and Biophysics*, Vol. 66, pp. 855-866, 2013.

87. Pessková, V., D. Kubies, H. Hulejová and L. Himmlova, “The Influence of Implant Surface Properties on Cell Adhesion and Proliferation”, *Journal of Materials Science: Materials in Med*icine, Vol. 18, pp. 465-473, 2007.

88. Chou, Y.F., W. Huang, J.C.Y. Dunn, T.A. Miller and B.M. Wu, “The Effect of Biomimetic Apatite Structure on Osteoblast Viability, Proliferation, and Gene Expression”, *Biomaterials*, Vol. 26, pp. 285-295, 2005.

89. Chen, L., C. Yan and Z. Zheng, “Functional Polymer Surfaces for Controlling Cell Behaviors”, *Materials Today*, Vol. 21, No. 1, pp. 38-59, 2018.

90. Vogler, E. A., “Protein Adsorption in Three Dimensions”, *Biomaterials*, Vol. 33, pp. 1201–1237, 2012.

91. Venturata, A., G. MacFarlane, J. Geng and M. Bradley, “Understanding Polymer-Cell Attachment”, *Macromolecular Bioscience*, Vol. 16, pp. 1864-1872, 2016.

92. Santerre, J.P., P. ten Hove, N.H. VanderKamp and J.L. Brash, “Effect of Sulfonation of Segmented Polyurethanes on the Transient Adsorption of Fibrinogen from Plasma: Possible Correlation with Anticoagulant Behavior”, *Journal of Biomedical Materials Research*, Vol. 26(1), pp. 39-57, 1992.

93. Toth, K., N. Nugay and J.P. Kennedy, “Polyisobutylene-Based Polyurethanes: VII. Structure/Property Investigations for Medical Applications”, *Journal of Polymer Science, Part A: Polymer Chemistry*, Vol. 54, pp. 532-543, 2016.

94. Kowalczyńska, H.M. and M. Nowak-Wyrzykowska, “Modulation of Adhesion, Spreading and Cytoskeleton Organization of 3T3 Fibroblasts by Sulfonic Groups Present on Polymer Surfaces”, *Cell Biology International*, Vol. 27, pp. 101–114, 2003.

95. Yuan, P., 2010, “*Protein Adsorption and Bacterial Adhesion on Hybrid Starch/ Polycaprolactone Block Copolymers*”, M.Sc. Thesis, The State University of New Jersey.

96. Yin, Y., K. Fisher, N.J. Nosworthy, D. Bax, R.J. Clarke, D.R. McKenzie and M.M.M. Bilek, “Comparison on Protein Adsorption Properties of Diamond-like Carbon and Nitrogen-containing Plasma Polymer Surfaces”, *Thin Solid Films*, Vol. 520(7), pp. 3021-3025, 2012.

97. Tiwari, A., B. Garipcan and L. Uzun, *Advanced Surfaces for Stem Cell Research*, 2016.

98. Kostadinova, A. and I. Keranov, “Modifications of the Polymer Surface Aimed at Improving Cell Adhesion and Interaction”, *Importance and Applications of Nanotechnology*, pp. 1-6, 2019.

99. Štrbková, L., A. Manakhov, L. Zajíčková, A. Stoica, P. Veselý and R. Chmelík, “The Adhesion of Normal Human Dermal Fibroblasts to the Cyclopropylamine Plasma

Polymers Studied by Holographic Microscopy”, *Surface and Coatings Technology,* Vol. 295, pp. 70–77, 2016.

100. Černochová, P., L. Blahová, J. Medalová, D. Nečas, M. Michlíček, P. Kaushik, J. Přibyl, J. Bartošíková, A. Manakhov, L. Bačáková and L. Zajíčková, “Cell Type Specific Adhesion to Surfaces Functionalized by Amine Plasma Polymers”, *Scientific Reports*, Vol. 10, pp. 9357, 2020.

101. Luo, J., Y. Deng and Y. Sun, “Antimicrobial Activity and Biocompatibility of Polyurethane-Iodine Complexes”, *Journal of Bioactive and Compatible Polymers*. Vol. 25, pp. 185-206, 2010.

102. Dumitru, R., J.M. Hornby and K.W. Nickerson, “Defined Anaerobic Growth Medium for Studying Candida albicans Basic Biology and Resistance to Eight Antifungal Drugs”, *Antimicrobial agents and chemotherapy,* Vol. 48(7), pp. 2350–2354, 2004.

103. von Wulffen, J., RecogNice-Team, O. Sawodny and R. Feuer, “Transition of an Anaerobic Escherichia Coli Culture to Aerobiosis: Balancing mRNA and Protein Levels in a Demand-Directed Dynamic Flux Balance Analysis”, *PLoS ONE,* Vol. 11(7), e0158711, 2016.

104. Ioannou, C.J., G.W. Hanlon and S.P. Denyer, “Action of Disinfectant Quaternary Ammonium Compounds Against Staphylococcus Aureus”, *Antimicrobial Agents And Chemotherapy,* Vol. 51(1), pp. 296–306, 2007.

105. Masalha, M., I. Borovok, R. Schreiber, Y. Aharonowitz and G. Cohen, “Analysis of Transcription of the *Staphylococcus Aureus* Aerobic Class Ib and Anaerobic Class III Ribonucleotide Reductase Genes in Response to Oxygen”, *Journal of Bacteriology*, Vol. 183, pp. 7260-7272, 2001.

APPENDIX A: COPYRIGHT LICENCES

Copyrights belonging to figures which were taken from articles and journals can be found below.

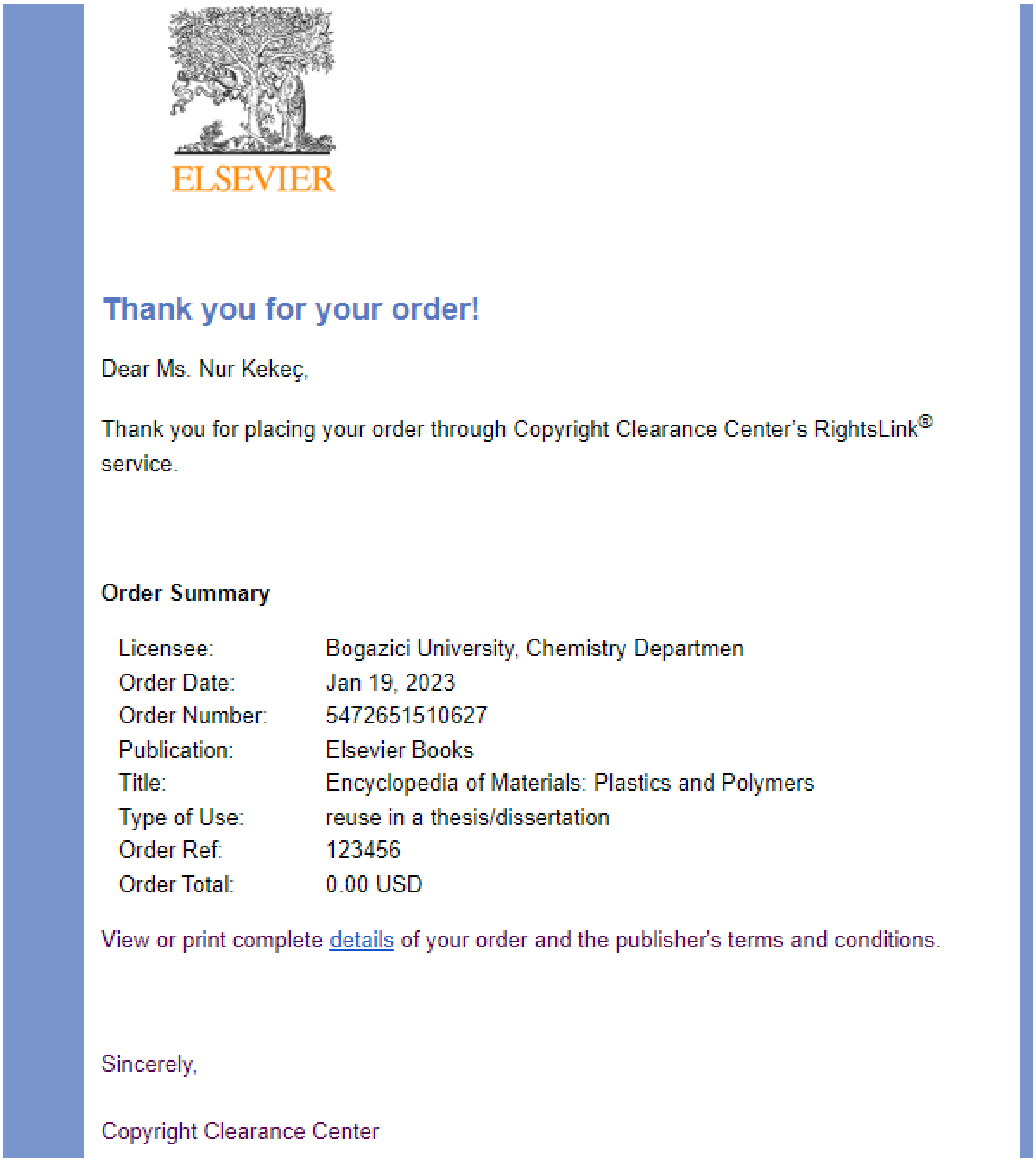

ELSEVIER

Thank you for your order!

Dear Ms. Nur Kekeç,

Thank you for placing your order through Copyright Clearance Center's RightsLink® service.

Order Summary

Licensee:	Bogazici University, Chemistry Departmen
Order Date:	Jan 19, 2023
Order Number:	5472651510627
Publication:	Elsevier Books
Title:	Encyclopedia of Materials: Plastics and Polymers
Type of Use:	reuse in a thesis/dissertation
Order Ref:	123456
Order Total:	0.00 USD

View or print complete details of your order and the publisher's terms and conditions.

Sincerely,

Copyright Clearance Center

Figure A.1: Permission from [23], Elsevier, Copyright (2022).

ELSEVIER

Thank you for your order!

Dear Ms. Nur Kekeç,

Thank you for placing your order through Copyright Clearance Center's RightsLink® service.

Order Summary

Licensee:	Bogazici University, Chemistry Departmen
Order Date:	Jan 19, 2023
Order Number:	5472651374709
Publication:	Elsevier Books
Title:	Clay-Polymer Nanocomposites
Type of Use:	reuse in a thesis/dissertation
Order Ref:	123456
Order Total:	0.00 USD

View or print complete details of your order and the publisher's terms and conditions.

Sincerely,

Copyright Clearance Center

Figure A.2: Permission from [20], Elsevier, Copyright (2017).

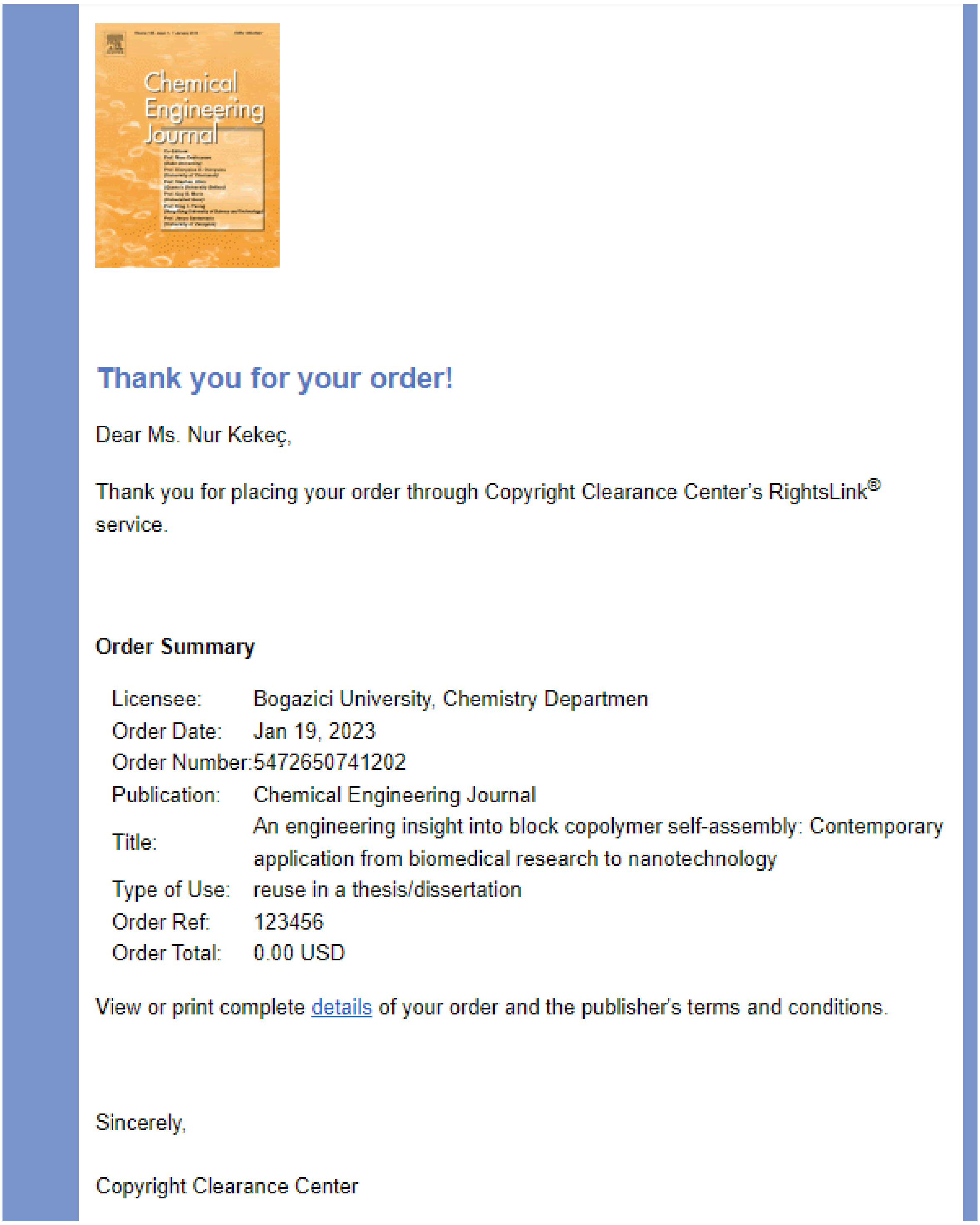

Thank you for your order!

Dear Ms. Nur Kekeç,

Thank you for placing your order through Copyright Clearance Center's RightsLink® service.

Order Summary

Licensee:	Bogazici University, Chemistry Departmen
Order Date:	Jan 19, 2023
Order Number:	5472650741202
Publication:	Chemical Engineering Journal
Title:	An engineering insight into block copolymer self-assembly: Contemporary application from biomedical research to nanotechnology
Type of Use:	reuse in a thesis/dissertation
Order Ref:	123456
Order Total:	0.00 USD

View or print complete details of your order and the publisher's terms and conditions.

Sincerely,

Copyright Clearance Center

Figure A.3: Permission from [6], Elsevier, Copyright (2018).

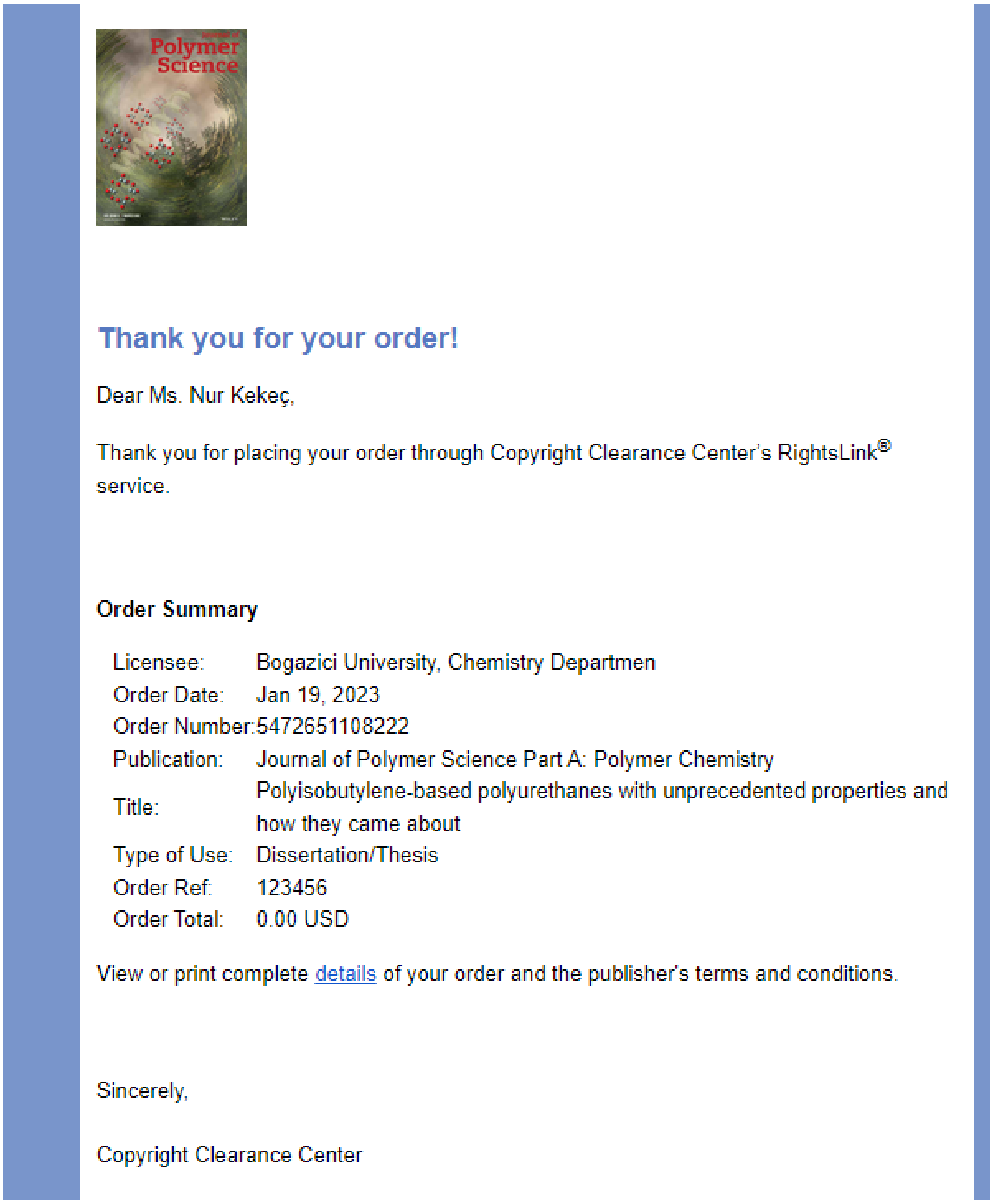

Thank you for your order!

Dear Ms. Nur Kekeç,

Thank you for placing your order through Copyright Clearance Center's RightsLink® service.

Order Summary

Licensee:	Bogazici University, Chemistry Departmen
Order Date:	Jan 19, 2023
Order Number:	5472651108222
Publication:	Journal of Polymer Science Part A: Polymer Chemistry
Title:	Polyisobutylene-based polyurethanes with unprecedented properties and how they came about
Type of Use:	Dissertation/Thesis
Order Ref:	123456
Order Total:	0.00 USD

View or print complete details of your order and the publisher's terms and conditions.

Sincerely,

Copyright Clearance Center

Figure A.4: Permission from [15], John Wiley and Sons, Copyright (2011).

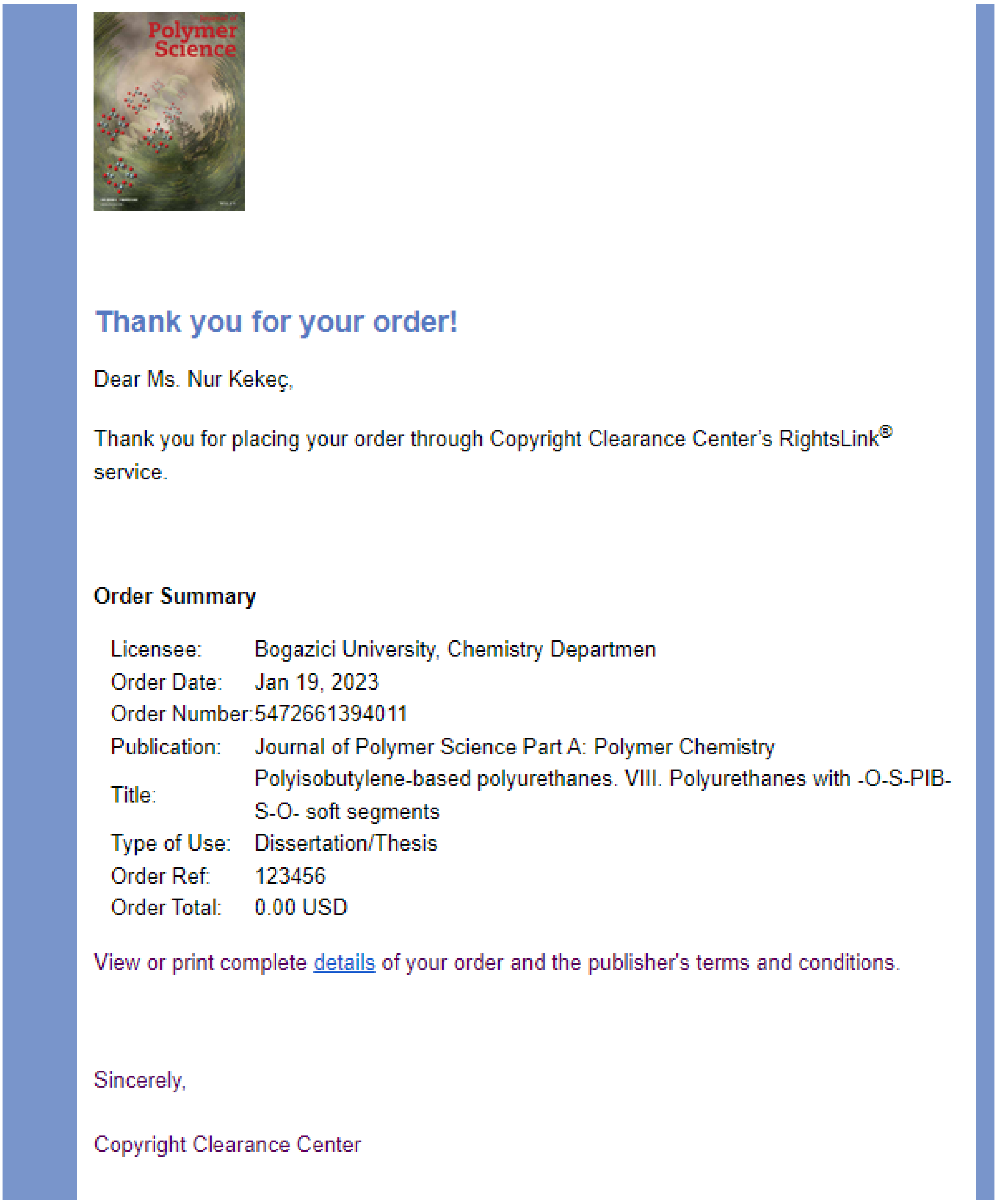

Thank you for your order!

Dear Ms. Nur Kekeç,

Thank you for placing your order through Copyright Clearance Center's RightsLink® service.

Order Summary

Licensee:	Bogazici University, Chemistry Departmen
Order Date:	Jan 19, 2023
Order Number:	5472661394011
Publication:	Journal of Polymer Science Part A: Polymer Chemistry
Title:	Polyisobutylene-based polyurethanes. VIII. Polyurethanes with -O-S-PIB-S-O- soft segments
Type of Use:	Dissertation/Thesis
Order Ref:	123456
Order Total:	0.00 USD

View or print complete details of your order and the publisher's terms and conditions.

Sincerely,

Copyright Clearance Center

Figure A.5: Permission from [16], John Wiley and Sons, Copyright (2015).

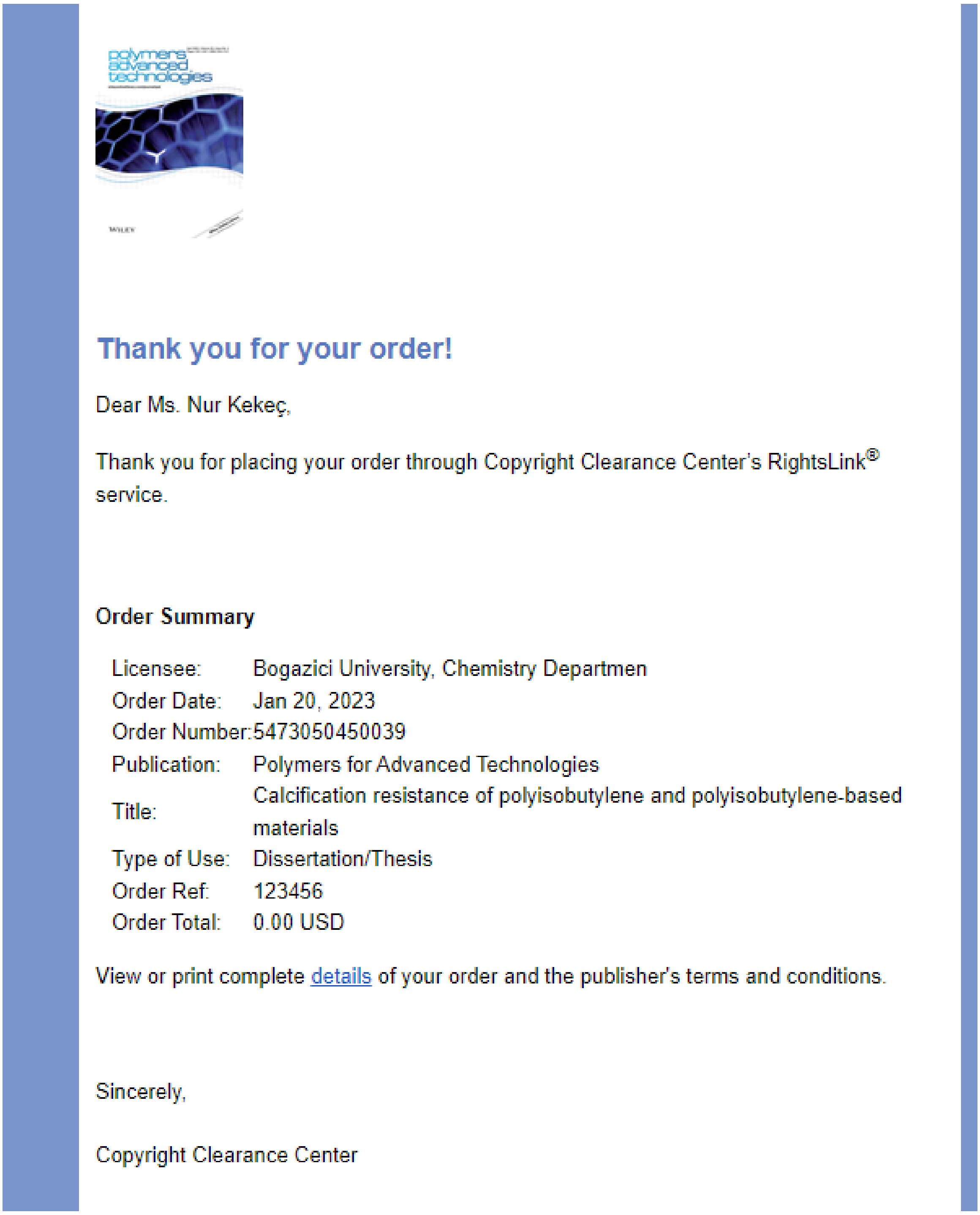

Thank you for your order!

Dear Ms. Nur Kekeç,

Thank you for placing your order through Copyright Clearance Center's RightsLink® service.

Order Summary

Licensee:	Bogazici University, Chemistry Departmen
Order Date:	Jan 20, 2023
Order Number:	5473050450039
Publication:	Polymers for Advanced Technologies
Title:	Calcification resistance of polyisobutylene and polyisobutylene-based materials
Type of Use:	Dissertation/Thesis
Order Ref:	123456
Order Total:	0.00 USD

View or print complete details of your order and the publisher's terms and conditions.

Sincerely,

Copyright Clearance Center

Figure A.6: Permission from [41], John Wiley and Sons, Copyright (2019).

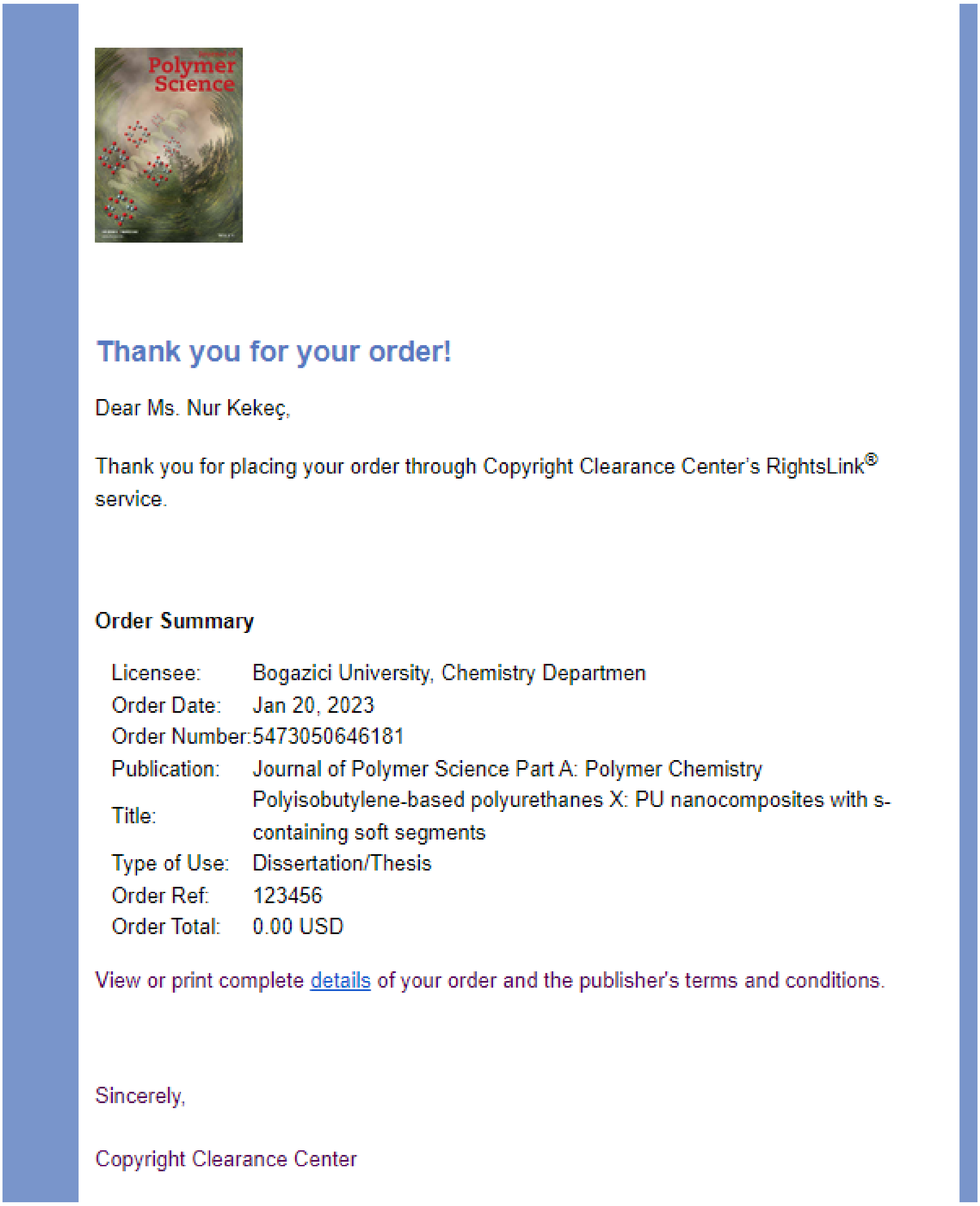

Thank you for your order!

Dear Ms. Nur Kekeç,

Thank you for placing your order through Copyright Clearance Center's RightsLink® service.

Order Summary

Licensee:	Bogazici University, Chemistry Departmen
Order Date:	Jan 20, 2023
Order Number:	5473050646181
Publication:	Journal of Polymer Science Part A: Polymer Chemistry
Title:	Polyisobutylene-based polyurethanes X: PU nanocomposites with s-containing soft segments
Type of Use:	Dissertation/Thesis
Order Ref:	123456
Order Total:	0.00 USD

View or print complete details of your order and the publisher's terms and conditions.

Sincerely,

Copyright Clearance Center

Figure A.7: Permission from [21], John Wiley and Sons, Copyright (2016).

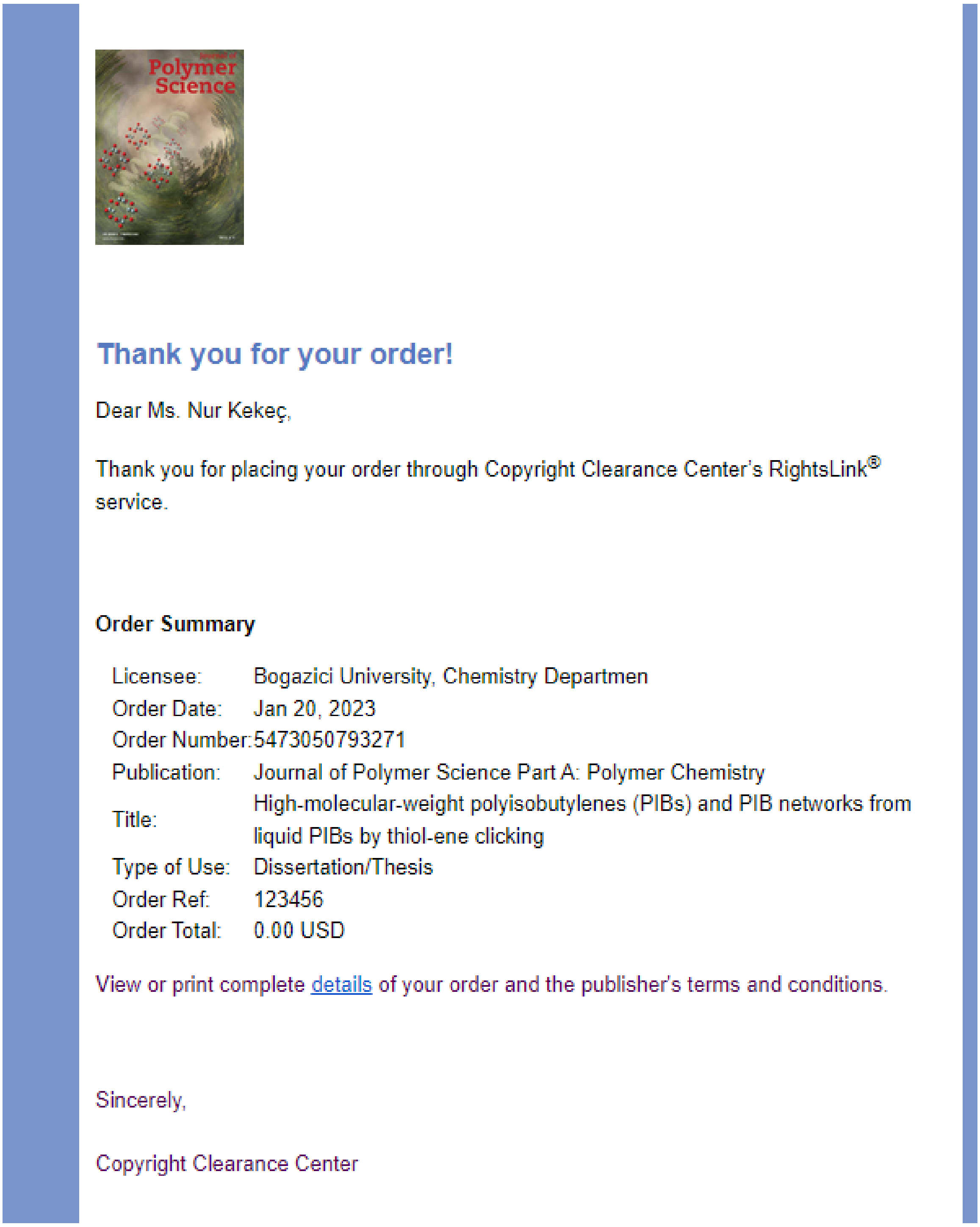

Thank you for your order!

Dear Ms. Nur Kekeç,

Thank you for placing your order through Copyright Clearance Center's RightsLink® service.

Order Summary

Licensee: Bogazici University, Chemistry Departmen
Order Date: Jan 20, 2023
Order Number: 5473050793271
Publication: Journal of Polymer Science Part A: Polymer Chemistry
Title: High-molecular-weight polyisobutylenes (PIBs) and PIB networks from liquid PIBs by thiol-ene clicking
Type of Use: Dissertation/Thesis
Order Ref: 123456
Order Total: 0.00 USD

View or print complete details of your order and the publisher's terms and conditions.

Sincerely,

Copyright Clearance Center

Figure A.8: Permission from [14], John Wiley and Sons, Copyright (2019).